Development of LoRa-based Wireless Sensing Technologies for Structural Health Monitoring

by

Hui Zhang

A thesis submitted in partial fulfilment of the requirements for the degree of Doctor of Philosophy

Supervised by

Associate Professor Sherif Beskhyroun

Department of Built Environment Engineering

School of Future Environments

Auckland University of Technology

New Zealand

June 2024

Abstract

As vital components of national service facilities, civil infrastructures must meet design standards for safety, sustainability, and longevity. However, the performance of structures in long-term service can be compromised or even destroyed by ageing and natural calamities. Therefore, monitoring the integrity of these structures enables the owner, users, and other stakeholders to have a better understanding of the safety state, allowing them to better maintain and extend the service lives of these structures.

Visual inspection is currently the most used non-destructive testing method, although it is unreliable, especially when monitoring huge structures and difficult-to-access locations. The Structural Health Monitoring (SHM) system can be a useful instrument for monitoring and evaluating structural performance. It refers to the process of adopting a strategy for structural damage detection. A typical SHM system operating procedure includes the monitoring of dynamic response via a sensory system, the extraction of damaged physical features, and the analysis of gathered data to determine the condition of the monitored structure. Strain is a metric that has a direct relationship with stress and deflection. In other words, aberrant structural symptoms, such as damage and degeneration, typically manifest as strain field anomalies.

Hence, the objective of this research is to build a new strain-based wireless sensory system for an integrated SHM system. Due to the strain gauge's extensibility and

high sensitivity, it is feasible to monitor the progression of local damage across a small area at an early stage. Besides, by incorporating strain-based sensors into the wireless sensor network design model, the SHM system's integration and management scope will be expanded to include the underlying sensor equipment and the user-graphical interface for monitoring data visualization, thereby achieving the integration of real-time monitoring and rapid evaluation of the structure. The strain-based flexible sensing system developed in this study not only fulfils the requirements for low power consumption but also exhibits excellent sensitivity, allowing it to accurately monitor minor strain changes in localised locations. The wireless sensor system is composed of three parts: a flexible strain-sensing plate, a wireless transmission communication system based on LoRa, and a visual real-time monitoring system.

The aim of this system is to overcome the problem of local damage detection in structural health monitoring (SHM) systems. Thus, it can be utilised as part of an intelligent SHM system to monitor, collect, and transmit strain changes in essential structural components. This research's primary objective is to reduce development and installation costs and the system's power consumption in order to enable long-term monitoring. Because the developed highly flexible strain sensing sheets can be easily mounted on the surface of the structure, as well as having the properties of being waterproof and heat and low temperature resistant, the installation and maintenance costs of the sensor are substantially reduced.

A series of experimental experiments were conducted on a full-scale concrete frame construction in order to evaluate the various properties of the flexible strain gauge. The performance of a flexible strain sensing device was investigated in terms of sensitivity, strain monitoring, and crack damage. The system was also designed to utilise LoRa wireless communication technology for low power consumption and long distance transmission in order to solve the need to install a large number of sensors to cover a

larger area in huge constructions.

The second component of the research involved the development of a hardware system for the continuous gathering of data for two strain measuring configurations: bending strain and axial strain. Utilising multiplixers to achieve seamless configuration switching. Additionally, LoRa technology is employed to enable long-distance wireless transmission. The strain data has a low transmission rate need and is well fitted to LoRa technology, allowing the designed sensing system to have extremely low power consumption and reducing the cost of battery replacement and system maintenance by a significant amount.

The third component of the research is developing an user interface for data management and visualisation for the integrated SHM system. Node-RED is used to create a dashboard for data visualisation, which is connected to The Thing Network (TTN) and Clould to enable real-time data transfer and demonstrate. It is entirely compatible with the deceloped flexible strain sensor system, allowing users to simultaneously monitor the minimum and maximum values of bending and axial strain. The Dashboard also includes the Timechart function to assist users in comprehending the pattern of strain data over time and detecting outliers. The visualisation tool additionally gives information on the number of sensors and Gateways in use, including their operational state and installation locations. Moreover, the original data is kept to permit in-depth analysis and extraction.

The experimental results presented in this thesis demonstrate that the developed system is practicable and possesses the qualities of high sensitivity, low power consumption, and low cost. It is conducive to the continuous real-time monitoring of multiple strains on the structure's main components and allows the flexible wireless sensor system to identify damage in a wide variety of structures.

Contents

Abstract **2**

Attestation of Authorship **15**

Acknowledgements **16**

1 Introduction **17**

1.1 Why Structural Health Monitoring (SHM) System? 17

1.2 Current State of Sensor System in SHM 19

1.3 Internet of Things (IoT) 21

1.4 Research Motivation and Objectives 22

1.5 Thesis Structure 23

1.6 Summary 25

2 Literature Review **27**

2.1 Current State of SHM System and Challenges 27

2.2 Damage Identification and Evaluation Process in the SHM Architecture 29

2.2.1 SHM Sensors and Parameters 31

2.2.2 Direct Sensing and Indirect Sensing Method 35

2.2.3 Overview of Strain-based Sensing Techniques 38

2.2.4 Recent Development of Strain Sensing 44

2.3 IoT and Smart Sensors 48
2.3.1 Challenges and Opportunities of IoT 52
2.3.2 Wired and Wireless Sensors Networks 58
2.3.3 Features of Wireless Sensors for WSNs-based SHM system . 59
2.3.4 Advantages of WSNs in SHM 63
2.3.5 The Major Challenges of WSNs in SHM 65
2.3.6 Comparisons of Existing Wireless Smart Sensor System . . . 69
2.3.7 Academic Prototypes 70
2.3.8 Commercial Wireless Sensor Platform 72
2.4 LoRa - Long Range Radio Communication 73
2.4.1 LoRaWAN Introduction 75
2.4.2 LoRa Performance Overview 77
2.5 Summary 81

3 Development of the Flexiabe Strain Sensing Sheet 83

3.1 Introduction 83
3.2 Strain Sensing Principle 84
3.3 Flexible Strain Sheet Prototype 88
3.4 Development of Strain Sensor Configuration Selector for Bi-axial Strain Measurement 95
3.5 Flexiabe Strain Sensing Sensors Calibration 99
3.5.1 Calibration Test 99
3.5.2 Test Results and Findings 103
3.6 Summary 105

4 Development of the Real-time Wireless Sensory System 108

4.1 Introduction 108

4.2 Design Goals and Considerations 109
4.3 System Level Architecture 111
4.3.1 Data Processing and Transmission 113
4.3.2 LoRa Gateway, Network Server, and Application server 120
4.3.3 Development of the LoRa Gateway 122
4.3.4 Data Storage and Extraction 129
4.3.5 Development of Data Storage System 131
4.4 Summary 132

5 Development of MQTT-based Data Visualisation and Storage for SHM Applications 136

5.1 Introduction 136
5.2 Related Work 138
5.2.1 MQTT Protocol 138
5.2.2 Development of the Application Layer - Data visualisation . . 139
5.3 System Architecture Overview 140
5.3.1 Design Requirements 142
5.3.2 System Implementation 143
5.4 Summary 151

6 Experimental Validation of Flexible Strain Sensors and LoRa-based Wireless Sensor System 153

6.1 Introduction 153
6.2 Full-Scale RC Frame Cyclic Loading Test 154
6.2.1 Experimental Sensors Setup 158
6.2.2 Cyclic Testing and Strain Field Monitoring 160
6.2.3 Hysteretic Response and Load Capacity 164
6.3 Full system Lab Bending Test 173

6.3.1 UTM Bending Test Setup 173
6.3.2 Bending Test Results 175
6.4 LoRa-based Wireless Sensor System Performance Test 179
6.4.1 Test Purpose and Scope 179
6.4.2 Indoor Test with Obstacles 180
6.4.3 Indoor Test Results and Findings 184

7 Future Work Exploration 192
7.1 Introduction 192
7.2 Deep Neural Network-Based Strain Values Prediction Models 194
7.2.1 Model Evaluation 195
7.2.2 Mean Square Error (MSE) 195
7.2.3 R-Squared (R^2) 196
7.3 Deep Neural Network Design Considerations 197
7.4 Training Neural Network Preparation 199
7.5 Model Training Results 201
7.6 Summary 202

8 Conclusion 206
8.1 Conclusion 206
8.2 Future Work 211

References 213

Appendices 222

A LoRa-Based Wireless Sensor Node Hardware Design 223

List of Tables

2.1 A summary of the characteristics of damage identification 32

2.2 The best performance of commonly used commercial strain sensors (Glisic, 2022) 43

2.3 Components of two major IoT architectures 53

2.4 Internet of Things research needs examples (Vermesan et al., 2022) . . 57

2.5 Comparison of LoRa, Bluetooth 5.0 and WI-FI technology 80

4.1 Circuit diagram symbols for the two different bridge connection modes 115

4.2 Power consumption of the main components of various operational states at 3.3 V 119

4.3 Unit price of the components and total costs of the wireless strain sensor node 120

6.1 Cyclic Test Procedure 162

6.2 LoraWAN communication range performance test 187

List of Figures

1.1 A typical SHM system running process 18

2.1 Example of 2D sensor sheets: (a) prototypes installed over cracks on a bridge foundation(b) crack measurement results. (Aygun et al., 2020) . 36

2.2 Strain sensors development progress (Glisic, 2022) 39

2.3 Examples of modern strain sensors: (a) resistive strain gauge (b) FBG strain sensor (c) vibrating wire strain sensor (image (a) Michigan Scientific Corpooration, www.michsci.com, last accessed on 12 December 2022); image (b) SMARTEC SA, Manno, Switzerland, www.smartec.ch, last accessed on 12 December 2022; image (c) Earth Sciences, Australia, www.essearth.com, last accessed on 12 December 2022. 42

2.4 Strain gauges installation: (a) to measure longitudinal deformation (b) to measure hoop strain. (J. Kim et al., 2012) 46

2.5 FBG sensors installation: (a) Inside of sensor encloser (b) 40 FBG installed on Tsing Ma bridge (Chan et al., 2006) 47

2.6 The skeleton of a basic IoT system 49

2.7 IoT reference modle by ITU-T Y.2060 (Chan et al., 2006) 51

2.8 Top 10 IoT segments of actual enterprise projects in 2018 (Lueth, 2018) 54

2.9 World Internet Users Stats in 2022 (a) World internet penetration rates (b) Internet users in the world. (*World Internet Users Statistics and 2022 World Population Stats*, 2022) 55

2.10 Internet service availability in the New Zealand in 2023 (a) 3G network coverage map (b) 4G network coverage map. (*Spark NZ network coverage*, 2023) 56

2.11 Sensor node block diagram 61

2.12 Academic wireless sensors prototypes in recent years: (a) AE sensor node (Y. Wu, Liu & Li, 2017) (b) Xnode smart sensor (c) WSHM platform. (Fu, Khodaei & Aliabadi, 2018) 72

2.13 LoRaWAN architecture (Gkotsiopoulos, Zorbas & Douligeris, 2021) . 76

2.14 Bandwidth and range comparasion of LoRa, Bluetooth, WI-FI and cellular (https://wifivitae.com/2022/12/14/lorawan-mapper-overview/) 80

3.1 A typical whetstone bridge circuit 87

3.2 Design of the strain sensing sheet: (a) Full-bridge configuration (b) half-bridge configuration. 89

3.3 Half-bridge flexible strain gauge prototype 90

3.4 Components of the strain sensin sheet 91

3.5 Full-Bridge Type II Rejecting Axial and Measuring Bending Strain (National Instruments, n.d.) 96

3.6 Full-Bridge Type III Measuring Axial and Rejecting Bending Strain (National Instruments, n.d.) 97

3.7 Design of the strain sensor configuration selector (a) 3D view of the design (b) prototype image. 98

3.8 An example of the use of the strain configuration selector 99

3.9 Dog-bone specimen for calibration 100

3.10 Dog-bone specimen drawings (a) for half-bridge flexiable strain snesors (b) for full-bridge flexiable strain snesors. 101

3.11 UTM tensile test setup (a) Specimen, flexible strain sensor and LVDT (b) UTM front view. 102

3.12 Flexible strain sensors tensile test - UTM Load and strain response (a) for half-bridge flexiable strain snesors (b) for full-bridge flexiable strain snesors. 104

3.13 Strain sensitivity and linearity test of the flexiable strain sensor. (a) for half-bridge flexiable strain snesors (b) for full-bridge flexiable strain snesors. 106

4.1 System architecture for the proposed wireless flexible sensor system . 113

4.2 Circuit diagram (a) measuring bending strain (b) measuring axial strain. (*National Instruments*, n.d.) 116

4.3 Final prototype of the Lora-bsaed wireless strain monitoring system . 118

4.4 Proposed architecture for the intergrated wireless SHM system 121

4.5 Raspberry Pi 3b+ interface 123

4.6 RAK2245 Pi HAT WisLink LPWAN Concentrator (a) top view (b) bottom view (https://docs.rakwireless.com/Product-Categories/WisLink/RAK2245-Pi-HAT/Overview/) 125

4.7 Devepoed LoRa gateway prototype 125

4.8 Proposed workflow for the intergrated wireless SHM system 127

4.9 TTN platform overview (a) TTN application page (b) Data received on TTN - min and max value 128

4.10 Nerwork configuration interface for the developed LoRa gateway . . . 129

4.11 PCB prototypes (a) data storage system (b) connected to the LoRa-based wireless system 133

4.12 End user access file (a) webserver main page (b) webserver test file . . 134

5.1 LoRa-based IoT system architecture diagram for the strain monitoring application 141

5.2 TTN server interface 145

5.3 Backend view of the designed dashbaord work flow on Node-RED . . 146

5.4 Backend view of the designed dashbaord work flow on Node-RED (CloudTern, 2021) 147

5.5 Docker desktop 148

5.6 Docker Desktop interface 149

5.7 The designed dashboard main interface 150

5.8 The designed dashboard download function interface 151

6.1 RC frame geometry 155

6.2 RC frame reinforcement (a) top view (b) side view 156

6.3 RC frame foundation installation 158
6.4 The RC frame installation (a) front view (b) side view (c) back view . 159
6.5 All sensors installation on the RC frame 161
6.6 Flexible strain sensors installation (a) 1 full-bridge installed on beam with LVDT 11 (b) 2 half-bridges connected as 1 full-bridge installed on column with LVDT 1 and 2. 161
6.7 Lateral loading protocol of the RC frame 162
6.8 Crack patterns of the bare frame in different drift levels (a) 0.5% drift (b) 1.0% drift (c) 1.5% drift (d) 2.0% drift. 164
6.9 Lateral load-displacement hysteresis of RC frame 165
6.10 Lateral load-drift hysteresis of RC frame 165
6.11 Crack patterns in different drift levels (half-bridge flexible strain sensors) 166
6.12 Crack patterns in different drift levels (full-bridge flexible strain sensors) 167
6.13 Strain measurements collected by the flexible strain sensor - column . 168
6.14 Column damage condition surrounding the flexible strain sensor - drift 1.5% 169
6.15 Cracks pattern on the beam (full-bridge flexible strain sensor) at 2%drift 169
6.16 Strain measurements collected by the flexible strain sensor - beam . . 170
6.17 Flexible strain sensor performance during cyclic testing - on column . 171
6.18 Flexible strain sensor performance during cyclic testing - on beam . . 172
6.19 UTM bending test setup - NI DAQ 176
6.20 UTM bending test setup - LoRa-based wireless flexible strain sensor system 177
6.21 Relative resistance change during the bending test 178
6.22 Strain and relative resistance change over time 178
6.23 Testing site - AUT WZ Building 3D view 181
6.24 Testing site - AUT WZ Building external view (Mann, 2019) 182
6.25 AUT WZ Building - internal view (Mann, 2019) 183

6.26 LoRa network installation top view 184
6.27 Field testing of Lora network performance in AUT WZ Building . . . 185
6.28 TTN server monitoring panel for indoor test - floor 4 188
6.29 PPR values for indoor test 189
6.30 RSSI values for indoor test - SF = 7 190
6.31 SNR values for indoor test - SF = 7 191

7.1 A typical DNN model architecture 194
7.2 Correlation heatmap of 19 data channels 198
7.3 Architecture of the proposed neural network 200
7.4 Flowchart of DNN model preparation and training 201
7.5 Training and Testing accuracy of proposed deep neural networks . . . 203
7.6 Comparison between experimental measurements and predictions . . . 204

Attestation of Authorship

I hereby declare that this submission is my own work and that, to the best of my knowledge and belief, it contains no material previously published or written by another person nor material which to a substantial extent has been accepted for the qualification of any other degree or diploma of a university or other institution of higher learning.

_____

Signature of candidate

Acknowledgements

To begin, I would like to offer my most heartfelt gratitude to my supervisor, Sherif Beskhyroun, for all of the assistance and support he provided me while I was working towards my PhD. I could never have dreamed that I would be able to complete my PhD studies without his trust and support four years ago. His excellent research insights and outstanding execution have always inspired and impacted me. I could not have finished this thesis without his stringent criteria and pursuit of quality in my study. I would also like to express my gratitude to Xuejun Li for acting as my co-supervisor during this project. His accomplishments in the realm of communication are remarkable, and I am grateful to him for providing me with insightful heuristic ideas that I was able to implement into my work. I hope I can carry on the knowledge and spirit I learned from my supervisors and pass it on to others.

In addition, I would like to express my gratitude to the expert technicians working in the AUT Structure Laboratory, to Justin Matulich, Allan Dixon, and Stephen Hartley, as well as to Pouyan Zarnani and his PhD student Sajad, both of whom were of great assistance to me in the course of the experiment's testing. During the course of my research, the employees at AUT provided me with both practical and emotional assistance, and I would like to express my gratitude to each and every one of them.

A special thank you to all of my friends and coworkers in the PhD office at the Auckland University of Technology, especially Sajad Veismoradi, Sherry Feng, and Fucheng Zheng, as well as everyone else I know, even if I can't remember their names right now. Without them, the whole experience of doing research for a doctoral degree would not have been the same.

Finally, I would like to express my deepest gratitude and love to all my family in China—my father, mother, grandmother and Zitong Fan, for their emotional support and encouragement. This thesis is dedicated to all of you.

Chapter 1

Introduction

1.1 Why Structural Health Monitoring (SHM) System?

Civil structures and infrastructure, such as residential and commercial buildings, bridges, dams, and tunnels, are significant social assets for a nation. To maintain its safety, the state and government must frequently invest a substantial amount of money in its construction and long-term maintenance. In spite of this, ageing, deterioration, and other damage problems are unavoidable as a result of the building's daily use, and it will eventually reach the end of its life cycle. In addition, the structure will be impacted by extreme environmental conditions and unpredictable natural disasters, such as earthquakes, hurricanes, and flooding, which will result in the structure's collapse, inflict enormous economic losses, and potentially endanger human lives. Therefore, it is vital to carry out regular inspections, long-term monitoring, and maintenance on any civil structures and foundations.

The Structural Health Monitoring (SHM) System is an efficient instrument for detecting and monitoring the condition and performance of structures. It is defined as a system

that integrates an identification and enforcement strategy for structural damage (Farrar & Worden, 2007). Apparently, the SHM system has a significant impact on the monitoring of the structural integrity of buildings. It offers both an early warning of structural deterioration and a rapid assessment of the structure's condition following unforeseen events such as natural catastrophes. A typical SHM system operation includes measuring the dynamic response with a sensing system, extracting damaged physical features, and analysing the collected data to determine the condition of the monitored structure (Sohn et al., 2003). As illustrated in Figure 1.1, the SHM system typically includes sensors to monitor the physical phenomena of the structure (also known as damage characteristics), after which the sensors generate electrical signals and transmit them via wired or wireless connection to the terminal. The collected data can then be used for damage detection analysis, and the results can be used for diagnosis and prediction to determine the state of structures.

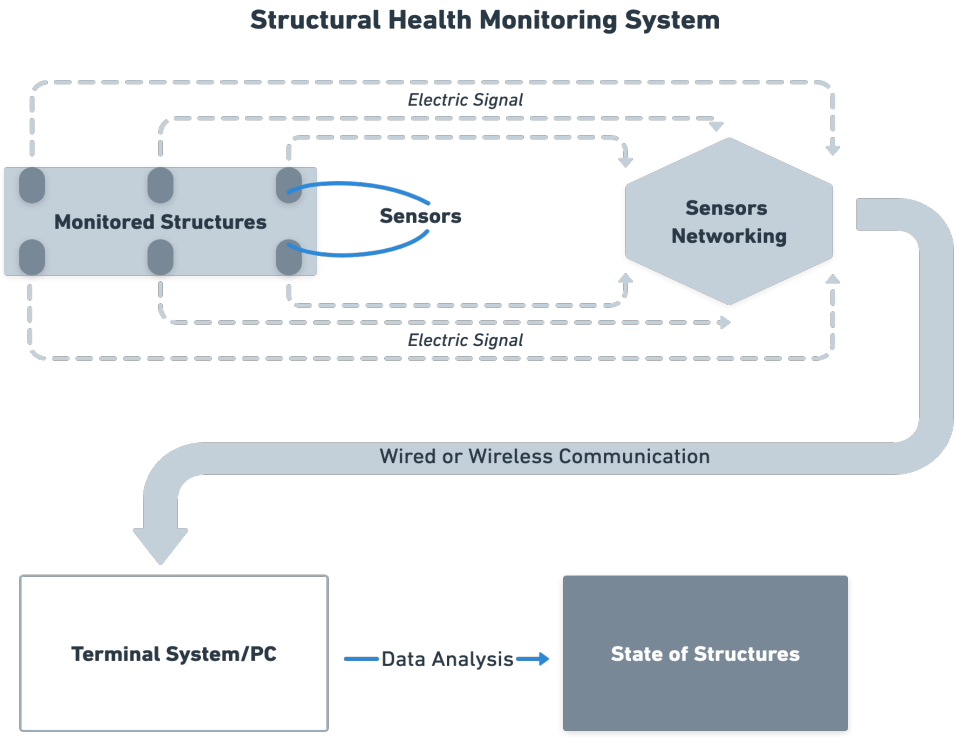

Figure 1.1: A typical SHM system running process

According to the "New Zealand Infrastructure Strategy 2022-2052" strategy report (*The New Zealand Infrastructure Strategy 2022-2052: A foundation for progress*, 2022) published by the New Zealand Infrastructure Commission, the difficulties that New Zealand's infrastructure will confront over the next three decades are outlined. It emphasises that repairing and maintaining existing infrastructure costs $60 for every $40 spent on new infrastructure. Infrastructure delivery, utilisation, and renewal in New Zealand cannot be disregarded, as is evident. Research and implementation of SHM systems in New Zealand are in their infancy at this time. This study aims to address this difficulty and introduce advanced SHM techniques to New Zealand.

1.2 Current State of Sensor System in SHM

In the SHM system, the collection of the properties of the object being evaluated is done with the assistance of sensors. There is a diverse selection of sensors available to meet the needs of a wide variety of criteria. In order to deliver the essential information in a precise way, it is required for these sensors to possess certain qualities, such as high sensitivity, stability, and efficiency.

There are two categories of current sensing technologies: wired sensing and wireless sensing. The traditional method of wired sensing technology relies mostly on wires that are directly attached to the sensing apparatus. These wires are exceptionally stable and long-lasting, making them perfect for situations in which they do not need to be replaced regularly. However, the installation of the limited sensor system necessitates a significant amount of both space and resources, and the conditions that must be met for subsequent maintenance are considerably more challenging. Installing wired sensors both outside and inside a structure is a difficult and time-consuming process, which drives up the cost of the project. This is especially true for multilayer, complicated

constructions as well as large-scale structures. It is impractical to use for monitoring things like bridges, dams, aircraft, etc.

In SHM applications, the use of wireless sensing is becoming an increasingly practical option as a means of overcoming the constraints of wired sensing systems and as an alternative to conventional sensing technologies. This is primarily due to the fact that they are economical, adaptable, and simple to install and maintain. Additionally, the quickening pace of advancement in communication technology gives a solid foundation for wireless transmission, which is a positive development.

The most popular method for deploying a SHM system involves first installing wired or wireless sensor devices on the building structure and then connecting the devices to computers in order to perform data collection and transfer. The environmental variables are essentially converted into electrical signals that can be sent, and the gathered data is then converted to digital format by the digital-to-analog converter (ADC) and uploaded to the computer. In the final step, the user applies the appropriate algorithms to the data in order to do additional analysis and interpret the results.

This research presents the development of a wireless intelligent sensor system that differs from the conventional transducer for SHM. The data collection, signal conversion, processing, and wireless transmission are all incorporated within the wireless smart sensor. The data that is gathered from the structural environment is preprocessed in the sensor system and stored locally on the sensor board. It will be consolidated into relevant information and then wirelessly communicated after going through these steps. The acquired data are then automatically evaluated and represented graphically. This newly developed wireless intelligent sensing system is dependable, adaptable, and resistant to defects. And the installation is both versatile and easy to maintain.

1.3 Internet of Things (IoT)

The Internet of Things (IoT) is basically a network comprised of data generated by various things (Madakam, Lake, Lake, Lake et al., 2015). It can be traced as far back as the 1830s. It was not until the most recent decade that it gradually evolved and drew the curiosity of researchers. This was made possible by the rapid spread of the internet. Through the process of information digitization, analogue forms of data such as text, images, sounds, and electromagnetic waves can be transformed into digital formats. These types of data can be processed on the network, which makes it simpler to store, transfer, and share the data. This procedure enables the extraction of information from any physical object to be digitized. The IoT is also based on the establishment of the concept of the Internet of Everything (IoE).

Since the Internet of Things lowers the cost of both the creation and implementation of hardware, it is widely employed in many embedded devices. Moreover, the Internet of Things accelerates up the process of taking SHM systems from the stage of experimental invention to the stage of industrial deployment. Despite the fact that most SHM technologies are not yet widely implemented in IoT devices (Mahmud, Abdelgawad, Yelamarthi & Ismail, 2017), there is significant research interest in this area. It can provide SHM systems with cloud computing capacity to manage massive sensor data. This new generation of IoT-based SHM systems typically consists of smart objects (SOs) that are sampled every few seconds, after which monitored/sampled data would either be saved or transmitted across the network to the cloud for data processing, and finally to the application layer (Gubbi, Buyya, Marusic & Palaniswami, 2013).

To identify and monitor the performance of critical structural elements and to limit the risk of partial or entire collapse owing to damage to structural elements, this study

extended the framework of the IoT to SHM systems with full-scale structures, such as reinforced concrete (RC) frames.

1.4 Research Motivation and Objectives

As a result of flexible technology's low weight and high strain capacity, it has enabled significant advancements to be made in a variety of industries, including communications and medical care. The exploration and implementation of flexible technology in the field of SHM is not very advanced currently. This is due to the fact that the majority of SHM applications are presently concentrated on the global monitoring of extremely large buildings. However, the deployment of sensors can be difficult for large structures as global monitoring requires a high density of sensors. Yao et al. (Y. Yao & Glisic, 2012) divided damage detection into two more intuitive forms according to different methods of obtaining damage identification parameters: the direct sensing method and the indirect sensing method. The objective is to acquire information regarding the structural damage through direct contact and measurement of the sensor with the structural damage, as well as through contact with potential damage areas. In this research, an integrated flexible SHM system is designed by combining a flexible strain sensor with a wireless sensor node. The concept for this system was inspired by direct monitoring techniques. The primary goals of the project are to apply direct sensing techniques in areas of increased structural critical damage and long-term, real-time monitoring of the strain field condition in areas that are particularly susceptible to strain.

Among the various types of sensors used in the SHM, strain sensors are one of the most important sensors for determining the elastic and health states of structures (Loh, Kim, Lynch, Kam & Kotov, 2007). Because a building material will fail when the tension applied to it at a particular point is greater than the inherent strength of the

material itself, this leads to serious structural issues, such as deterioration and potentially even collapse of the structure. Researchers make extensive use of strain sensors in order to monitor mechanical strain. This is due to the fact that the initial indicators of structural damage are typically confined and appear as abnormal changes in the strain field. Cracks in concrete surfaces and bending in steel structures are two examples that are typical of this phenomenon. Because these early symptoms of structural fatigue and loss of stability can be reflected by changes in strain, it is important to monitor the status of structural strain. Therefore, any observed strain changes on the surface of the structure can provide the SHM system with the most direct first-hand knowledge about the overall structural integrity. This is because, in comparison to other structural responses (such as acceleration and displacement), the strain difference can be measured directly on the surface of the structure. However, in order to determine the condition of the structure, the structural data that is gathered by the accelerometer is typically subjected to additional analysis by a damage detection algorithm. These are the primary justifications behind the selection of strain as the candidate for the sensor parameter in this study.

1.5 Thesis Structure

The thesis is structured as follows and is comprised of eight chapters:

Chapter 2: Chapter 2 reviews the current development and challenges of the SHM system. This thesis reviews the background information as well as the current literature on the various components and sensing technologies used in SHM systems. The literature review of sensing technology focuses primarily on direct sensing technology and indirect sensing technology, as well as the technology that is based on strain sensing and the latest developments in strain technology. This chapter also provides

an extensive review and discussion surrounding wireless sensing technology and the Internet of Things, including the challenges and opportunities in IoT; the challenges and applications of wired sensing and wireless sensing systems in the field of SHM; and the representative of long-distance transmission technology—the development of LoRa communication and the application potential in SHM.

Chapter 3: Chapter 3 introduces the development process of flexible strain sensors and strain configuration selectors. The fundamental principles behind their development and the selection of their materials are discussed. In order to validate its performance, both a calibration test and a tensile test were carried out.

Chapter 4: Chapter 4 presents the hardware development of the Lora-based wireless sensor node. Firstly, the development of a master system is introduced, including configuration control of flexible strain sensors, data acquisition, and transmission. Other than this, it also describes the process of developing a subsystem, which primarily serves for the extraction and storage of data.

Chapter 5: Chapter 5 provides the development of a data visualisation dashboard based on the TTN network server application layer. This application not only integrates with the LoRa network, but it also provides users with the ability to monitor data in continuous time.

Chapter 6: Chapter 6 mainly develops the system to perform a variety of performance tests to verify its capabilities. The system was initially put to use for cyclic loading experiments on a full-scale RC frame. The purpose of these tests was to validate the capability of the flexible strain sensor to identify crack damage. Furthermore, the effectiveness of the wireless system's long-distance transmission was evaluated in a medium-rise engineering building that is located at the Auckland University of Technology in New Zealand. After that, the test findings that pertain to the functionality

of the system are presented and summarised.

Chapter 7: Chapter 7 the strain prediction model based on deep neural network is introduced. This model uses RC frame cyclic loading test data as a training set, and designs a model that can be used for full-scale strain prediction.

Chapter 8:This is the final chapter, and it contains a summary of the primary original concept and development of this thesis, as well as a discussion of potential future studies and applications.

1.6 Summary

The exploration and implementation of SHM systems involve a wide range of disciplines and approaches. The long-term stability, reliability, and service life of the equipment is going to be one of the most major challenges that will be faced in the future. It is essential that SHM systems have the lifespan that they are supposed to have given that the majority of the building's structures and infrastructure are often designed to be operated for decades. Although the recent advancement of SHM systems shows that the majority of the developed devices have good long-term stability, many sensors (as an important part of the SHM system) are subject to a variety of environmental factors during installation and use, which results in internal component ageing and failure issues. Furthermore, it is important to keep in mind that the SHM system incorporates the progress made in the creation of a wide variety of scientific and engineering disciplines, and as a result, extending its service life is not an easy task. It requires the advancement of a variety of scientific domains from a multitude of different points of view. One of the primary goals of this study is to design and develop a replaceable SHM system that is relatively inexpensive as one of the key strategies for responding to this challenge.

When it is required to extend the life of the SHM system, this can be achieved by replacing the portable sensing equipment, which leads to a significant reduction in the expenses associated with installation and maintenance.

Chapter 2

Literature Review

2.1 Current State of SHM System and Challenges

Infrastructures such as highways and highway bridges are built to withstand the dead loads, live loads, and ultimate loads imposed by natural disasters or humans. Unanticipated structural damage has the potential to wreak havoc on human life, society, and the economy. Therefore, socioeconomic and human life safety concerns have been the primary impetus for the rapid development of modern SHM technology. More and more researchers are focusing their attention on the process of monitoring and evaluating the structure in order to guarantee the public's and the nation's security. Despite the fact that modern systems are safer and more reliable than in the past, operating and maintenance costs have climbed significantly. Consequently, numerous academics have spent the last few decades optimising SHM systems (Gordan et al., 2022; He, Zhang, Chen & Li, 2022; Corbally & Malekjafarian, 2022; An, Youn & Kim, 2022; Lin, Guo, He, Li & Yang, 2022). In this chapter, the prior study findings pertaining to crucial SHM process components are reviewed.

The operation procedure of the SHM system may be summarised into a paradigm, including: (1) data gathering, fusion, and cleaning; (2) data storage and transmission; (3) damage feature extraction and in-depth analysis; and (4) structural performance diagnostics and prediction. In the evaluation stage, a number of non-destructive evaluation techniques have been studied in recent years, such as visual detection, infrared thermography (Doshvarpassand, Wu & Wang, 2019), ultrasonic waves (Mutlib, Baharom, El-Shafie & Nuawi, 2016), modal vibration analysis, laser ultrasonic detection (Zhao, Zhu, Yuan, Wang & Zhu, 2016), and so on. These approaches have certain limitations, such as the requirement to further locate the damage once it has been discovered, which requires technicians to be able to enter the potentially damaged region directly, which may be difficult to reach. In the event of natural calamities, such as the fragility of a structure following an earthquake, the inspector may also be at risk. NDE has been developed for over forty years and is extensively used to evaluate the performance of materials, components, and systems. It is characterised by the fact that there is no harm to the object being tested, and it also indicates that the evaluation is carried out without having an effect on the operation of the tested object. In general, NDE techniques can be classified into two main categories: global nondestructive evaluation (NDE) and local nondestructive evaluation(NDE). Global NDE monitors and evaluates the entire structure by collecting responses from different locations within the structure (such as structural vibration and displacement), while local NDE applies to local damage phenomena (such as cracks and corrosion) occurring on structural components or surfaces.

Visual inspections are currently the most used non-destructive evaluation (NDE) technique; however, they are unreliable, particularly when monitoring large structures and inaccessible sites. Currently, the traditional visual inspection method relies heavily on experienced inspectors on-site. This conventional approach, however, is prone to

human error and cannot provide an accurate assessment of the structure's condition when inspectors are unskilled or must investigate inaccessible areas. This is also a less efficient inspection method for large-scale structures, as it necessitates more inspectors and extended field assessments to maintain massive facilities. The most major limitation of visual inspection is that it cannot ensure continuous or long-term real-time monitoring over an extended period of time. If there are cracks in the structure, the long-term monitoring of the status of the cracks needs to establish if it is a live crack or a dead crack and whether or not the crack is actively expending. If it is a live crack, the SHM system can track its direction and condition. This is, to some extent, challenging for visual detection. While with the assistance of high-resolution sensory system, the SHM system is capable of providing an accurate assessment in comparison to conventional visual inspection, lowering the risk of evaluation failure. Long-term real-time diagnostic data also aids in predicting structural performance and required maintenance, thereby maximising the structural integrity and safety and extending its lifespan.

2.2 Damage Identification and Evaluation Process in the SHM Architecture

In general, structural damage generates changes in modal parameters; therefore, researchers introduce a variety of sensitive measures, such as vibration characteristics, strain, power flow, and so on, to detect damage status (Morassi & Vestroni, 2008; Montalvao, Maia & Ribeiro, 2006; Alvandi & Cremona, 2006; Carden & Fanning, 2004). Damage identification or detection is the basis of structural repair or replacement decisions in the SHM system (J.-T. Kim, Ryu, Cho & Stubbs, 2003). The deterioration caused by the structure can be broken down into two distinct categories: linear and

nonlinear. Damage that can be classified as "linear" occurs when an initially linearly elastic structure is unable to retain its linearly elastic state after being damaged. On the other hand, the initial linear elastic structure demonstrates nonlinear damage by transitioning into a nonlinear state after being damaged. Linear equations of motion can be used to represent the structural reactions to changes that are generated by modal features.

According to Rytter (Rytter, Brincker & Hansen, 1991), the procedure for the complete detection and evaluation of damage consists of the following four steps:

a) Step 1: Whether or not the damage is present in the system.

b) Step 2: Determine the location of the damage.

c) Step 3: Identify the nature of the damage.

d) Step 4: Evaluate the extent of the damage and estimate the remaining life of the structure.

It is clear from Rytter's findings that a typical SHM system architecture needs to have a damage identification and evaluation mechanism. The SHM procedure entails gathering data from sensors that have been installed in the monitored structure on a regular basis. This enables the recognition of damage to the structure. When such data are used, sensitive properties that can be exploited for structural state analysis are typically damaged. The term "damage identification" refers to this stage in the SHM process. The concept of "damage identification" comes from the idea that a structure that has been damaged will have changes in its material or geometric qualities that may have an undesirable effect on the structure either now or in the future. For instance, changes in the geometry of a structure that are brought on by cracks in the structure might bring about shifts in the element's stiffness.

Analyzing the ways in which structural vibration characteristics have changed can be a relatively straightforward way to determine the extent of global damage. Doebling et al. (Doebling, 1996) addressed and extensively reviewed various vibration-based damage monitoring approaches. The literature review was then brought up to date by (Sohn et al., 2003), who covered the years 1996 to 2001. Throughout the course of the past few decades, scholars have conducted a significant amount of research in three sectors that are based on time, frequency, and mode shape, and they have accomplished excellent achievements (Hou & Xia, 2021; Das, Saha & Patro, 2016; Fan & Qiao, 2011). A significant number of studies find and localise damage by detecting fluctuations in the natural frequency, which is straightforward to measure. However, because the natural frequency only causes extremely minute shifts, it is exceedingly difficult to identify, particularly in the case of huge structures. Inaccurate frequency measurement can also be caused by external factors such as the influence of fluctuating temperatures or changes in the mass of the structure. In the field of SHM, researchers have also delved deeply into multidisciplinary topics, such as the intersection of computer science and mathematics in the form of damage algorithms. A review of the variables utilised by Lee et al. for the purpose of damage identification can be found summarised in Table 2.1.

2.2.1 SHM Sensors and Parameters

The selection of sensor type and specifications is the initial step in the design and development of a SHM system. As mentioned above, there are two distinct approaches to detecting the extent of damage: local damage detection and global damage detection. It is better to choose sensor characteristics in accordance with a variety of damage detection purposes. Sensor parameters can be roughly classified into the three categories that are listed below (Ou & Li, 2010):

Table 2.1 A summary of the characteristics of damage identification

Category		Methodology
Modal Parameters	Natural Frequencies	• Frequency changes • Residual force optimization
	Mode Shapes	• Mode shape changes • Modal strain energy • Mode shape derivatives
Matrix Methods	Stiffness-based	• Optimization techniques • Model updating
	Flexibility-based	Dynamically measured flexibility
Machine Learning	Genetic Algorithm	• Stiffness parameter optimization • Minimization of the objective function
	Artificial Neural Network	• Back-propagation network training • Time delay neural network • Neural network systems identification with neural network damage detection
Other Techniques		• Time history analysis • Evaluation of frequency response function (FRFs)

- ***Local load response.*** The local load response of a structure is the response of the structure itself to a given load. This reaction may only be evaluated from a particular area of the structure (local region). The measurement parameters include strain, cracking, etc.

- ***Global load response.*** The global load response requires that the entire structure be measured. Take, for instance, the load that is generated by the passing of vehicles over the bridge. Acceleration and velocity are the types of parameters that are often measured by the sensor in this scenario.

- ***Environmental factors.*** Environmental factors are factors that are not directly related to the structure itself but are instead related to the environment in which the structure is located. Temperature and humidity are examples of common measurement parameters.

The sensitivity, resolution, signal-to-noise ratio, and other performance characteristics of the sensor are all adjustable, giving users granular control over the device's capabilities.

According to the types of the aforementioned detection parameters, the following SHM sensors are commonly used:

- ***Accelerometers.*** The accelerometer is the sensor that is utilised most frequently for detecting the structural vibration response in global monitoring. Accelerometers are typically piezoelectric or spring types. The sample frequency of the accelerometer can be increased to more than 100 Hz, and the minimum sampling resolution of the accelerometer is 16 bits. In recent years, there has been a significant increase in the use of accelerometers that are based on MEMS. Presently, the most prevalent form of accelerometer is the piezoelectric accelerometer. It offers the benefits of being compact, lightweight, and capable of operating across a broad frequency range (De Reus, Gulløv & Scheeper, 1999).

  Zhu and colleagues (Zhu et al., 2018) conducted research on a new high-sensitivity wireless sensor that was based on a MEMS accelerometer. Their findings demonstrated that the wireless accelerometer has superior performance. Kohler et al. (Kohler, Hao, Mishra, Govinda & Nigbor, 2015) built a portable vibration sensor called ShakeNet, which was successfully tested on a California bridge.

- ***Strain sensor.*** The strain sensor is commonly applied in SHM because of its affordable pricing. It is particularly sensitive to the presence of possible risks in critical components or in local areas of the structure. Strain sensors are typically implemented for the purpose of doing local monitoring. In recent years, there has been a lot of research done on embedded strain gauges, such as embedding the strain gauges into cement materials. However, because of its great sensitivity, once it is incorporated into the material or the structure, it will also be impacted by the conditions of the environment outside of it (for example, temperature). As a result, it is essential to ensure that the exterior of the strain gauge is protected.

  Jo et al. (Jo, Park, Spencer, Jung et al., 2013) came up with a wireless strain sensor

panel called SHM-S. It has the ability to measure strain at low levels caused by the environment. Moreu et al. (Moreu, Kim & Spencer Jr, 2017) installed a wireless strain gauge on a bridge in combination with an accelerometer in order to assess, respectively, the load and the structural characteristics of the bridge.

- ***Linear Voltage Differential Transducers (LVDTs).*** The linear variable displacement transducer, or LVDT, is a precise electromechanical sensor. It provides resolution on an infinite scale. Its operating principle is that when the structure is shifted, the LVDT's magnetic core moves, and as a result, the output voltage varies in a linear way in relation to the magnitude of the magnetic core displacement. Its primary characteristics are frictionless quantity measurement, excellent resolution, and great repeatability.

- ***Optical Fiber Sensors (FOSs).*** In recent years, FOSs have also become a popular area of study in SHM. In most cases, it is fixed directly to the surface or inside structures during the construction of existing buildings. Not only are FOSs capable of operating in severe environments, but they can also be used to measure parameters such as strain, temperature, and force. FOSs have a large measuring range, are distributed, have minimal transmission loss, and offer additional advantages. At present, high-precision fibre Bragg grating sensors are widely used (Lu et al., 2019).

The primary objective of this research is to identify and keep monitoring any localised damage that may have occurred to the structure; hence, a strain-based wireless sensor system is being developed. The literature review pertaining to strain sensing is going to be covered in the following chapter section.

2.2.2 Direct Sensing and Indirect Sensing Method

One of the major aims of the SHM is to have the ability to determine with accuracy whether or not the structure is damaged. As previously indicated, damage monitoring can be broken down into two categories: local monitoring and global monitoring. These techniques, in turn, require the employment of distinct kinds of sensors to detect damage, extract structural modal parameters, and determine other aspects of structural state.

Yao et al. (Y. Yao & Glisic, 2012) divided damage detection into two more intuitive forms according to different approaches to obtaining damage identification parameters: the direct sensing method and the indirect sensing method. As its name implies, the purpose of the direct sensing method is to obtain information on structural damage through the direct contact and measurement of sensors and structural damage, as well as through contact with potential damage areas and structural components. For instance, strain sensors can be utilised to detect structural cracks as well as the propagation of damaging waves through the structure. When using the direct sensing approach, the sensor is pre-positioned at the presumed area of the damage. This allows the sensor to identify damage anomalies, such as high strain anomalies, in a direct and expedient manner. The outstanding benefit of utilising this technique is that it generates measurement results that are characterised by a high level of reliability and consistency. The challenge of this strategy, however, is that because it focuses on local damage, the presumed position of the structural damage needs to be pinpointed with as much precision as is feasibly possible. To put it another way, the approach of direct sensing necessitates the accurate positioning of the sensor in the area that is at risk of being damaged. Although deploying a large number of densely distributed discrete sensors is a viable solution to this challenge, doing so will result in a significant rise in the cost of both the equipment and its installation. In order to monitor and track the growth of

cracks in the structure, Aygun et al. (Aygun et al., 2020) developed a 2D sensor sheet to cover larger portions of the structure's surface. As shown in Figure 2.1, this sensor system was successfully used to monitor and track the formation of cracks. However, because two-dimensional sensor systems incorporate numerous sensor arrays, if a single sensor element in the sensor array is broken, the detection performance and effect of the entire system are directly compromised, resulting in false measurement data.

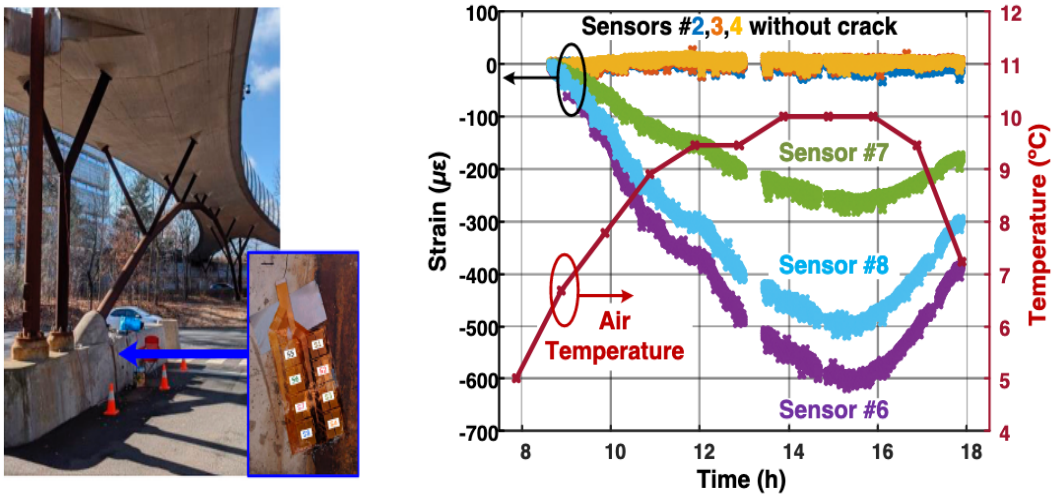

(a) (b)

Figure 2.1: Example of 2D sensor sheets: (a) prototypes installed over cracks on a bridge foundation(b) crack measurement results. (Aygun et al., 2020)

The term "indirect sensing" refers to a scenario in which the sensing system does not come into direct contact with the structure at the location where damage exists (or where damage is potentially present). Common sensors used for indirect sensing technologies include accelerometers, LVDTs, and other devices not installed at the location of the damage, as they are normally used for monitoring the global response. The indirect sensing method makes use of sensor equipment that is presumed not to be placed at the damaged location of the structure. In this case, the damage may or may not cause a change in the strain field of the sensor as well as its location. Indirect sensing is also known as global sensing or non-contact sensing. There are a lot of obstacles to

overcome while taking such an approach. If the sensor is situated at a location that is a significant distance from the actual site of the damage, the strain change that is measured by the sensor will be extremely minimal and impossible to detect, because it is difficult to differentiate changes in strain from other factors such as load and ambient noise. Indirect sensing, on the other hand, cannot rely solely on strain as a single indicator; rather, it necessitates the application of sophisticated data analysis algorithms in order to identify the existence of damage and its precise location, which results in additional and significant financial outlays. In addition, most of them are mainly used in the context of laboratory tests, which cannot guarantee the same outcomes as examinations conducted in real life. Therefore, despite the fact that the technique of indirect sensing is widely employed in a variety of applications, its restrictions are difficult to overcome.

In SHM applications, the difference between direct sensing detection techniques and indirect sensing detection methods is that damage can be identified immediately from the sensor's output of evident outliers. This is one of the characteristics of direct-sensing detection methods, despite the fact that the two detection techniques each have their own different objectives. Indirect sensing, on the other hand, requires that the structure be monitored for a long period of time, that a large amount of data be continuously collected, and that a variety of algorithms be used to analyse the data in order to establish whether or not damage exists and what its features are (damage location and quantification).

In previous sections, the benefits and drawbacks of direct and indirect sensing have been outlined in terms of the sensors employed in the SHM and their corresponding difficulties.The ultimate purpose of this research is to investigate and develop a sensing system that is low-cost, highly sensitive, and chemically durable for the purpose of putting SHM into practical application in the context of local damage monitoring. As a result, direct sensing forms the foundation of the damage detection system that is

presented in this study. The primary hypothesis for this line of exploration is that the proposed system will be capable of rapidly extracting the characteristics of structural damage by developing a portable direct-sensing device with increased sensor exposure to local damage.

2.2.3 Overview of Strain-based Sensing Techniques

Lord Kelvin made the hypothesis in 1856 that the resistance of metal conductors is proportional to the mechanical strain, which laid the foundation for the invention of the resistance strain gauge. In the 1920s, strain-based sensors began to be employed in the SHM field, which is primarily classified into two categories: discrete electrical sensors for local damage monitoring and distributed sensors for structure integrity monitoring. Through the introduction of the above principles and related literature reviews, it is obvious that the use of sensitive modal parameters is the key to accurate local damage identification. The great sensitivity of strain-based sensing techniques has emerged as a popular field of research in recent years, and numerous strain-based sensors have also been the focus of extensive study and development.

More than a century has passed since strain sensors were first developed, during which time they have found widespread use in the construction of civil engineering projects and have significantly broadened the application range and evaluation capability of SHM systems in terms of structural safety and integrity. Glisic (Glisic, 2022) classifies them as belonging to three generations of strain sensors according to the procedure through which they were developed, as illustrated in Figure 2.2. Green means that it is relatively mature in the market and has been well developed; orange means that it is partially mature but still needs a lot of research; and red means that it is currently being researched and developed.

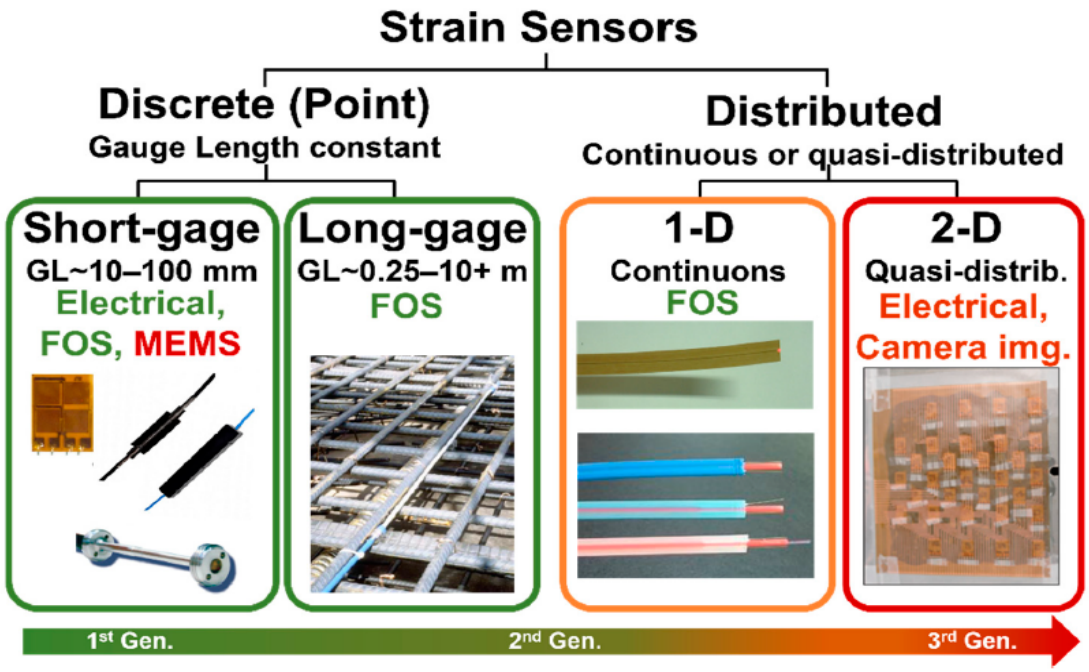

Figure 2.2: Strain sensors development progress (Glisic, 2022)

Strain gauges, which operate according to electrical principles and are typically attached to the surfaces of materials, are the most prominent examples of the first generation of sensors. After that, embedded strain sensors variations were developed, which are usually pre-installed inside structures when buildings are being constructed. However, it was difficult to utilise these sensors to measure structures that are already in existence. They are able to monitor and assess the levels of strain in localised parts of the material, establishing the basis for strain-based sensors.

The development of optical fibre technology enabled the invention of the second generation of strain sensors, which comprises discrete short-gauge and long-gauge strain sensors as well as one-dimension distributed sensors. These sensors were made possible by the advancement of technology. The second generation of sensors has the potential to carry out spatial coverage of structures, monitor buildings from a more macro perspective, and have a high capability for detecting structural damage. Not only can it be used in combination with strain sensors of the first generation, but it can also bring

about sustainable management of building safety and structural integrity monitoring.

The reliability and accuracy of damage detection are both improved as a result of the third-generation strain sensor's excellent efficiency. This improvement is primarily due to the fact that the third-generation strain sensor covers a larger spatial range and has a higher spatial resolution than its predecessors. At this point in time, continuously distributed or quasi-distributed two-dimensional strain sensors are the main part of the third generation of strain sensors. These sensors can be divided into two primary categories: contact sensors and non-contact sensors, each of which is determined by the type of sensing technology used. In the new generation of strain sensors, strain is chosen as the primary indicator of damage detection rather than the observation parameter. This is the most distinguishing aspect of this new generation of strain sensors. They can also use the same direct sensing technology as the first generation, which involves making direct contact with the surface of the testing material in order to detect material properties. As a result, the accuracy of damage identification can be significantly improved, regardless of the environment. However, the third generation of strain sensors also faces some major challenges, such as how to apply them to full-scale structures, how to deploy sensors on a large scale, how to efficiently transmit and manage a large number of long-term monitoring data, how to avoid systemic problems caused by the damage of a single sensing element in a sensor array, and so on. These challenges are not insurmountable, but they do present some difficulties. Nevertheless, the strain sensor of the third generation will become increasingly prevalent in the SHM system's real-world applications in the near future.

It is worth mentioning that strain sensors are particularly useful for SHM applications since they are the most effective technology now available to analyse structural safety and performance indicators (such as stress and deflection). Strain gauges, fibre optical sensors (FOS), and piezoelectric (PZT) strain sensors are the common types of strain

sensors that are employed in SHM applications with the highest frequency at the present time. Figure 2.3 illustrates the some examples of modern strain sensors that finds the most widespread application on the market today. The contribution that their presence has made to the monitoring of the growth of building structures and SHMS has been invaluable. Typically, this form of strain gauge is bonded to the polished structure's surface. The use of resistive strain gauges is appropriate for a wide variety of structural materials, including, but not limited to, wood, metal, composite materials like concrete, and other synthetic fibers. Glisic (Glisic, 2022) provided a concise summary of the advantages and challenges that strain sensors bring to SHM applications.

Advantages

- ***The costs of production are fairly affordable.*** Its sensing components are low-cost, readily available through mass production, and well-suited for the attachment of sensor arrays to large structures.
- ***Outstanding testing performance.*** With its high resolution, its test performance is generally in the $1\mu\varepsilon$ range, which is ideal for SHM systems.
- ***Potentials for wireless communication systems.*** Based on their electrical principles, it is easy to develop wireless transmission functionalities for strain sensors in conjunction with wireless sensor network technology for remote monitoring.

Challenges

- ***Electromagnetic Interference (EMI).*** Despite the fact that the electrical principle behind the strain sensor makes it possible for it to operate wirelessly, it is also sensitive to electromagnetic interference (EMI) when it is located close to the monitoring structure, such as wires or radio waves. Electromagnetic interference will not only have an effect on the measurement data; in extreme circumstances, such as when lightning, lightning, or other uncontrollable natural forces are present, it will also lead to the failure of sensor electronics or the irreversible damage of such system.

- ***Need Temperature compensation.*** With the exception of the Carlson strain metre, the vast majority of modern strain sensors are sensitive to variations in temperature. As a result, it is necessary to perform temperature compensation on the strain that is obtained using these sensors.



(a) (b) (c)

Figure 2.3: Examples of modern strain sensors: (a) resistive strain gauge (b) FBG strain sensor (c) vibrating wire strain sensor (image (a) Michigan Scientific Corpooration, `www.michsci.com`, last accessed on 12 December 2022); image (b) SMARTEC SA, Manno, Switzerland, `www.smartec.ch`, last accessed on 12 December 2022; image (c) Earth Sciences, Australia, `www.essearth.com`, last accessed on 12 December 2022.

It is clear that each of these widely utilised strain sensors currently available on the market come with their own unique set of advantages and disadvantages. The features of three common commercially available strain sensors are outlined in Table 2.2 by Glisic (Glisic, 2022). This table provides a comparison of the sensor qualities that are critical to SHM civil applications. Some of these characteristics include stability, resolution, linearity, and so on.

In recent years, in order to fulfil the requirements of integrity monitoring, the strain sensor has evolved from a one-dimensional (1D) measurement to a two-dimensional (2D) measurement and then gradually to a three-dimensional (3D) measurement. For instance, 2D paint, 2D sensing sheets, and 3D intelligent self-sensing materials In order to determine whether or not strain is useful in the process of damage localization,

Table 2.2 The best performance of commonly used commercial strain sensors (Glisic, 2022)

Property	**Vibrating Wire Strain Sensor**	**Resistive Strain Gauge**	**Carlson Strain Meter**
Gauge length	Typical: 50-150 mm Special (long): 300 mm	Typical: 0.3-20 mm Special (long): 150 mm	Typical: 203-508 mm Special (short): 102 mm
Multiplexing (the way multiple sensors are accessedby the reading unit)	Parallel (one by one)	Parallel (one by one)	Parallel (one by one)
Maximum number of sensors per reading unit (with a channel switch or multiplexer)	32 *	1200 *	24 *
Stability	Long-term stable	Long-term drift (typical)	Long-term stable
Resolution	Typical: 1 $\mu\varepsilon$ Best: 0.35 $\mu\varepsilon$	Typical: 1 $\mu\varepsilon$ Best: 0.5 $\mu\varepsilon$	Typical: 2-3 $\mu\varepsilon$ Best: 1.5 $\mu\varepsilon$
Linearity (repeatability precision)	Typical: ±0.5% Full Scale Best: ±0.1% Full Scale	0.2-2%	N/A
Sensor range	Typical: 3000 $\mu\varepsilon$ Extended: 10,000 $\mu\varepsilon$	Typical: 10,000 $\mu\varepsilon$ Extended: 100,000 $\mu\varepsilon$	Typical: 2000 $\mu\varepsilon$ Extended: 3900 $\mu\varepsilon$
Temperature sensitivity	Compensated with an integrated temperature sensor	Compensation needed	Self-compensated (by measurement principle)
Measurement frequency	Typical: 0.25-1 Hz Dynamic: 20 to 333 Hz Max.: 1 kHz *	Typical: 100-200 Hz Max. 100 kHz	N/A
	* Unconfirmed		

Herrera-Iriarte et al. (Herrera-Iriarte, Alvarez-Montoya & Sierra-Pérez, 2020) carried out a comparative experiment with the strain values of two different groups of FOS. Xu and coworkers created an innovative self-powered strain-temperature dual-functional sensor based on composite films of carbon nanocoils (CNCs). When used in conjunction with wireless networks, PZT sensor skins that have been integrated into flexible layers can be effective for damage detection in applications linked to aeronautics (Schulz & Sundaresan, 2006; Qiu, Deng, Yuan, Huang & Ren, 2018; Liu, Yuan & Qiu, 2012). In recent years, a number of researchers have started making use of strain sensors based on graphite in SHM systems (Zymelka et al., 2017; Zymelka, Yamashita, Takamatsu, Itoh & Kobayashi, 2018).

All of these experiments show a great deal of potential, but they are hampered by a number of obstacles, including a high cost, poor durability, and the requirement for costly auxiliary electronics, such as lasers, in order to combine. For instance, the fibre sensor or fibre Bragg grating (FBG) that was discussed earlier is capable of providing high-precision data on strain and temperature, but the practical use of SHM has to find a solution that addresses the issue of the high cost that is associated with deploying fibre on a structure. Strain gauges are characterised by a high level of sensitivity and an affordable price. When combined with materials that are flexible and elastic, it is possible to acquire detection results of high quality at a reduced cost. As a result of this, the new sensing system that was developed in this study is based on strain sensing techniques.

2.2.4 Recent Development of Strain Sensing

The design of the civil structure is performed in accordance with the requirements of the standard regarding stress and deflection. Stress and deflection, on the other hand, cannot

be directly measured in real-world applications because of limitations in structural material performance, sensing technology, and other factors. The parameter known as strain is directly related to both stress and deflection. In other words, abnormal symptoms of structures, such as deterioration, decay, and other damages, typically manifest in the form of anomalies in the strain field. In addition, the strain-based technique can be utilised in SHM applications to address the issue of difficulty detecting minor damage, which is a common issue. The basic principle underlying this concept is that although small damage cannot be diagnosed by changes in displacement, it may be identified by changes in strain (Xu, Fan, Yang, Zhao & Pan, 2021).

The strain-based sensing technology has very promising application prospects in real-world engineering contexts. For instance, subterranean pipelines are sensitive to permanent ground deformation (PGD) and wave propagation due to the seismic action that occurs during an earthquake. The bending of a pipe causes stress because the pipe is either compressed or stretched in its axial direction as a result of the bending. A study was carried out by Kim et al. (J. Kim et al., 2012) in 2012 with the purpose of determining the magnitude of damage that earthquake-induced PGD causes to buried pipelines. In their experiment, a large number of strain gauges were applied to monitor the pipeline's progression toward deformation and eventual failure. As can be seen in Figure 2.4, the strain gauge is mounted in the middle of the pipe section as well as at the mouth of the pipe so that both the longitudinal strain and the hoop strain can be measured.

The Fiber Bragg Grating (FBG) sensor is another common type of strain sensing instrument. It functions on the premise that the refractive index of the fibre core undergoes cyclical shifts at periodic intervals (Sahota, Gupta & Dhawan, 2020). When the broadband wave propagates through the grating, the wave with a certain peak value will be reflected, and when external factors, such as stress, induce changes in the



(a) (b)

Figure 2.4: Strain gauges installation: (a) to measure longitudinal deformation (b) to measure hoop strain. (J. Kim et al., 2012)

characteristics of the FBG, the reflected wavelength will be altered, making it possible to measure the required parameters. As can be seen in Figure 2.5, Chan et al. (Chan et al., 2006) deployed forty developed FBG sensors on the Tsing Ma Bridge in Hong Kong in order to measure different strains and temperature under railway and traffic loads. The sensors are split into three individual sensor arrays, which are then attached to the rocker bearings, truss beams, and hanger cable of the bridge, respectively.Although FBG is capable of providing high-accuracy strain and temperature acquisition, its fabrication and installation are both labor-intensive, time-consuming, and expensive. There is more work to be done to address these challenges in order to make practical engineering applications of SHM systems.

Crack detection is another one of the most prevalent application scenarios for strain-based sensing techniques, and it is often used as damage indicators in SHM damage identification. Cracks are typically the result of local failures in structural components and building materials. These failures can be produced by a wide variety of reasons, including buckling, external stresses, fatigue, and corrosion. It's possible that the growth

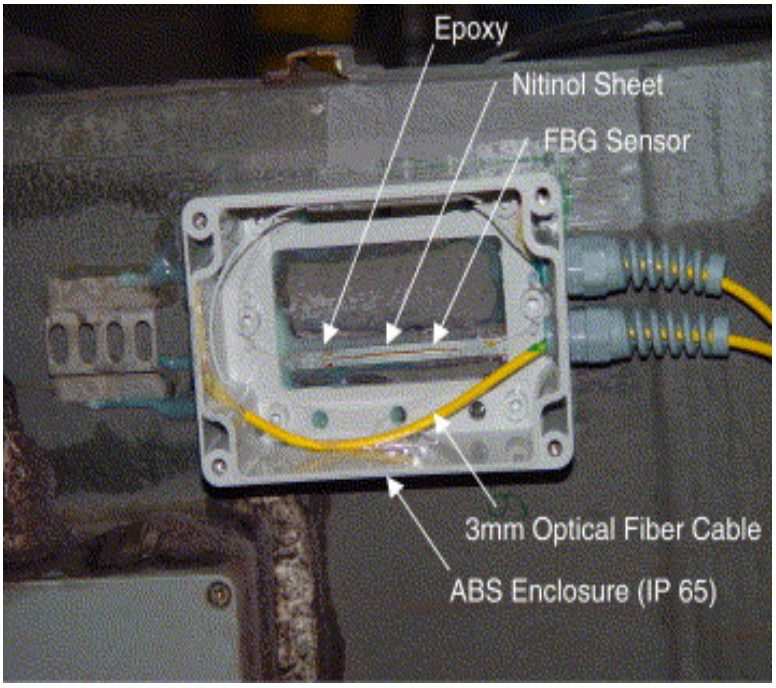

(a)

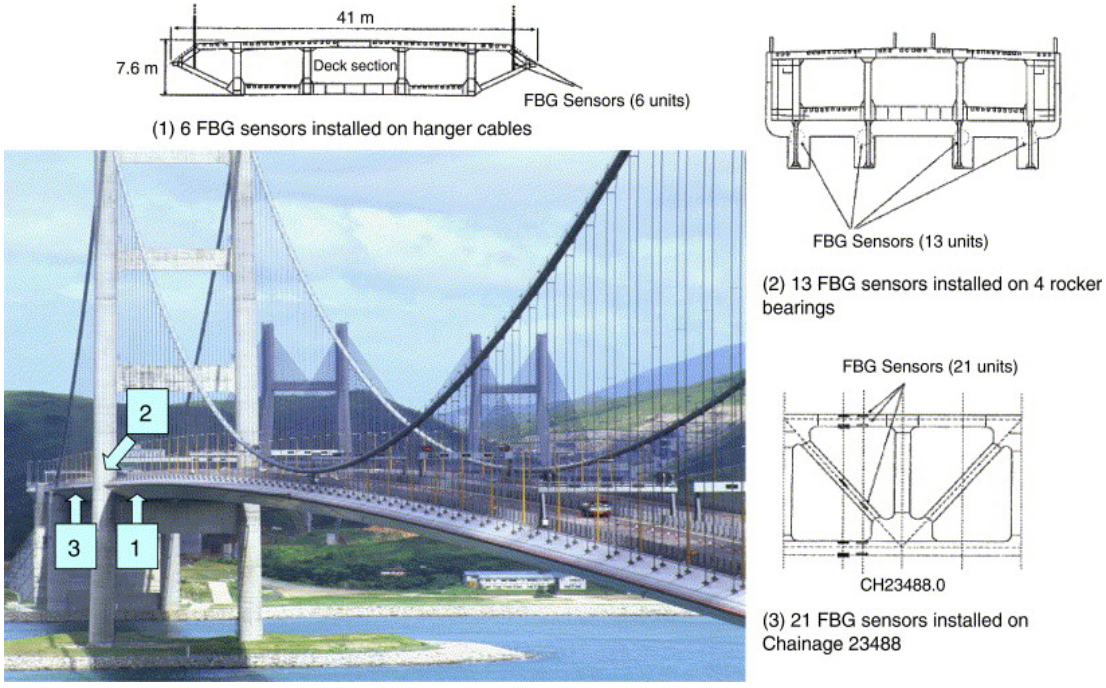

(b)

Figure 2.5: FBG sensors installation: (a) Inside of sensor encloser (b) 40 FBG installed on Tsing Ma bridge (Chan et al., 2006)

of a few small cracks at the beginning will have only a minor impact on the building's overall integrity. But once a crack is identified in any structure, the first step is to figure out whether it is a live crack or a dead crack. Live cracks tend to grow larger with time, whereas dead cracks don't. In order to avoid structural failure that is brought on by major cracks, such as damage and collapse of key structural components, long-term monitoring of the growth trend of the crack is required if it is a live crack. Additionally, early ageing cracks can have a significant impact on the structure's inherent durability, which is especially dangerous for complex composite materials such as concrete. It is therefore extremely crucial to identify the presence of cracks and the status of such fractures before the cracks reach a critical level and cause the failure of structural components or the entire building. The strain sensing system that is in contact with the structure surface can accurately monitor, through the outliers of the output signals, whether or not the strain field is abnormal due to cracks in the structure. This is also one of the objectives of the strain-based sensing system developed in this study. In Chapter 3, the principles of the strain sensing technology used in this paper as well as its development process are introduced in detail.

2.3 IoT and Smart Sensors

The IoT refers to the core notion of connecting objects to networks (wired or wireless) using various information-detecting devices or technologies. It is an internet-based information carrier, which can realise the interconnection between things and things, things and people. Even though the modern technical specifications and architecture of the IoT have not been standardised (Nicolescu, Huth, Radanliev & De Roure, 2018) and despite the fact that the architecture models that researchers refer to are slightly different from each other, the IoT system typically consists of the following four layers:

(1) the perception layer or sensing layer of the physical environment; (2) the network layer, which is used to connect all sensor devices; (3) the data processing layer for the purpose of converting and processing data; and (4) the application layer that actually provides intelligent services. Figure 2.6 shows the structure of a basic IoT system. IoT can be implemented in numerous fields. It is possible to achieve sensing, data gathering, storage, and processing by connecting physical or virtual devices to the Internet. The merger of integrated sensing technology and the IoT can meet the requirements for processing massive data volumes, but at the same time, it will bring data security challenges in both storage and transmission (J. Lee, Stanley, Spanias & Tepedelenlioglu, 2016).

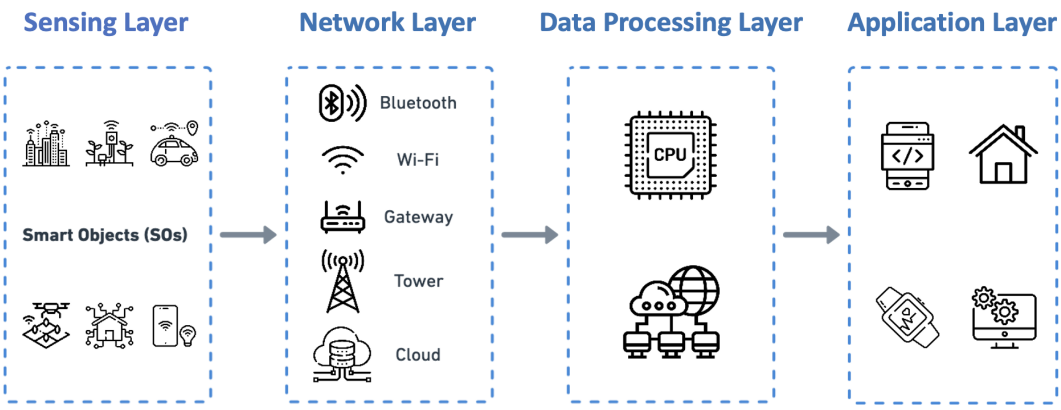

Figure 2.6: The skeleton of a basic IoT system

The primary components of the IoT architecture are, in general:

1. ***Perception/sensing layer***: As the first layer of the IoT, the Perception layer is responsible for converting analogue models into digital information. The typical components of this layer are as follows:
    - Sensors: Instruments used to evaluate and monitor changes in physical properties,
    - Actuator: Device that converts electrical signals into physical signals,
    - Deveces: Comprising both a sensor and an actuator.

2. ***Network/connectivity layer***: The communication of data is at the heart of this layer; its primary purpose is to facilitate effective coordination with other layers as well as the storage and processing of data. The IoT encompasses a variety of network technologies for communication, data storage, and processing, including Bluetooth, Wi-Fi, and Low-Power Wide Area Network (LPWAN).
3. ***Data processing layer***: The data processing layer is typically composed of two stages: the data accumulation stage and the data abstraction stage. These stages are designed to collect, store, and process data, respectively.
4. ***Application management***: In this layer, the data will be further processed and analysed in order to more precisely interpret the qualities and significance of the extracted data, as well as to assist users in making decisions. The application layer is responsible for its own unique applications in a variety of different commercial sectors.

A specific IoT reference model that is specified by ITU-T Y.2060 (International Telecommunications Union) is shown in Figure 2.7. The model contains important capabilities and components of the IoT, which contribute to reducing the complexity of developing and implementing the IoT while also providing academics with a shared understanding. The application layer is located at the very top of the reference model. This layer encompasses typical Internet of Things applications that are now available on the market, such as smart homes, artificial intelligence health monitoring, and smart grids. The service and application support layer is the second layer that is presented. Its primary objective is to offer support for a wide variety of applications, both general and specialized. Accessing the network, connecting various devices, and managing communication are the responsibilities of the network layer, which is the third tier of a network system. The device layer is the fourth layer, and it is comprised of several sensors that come together to form a sensor network. This layer is able to manage sensor devices and gateways, as

well as facilitate communication between gateways and devices. The reference model for managing devices includes the management layer in addition to the security layer. Examples of this include remote access, activation, monitoring, management, traffic control, protection of privacy, authorisation, and authentication.

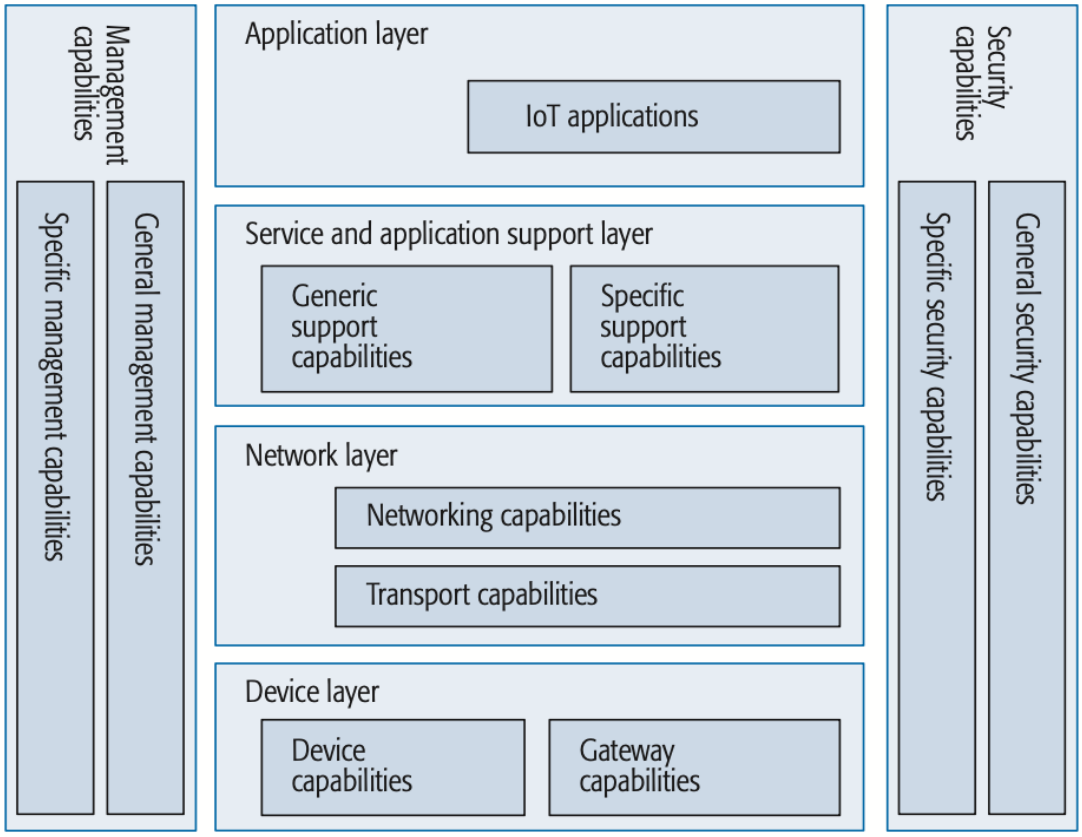

Figure 2.7: IoT reference modle by ITU-T Y.2060 (Chan et al., 2006)

In recent years, researchers have created SHM systems for a variety of applications as a direct result of the rapid growth of the IoT. The possibility of IoT research in the field of SHM has been examined in terms such as eliminating environmental consequences and expanding sensor applications and communication technologies. Misra et al. (D. Misra, Das & Das, 2020) built a building monitoring system that is compatible with mobile device applications by making use of piezoelectric sensors, low-cost Arduino, and ESP8266 Wi-Fi modules. Another study that utilises piezoelectric

sensors is the integrated IoT SHM system that was developed by Myers et al. (Myers, Mahmud, Abdelgawad & Yelamarthi, 2016) This system was designed to detect the location of damage as well as its severity. Research on SHM systems that use machine learning techniques (Zhang, Zhou, Han, Lin & Wu, 2018) to minimise environmental consequences is also ongoing, and other IoT devices for complex structures, such as foundations (Day-Lewis et al., 2017) and bridges (J.-L. Lee, Tyan, Wen & Wu, 2017), are also attracting widespread interest.

In order to construct a typical IoT communication architecture, these four core layers integrate a variety of software and hardware technologies. It not only makes it possible for simple sensing devices to connect to the internet by utilising the wireless network paradigm, but it also makes it possible for devices to communicate with each other in an independent way (Petersen, Baccelli, Wählisch, Schmidt & Schiller, 2014). Madakam et al (Madakam et al., 2015) compiled five typical IoT projects developed by some researchers and industry practitioners. The two major IoT architecture of as well as the components that make up their models are extracted in Table 2.3, which can be found below.

2.3.1 Challenges and Opportunities of IoT

The IoT has been implemented in a broad variety of domains, which has benefited the growth of numerous industries that are closely related to it. According to Atzori et al., (Lueth, 2015) the applications of the Internet of Things can be broken down into four categories: (1) transportation and logistics, (2) healthcare, and (3) intelligent environments (such as personal homes, offices, factories, etc.). (4) social areas (e.g., infrastructure construction services). In a survey on IoT applications conducted by Lueth, the top three IoT applications, as measured by people's Google searches, Twitter

Table 2.3 Components of two major IoT architectures

Organisation	Architecture Layers
International Telecommunications Union (ITU) architecture	• Sensing layer • Access layer • Network layer • Middleware layer • Application layer
IOT forum architecture	• Applications • Transportation • Processors

postings, and LinkedIn content, were smart homes, wearable gadgets, and smart cities (or smart buildings). Lueth also (Lueth, 2018) verified that, as of 2018, a total of 1600 enterprise IoT projects had been put into practical application. As shown in Figure 2.8 The smart city, connected industry, and connected building were three of the most successful projects that had been put into real-world implementation. It is not difficult to observe that despite the fact that IoT is still an emerging technology with a comparatively short history, the characteristics of IoT determine that it can affect and spread a wide variety of fields and human life.

The accessibility of the Internet in the geographic area in which IoT applications are deployed is yet another factor that should be taken into consideration. It can be seen from Figure 2.9, in addition to Africa, the utilisation rate of the internet is far above 70% in Asia, Europe, Latin America, South America, the Middle East, and Oceania, as shown by the most recent data collected by Internet World Stats in 2022. When compared with the situation just ten years ago, more than 50% of the population in most regions of the world does not have access to the internet. As a result, the rapid

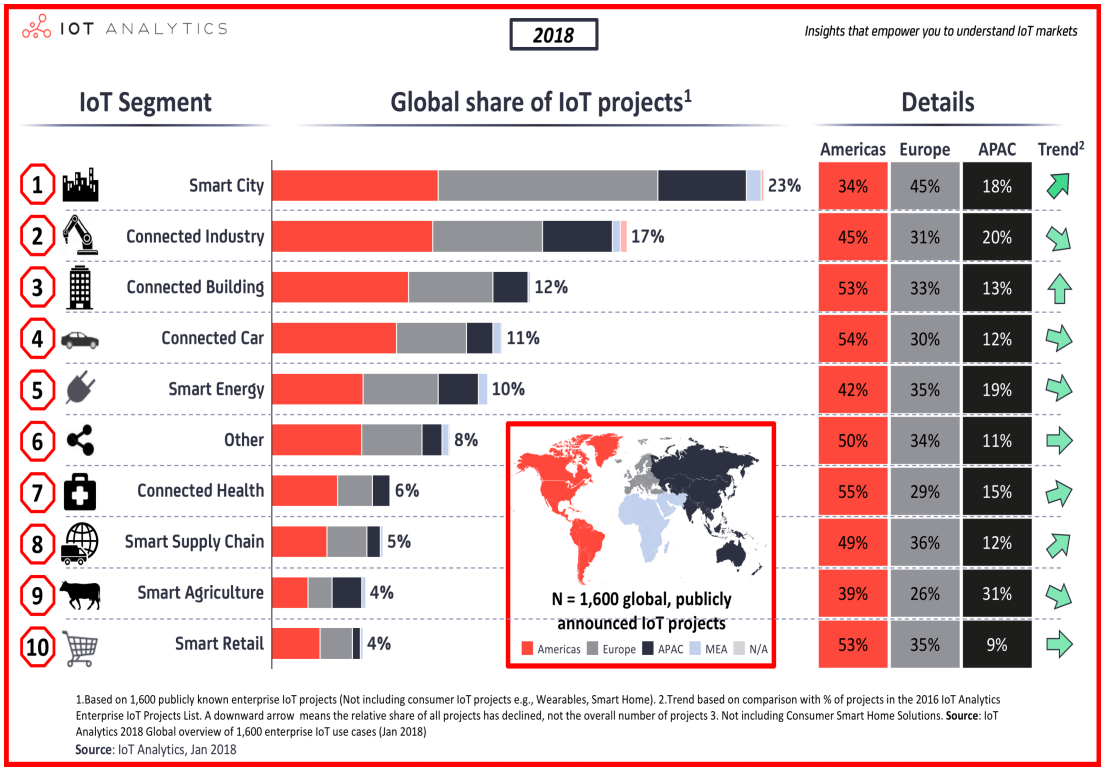

Figure 2.8: Top 10 IoT segments of actual enterprise projects in 2018 (Lueth, 2018)

growth and widespread use of the internet also provide an excellent service platform for the IoT. As an illustration, take the Internet service provider Spark as an example, which operates in New Zealand. The scope of its Internet coverage in New Zealand is demonstrated in Figure 2.10. The company's 3G network coverage reaches 97.5 percent of New Zealanders, and its 4G network coverage is also available in most cities and regions across New Zealand. As a result, the existence of a network in New Zealand with such a high coverage provides an excellent environment for the development of an intelligent sensor system based on a wireless network in this study.

The advancement of IoT technology is predominantly dependent on the development of various applications in both software and hardware; consequently, it involves a great deal of research needs, such as in IoT architecture, communication technology, network technology, algorithms, sensing devices, and so on. Because of the inherent

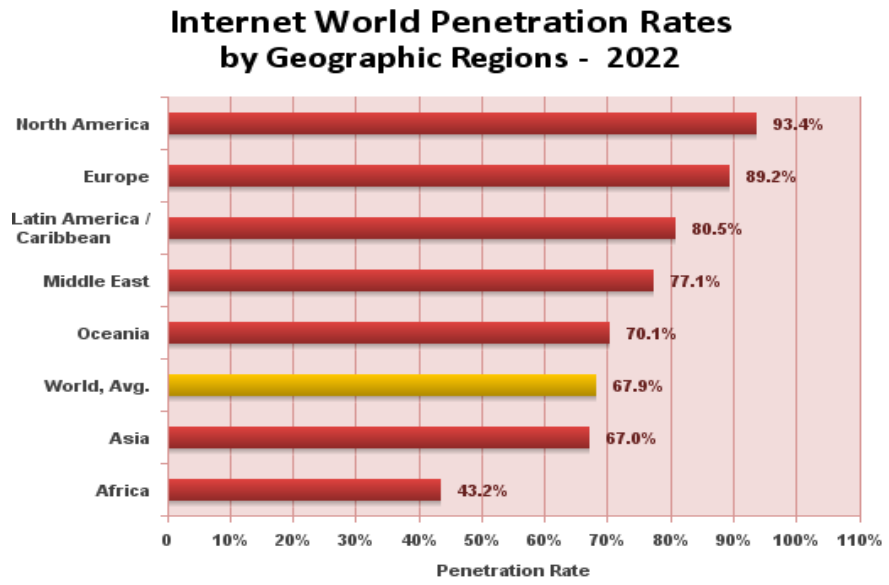

(a)

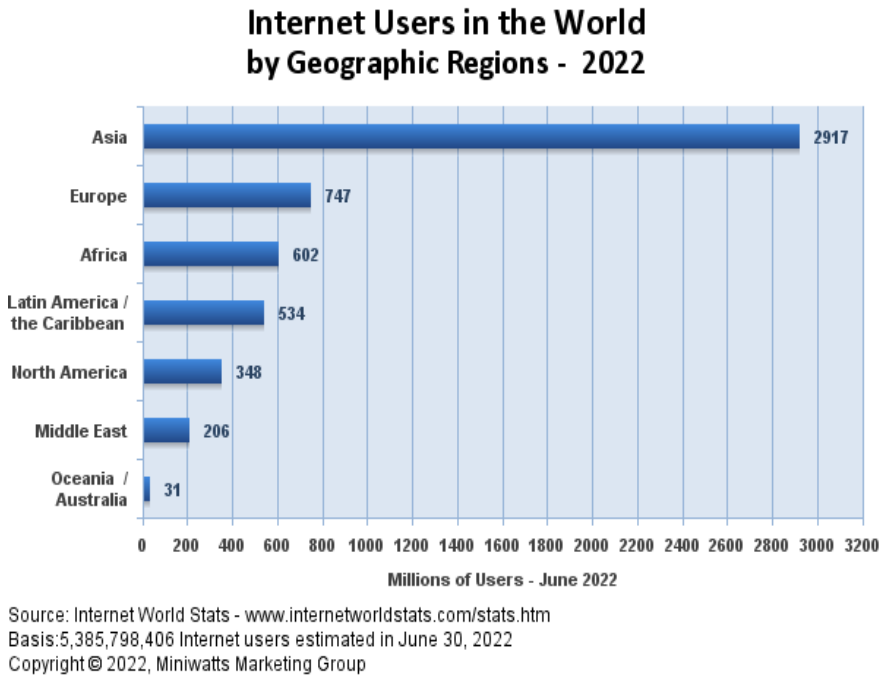

(b)

Figure 2.9: World Internet Users Stats in 2022 (a) World internet penetration rates (b) Internet users in the world. (*World Internet Users Statistics and 2022 World Population Stats*, 2022)

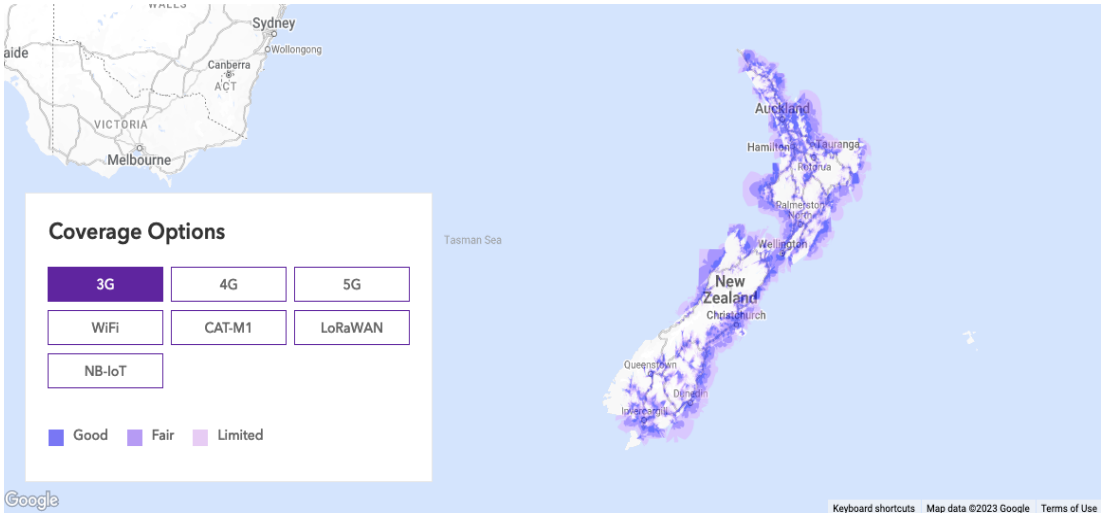

(a)

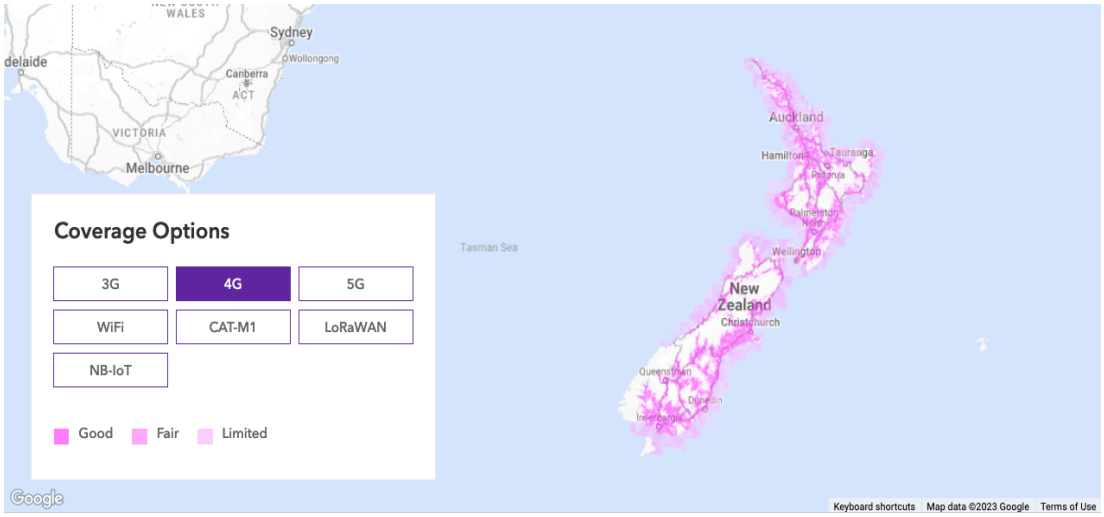

(b)

Figure 2.10: Internet service availability in the New Zealand in 2023 (a) 3G network coverage map (b) 4G network coverage map. (*Spark NZ network coverage*, 2023)

complexity of the IoT, the demands for research can be broken down into a wide variety of specialised subfields. The examples that are used to illustrate this point are taken and summarised in Table 2.4. For further details, refer to Vermesan et al.'s (Vermesan et al., 2022) paper.

In spite of the promising studies and applications of IoT systems that were discussed above, there are still a number of design obstacles that developers, engineers, and

Table 2.4 Internet of Things research needs examples (Vermesan et al., 2022)

Research Needs	2011-2015	2015-2020	Beyond 2020
IoT Architecture	Extranet (Extranet of Things) (partner to partner applications, basic interoperability, billions-of-things)	Internet (Internet of Things) (global scale applications, global interoperability, many trillions of things)	
	Adaptation of symmetric encryptionand public key algorithms from activetags into passive tags		
	Universal authentication of objects		
	Graceful recovery of tags following	Code in tags to be executed in the tag or intrusted readers	
Internet of Things Architecture	power loss	Global applications	
	More memory	Adaptive coverage	Intelligent and collaborative functions
Technology	Less energy consumption	Object intelligence	
	3-D real time location/position embedded systems	Context awareness	
	IoT Governance scheme		
	Long range (higher frequencies —		
Communication	tenth of GHz)	On chip networks and multi standard RF architectures	
Technology	Protocols for interoperability	Plug and play tags	Self configuring, protocol seamless networks
	Protocols that make tags resilient topower interruption and fault induction	Self repairing tags	
	Collision-resistant algorithms		
	Grid/Cloud network		
	Hybrid networks		
	Ad hoc network formation	Service based network	Need based network
Network Technology	Self organising wireless mesh networks	Integrated/universal authentication	Internet of **Everything**
	Multi authentication	Brokering of data through market mechanisms	Robust security based on a combination of ID metrics
	Sensor RFID-based systems		Autonomous systems for non stop information technology service
	Networked RFID-based systems — interface with other networks —hybrid systems/networks		
	Paper thin electronic display with		
	RFID		
	Ultra low power EPROM/FRAM		
	NEMS	Polymer based memory	
	Polymer electronics tags	Molecular sensor	
	Antennas on chip	Autonomous circuits.	
	Coil on chip	Transparent displays	
Hardware Devices	Ultra low power circuits	Interacting tags	
	Electronic paper	Collaborative tags	
	Devices capable of tolerating harsh	Heterogeneous integration	
	environments (extreme temperaturevariation, vibration and shocks conditions and contact with different chemical substances)	Self powering sensors	
	Nano power processing units	Low cost modular devices	
	Silent Tags		
	Biodegradable antennae		
	Common sensor ontologies (cross		
Data and Signal	domain)	Autonomous computing	Cognitive computing
Processing Technology	Distributed energy efficient data pro-	Tera scale computing	
	cessing		

researchers need to overcome. For instance, the development of wireless devices as well as wireless sensor networks is extremely important to the IoT. The following is an overview of some of the significant challenges faced by the IoT:

- Energy problem
- Concerns pertaining to the safety of wireless networks;
- The amount of electricity that is consumed by the device
- Fault tolerance of data ;collected and transmitted by sensing equipment;
- And application to real-life and industrial scenarios.

There are some more specific concerns, like the illegal exploitation of the IoT to extract private information using already installed IoT sensing devices. As a result, it is an extremely challenging task to design and build IoT systems that are immune to any security threats.

2.3.2 Wired and Wireless Sensors Networks

SHM systems that are based on wired sensing usually involve the use of wires to connect a number of transducers that are mounted on the structure to a central data processor. The majority of these systems convey peak data using alternating current (AC) power (Farrar, Park, Allen & Todd, 2006). When the measurement goes beyond a predetermined threshold, the user will receive an alert. The primary drawback of a wired sensor system is that it requires the laying of dozens or even hundreds of data channels in order to monitor the full-size structure, which results in a significant increase in cost. One example of this is the Tsing Ma bridge in China (Ni, Wang & Ko, 2000).

In order to circumvent the impracticality of wired sensor systems, wireless sensor systems have been investigated and widely implemented in SHM. The cost of installing

numerous sensor nodes is also far lower than the cost required to deploy cables in a wired system. Also, it ensures that each node is transmitted to the gateway in an effective manner and reduces the overall cost of the project. In addition, wireless networks are extremely versatile and can accommodate a broader range of user demands, such as data transmission and monitoring in real-time. This kind of integration of network information technology and wireless communication offers a cost-effective alternative for the monitoring and evaluation of full-size and large-scale structures.

Despite the numerous benefits of wireless sensor systems, there are still some obstacles in the practical industrial applications of SHM at present, such as long-distance transmission, as data transmission rates are affected by distance limitations. Other electronic devices, such as mobile phones and radio equipment, will also cause interference with wireless sensor networks (WSNs). This interference will result in disruptions to signals, the loss of data, and other issues. In addition, even though wireless sensor networks provide the opportunity for real-time monitoring, the more sophisticated raw data that is gathered by sensors still needs to be artificially evaluated in more detail.

2.3.3 Features of Wireless Sensors for WSNs-based SHM system

In general, the wireless sensors that is utilised in a WSNs-based SHM system requires four fundamental components in order to realise the process of installing sensors in the structure, gathering inductive data, and then transferring and processing it. These components come together to make up the sensor node. In SHM systems, it is essential for WSNs to construct a sensor node that possesses the necessary level of functionality. Because the entire process of data collection and transmission within the SHM system is extremely reliant on sensor nodes, As an essential step in the process of extracting damage features and processing data signals, the design of wireless sensor nodes

typically needs to take into consideration the following functions (including, but not limited to, others):

1. Adequate data should be obtained in accordance with the differences in the extracted damage characteristics.
2. Has the ability to temporarily retain a specified amount of gathered measurement data.
3. Is capable of doing signal processing on the data that has been collected.
4. If put in harsh environmental conditions, the system is able perform self-monitoring, such as monitoring the power supply or the damage to built-in components.
5. The base station has the ability to reassign certain degrees of freedom, such as the sample rate.
6. Capable of receiving and transmitting data in a consistent and dependable manner.

The wireless sensor node is not a simple device, and its design as well as its use in the real world face a variety of challenges. Particularly concerning is the issue of power consumption; an increase in the functionality of sensor nodes will result in an increase in the amount of power consumed by the system. The primary components of the sensor node are depicted in Figure 2.11. These components include the sensing unit, communication unit, processing unit, and power supply. The power supply for sensor nodes is provided primarily by batteries. The sensor unit is the initial component that works to ensure that data collection takes place. After that, the data is sent through signal processing and conversion to either the base station or the terminal devices. The primary purpose of sensor nodes in WSNs is to operate as a bridge between the real world and the network, to extract the characteristics of objects that are able to be perceived, and then to turn those characteristics into data that people are able to read and comprehend. The data may alternatively be stored in the terminal device or temporarily stored in the sensor node. Either option is available.

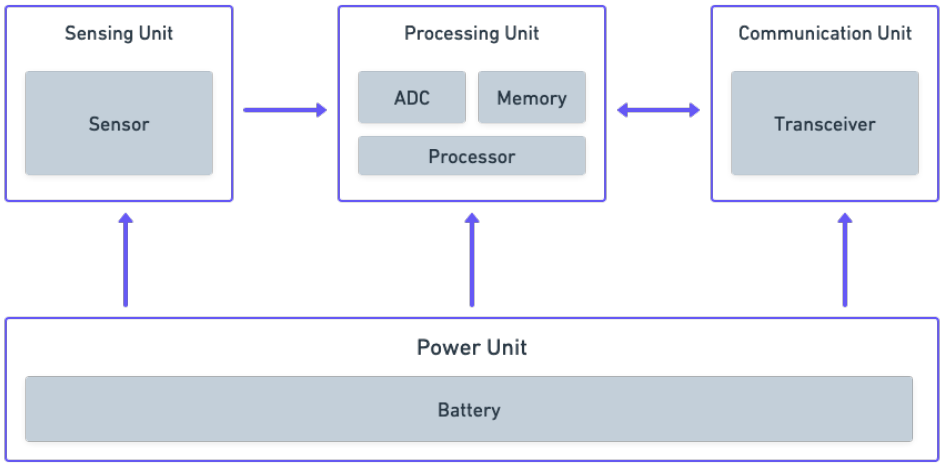

Figure 2.11: Sensor node block diagram

The following section provides a brief overview of the key components function, which include sensor interfaces (sensors and data acquisition systems), the computing core (microcontroller and memory), wireless transceivers, and power sources (Lynch & Loh, 2006).

Sensor Interface: Sensors are always going to be the most crucial component of any wireless sensor network. It is critical to select the suitable sensor type in order to extract the structural information of the object. Because the performance of the sensors determines the quality of all the data and the overall SHM system evaluation accuarcy. An analog-to-digital converter is a common interface used in sensors system that converts analogue signals into digital output (ADC). The accuracy of the ADC is determined by the resolution of the device itself, as well as the sampling frequency and the number of channels. When it comes to accuracy, an ADC's resolution is directly correlated to its performance. However, this results in a rise in both the price of the sensors and the amount of power they consume. Not necessarily the most powerful components should be used; rather, the proper ones should be chosen based on the monitored characteristics.

Computing Core: When the sensor interface is connected to the sensor in order to start the data collection, the microprocessor will control multiple wireless sensor nodes by utilising pre-programmed algorithms for various functions, including sampling, transmission, and storage. The size of its data bus can typically range from 8 to 32 bits. It is important to keep in mind that a large data bus will lead to higher throughput, yet it will also cause problems with high costs and high power consumption. Every microprocessor has its own internal clock that can be used to determine how quickly embedded programmes run. Additionally, it possesses memory and has the ability to add additional external memory to the sensor system if the RAM, ROM, and storage capacity are insufficient.

Wireless Transceivers: Data can be transmitted to remote storage devices via wireless transceivers, which are designed to communicate with a number of sensors or gateways simultaneously. The communication range of the SHM application may need to be greater than 100 metres or even cover a bigger area if it is to be used for the monitoring of civil buildings. For this purpose, a wireless transceiver with a large communication capacity is required. Radios with shorter communication ranges can be used for monitoring mechanical systems like aircraft.

The communication range of a wireless transceiver has a direct impact on the amount of power that it requires to run. According to the findings of Rappaport's investigation (Rappaport, 2002), the amount of power that is lost by a wireless signal while it is being sent in an open area is directly proportional to the radio's wavelength and inversely proportional to the square of the distance between the transmitter and the receiver.

Power Source: In contrast to wired systems, which get their power from cables that are physically attached to the sensor devices, wireless sensor systems rely mostly on batteries as their primary source of power. As a result, one of the most important aspects

of the design of wireless sensors is the design of a power distribution system that is reasonable (Spencer Jr, Park, Mechitov, Jo & Agha, 2017). As mentioned above, the development of this wireless sensor system and the selection made about its primary components will directly impact the amount of energy that is needed to drive it. In order to achieve monitoring over a longer period of time, it is required to optimise them to some degree in order to lower the amount of power that is consumed overall (S. Jang & Spencer Jr, 2015). In addition, human interventions, such as pre-set time triggers or periodic sampling, can also be taken into consideration, and natural resources, such as solar power, can be used as a backup source of energy.

2.3.4 Advantages of WSNs in SHM

The swift advancement of wireless sensor networks (WSNs) and technology for micro-electromechanical systems (MEMS) provides a robust research foundation for low-cost wireless structural monitoring systems (Lynch & Loh, 2006; Bhuiyan, Wang, Cao & Wu, 2013; Caballero-Russi, Ortiz, Guzmán & Canchila, 2022; R. Misra, Jalali, Rizzo & Dickerson, 2021). The installation of wireless sensor nodes on the structure allows for the collection of vibration characteristics, structural response, strain values, and other important parameters. These kinds of systems have the potential to avert catastrophic events like the collapse of a structure.

The advantages of WSNs application in SHM mainly include the following aspects:

Low Cost: Conventional wired sensors installed in the structure require the use of long cables to transmit data to the centralised data acquisition system. This particular installation method is quite expensive. According to Jang et al. (W.-S. Jang, Healy & Skibniewski, 2008), the cost of setting up cables on a new building is approximately $2.20 per metre, while the cost of installing cables on an existing building is approximately $7.19 per metre. The cost of installing approximately 15 wired sensors to create a

sensor network can reach up to $5,000. However, the cost of each WSN is typically between $50 and $100. Due to the low cost, it is now possible to deploy large-scale sensors in huge and complicated buildings, which not only ultimately decreases overall costs but also lowers the expenses of ongoing maintenance.

Network Scalability: The term "scalability" in the network context refers to the concept that the initial benchmark of the application can be met, and on this basis, the sensor network can be expanded to a large scale. The scalability of the network indicates an increase in both the complexity and the practicability of the application (Aygün & Gungor, 2011).

This scalability is represented by an increasing number of sensors, increased sensor sensitivity, a more complex network topology, and enhanced data quality. This allows robust, real-time, and long-term monitoring of the SHM system. The increased cost of wireline-sensor network scalability is still considerably cheaper than the additional installation of wired cables, especially for full-scale or large structures.

Deployment Time: The deployment of wireless sensor nodes is relatively simple. In contrast to wired sensors, the distance between many sensor nodes in wireless sensor networks is typically several metres or more than ten meters. The process of installation is made much easier because there is no need to install wires, which significantly cuts down on the amount of time required for the installation. A good illustration of this would be the comparison experiment that Chintalapudi et al. (Chintalapudi et al., 2006) carried out. Before each trial, it took them several days to put up wired sensor nodes for a four-story office building, but it only took them around thirty minutes to set up wireless network sensor nodes.

On-site Monitoring vs Remote Monitoring: It is important to point out that the fundamental purpose of a wired sensor network is to connect a number of sensor nodes

to a centralised data collection and processing system. This emphasises that experienced specialists are typically required to perform the onsite monitoring in order to guarantee that the equipment is functioning properly. However, wireless sensor nodes are capable of realising remote monitoring, and users can enter the network system at any time and from any location to track and retrieve monitoring data when there is a network present.

2.3.5 The Major Challenges of WSNs in SHM

Integrating WSNs with SHM systems in order to monitor civil structures presents a number of obstacles, despite the fact that WSNs have many of the benefits discussed above. Some issues are due to the constraints that are imposed on account of the nature of civic structures. Many are because of the constraints that are imposed on account of the nature of civic structures. For instance, the location of the structure, the intricacy of the structure, and the impact of characteristics that are associated with adverse environmental conditions The connection between wireless sensor nodes can also give rise to complications such as signal instability and difficulties in synchronising the sensors.

In the past decade of research, researchers have developed various prototypes of wireless sensing SHM systems. Having said that, it does also offer certain obstacles. When a SHM system is integrated with wireless sensor networks, its limitations will be exacerbated as a result of its inherent characteristics. For instance, the issue of generating an excessive amount of data when covering wide areas and conducting long-term monitoring, as well as the issue of time synchronisation in dense sensor networks, etc. In this section, the present SHM-related problems in WSNs, such as sampling rate limitations and power efficiency requirements, are discussed.

Limited Bandwidth/data rates: Bandwidth is an essential feature that must be considered for any network connection. The term "rate" is more frequently used in place of the word "bandwidth." Due to the fact that the bandwidth of WSN is limited, it is not practical for it to transmit huge volumes of data effectively, which in turn restricts the sampling frequency. In most cases, the sample frequency is determined by the principal mode of vibration of the structure. To put it in other words, the low data rate and small volume of the data transmission will limit both the types of sensors that are available and the applications that can be used with SHM. For instance, sensors like accelerometers that measure structural response need to be deployed intensively in SHM. Because of this, the wireless sensor network needs to meet certain requirements, such as a high data rate, a large data transfer volume, and other criteria.

Power Consumption: Power consumption is one of the key factors that must be considered while designing a sensor system. In wireless systems, battery power is typically utilised, which means that the amount of energy that is consumed is relatively constrained. Typically, sensors can operate for 5 to 10 years while maintaining stability and reliability. The design life of a building facility is much shorter than a few decades. The performance of the structure deteriorates over time, resulting in a reduced level of safety. To achieve long-term or real-time monitoring, the sensor system needs to match the service life of the structure.

In most cases, a basic SHM system will continue to function for several months or even years after it has been deployed. This has a significant influence on the amount of energy that is consumed. While the actual working environment of the SHM system usually does not provide access to a direct power source. Although many buildings have power outlets or power sources for lamp posts, sensors are not always installed close to the power source.

The high power consumption of SHM systems shortens battery life, and if the SHM

system is installed in low-access locations, it is not possible to arrange for regular replacement maintenance. Also, the power depletion of sensor nodes will directly cause the SHM system to break down. Therefore, reducing energy usage is a key challenge for wireless sensors that rely on batteries as their primary source of power (Nagayama, Spencer & Rice, 2008).

WSNs generally prioritise the usage of batteries as their primary source of power supply. When choosing batteries to provide the necessary energy for sensor signal processing and communication, the following criteria should be taken into consideration:

- Battery type (e.g., alkaline, nickel metal hydride (NIMH), and lithium-ion.)
- capacity
- Cost
- Environmental impact
- Service life
- Energy consumption
- Security issues

Sampling Rate: Real-time wireless sensor networks require a number of key parameters, one of which is the sampling rate of the data. A better application quality of service (QoS) and improved data gathering capability can be obtained through the achievement of a higher sampling rate. When monitoring a particular structure, a SHM sensor network needs to be deployed in a variety of locations across the structure. The Nyquist theorem states that the sample rate must be at least twice as high as the component with the highest frequency. As a result, this frequently calls for a sufficient quantity and data size. In addition, the features required for structural analysis can only be generated using data that is collected from sensors over an extended period of time. In the event of long-term monitoring and a high sampling rate, the problem that

WSNs will cause is that the queue for processing sample activities can get full, causing real-time monitoring to lose its significance (*Measuring Strain with Strain Gages*, n.d.). So, one of the most important challenges in a SHM system that utilises a wireless sensor network is determining how to equitably distribute system resources in order to achieve the highest possible sampling frequency.

Fault Tolerance: The fault with the sensor network can be broken down into two categories: a data fault and a function fault. A function fault is quite easy to identify, and this includes communication network faults, base station faults, and sensor faults. Failures in data collection can have a wide variety of root causes, including inaccurate readings brought on by a decline in sensor performance or erroneous information produced by the destruction of sensor nodes as a result of inadequate network protection (Aygün & Gungor, 2011). As a consequence of this, the architecture of a wireless sensor network needs to be fault-tolerant so that even in the event of a malfunction, the system is still able to accomplish the objective it is intended to.It should be noted that WSNs key design indicators include communication rate, power consumption, and communication range. The communication rate has an effect on the performance of the nodes, and a high communication rate can provide WSNs with a shorter amount of transmission time and a lower amount of overall network power consumption. Sensor nodes should not be placed too far apart in order to develop an interconnected network architecture. If wireless communication is extensively used, it must adapt to higher design criteria, such as an increase in the number of sensor nodes (adding nodes).

Time Synchronization: A better understanding of sensor system runing time and fewer mistakes can be achieved by the use of time synchronisation, which can guarantee the simultaneous sampling of sensor nodes. Synchronization of the network is necessary in wireless sensor networks in order to facilitate significant data sharing among sensor nodes. The research that has been done up until now has made tremendous progress

toward offering quality time synchronisation. In this study, it is still necessary to take into consideration the synchronisation of multiple sensors as an essential component of the design.

2.3.6 Comparisons of Existing Wireless Smart Sensor System

In light of the characteristics and benefits that WSNs bring to SHM applications, many researchers have been trying to design reliable wireless sensing devices over the past decades. In spite of the enormous number of systems that have been developed, only a limited number of devices have been utilised for full-scale monitoring of structures. Abdulkarem et al. (Abdulkarem, Samsudin, Rokhani & A Rasid, 2020) presented an overview of the experiences, challenges, and future research prospects of WSNs in the development of SHMs. In addition to this, it provides a thorough summary of the wireless sensor prototype that was built by researchers between the years 2005 and 2019, and it classifies the prototype into two groups: the academic type and the commercial type.

Currently, there are two different approaches that can be used to develop academic prototypes. The first method is to create sensor panels for particular research objectives and applications by making use of some components that have previously been commercialised and are considered mature. This makes the development process much quicker and is also very convenient. The other option is to fully customise the system by developing cutting-edge sensors, which necessitates a complicated design and an extremely lengthy development cycle. The associated investment and research costs will be high. Because of the customised nature of their features, these types of sensor systems can only be utilised on a limited number of objects. Commercial prototypes are platforms that are developed by industry and then commercialised by technology

companies for usage by the general public, either through purchase or open-source license. One of the most successful examples is the microelectromechanical system (MEMS) sensor, which is also known as the mote and is the most common commercial platform. These commercial platforms typically consist of various hardware elements along with their respective operating systems. And because it is compatible with a wide variety of sensor interfaces, it can be installed in a variety of civil structures. In the following section, a brief summary of some examples on academic and commercial prototypes over the past few years is presented.

2.3.7 Academic Prototypes

In place of the traditionally wired network strain measuring method, Yao et al. (H. Yao, Cao & Li, 2016) developed an integrated portable wireless strain monitoring system (PWSMS) for the purpose of improving the monitoring efficiency of large metal structures. The MSP430F149 microprocessor and the ZIgBee CC2530 radio frequency chip were used by the system. Because of its portability and miniaturisation, the work that needs to be done to monitor may be completed more quickly, and the precision of the measurements can be guaranteed.

As shown in Figure 2.12 (a), Wu et al. (Y. Wu et al., 2017) created a wireless acoustic emission (AE) sensor platform that can accurately detect and determine the location of cracks in a material. An ARM processor (STM32F407) that is capable of a data sampling frequency of up to 5 Msps and an improved IEEE 802.11b/g/n CC3200 wireless data transceiver that is capable of data transmission rates of up to 6 Mbps are both utilised in this system. However, the system does have a few drawbacks. Due to the use of Wi-Fi communication technology, the energy consumption of the AE platform is considerable, and it will quickly devour the entirety of the system's reserve power.

Despite the fact that the platform possesses good data sampling and fault detection capabilities, as well as sensor nodes that are equipped with dual channels, it still has a high level of energy consumption.

In order to take advantage of recent developments in micro-electromechanical systems (MEMS) technology as well as wireless data transmission, Zhu et al. (Zhu et al., 2018) designed a sensor node named Xnode that is equipped with a three-axis digital MEMS accelerometer. The sensor node has a number of desirable characteristics, including low noise and excellent resolution. It is composed of three PCBs, which are a processor board, a sensor board, and a radio/power board, as can be seen in Figure 2.12 (b). It contains an ARM Cortex-M4 LPC4357 CPU that is capable of operating at frequencies as high as 205 MHz. Additionally, it uses an Atmel AT86RF233 radio frequency that operates at 2.4 GHz and has an outdoor transmission range of one kilometre. The rate of transmission is 250 kilobits per second. This sensor node not only satisfies the requirements for accelerometer sensors that are necessary for large-scale applications in civil infrastructure, but it also provides a software framework that can be used for the computation of data.

Fu et al. (Fu et al., 2018) designed a wireless SHM system (Figure 2.12 (c)) for impact detection of composite structures. The system has 24 sensor input channels, each of which is capable of correctly capturing the structural reaction and exhibiting high levels of robustness when exposed to environmental vibration noise. Filters, impact detection, local data processing, and wireless connection are the primary components that make up the system as a whole. The utilisation of an event-triggered mechanism is a key characteristic of this system. When the structural material is not impacted by external forces, it always adopts an operation that has a low level of energy consumption. The response time is approximately 12 µs, and the average current is lower than 1 mA when the impact activity is less than 0.1%. When the structure is impacted, the activation of

the trigger causes the system to perform at a high level.

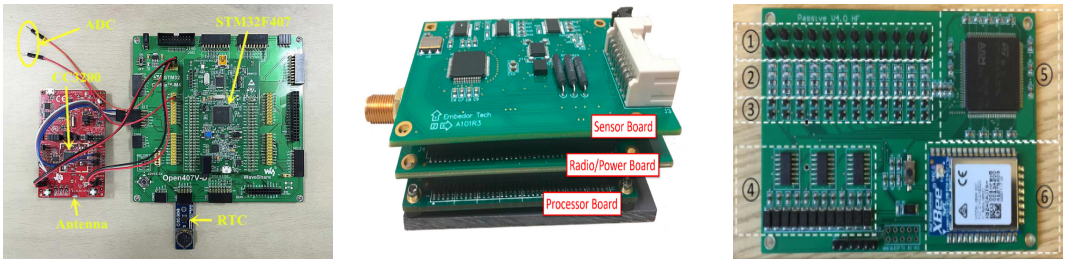

(a) (b) (c)

Figure 2.12: Academic wireless sensors prototypes in recent years: (a) AE sensor node (Y. Wu et al., 2017) (b) Xnode smart sensor (c) WSHM platform. (Fu et al., 2018)

2.3.8 Commercial Wireless Sensor Platform

Waspmote Pro. Waspmote Pro is a wireless system that has a low price point and consumes a low amount of energy. This platform is open-source, developed by the Spanish business Libelium (IoT, 2022). It can be used to monitor environmental humidity, temperature, acceleration, and other parameters. It has applications in agriculture as well as intelligent environmental monitoring, gas monitoring, and radiation detection. Outdoor coverage of up to 100 metres is achieved by the system through the use of an ATmega1281 microprocessor operating at a frequency of 14 MHz and an XBee radio module operating at a data transmission rate of 250 kbps.

Shimmer3. The Shimmer3 platform is designed specifically for the development of wearable sensors. It was established by Shimmer (Ltd., 2022) and is now available for a variety of mature applications. This platform has a central processing unit (CPU) with an MSP430F5437A, 16 KB of random access memory (RAM), 256 KB of flash memory, and a slot for a microSD card with a capacity of up to 32 GB. Because of the system's adaptability and freedom of customization, it is able to deliver to software developers a fully functional user environment that comprises both a software

and hardware framework. Dondi et al. (Dondi, Di Pompeo, Tenti & Rosing, 2010) developed a battery-free wireless embedded system with the help of Shimmer3, and they demonstrated that systems built on the Shimmer3 platform are capable of doing up to 350 analyses in a single day.

LRWAN1. The B-L072Z-LRWAN1 development tool was created by STMicroelectronics (STMicroelectronics, n.d.). It is compatible with the LoRa, Sigfox, and FSK/OOK wireless protocols. The toolkit features an SX1276 transceiver along with a Murata open-source CMWX1ZZABZ-091 integrated module. This module is driven by an STM32L072CZ microcontroller. The B-L072Z-LRWAN1 is capable of providing ultra-long range spread spectrum communication, and it has high anti-interference to environmental noise, which helps to minimise the amount of power that equipment needs to use. Because the CMWX1ZZZABZ-091 is an open module, users have full access to its various capabilities, including the ADC, 16-bit timer, I2C, SPI, etc.

2.4 LoRa - Long Range Radio Communication

Whether it is the Internet of Things or wireless sensor networks, it brings conventional construction and infrastructure into a world of unimaginable new possibilities. The development of the Internet of Things, which was discussed before, has significantly boosted the demand for low-cost wireless technology as well as wireless sensor networks. One of the most essential is the Low Power Wide Area Networks (LPWANs), which has been the most rapidly developing technology in recent years.

For the wireless devices used in IoT, they frequently need to be integrated into low-cost wireless devices generated by LPWANs in order to be utilised in actual industrial usage scenarios. For instance, it can be installed deep into buildings (bridges, tunnels),

underground (pipes), or even in high-rise buildings, among other places. In order to achieve this, the device's communication capabilities need to have a high level of both penetration and range coverage. In addition, low power consumption is very significant due to the particular location where the equipment is installed, which makes it impossible for people to access or frequently replace the power source. This makes it essential that the equipment have low power consumption.Most widely used wireless communication technologies are based on the IEEE 802.15.4 standard, such as ZigBee, which uses mesh network topology to extend its coverage. The distance between the connections that link each node must be less than roughly 100 metres.

LPWANs make use of a star network topology, which streamlines the process of managing the network and possesses receivers that are highly sensitive. LPWANs communication technology is distinguished by low cost, long-distance coverage, and low power. However, because of its extensive range and long-distance coverage, the transmission rate has to be lowered, making it more appropriate for low-rate data transmission than higher-rate transmission. Although the cellular network that is used the most in day-to-day life is capable of satisfying a vast range of long-distance transmissions, the cost of data transmission and the power consumption that it requires are incredibly high (Marais, Malekian & Abu-Mahfouz, 2017).The majority of the products that are offered by LPWANs at present are proprietary technologies. One example of a technology that may effectively meet the needs of LPWANs in terms of cost, range, and power consumption is the LoRa (Physical Layer) communication technology that Semtech developed. LoRaWAN defines the communication protocol as well as the network system architecture. The sensor system that was developed for this research made use of LoRa wireless sensor technology. As a result, the following section will provide a comprehensive overview of LoRa technology.

2.4.1 LoRaWAN Introduction

In LoRWAN, the term "Long Range" is abbreviated as "LoRa." The fact that it has a large coverage area and a long transmission distance is made abundantly clear by the fact that its name describes it in exactly those terms. To ut it simple, LoRaWAN is an IoT platform for wireless transmission and receiving that has low frequency, low power, and low bit rates (usually 0.3 to 50 kbits/s).

The primary characteristics of LoRa include, but are not limited to:

1. Long range: Supports connections up to 50 kilometres distant in flat, rural regions; has good penetration in complicated, obstructed situations such as cities or inside.
2. Low power: It has a low power consumption and a long duration during which it can be run on button batteries. Some ultra-low-power LoRa devices have their power management systems designed to last for several years before requiring recharges.
3. End-to-end security: With AES 128-bit encryption, mutual authentication, integrity protection, and confidentiality are highly guaranteed.The GPS feature of geolocation enables the ability to find and monitor the measuring device or object.
4. High capacity: Not throughput, but rather the centralised processing capability of millions of individual bits of information that LoRa supports per base station
5. Cost-effective: Reduced expenses associated with investments in infrastructure (such as telecommunication towers).

In general, LoRaWAN is a communication protocol that is maintained by the LoRa Alliance. Currently, LoRaWAN is the only standard for developing LoRa-based devices; hence, devices that are produced using LoRa technology are needed to comply with LoRaWAN. The LoRaWAN architecture consists of the following elements, as shown in Figure 2.13 (Gkotsiopoulos et al., 2021): (1) a terminal device that transmits sensor

data; (2) a gateway that receives sensor data and transmits it to the server; (3) a network server that manages network functions and all device connections; and (4) an application server that evaluates and analyses the data. The LoRa-based devices for building the IoT can implement any one or more of the following: Utilise a publicly operated commercial LoRa gateway; nevertheless, take into consideration the associated costs and any limits placed on the application's installation. Construct and deploy private LoRa gateways; however, this may necessitate the installation and ongoing maintenance of accompanying network servers. Terminal devices and gateways are connected to a communal cloud platform by utilising the community network. The research adopts the above combination to build a private gateway, establish communication between the terminal device and the gateway, and access LoRa devices through the cloud platform of the community network to realise wireless data cloud transmission. This is done with the goal of decreasing the cost of the developed wireless detection system as much as possible. In conclusion, LoRa bridges the gap between the bandwidth and range models provided by conventional wireless technologies, all while requiring a substantially lower investment in infrastructure.

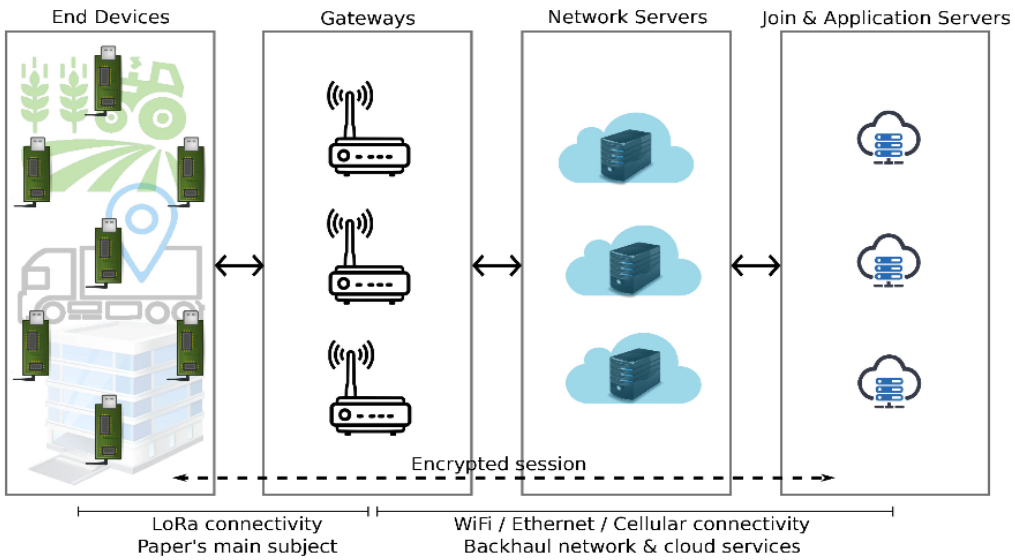

Figure 2.13: LoRaWAN architecture (Gkotsiopoulos et al., 2021)

2.4.2 LoRa Performance Overview

The primary focus of this section is an overview of the performance and characteristics of the LoRa technology that is currently available. LoRa has shown itself to be extraordinarily competent in a variety of fields, including the following (Gkotsiopoulos et al., 2021):

1. Smart cities and environmental monitoring, such as forest fire detection, street lighting, trash management, and monitoring for pollution (Sánchez Sutil & Cano-Ortega, 2020; Cruz, Cota & Tremoceiro, 2021; Alvear-Puertas, Rosero-Montalvo, Michilena-Calderón, Arciniega-Rocha & Erazo-Chamorro, 2021; Vega-Rodríguez, Sendra, Lloret, Romero-Díaz & Garcia-Navas, 2019).

2. Smart homes and buildings, including the automation of household appliances and the testing of the safety of building materials (Islam et al., 2022; Sidorov, Nhut, Matsumoto & Ohmura, 2019).

3. The business and agricultural sectors, which involve automatic irrigation, intelligent metering, intelligent tracking and location, and farm monitoring (Baghrous, Ezzouhairi & Benamar, 2020; Iyer et al., 2020).

4. The management and monitoring of medical and health care (Lousado & Antunes, 2020; Jain, Soni, Goyal & Sharma, 2020; Han et al., 2020).

Mikhaylov et al. (Mikhaylov, Petaejaejaervi & Haenninen, 2016) conducted research to assess the uplink throughput of a LoRaWAN end device as well as the data transmission times. A single LoRaWAN base station is connected to a number of different devices in order to analyse the impact of data transmission in a range of application contexts. The goal of this evaluation is to determine how different types of devices interact

with data transmission. According to the findings, a single LoRaWAN base station has the capability of providing service to a number of terminal devices, despite the substantial distance that separates them from one another. After then, Mikhaylov et al. conducted experiments in 2017 to evaluate the effectiveness of the LoRaWAN network interference (Mikhaylov, Petäjäjärvi & Janhunen, 2017). According to the findings of the experiment, data that is transmitted at a high rate has a greater chance of being disrupted by interference than data that is transmitted at a low rate does. The LoRa technology has a number of advantages, one of which is that it is beneficial for low-rate transmission. As a result, it is less exposed to interference and more suitable for usage in international networks. Based on the LoRa and MQTT network protocol architectures, Gambi et al. (Gambi, Montanini, Pigini, Ciattaglia & Spinsante, 2018) built a home automation device that has low power consumption, a low price, and the ability to communicate over long distances. The researchers Wixted et al. (Wixted et al., 2016) evaluated the LoRa technology in the Central Business District (CBD) of the city of Glasgow, which is located in Scotland. This location features glass buildings, sandstone structures with 7 stories, and a variety of geography, including river flats and hills that are 50 metres high. According to the findings of the testing, the signal strength in an open environment outside is exceptionally strong and has the capacity to remain stable during propagation despite the changing terrain. Additionally, the signal strength has the potential to remain stable during the entire process. In indoor testing, closed stairwells can reduce signal strength; however, the deployment of additional gateways can make up for this weakness, establishing a stable wireless communication network.

The previous literature review reviewed the application of IoT related technologies. LoRa is the most promising new technology in the Internet of Things. Bluetooth, Wi-Fi, and cellular technology are the three forms of wireless communication that are used the most commonly these days. When it comes to the transmission of data over relatively

small distances, these forms of wireless communication are quite efficient. Mobile phones and various other portable electronic devices are the most prevalent applications for cellular technology. It was one of the early forms of wireless communication technology and had extensive use in a variety of contexts across the world. The construction of the infrastructure is not a very cost-efficient activity, despite the fact that its communication range is quite extensive. The installation of cellular technology normally requires the building of a significant number of communication towers in a wide variety of different locations. These towers can be found almost anywhere. It is essential to increase the tower density if one wants to extend the range of coverage provided by the network. In addition, the amount of power consumed by cellular networks is substantially greater than that consumed by Bluetooth and LoRa. Bluetooth is often used with a diverse assortment of devices and pieces of equipment that are used on a daily basis, such as computers, mobile phones, Bluetooth headphones, and other items of a similar nature. The Bluetooth transmission is the one that is most likely to be affected by the distance between the sender and receiver. In spite of the fact that Bluetooth can now communicate up to a distance of about 240 metres as a result of the development of Bluetooth 5.0, the transmission distance is still rather restricted in comparison to the long-distance communication that is provided by LoRa. Wi-Fi transmission, on the other hand, is generally considered to be superior. However, the transmission capacity and signal strength of Wi-Fi will be greatly diminished if there are other objects or structures in the path of the signal. The environment in which any communication technology is transmitted will almost certainly have an effect on the distance it can travel. It is possible for LoRa to communicate over a distance of up to 10 kilometres in rural areas that are level and devoid of obstructions; however, its range is restricted to no more than 3 kilometres in places that have a higher population density. If LoRa weren't limited by its low throughput and low bandwidth, it would be very simple and quick to apply it to more practical applications. Table 2.5 presents

Table 2.5 Comparison of LoRa, Bluetooth 5.0 and WI-FI technology

Specifications	LoRa	Bluetooth 5.0	WI-FI
Modulation	Chirp spread spectrum	Frequency hopingspread spectrum	Frequency hoping spread spectrum
Frequency	AU915/AS923 South America and Asia EU 868 MHz (Europe) US 915 MHz (North America)	2.45 GHz	2.4 GHz, 5 GHz and 6 GHz
Range	urban areas: up to 5kms rural areas: up to 10kms	approximately 240 meters	approximately 200meters
Roaming	Enables different networks across various countries to combine their coverage zones	Securely paired to a single base station	Can roam between multiple access points
Security	Mutual authentication is established between a end-device and the network as part of the network join procedure	16-digit(128-bit) PIN authentication and frequency hooping	Wi-Fi Protected Access(WPA)
Power Consumption	Low	Low	Medium
Data Rate	0.3 kbit/s ~27 kbit/s	<2 Mbps	<54 Mbps

the results of a comparison of the Internet of Things (IoT) connectivity protocols LoRa, Bluetooth and WI-FI.

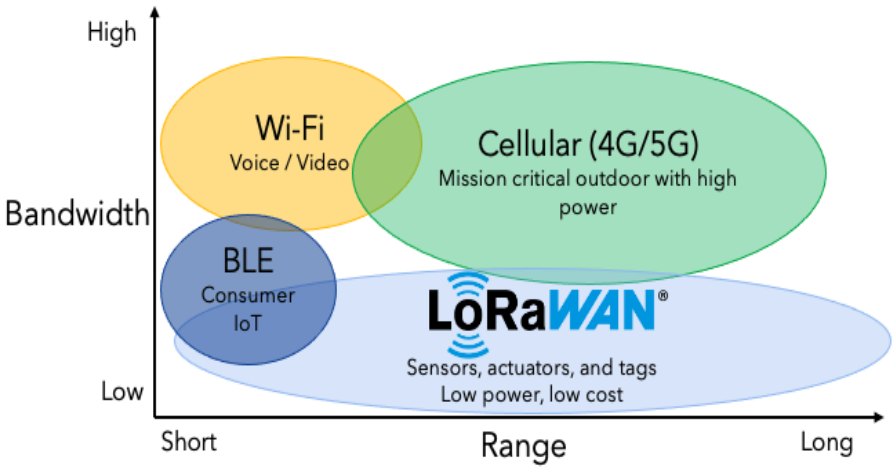

Figure 2.14: Bandwidth and range comparasion of LoRa, Bluetooth, WI-FI and cellular (https://wifivitae.com/2022/12/14/lorawan-mapper-overview/)

2.5 Summary

It is important to emphasise that the successful development of a competent SHM application is the result of the effective achievement of many scientific and engineering breakthroughs as well as the great fusion of technologies. The swift advancement of data science, network communication technology, and electronic information technology are all significant milestones. The emergence of IoT and wireless communication technologies, for example, makes smart sensors practical and substantially improves the remote monitoring capabilities of SHM systems. The advancement in machine learning has made the data analysis and damage identification indicators more diverse, and the reliability has improved dramatically, enhancing the comprehension of the gathered data. Therefore, in this chapter, a comprehensive literature review was undertaken on the various components of the SHM system. These components include sensing technology, data transmission, and damage identification. The requirements for local damage monitoring need to include the implementation of rapid damage identification. As a result, both the evolution of strain sensors and strain-based damage detection techniques were discussed.The Internet of Things (IoT) and smart sensors, as well as wireless network-based data communication technology and LoRa communication technology, are all topics that were covered in the area of the SHM system related to data transmission. In addition, a summary is provided on the development status, advantages, limitations, and challenges of their implementation in the SHM system. The properties of wireless smart sensors and the IoT were also examined with regard to their applications in SHM. Comparisons and summaries of the currently available SHM wireless sensors were also presented. The need for real-time monitoring and management of building structures was then presented to establish a long-term, reliable SHM system. One of the primary goals of this study is to meet this need, as it is an

essential part of the implementation of SHM.

Chapter 3

Development of the Flexiabe Strain Sensing Sheet

3.1 Introduction

The description of a flexible strain sensing system that is capable of use in full-scale structures is going to be the primary emphasis of this chapter. The flexible strain gauge that was suggested for usage in this study makes use of two different affordable configurations, including a full bridge and a half bridge, in order to fulfil the strain measuring requirements of a variety of structural elements in a number of different orientations. These criteria were designed to take into account the fact that strain might be measured in a number of different directions simultaneously. A strain configuration selector has been developed as part of this research project in order to support the capability of measuring strain in two separate orientations at the same time. These orientations include axial strain and bending strain, respectively. The selector is developed in such a way that it enables the system to switch strain modes for the purpose of detecting

axial or bending strain in an adaptive manner without having the user make adjustments to the mounting location of the strain sensor. In the first section of this chapter, the primary focus is given to the development principle of strain gauge configuration, in addition to other issues such as material selection and so on. The methodology that was utilised in the development of the flexible strain system is dissected and discussed in the second section. The aim of this study is to achieve the target of quick local detection by detecting the anomalous strain field generated by structural damage. The proposed flexiable strain sensory system enables the goal of local damage detection and identification to be achieved. In addition, the development of a strain configuration selector makes it possible to switch, if necessary, between two different measurements of strain without having to relocate the sensor installation to a new location. This helps to significantly reduce the costs associated with the deployment of sensors.

3.2 Strain Sensing Principle

In this chapter, the fundamental notion behind the construction of a strain sensor system is broken down and discussed. At the beginning, a fundamental description of the Wheatstone bridge configuration of the resistance strain sensor is provided. Following this, there is an overview and description of the layered structure of the materials that were constructed. The design details of the strain configuration selector are described in the final part of this section.

In the 1920s, strain-based sensors were first implemented in the field of structural health monitoring (SHM), which is fundamentally divided into two categories: discrete electrical sensors for the monitoring of local damage and distributed sensors for the monitoring of structural integrity. The effective use of modal parameters with a high degree of sensitivity is one of the most significant aspects of fulfilling the goal of precise

local damage identification. Due to the great level of sensitivity that strain-based sensors possess, strain sensing techniques have recently emerged as a key topic of research in recent years. The technology of the strain sheet has been used to a significant degree in a broad variety of applications, including the monitoring of the structural health of a building, load testing, and force sensing. For the purpose of structural health monitoring, for instance, strain sheets can be attached to the surface of a structure in order to monitor the behaviour of the structure while it is being loaded. This enables a more accurate assessment of structural health to be carried out. In general, strain sensing can be implemented for both local and global damage diagnosis. It can also assist in predicting damage at an early stage to the structure as well as providing crucial information regarding the current status of the building.

There are many different types of strain sheets available, such as uniaxial strain sheets, biaxial strain sheets, and multiaxial strain sheets. One constraint that applies to all varieties of strain gauges, whether uniaxial, biaxial, or multiaxial, is that a single strain gauge attached to a structure can only detect strain in one direction at a time. If strain measurements need to be taken simultaneously in more than one direction, then additional strain sensors will need to be used and positioned in each of the directions that need to be measured. The full-bridge sensor that was built for this study as an approach to this challenge is able to switch freely between bending strain and axial strain without the requirement for the installation of a new sensor or the adjustment of the measurement direction of the existing sensor. In the following part, both general design principles and specific design aspects will be discussed.

The configuration of a strain sensor typically consists of a quarter bridge, a half bridge, and a full bridge, though this is not always the case. Throughout the course of this research, the configurations of a full bridge and a half bridge are utilised on a variety of structural members. It is necessary for strain sensors to have the ability to compensate

for variations in temperature. This is because the vast majority of strain sensors are particularly sensitive to temperature in real-world scenarios. In this aspect, the entire bridge circuit of the Wheatstone bridge is an extremely dependable method for accomplishing the objective of temperature compensation. The configurations of a half-bridge and a full-bridge are employed in this study, as was mentioned previously; however, the half-bridge is also connected to the full-bridge via the strain configuration selector, which helps to ensure that the temperature compensation function works exceptionally well. A comprehensive overview of the strain configuration selector is described in Section 2.2.The essential concept that resides at the heart of strain sheet technology is that the amount of strain that is given to a metal sheet will cause the sheet to respond differently in terms of the degree of resistance it exhibits. When a sheet of metal is stretched, its dimensions shift, which causes the material's resistance to change as a direct consequence of the change. Because the amount of strain is proportional to the size of the change in resistance, it is simple to calculate the amount of strain by measuring the amount of change in resistance. This is because the size of the change in resistance is proportionate to the size of the change in strain. The full-bridge strain gauge, as shown in Figure 3.1, R1, R2, R3, and R4, contains four resistance units inside its structure. These resistance units are referred to as wheatstone bridges. Throughout the entirety of this particular research project, an excitation voltage that is always set at 3.3 volts is passed between the two electrodes that are denoted as Vex+ and Vex-. The ratio relationship between the observed output voltage Vout and the excitation voltage (input) Vin can be determined by applying the equation (3.1):

$$Vr = \frac{Vout}{Vin} = \frac{R4}{R4 + R3} - \frac{R3}{R3 + R2} \tag{3.1}$$

When there is no strain being applied to the bridge, it will be in a state of equilibrium,

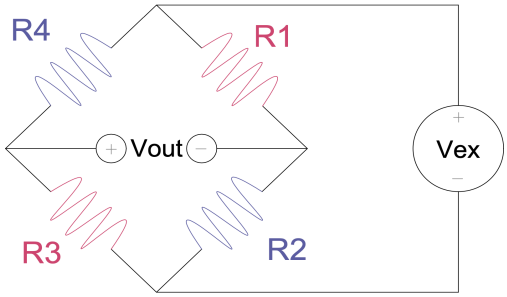

Figure 3.1: A typical whetstone bridge circuit

as shown by the equation above. During this stage, all of the resistance values will be equal to one another, and the output of the bridge will be zero. The thermal resistance coefficient of each resistor has the same value since each resistor is made from the same material during the manufacturing process. To put it another way, the rate of change in resistance stays the same regardless of the temperature. Because of this, the bridge's output voltage, denoted by Vout, can continue to be constant even while it is operating in equilibrium. This is the theory that underlies the fact that the full bridge configuration of the strain gauge can achieve temperature compensation. In addition to this, the resistance of the strain gauge is constructed out of wire, and the sensitivity of the strain can be expressed in terms of the gauge factor (GF) (3.2):

$$GF = \frac{\Delta R/R}{\Delta L/L} = \frac{\Delta R/R}{\epsilon} \tag{3.2}$$

Where R is the value of the wire's initial resistance, L is the length of the wire when it is first measured, ΔR and ΔL reflects the changing resistance value and length and ϵ indicates the mechanical strain.

3.3 Flexible Strain Sheet Prototype

The sensitivity of strain gauges that come in a half-bridge or full-bridge design is the highest among those available. Strain gauges can be used in a wide range of real-world applications since they are available in a variety of configurations, each with its own unique advantages. When dealing with natural environmental circumstances, it is essential to give thought to the means by which a negative impact caused by fluctuations in temperature can be reduced. It is not possible to place complimentary strain gauges on opposing sides of the test specimen since the full bridge configurations that are now available on the market only contain a single strain gauge. As a result of this research, a flexible strain sensor was developed in this research. This sensor makes use of two distinct full-bridge configurations, which National Instruments (National Instruments, n.d.) refers to as Configuration Type II and Configuration Type III, respectively. Both configurations measure strain in the same manner. In order to determine the amount of strain that essential components of a half-bridge construction are put under, a flexible strain gauge has been devised for use in these types of systems. In addition, a strain configuration selector is built in order to connect two half-bridge strain gauges in order to make a full-bridge configuration. This was accomplished by developing a strain configuration selector. Both of these innovations are carried out with the purpose of measuring the strain that essential elements of the structure are exposed to. A detailed explanation of the strain configuration selector will be presented in the following portion of this article.

Despite the fact that the four resistance elements that make up a standard strain gauge are normally the same size, the performance of these gauges is not very good when it comes to measuring the strain in slender structural members. Both a half-bridge configuration and a full-bridge configuration are put into practise as part of this study's

overall objectives. In contrast to the half-bridge configuration, which can be positioned on the opposite side of the member in order to measure the strain closer to the base of the column, the full-bridge configuration can be directly inserted in the span of the beam. In contrast, the configuration of the half-bridge has the advantage of being able to be mounted on either side of the member that is opposite the beam in order to measure the strain towards the top of the beam. Additionally, the frame of the suggested design is a long rectangle, which ensures both the sensitivity and temperature compensation performance of the device while simultaneously covering as much surface area as is practically possible. Its size is four to five times greater than the sensors that are now available on the market, and it is able to be attached to the majority of members that are slender. Figure 3.2 provides an illustration of the particular design prototype.

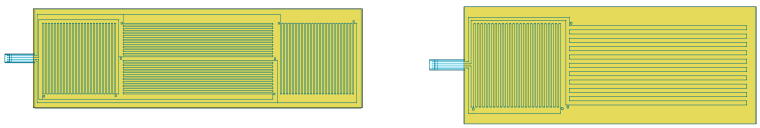

(a) (b)

Figure 3.2: Design of the strain sensing sheet: (a) Full-bridge configuration (b) half-bridge configuration.

Strain is defined as the ratio of the amount of elongation of a material (or object) under the action of an external force to the original length. Axial, bending, torsional, and shear strain are the four main types of strain. The axial and bending stresses are the primary focuses of this research, and Figure 3.3 displays the fundamental elements that make up the half-bridge flexible strain gauge that was developed as part of this research. In order to obtain the most accurate readings possible, the conductive layer is designed in the form of a grid. The deformation that occurs as a result of the flexible strain gauge

being subjected to external forces is due to the gauge being stretched. The strain that corresponds to the change in resistance is measured, and it is proportional to the change in length of the material that is caused by the deformation.

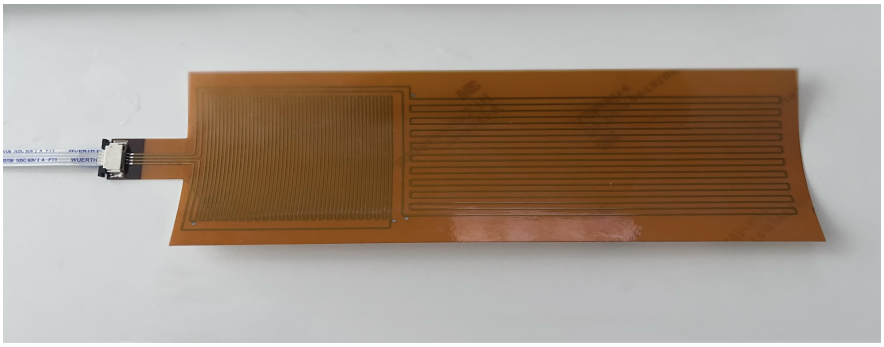

Figure 3.3: Half-bridge flexible strain gauge prototype

In the full-bridge design, there are four sensing elements, whereas in the half-bridge configuration, there are only two sensing elements. The layers of both designs are principally composed of three different types of materials: a 25μm polyimide (PI) subtract layer, a 20μm Constantan conductive layer, and a 25μm glue layer for glueing the layers together 3.4. Both configurations also include a 25μm glue layer for bonding the layers together. Due to its ultra-high resistance to high temperatures, superior mechanical qualities, and resistance to chemical corrosion, polyimide is widely used in a variety of industries, including the chemical industry, the environmental industry, and the aerospace industry. In terms of modulus, strength, density, elongation at break, and temperature resistance, the fibres that are utilised to manufacture PI materials are among the strongest fibres that are commercially available (Maurya, Kumar, Singh & Manik, 2022).This is the characteristic of PI materials that stands out the most. In order for flexible strain gauges to perform their intended functions, they require a significant amount of stretchability. The standard strain gauges that are most widely used on the market today not only have a small sensing area but also the compressive and tensile strength of the material itself, which is not suitable for long-term structural damage

detection. There is a solution to this challenge, however, and it can be found in the form of a new type of strain gauge. Polyimide (PI) is the principal material used for the proposed flexible strain gauges in this study. Polyimide is resistant to high temperatures and corrosion and has high stretchability, making it an ideal material for flexible strain gauges. This is also due to the possibility that PI can provide more options for the practical application of strain sensors in structural health monitoring.

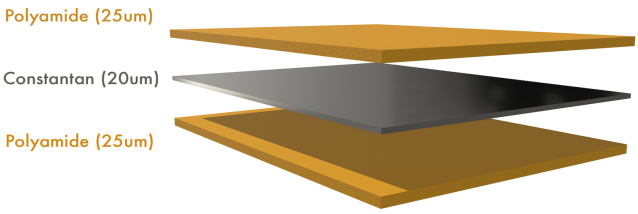

Figure 3.4: Components of the strain sensin sheet

The performance and sensitivity of a strain sensor are both significantly impacted by the material that is chosen for the conducting layer of the sensor. Copper-nickel Constantan has garnered a lot of attention as an ideal material for conducting layers of strain sensors thanks to the distinctive qualities that it possesses. The following is an overview of the material characteristics possessed by Constantan, which was used in this research as a conductive layer material for flexible strain gauges:

1. High gauge factor: The fact that Constantan has a high gauge factor, which indicates the sensitivity of the material to strain, is one of the main advantages of using this material. The gauge factor of constan is in the range of 2-4, which results in the material's great responsiveness to mechanical deformation. Because of this quality, it is possible to obtain accurate and consistent measurements of strain, which enable the detection of tiny variations in the environment.
2. Low thermal sensitivity: In comparison to other materials that are usually used in strain sensor applications, Constantan has a low thermal sensitivity. The term

"thermal sensitivity" refers to the vulnerability of the material to variations in temperature, which can lead to inaccurate readings and measurements. The low thermal sensitivity of constanan means that the strain readings acquired are unaffected by temperature swings. This makes constanan the ideal material for use in strain sensors in a wide variety of operating circumstances because of its versatility.

3. Excellent linearity: A close examination of the stress-strain relationship reveals that Constantan possesses very good linearity. Due to the fact that this behaviour is linear, it is possible to easily calibrate and obtain precise conversions of changes in electrical resistance to strain measurements. The outputs of the strain sensor are guaranteed to be accurate and reproducible because of the predictable and constant reaction of the Constantan material.
4. Stability under mechanical stress: It is essential for the long-term functioning of strain sensors that the conducting layer maintain its mechanical stability under mechanical stress. The material known as constan has a high level of mechanical stability, which enables it to survive repeated and lengthy deformations without suffering any major degradation. Because of its resilience, the risk of fatigue failure is reduced, which in turn ensures the endurance and longevity of strain sensors in demanding applications.
5. Wide range of applications: Due to its unique combination of characteristics, Constantan is ideally suited for use in a wide variety of strain sensor applications. It is useful in monitoring the structural health of buildings, bridges, and other types of infrastructure since it can correctly detect and quantify any deformations that may occur. Additionally, strain sensors based on the Constantan method have been used in robotics to assess joint angles and deformation in robotic limbs. This allows for accurate control and feedback to be provided. In the study of biomechanics, the use of Constantan is essential for tracking human movement and analysing muscle activation; this helps with rehabilitation and provides insight into overall

performance.

As mentioned above, in this study, polyimide was used as the top layer and substrate of a flexible strain sensor. Due to its high degree of flexibility, polyimide is a great choice as a material for use in flexible sensing devices. Because of its low elastic modulus, it can resist repeated bending and stretching without losing its mechanical integrity. This property allows it to be very versatile. Polyimide films can also be fabricated into thin layers, which enables conformal integration of a wide variety of substrates and intricate geometric designs. Because of this flexibility, the strain sensor is able to adjust to uneven surfaces and maintain dynamic mechanical deformation. The sensing element benefits from polyimide's exceptional mechanical strength, which contributes to the material's overall resilience. The sensor is able to tolerate severe environments and continue to function normally even after being used for extended periods of time thanks to its high tensile strength and wear resistance. The high tear strength of polyimide allows the flexible strain sensor produced in this study to remain extremely usable in severe conditions. In addition, polyimide is an efficient electrical insulator, making it an ideal material for use in strain sensors because of its compatibility with this property. A high dielectric strength helps to avoid leakage and interference, which in turn helps to improve the sensor's accuracy and sensitivity. Polyimide also has a low electrical conductivity, which helps to improve the signal-to-noise ratio by limiting the likelihood of unwanted electrical impulses and lowering the background noise level. Because of these qualities, polyimide is an excellent choice for use in applications that call for isolated currents. Some examples of such applications include biomedical monitoring and human-machine interfaces. Temperature stability is also one of the material properties of polyimides. Polyimide is able to sustain high temperatures without suffering considerable deterioration or loss of mechanical characteristics due to its high glass transition temperature and strong heat resistance. Since the strain

itself is quickly impacted by changes in temperature, the temperature resistance of polyimide enables the sensor to be used in demanding environments, such as the automotive and aerospace sectors, where temperature swings are prevalent. Besides, its compatibility with manufacturing technology is another outstanding characteristic. It may be processed using conventional techniques such as rotary coating, solution casting, heat curing, or ultraviolet light curing, among others. Polyimides can be depicted through the use of methods such as lithography, which enables the development of intricate sensor designs. Because of their adaptability, polyimide strain sensors can be easily integrated into a wide variety of devices and systems, which contributes to their growing popularity.

The full-bridge flexible strain gauge has overall dimensions that measure 220mm by 56mm, and the diameters of the resistance trace are 0.02mm thick and 0.04mm wide. The entire dimensions of the gauge are 220mm by 56mm. The temperature correction induction units that are located on the left and right ends are resistors. Both of these resistors measure 50 mm by 40 mm and are made up of 50 traces. The resistors that are used for the two parallel induction elements in the middle are each composed of 20 traces, have a size of 100 mm by 20 mm, and measure 100 mm by 20 mm. The overall length of the trace designs for all four induction components comes to a total of 2,000 millimetres when measured to their full extent. The flexible strain gauge in the half-bridge format has overall dimensions of 165 millimetres by 56 millimetres, and the induction components have the same size as the full-bridge configuration. The trace itself is made of a conductive material Constantan in order to maximise the effect of the wire itself on the strain measurement and the power consumed by the sensor during long-term monitoring. The size of this material is determined by the manufacturer's lithography capabilities, which in turn maximises the effect of the wire itself on the strain measurement. Constantan is an alloy material made of copper and nickel that has

a very low temperature coefficient (±20ppm/∘C) and is very resistant to potential drift in strain measurements caused by changes in ambient temperature (Aygun et al., 2020). The resistance values of the two distinct configurations of a single sensor element are both 122.5 ohm in the case where there is no change in strain (the resistance values of the most common strain gauges available on the market are 120 ohm, 300 ohm, and 1000 ohm). In addition to this, the flexible strain gauges that were utilised in this study have the capability of being scaled proportionally to fulfil the requirements of a range of different applications that are intended to be used in real-world scenarios.

3.4 Development of Strain Sensor Configuration Selector for Bi-axial Strain Measurement

In the study described here, both half-bridge and full-bridge structures were implemented, as pointed out previously. In order to install flexible sensors on both sides of various structural members while still making use of the temperature compensation performance of the full-bridge configuration, a strain configuration selector was developed in accordance with the definition that was provided by National Instrument. This enabled the installation of flexible sensors on both sides of various structural elements. The configurator enables the half-bridge structure to be connected on both sides of the mounting structure to form full-bridge type II and full-bridge type III (National Instruments, n.d.). Additionally, the configurator enables the configuration selector to be freely switched to measure bending and axial strain without changing the sensor installation position or installing a new sensor. This section first discusses the foundation of these two types of full-bridge configurations and then introduces the design concepts and applications of strain selectors developed according to the strain configuration type.

The full-bridge type II only measures the bending strain, and Figure 3.5 demonstrates the direction in which it should be positioned on the sample that is being measured in order to obtain accurate results. There are a total of four active strain elements, and two of them (R3 and R4) are positioned in the direction of the bending strain. One of these active strain elements is located at the top of the specimen, while the other one is located at the bottom of the specimen, which correlates to it. The other two strain components, R1 and R2, operate as Poisson gauges and are positioned laterally (vertically) on both sides of the sample. The output measurements of this type can be translated to strain using equation (3.3).

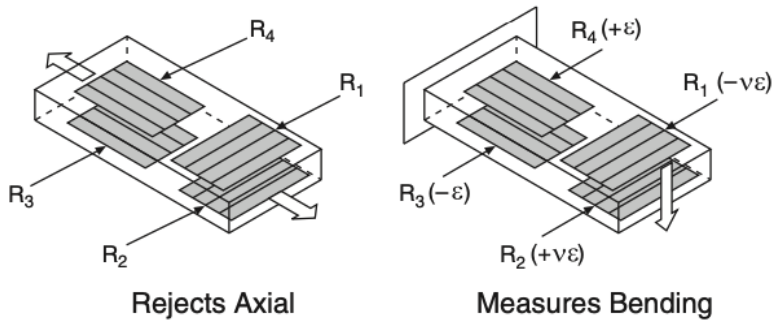

Figure 3.5: Full-Bridge Type II Rejecting Axial and Measuring Bending Strain (National Instruments, n.d.)

$$strain\,(\varepsilon) = \frac{-2Vr}{GF\,(1+v)} \tag{3.3}$$

The axial strain is the only strain that the full-bridge type III is capable of measuring. Figure 3.6 illustrates the axial direction that the strain gauge mounting specimen should be installed in. There are a total of four active strain elements, two of which are installed in the direction of axial strain (R2 and R4), one of which is installed at the top of the specimen, and the other of which is installed at the bottom corresponding to the top. One of these active strain elements is installed in the direction of radial strain (R1), while the other two are installed in the direction of axial strain (R2). Poisson gauges are

made up of two additional strain elements that are positioned transversely (in a direction that is perpendicular to the sample) on either side of the specimen. These aspects of strain are represented by the symbols R1 and R3, respectively. Equation (3.4) provides a means by which the strain values for this kind of installation can be transformed.

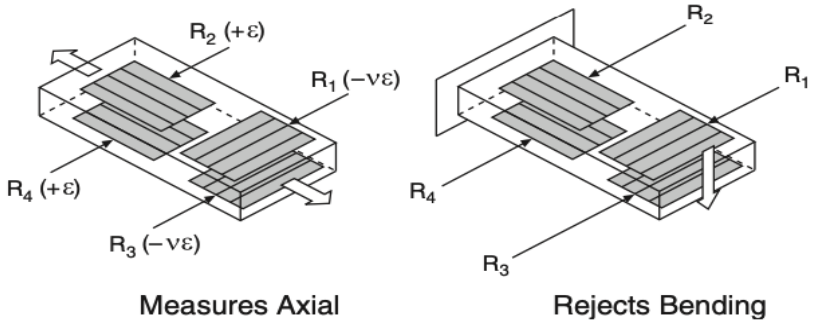

Figure 3.6: Full-Bridge Type III Measuring Axial and Rejecting Bending Strain (National Instruments, n.d.)

$$strain\,(\varepsilon) = \frac{-2Vr}{GF[(v+1) - Vr\,(v-1)]} \tag{3.4}$$

For both configurations, the principle behind the strain measurement is shown as following:

$$Vr = \left(\frac{V_{CH}\,(strained) - V_{CH}\,(unstrained)}{V_{EX}}\right) \tag{3.5}$$

Which V_r is offset compensated ratiometric bridge output, V_{CH} is measured voltage of the bridge, V_{EH} is the excitation voltage.

The two full-bridge arrangements for measuring strain that were introduced above make it clear that the vast majority of strain gauges that are used today are only capable of measuring strain in a single direction (either bending or axial), which corresponds to the Type II and Type III full-bridge strain sensor configurations that were covered

above in this section. In real-world situations, it is necessary to adhere the strain gauge to the surface of the specimen in order for it to be read. The strain gauge can only be installed in one direction since its installation typically requires the use of strong glue to secure it in place. Once it is installed, the position of the strain gauge cannot be easily altered, which means that the strain can only be measured in one direction. As an approach to this challenge, the researchers in this study came up with a strain configuration selector, which can be seen in Figure 3.7. The configuration selector enables unrestricted switching between axial strain measurements (full-bridge type II) and bending strain measurements (full-bridge type III), all without the need to adjust the mounting location of the strain sensor. An RJ50 port, which functions as a connecting point for wired transmission and data acquisition, can be found at the leftmost end of the selector. The switch key component, which monitors bending and axial strain, is located in the middle, and the jumper, which can be used to easily connect or switch between two different modes, is located on the outside. For the purpose of welding external strain sensors, solder interfaces (R1, R2, R3, and R4) are utilised(Figure 3.8).

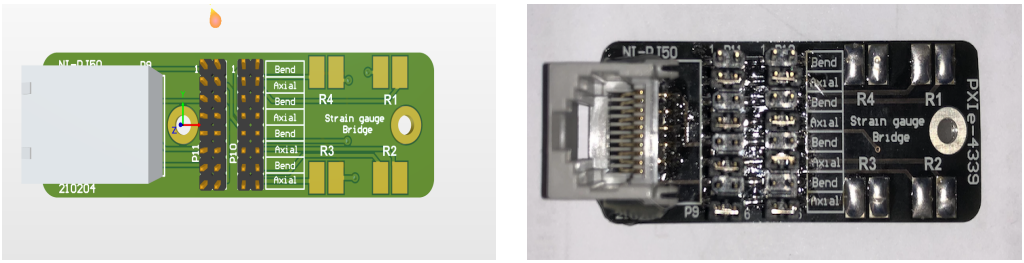

(a) (b)

Figure 3.7: Design of the strain sensor configuration selector (a) 3D view of the design (b) prototype image.

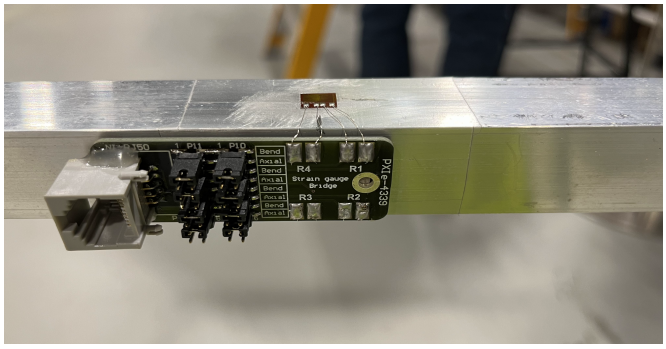

Figure 3.8: An example of the use of the strain configuration selector

3.5 Flexiabe Strain Sensing Sensors Calibration

The calibration of the sensor is a crucial step in determining how well the sensor will operate. The output of strain sensors needs to be measured after a known load has been applied for the calibration process to be complete. As was discussed previously, it is preferable to load the device with a strain distribution that is already known, and because the resistance is also known, it is possible to obtain the strain coefficient from those two variables. This train coefficient is also known as the Gauge Factor (GF) (refer to the equation (3.2)).

3.5.1 Calibration Test

The calibration experiment made use of two dog-bone-shaped mild steel flat bars (grade 300), as can be seen in Figure 3.9. The specimen size that was used for the calibration of the half-bridge flexible strain sensor is illustrated in figure 3.10 (a). The size of its cross section is 165mm(H) * 63mm(W) * 8mm(T). The size of the cross section of the specimen that is used for calibration of a full-bridge flexible strain sensor is 220mm(H) * 63mm(W) * 8mm(T) (Figure 3.10 (b)). In order to properly calibrate the sensor, the section width and length of the specimen that is created should have dimensions

that are extremely close to the section width and length of the flexible strain sensor in both configurations. The flexible strain gauge is placed precisely in the middle of the specimen (the narrow part of the dog-bone specimen), with the long side facing in the direction that is parallel to the direction in which the load is being applied.

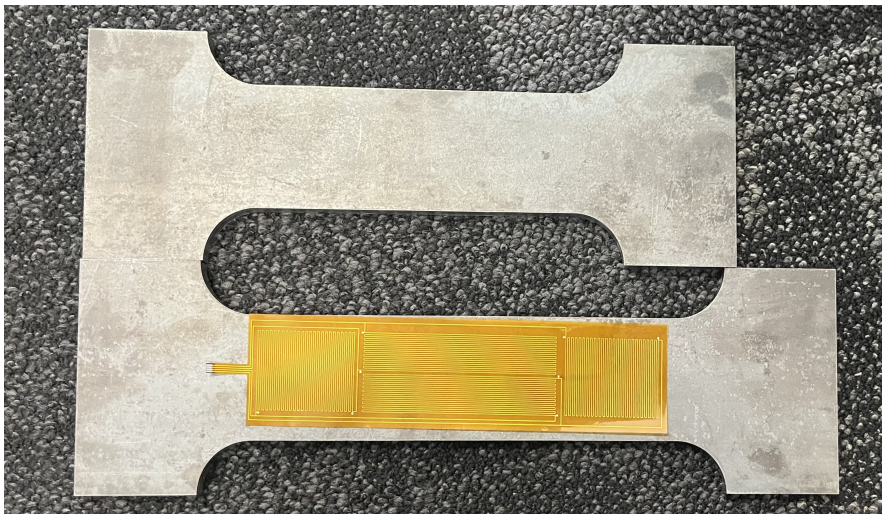

Figure 3.9: Dog-bone specimen for calibration

In order to determine the level of longitudinal strain during tensile testing, flexible strain gauges will be implemented. The apparatus used in the experiment to measure tensile strength is shown in Figure 3.11(b). The dog-bone specimen was mounted on the MTS tensile machine, which was a Model C45. The device is outfitted with a mechanism that can apply loads of up to 600 kN, and it possesses both high speed and low vibration levels. In addition to the strain gauge, an LVDT was also attached to the specimen so that it could act as a measuring reference for the tensile length. The RJ50 interface of the configurator was utilised by the strain configuration sensor that was produced throughout the course of this experimental test in order to establish a connection between the flexible strain gauge and the data gathering system manufactured by National Instruments (NI). In conclusion, the Universal Test Machine (UTM) was used to perform tensile testing on the mild steel dog-bone-shaped specimen in order to calibrate the flexible strain gauge. As can be seen in Figure 3.11(a), the direction of

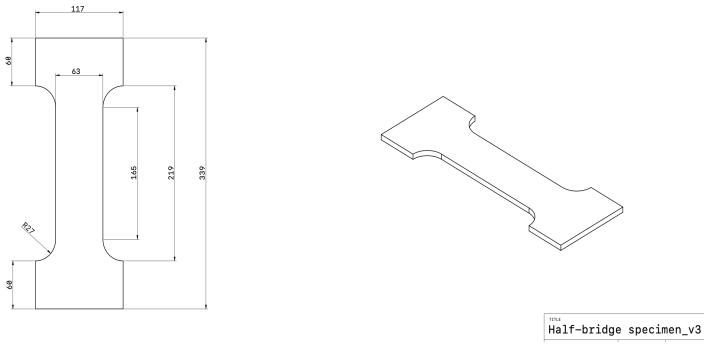

(a)

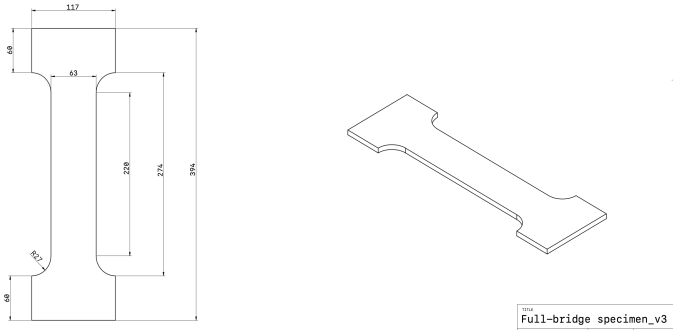

(b)

Figure 3.10: Dog-bone specimen drawings (a) for half-bridge flexiable strain snesors (b) for full-bridge flexiable strain snesors.

the compass runs in a direction that is parallel to both the specimen (the direction in which the flexible strain gauge is mounted) and the direction in which the load is being applied.

In order to determine the linear relationship between strain and voltage, the flexible strain gauge must first be calibrated, then its sensitivity must be confirmed, and lastly, the specimen must be loaded incrementally within the elastic range. Following this process, the linear relationship between strain and voltage can be determined. The full-bridge flexible strain gauge attached to the dog-bone specimen undergoes an elongation of 0.05mm/s, after which the observed signal is amplified by the National Instrument (NI) data acquisition with a sampling rate of 50 MHz. The specimen is kept under a constant load during the experiment so that tensile tests may be performed on it. This



(a)



(b)

Figure 3.11: UTM tensile test setup (a) Specimen, flexible strain sensor and LVDT (b) UTM front view.

enables the researchers to observe the hysteresis that is generated by the elastic material. When it comes to strain sensors, sensitivity testing is of the utmost importance. The Gauge Factor (GF) coefficient of a strain sensor modifies the sensitivity of the sensor in relation to variations in resistance. The value is stated to be 2.1 in accordance with the Constantan gauge factor that was proposed by Hu et al (Hu, Gao & Sheng, 2000). This theory has also been successfully proven by the studies of Aygun et al (Aygun et al., 2020). As a result, GF also needs to be validated in the flexible strain sensor that is being utilised in this research. This guarantees that the newly developed flexible strain sensor will have the capability to reliably detect even minute shifts in strain.

3.5.2 Test Results and Findings

The approach for the experiment consisted of performing a tensile test on a dog-bone specimen while the load was being controlled. During the test, the load was steadily increased in a repetitive way, and it was then cycled. During the entirety of the test, this loading strategy was utilised to make certain that the specimen never deviated from the linear elastic regime it was supposed to be in. The cyclic loading procedure that was applied to the specimen by using the MTS Criterion 45 equipment is depicted in Figure 3.12, for both half-brigde and full-brgde configurations, along with the matching response of flexible strain sensors that was attached to the surface of the specimen. Notably, as the test result shows, the length of each cycle stayed the same throughout, and the response of the flexible strain gauge showed no signs of latching throughout the course of the different cycles. In addition, it showed that the recorded strain measurements aligned with the cyclic loading process, with peak values that were almost identical to one another. These findings provide a solid foundation for the outstanding stability and linearity qualities of the flexible strain gauge developed in the course of this study.

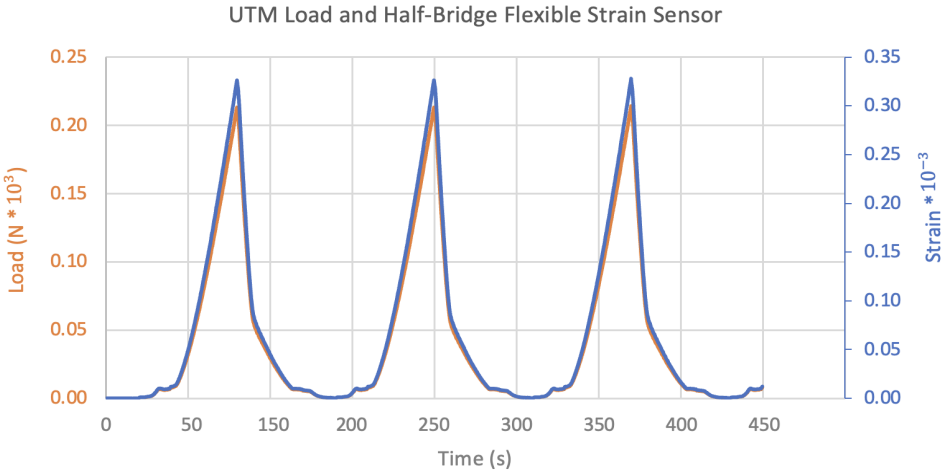

(a)

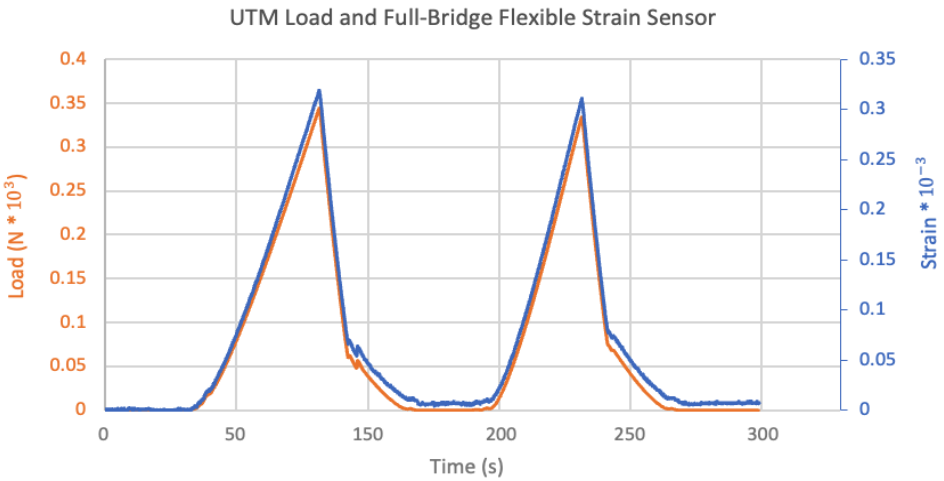

(b)

Figure 3.12: Flexible strain sensors tensile test - UTM Load and strain response (a) for half-bridge flexiable strain snesors (b) for full-bridge flexiable strain snesors.

Based on the results of the experiments, the relative values of the sensitivity, or GF, of two configuration types of flexible strain sensors were calculated and are shown in Figure 3.13. The GF value of the structure with the half-bridge is around 2.15, while the GF value of the structure with the complete bridge is 2.11. Each one is relatively close to the hypothetical figure of 2.1. As was just indicated, the primary objective of the strain sensor is to identify abrupt and large shifts in the strain field that are the result

of damage to the structure. Therefore, the sensitivity that was attained is more than adequate for use in the real-world applications of integrated SHM systems. In addition to this, the newly created flexible sensor has excellent linearity and demonstrates no lag in its structural response. The relationship between the load and the relative resistance of the strain gauge is depicted in Figure3.13. When compared to a variety of load settings, the linear behaviour of the resistance of the strain gauge demonstrates a high level of consistency. Calculating the R-squared number is one way to quantify linearity. This value demonstrates that all trendlines for both half-bridge and full-bridge configurations are greater than 0.99, which demonstrates that linearity has been achieved.

3.6 Summary

This chapter provides a comprehensive analysis of the design and development processes that went into creating a flexible strain sensor that is able to freely monitor both axial strain and bending strain. A configuration selector is being developed as well in order to allow for the switching of the configuration of the strain sensor. The installation location of the flexible strain sensor does not need to be altered for the selector to make the necessary adjustment to the bridge connection mode within the sensor. This makes it feasible to detect strain in two dimensions simultaneously. The flexible strain sensor has PI as its foundational material, and Constantan makes up the sensor's conducting layer. The developed flexible sensor is resilient and durable to the surrounding environment in practical applications of SHM frames due to the high stretchability of PI and the low temperature coefficient of Constanstan. In addition, tensile tests were carried out on the flexible strain sensor in order to validate its sensitivity and calibrate it. Both of these goals were accomplished through the process. For the purpose of testing the full-bridge and half-bridge flexible strain sensors, two different sizes of dog-bone samples were

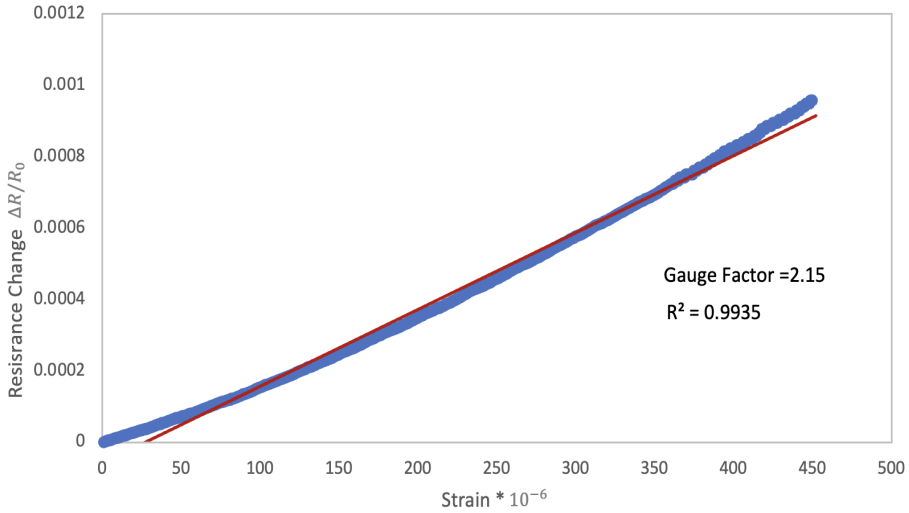

(a)

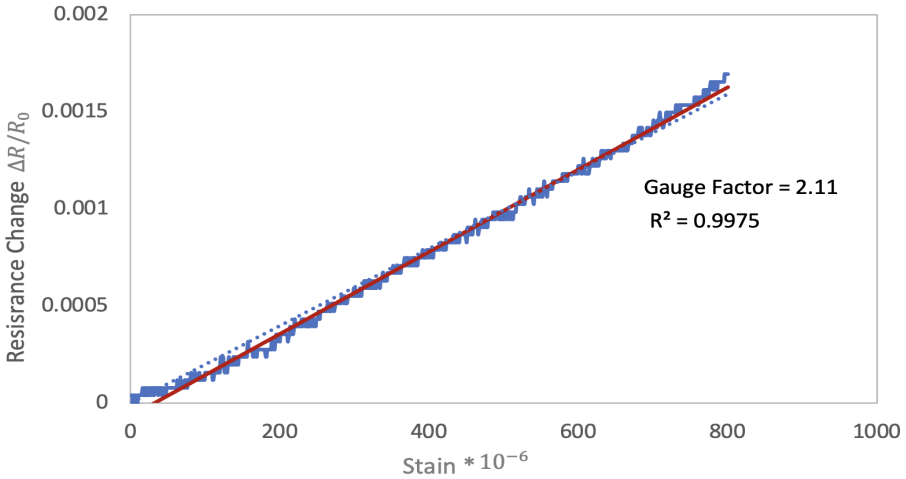

(b)

Figure 3.13: Strain sensitivity and linearity test of the flexiable strain sensor. (a) for half-bridge flexiable strain snesors (b) for full-bridge flexiable strain snesors.

constructed. To guarantee that the results of the measurements are accurate, the sensor is placed in the middle of the sample, and its cross-section size is matched as closely as possible to that of the flexible strain sensor at the narrowest area of the sample. The results of the experiments show that the GF of the two different designs is about 2.1, which meets the SHM system's requirements for abnormal strain field monitoring and accurately shows the beginning stages of structural damage. The results of the tests

further indicate that the flexible strain sensor that was produced has excellent linearity and is highly compatible with the structural response without any lag. The following chapter focuses mostly on presenting an overview of the hardware development of flexible strain sensors. The flexible strain sensor is further developed to have the capability of wireless transmission so that it may be used in a real-world structural scenario.

Chapter 4

Development of the Real-time Wireless Sensory System

4.1 Introduction

In this chapter, an introduction to the development of a wireless smart strain sensor that is based on LoRa WAN for long-distance transmission is provided. The strain field monitoring and evaluation of civil structures is one of the primary motivations behind the development of the wireless intelligent strain sensor that was included as part of an integrated SHM system. It is possible to simply change the interface of the flexible strain sensor and equip it with a Lora communication node, which has the capability of being used for long-distance transmission. The architecture for a wireless sensor system that is proposed in this research can, most significantly, simultaneously carry out two different forms of data transmission. The first method is to actively monitor the strain field of the building structure to determine whether or not there are any outliers. This is done by broadcasting the highest and minimum values (at sample rates of 30 Hz) in real

time via LoRa. The second transmission method is to send all of the acquired raw data to the ESP32 module at the same time using the RP2040 microcontroller and then store it on the SD card so that users can freely access all of the data files. In order to realise real-time monitoring and evaluation of the state of the civil structure, the sensor node engages in real-time communication with the LoRa gateway and also intervenes in The Things Network (TTN) cloud platform, which provides a network Server, join Server, and application server. In addition, a web server has been established, and users who are within a particular range (up to 100m in an open area) can connect to the sensor's network for free in order to browse and download sensor data in real time. The purpose of the newly developed strain wireless sensor is to make it possible for flexible strain sensors to be outfitted with wireless transmission capabilities, to minimise cost and power consumption, and to make it easier to install and use than the strain sensors that are used in the currently implemented SHM framework. In addition, the use of LoRaWAN makes it possible for the SHM system to accomplish real-time, dynamic, long-term monitoring in real-world applications.

4.2 Design Goals and Considerations

In the first stage of designing sensor nodes for a structural health monitoring system, the design objectives and challenges to be addressed need to be considered first. In the context of this study, the main goal of the development of a flexible strain sensor is to identify the abnormal response of the local strain field exhibited by the building structure. In order to achieve this, flexible strain sensors will need to feature integrated wireless transmission capabilities. There have previously been discussions on various wireless communication technologies, and LoRa technology has been determined as the purpose of this research. Not only does LoRa make long-distance communication

possible, but it also has the advantage of requiring an extremely small amount of power. However, in order to provide coverage over longer distances, LoRa must reduce the transmission bandwidth. Nevertheless, this is not a limitation for the strain sensor that was used in this investigation because the strain sensor does not require high data transmission rates or large amounts of data to be transmitted. It is possible to monitor in real time the maximum and minimum values of the strain, and it is also possible to record the strain values that are abnormally high or abnormally low in order to make a speedy first assessment regarding the existence of an anomaly in the strain field. As a result, the flexible strain sensor that is outfitted with a wireless transmission function that makes use of LoRa is able to satisfactorily meet the criteria of the SHM practical application. The wireless communication function based on LoRa that was designed for flexible strain sensors in this study has, all things considered, the following functional characteristics:

- Transmission over great distances with extremely low power requirements
- Continuous and real-time monitoring
- Send the highest and lowest values that fall within a specified rate range
- An immediate and preliminary evaluation of structural strain field anomalies

The second factor to take into account is that the bi-axial strain that is being measured by the flexible strain sensor that was built for this investigation requires unlimited switching. As a result, it is essential to incorporate the strain configuration selection developed earlier into the wireless sensor system. This study makes use of two multiplexers in order to reach this objective. These multiplexers are interconnected with ZIF connectors in order to resolve the issue of the strain configuration selector having to manually switch between two strain measurement modes.

Because the application of LoRa technology in this study is only responsible for transmitting the maximum and minimum values within a certain sample rate, the third

design requirement that needs to be considered is the fact that the end user can see the real-time data through The Things Network (TTN), but they cannot see all of the raw data. And taking into consideration that the sensor in the real-world application of SHM will be positioned either inside or outside the structure at various heights and positions, it will not be easy for the user to remove the SD Card in order to retrieve all of the historical data. In addition, the existing difficulties of data extraction in SHM applications include the fact that the sensor system needs to temporarily cease working if the user removes the SD Card directly from the sensor. This means that the system is unable to do genuine, continuous, real-time monitoring over the long term. In order to overcome these obstacles, the wireless sensing system was developed with an additional sub-system for the storage and extraction of data. This data storage and extraction sub-system is outfitted with a second microcontroller processor and is separately externally connected to the data storage module. In open areas, the coverage provided by the subsystem extends up to 100 metres and includes free built-in hot spots. End users can simply enter the static IP address on their own electronic devices to obtain all of the historical data in the memory in real time. This does not affect the data acquisition of the sensor itself, and data storage and data extraction can be carried out in parallel so as to achieve continuous monitoring of users and download or obtain the latest real-time data.

4.3 System Level Architecture

The architecture and design of a wireless strain sensor system are presented in this section. The primary objective of the design is to facilitate long-distance wireless transmission that consumes a low amount of power in order to meet the requirements of SHM applications. Additionally, the design aims to make it feasible for flexible strain

sensors to monitor strain field anomalies in real time and provide an early assessment of the structural damages. Furthermore, the architecture supports simultaneous measurement of multi-axial strain, which, in place of the formerly developed wired strain configuration selector.

Figure 4.1 illustrates the structure of the proposed system that comprises a wireless flexible strain sensor. The primary elements that compose the structure can be broken down into the following three parts:

- Data acquisition
- Data processing and transmission
- Data storage and extraction

The data collection system employs the flexible strain sensor that was developed earlier in this study. This sensor is coupled to the data processing and transmission system by using the flexible flat cable (FFC). The data processing and transmission system is made up of the following components: (1) a micro-power microcontroller (RP2040), (2) a power supply system, (3) a LoRa transceiver, (4) two Mutiplixers, and (5) an Amplifier that utilises amplification and digital-to-analogue conversion. (6) Pin header connectors that allow for the integration of external devices to transmit full raw data. The final part of the data storage and extraction process utilises a microcontroller (an ESP32) and an SD card module for the storage of the data.

As the design of the data extraction part (flexible strain sensors) has already been presented, the primary focus of this chapter is on presenting the design of the system that manages data processing, transmission, and raw data storage and extraction.

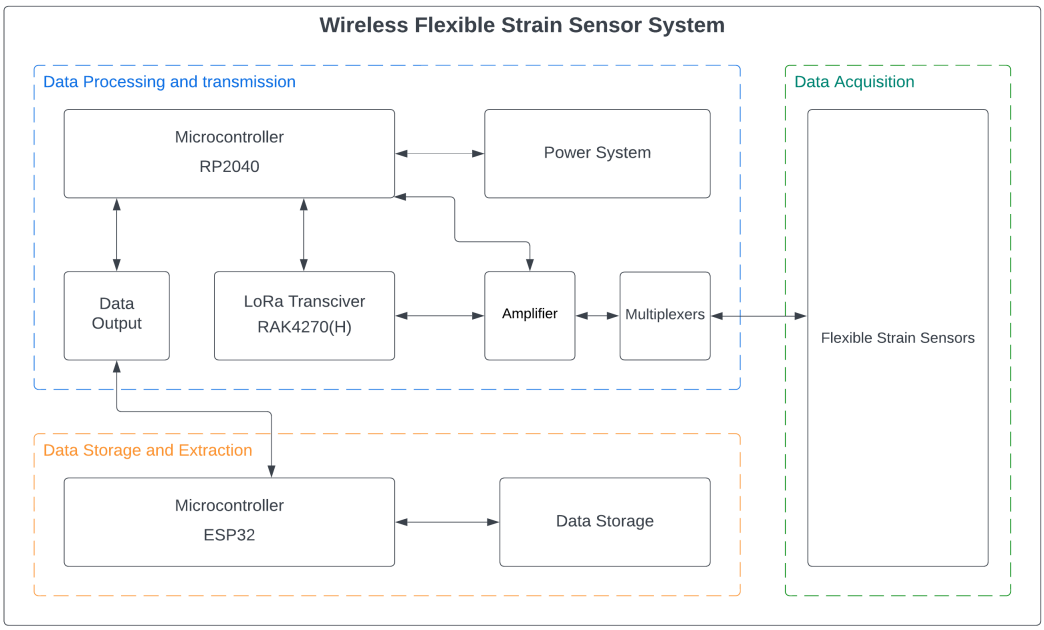

Figure 4.1: System architecture for the proposed wireless flexible sensor system

4.3.1 Data Processing and Transmission

The RP2040 was selected for the design of the data processing and transmission module as the microtronller. The RP2040 is the first self-developed chip produced by the Raspberry Pi and has the following technical specifications:

- Dual ARM Cortex-M0+ @ 133 MHz
- 264 kB of on-chip SRAM in six independent banks
- Support for up to 16MB of off-chip flash memory via dedicated QSPI bus
- DMA controller and fully connected AHB crossbar
- Interpolator and integer divider peripherals
- On-chip programmable LDO to generate core voltage
- 2 on-chip PLLs to generate USB and core clocks
- 30 GPIO pins, 4 of which can be used as analogue inputs

The fact that the RP2040 can achieve great performance while maintaining low power

consumption and minimal leakage is perhaps the most compelling argument in favour of using it as a microcontroller for data processing and transmission. The RP2040 is also very cost-effective. Additionally, its low-power mode can allow an extended battery working duration, which in turn extends the life cycle of embedded devices when used in real-world industry applications. In addition, it is compatible with a wide range of peripherals, including two UARTs, two SPI controllers, two I2C controllers, sixteen PWMs, a USB 1.1 controller and PHY (both for the host and the device), and eight PIO state machines. This not only provides the foundation but also the basis for simultaneously implementing two different data transmission techniques within the scope of this study.

In computer networks, multiplexing is one of the strategies that may be used to combine signals on a single medium and send numerous data signal streams. This method is also used as one of the ways that signals can be transmitted. The many-to-one concept is adhered to by this method, which merges n input lines into a single output stream. A multiplexer can function as an analogue switch within an analogue circuit, allowing the user to manage the connections and disconnections that occur within the circuit and, as a result, connect several input signals to a single input. In this particular study, two multiplexers(MAX14662ETI+T) were used to regulate the bridge connection mode of the flexible strain sensor. This allows for the formation of two different circuit modes, which enable free switching between axial strain measurement and bending strain measurement.

These two multiplexers are primarily intended to serve as replacements for the strain configuration selector that was developed before. That selection involves the manual switching of bridge connections, which is adequate for short-term measurements. However, if it needs to be applied to the SHM framework, manually switching on the actual

building structure is an unrealistic expectation. The multiplexer sets the circuit connection mode in advance through the programming class. Since the basics of the two ways to measure strain were talked about in Chapter 3, which was about developing the strain configuration selector, the following section will focus on the bridge connection principle of bending strain and axial strain.

Figure 4.2 (a) illustrates the bridge connections that are necessary for measuring bending strain. Each of the four bridges in this figure represents one of the four resistors that make up the flexible strain selector. Figure 4.2 (b) shows the bridge connection that is used to measure axial strain in a specimen. It is important to highlight that the NI PXIe-4339 data acquisition system is the source of the schematic diagram and that the relevant design modification is made in this study to adapt to the multiplexer. Table 4.1 illustrates the specific interpretation of the circuit configuration symbols that are used.

Table 4.1 Circuit diagram symbols for the two different bridge connection modes

Symbols	Full-Bridge Type II - Bending Strain	Full-Bridge Type III - Axial Strain
R_1	Active element measuring compressive Poisson effect ($-\nu\varepsilon$)	Active element measuring compressive Poisson effect ($-\nu\varepsilon$)
R_2	Active element measuring tensile Poisson effect ($+\nu\varepsilon$)	Active element measuring tensile strain ($+\varepsilon$)
R_3	Active element measuring compressive strain ($-\varepsilon$)	Active element measuring compressive Poisson effect ($-\nu\varepsilon$)
R_4	Active element measuring tensile strain ($+\varepsilon$)	Active element measuring the tensile strain ($+\varepsilon$)
V_{EX}	Excitation voltage provided by power system	Excitation voltage provided by power system

In the previous review of the literature, it was found that, compared to other wireless data transmission technologies like cellular, Bluetooth, WiFi, or Zigbee, the characteristics of LoRa, such as its low bandwidth and wide coverage, are suitable for strain sensor applications within the SHM framework required by this study. This was discovered based on the findings of the previous literature review. For the purpose of industrial deployment of SHM applications, LoRaWAN, which is a communication protocol,

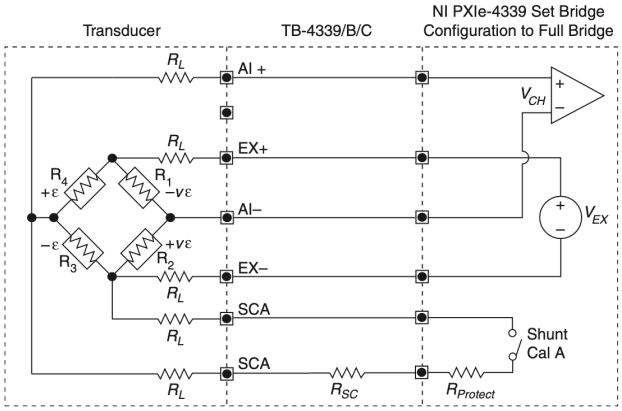

(a)

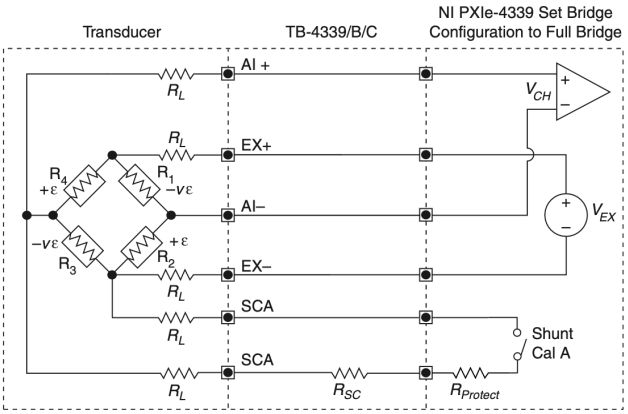

(b)

Figure 4.2: Circuit diagram (a) measuring bending strain (b) measuring axial strain. (*National Instruments*, n.d.)

is perfect since it makes use of LoRa modulation technology to send small packets over great distances.LoRaWAN's low power consumption features are excellent and can support up to 10 years or more of battery life.Its gigahertz radio modulation capability enables deep indoor coverage, such as connecting terminal devices located in underground parking lots. This is also one of the primary reasons for this study to consider it as a wireless transmission technology for sensors used to monitor the performance of high-rise or large buildings.

This research made use of a LoRa transceiver that was the RAK4270 (H) type, which was developed by RAK Company. The LoRaWAN protocol is utilised by the module in

order to perform point-to-point or LoRa network connections. The module is equipped with an STM32L071 MCU as well as an SX1262 LoRa chip. Through the use of AT commands that are transmitted via the UART interface, the module is able to communicate with a number of LoRa receivers, gateways, and other equivalent devices. Its bandwidth ranges from 7.8 kHz to 500 kHz, SF5 to SF12, BR = 0.018 to 62.5 kb/s. The following is a list of the specific parameters that the module has:

- Frequency plan AS923, AU915, EU868, KR920, US915, IN865,CN470, EU433 (AS923 is used in this study)
- Perfect for ultra-long transmission
- Highly sensitive in LoRa modulation (138dBm)
- Stronger signal transmission capability (up to 20dBm)
- Easy-to-use and low cost

As was discussed in the chapter's introduction regarding the design and consideration, this research makes use of two different ways of communication, both of which are carried out concurrently. The first option is the technology known as LoRa. However, it should be emphasised that the limited bandwidth of LoRa is only responsible for the alternating transmission of the maximum and lowest values of the two strain modes at a specified sample rate of 30 Hz in the SHM framework that was established for this study. The LoRa transceiver will communicate with a LoRa gateway, the data collected by the flexible sensor will be compiled by embedded, only the maximum and minimum values described above will be extracted, and then the data will be transmitted to the LoRa gateway and then transmitted to the TTN platform by the LoRa gateway in order to achieve real-time transmission of data flow and real-time monitoring of the SHM system. In the second mode, the raw data that is collected is transmitted concurrently to a separate microcontroller (an ESP32), and then it is completely stored on an SD card. This allows the end user to retrieve the data and perform further in-depth analysis on

it. This particular aspect of the design and development will be elaborated upon in the section devoted to data storage and extraction.

The primary objective of this development is to reduce the cost of sensor monitoring systems for the SHM framework by integrating all functions onto a single board. The second goal is to provide reliable local damage monitoring of essential structural parts of the building structure. The prototype of the LoRa-based wireless strain monitoring system is shown in Figure 4.3. As was discussed prior, the LoRa-based wireless strain sensing system was developed to integrate the SHM framework. As a result, there is a compromise that must be made in terms of sensitivity, cost, and power consumption when it comes to SHM applications. The previous section of the paper presented the testing that was done to validate the wireless flexible strain sensor's sensitivity. Therefore, when it comes to the design of the hardware, the primary factors that are taken into consideration are the amount of power that is consumed and the cost of the system that is being produced.

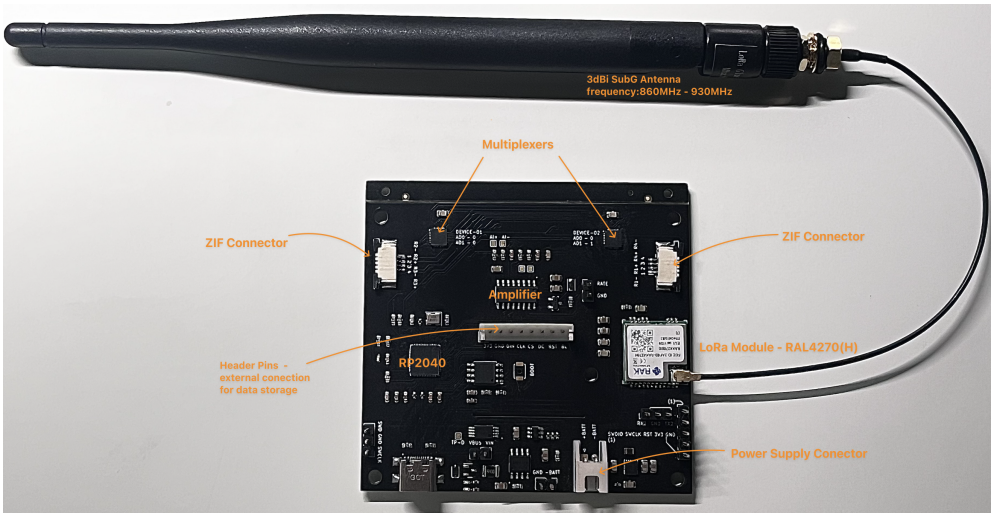

Figure 4.3: Final prototype of the Lora-bsaed wireless strain monitoring system

In Table 4.2, the power consumption of the primary components of the Lora-based wireless strain sensor node is displayed both when it is in the sleep state and when

it is in the working mode. It can be seen that the power consumption of the infinite strain sensor node in sleep mode is only between 4 and 5 microamperes, while its power consumption in full operational mode is close to 40 milliamperes. The power consumption of other components on the sensor circuit board is only approximately 3 to 4 microamperes. This results in low power consumption for wireless strain sensor systems that are based on the LoRa protocol and used in SHM applications.

Table 4.2 Power consumption of the main components of various operational states at 3.3 V

Components	**Sleep Mode(μA)**	**Normal Operation (mA)**
Multiplexer (MAX14662)	0.01	0.3
LoRa Module RAK4270(H)	2.31	TX mode - 35.4 RX mode - 15.8
Microcontroller RP2040	0.39	1.2
Amplifier (HX711)	< 1	< 1.5
Total Power Consumption	~ 4 - 5	~ 55

The component specifications for the data collection and transmission section of the wireless intelligent strain sensor node used for design are listed in Table 4.3. This table also includes the manufacturer, unit price, and overall cost of the hardware system. As can be seen from the table, the design that is the subject of this investigation has a total hardware cost of only around 63USD. The cost of this solution is considerably lower than that of the SHM systems that have been developed throughout the years. This has the potential to result in significant cost savings and an improvement in the deployment density of sensors due to the extensive deployment of sensor nodes required by the SHM framework.

Table 4.3 Unit price of the components and total costs of the wireless strain sensor node

Components	Manufacture	Unit Price(USD)
LoRa Module-RAK4270(H)	RAKWireless	7.8
3dBi SubG Antenna	RAKWireless	7
FPC Cable	Wurth Elektronik	3.5
3dBi SubG Antenna	RAKWireless	7
SD Card - 16GB	Strontium	7.45
PCB Prototype	JLC	30
Total Cost		62.75 USD(103 NZD)

4.3.2 LoRa Gateway, Network Server, and Application server

LoRaWAN is used in the field of monitoring systems, where it serves both as a communication protocol for networks and an architecture for system implementation. The design and development of LoRa sensor nodes that are employed in this study were discussed in the previous subsection, and the primary focus of the following part is to discuss the LoRaWAN network architecture that was utilised in this research project. The end node (such as the LoRa transmitter that was inserted inside the sensor for this study), the gateway, the network server, and the application server are the standard components that make up the LoRaWAN architecture. The user stores and processes the data on either the network server or the application server by establishing a communication link between the terminal node and the LoRa gateway. This study aims to develop a low-cost gateway that is end-user-friendly and can communicate with multiple sensor nodes. It is further integrated with The Thing Network (TTN), which will enable users to access the network server at any time and from any location for real-time monitoring and data visualisation without being constrained by geographic boundaries. When compared to the standard architecture of a LoRa network, the proposed design

is not only simpler but also easier to implement and more cost-effective, and it can be applied to the framework of an integrated SHM system, which allows it to fulfil the requirements of an application for a monitoring system. As shown in Figure 4.4, it illustrates the specific network architecture that is proposed by this research.

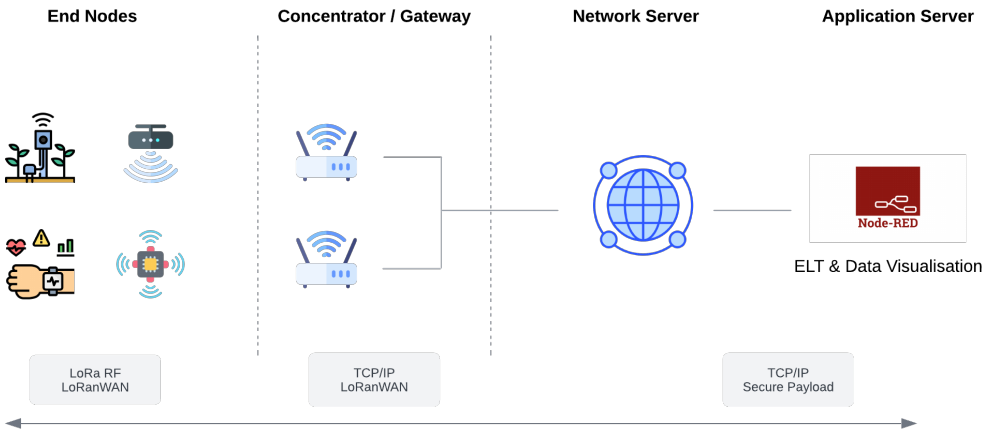

Figure 4.4: Proposed architecture for the intergrated wireless SHM system

The end node layer, which is also known as the physical layer, is for flexible strain sensors used in this study to collect data regarding bending strain and axial strain. In order to set up a network of communication, this layer incorporates LoRa sensor nodes for the purpose of data transmission with the gateway of the subsequent layer. transmits the encrypted payload containing the data that is being collected by the sensor to the system that is hosting the network. TTN was chosen to be the network server used for this investigation. The application server constitutes the topmost layer. In this layer, the research builds and develops the data visualisation software based on Node-RED in order to carry out centralised data processing. It is integrated with TTN, and the data that is collected by TTN in the network server layer is delivered to the visualisation programme in real time. The programme just needs to be installed once by end users, after which strain data may be instantaneously visualised for real-time monitoring. It is important to point out that the programme is dockerized, which makes it easier for users

to deploy applications on the end devices they use. Additionally, the application can be rapidly loaded and operated locally in any container or system environment without requiring any modifications. The design and development of this data visualisation application will be discussed in the next chapter. The LoRa architecture that has been proposed as part of this research is, in general, primarily geared towards the monitoring system that will be employed in the SHM framework. In addition to the LoRa gateway layer, which is necessary for the transmission and transfer of data and requires Ethernet and TTN, data communication between other levels in LoRaWAN is established. As a result, the data transmission of its LoRa nodes can be accomplished without the use of any Wi-Fi or Ethernet network. This results in a very low cost for the data transmission of LoRa-based sensor nodes.

4.3.3 Development of the LoRa Gateway

In the context of this study, a Raspberry Pi 3b+ serves an important role as one of the primary devices for the creation of an intelligent gateway. The Raspberry PI is a lightweight and highly compact computing device that resembles a little computer and has the capability of running computer programmes. In addition, it possesses properties such as relatively high computing power, a sophisticated interface, and free programming that may be customised however the user sees fit. Because of this, it is also one of the finest choices for designing edge-layer devices like gateways or local servers. During the development of an intelligent gateway that operates within the SHM framework, the device volume needs to be taken into consideration in order to accomplish successful installation in challenging locations.The Raspberry Pi 3b+(Figure 4.5), which was chosen for this study, is the latest and most up-to-date model in the Raspberry Pi 3 series. Its technical specifications are as follows:

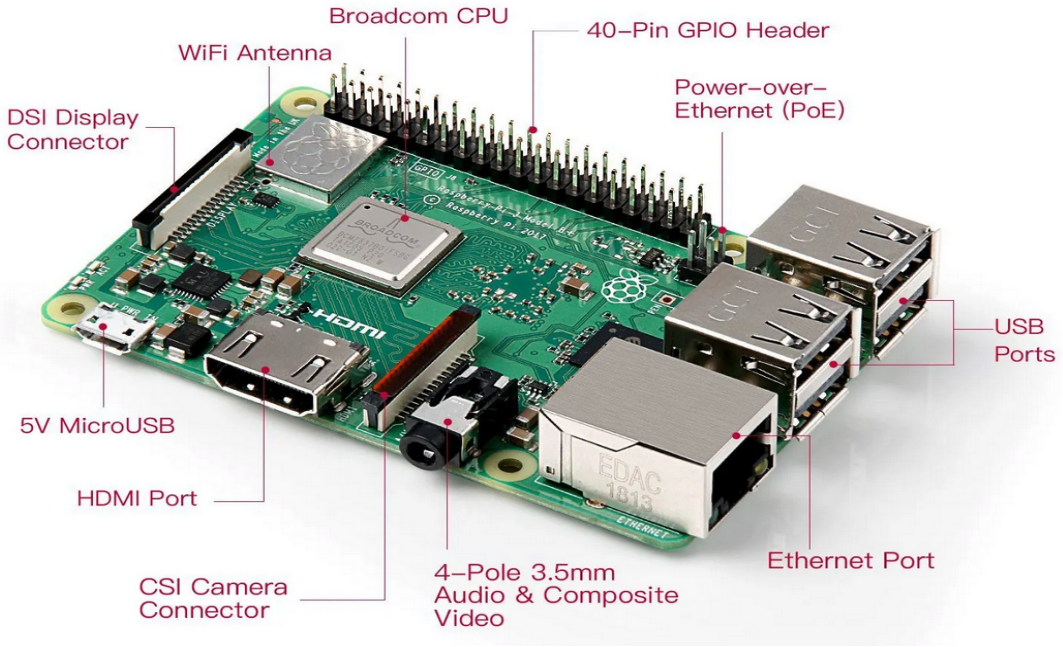

Figure 4.5: Raspberry Pi 3b+ interface

- 1.4 GHz Cortex-A53 (ARMv8) 64-bit SoC processor
- 1GB LPDDR2 SDRAM
- 2.4GHz and 5GHz IEEE 802.11b/g/n/ac wireless LAN, Bluetooth 4.2, and BLE
- Gigabit Ethernet over USB 2.0 (maximum throughput: 300 Mbps)
- Extended 40-pin GPIO header
- Full-size HDMI@ and 4 USB 2.0 ports
- CSI camera port for connecting a Raspberry Pi camera
- DSI display port for connecting a Raspberry Pi touchscreen display
- 4-pole stereo output and composite video port
- Micro SD port for loading the operating system and storing data
- 5V/2.5A DC power input

Based on the findings of this research, the RAK2245 Pi HAT WisLink LPWAN Concentrator (Figure 4.6) was chosen to serve as the whole RF front end of the gateway. It is compatible with the LoRaWAN global frequency band and has support for eight

different channels. This board, which combines the Ublox MAX-7Q GPS module as well as a heat sink, is the most compact gateway concentrator available. The board is capable of providing a LoRa wireless link operating at very high speeds while maintaining a modest data transfer rate. It is able to manage data packets from a large number of remote decentralised terminals since it is powered by a Semtech SX1301 transceiver concentrator. There are two Semtech SX125X integrated inside the RF front-end I/Q transceiver. As shown in Figure 4.7, the RAK2245 Pi HAT is integrated into the Raspberry Pi 3 Model B+ that was used in this research in order to produce a complete and cost-effective gateway solution. The primary objective of this research was to develop a relatively affordable LoRa network system that is compatible with the SHM framework. The features of RAK2245 Pi HAT WisLink LPWAN Concentrator are as follows (RAKWireless, 2023):

- Compatible with the Raspberry Pi 3 Edition B+ model
- Integrated Ublox MAX-7Q GPS Module
- Heat sink SX1301 base band processor
- Emulates 49 LoRa demodulators
- 10 parallel demodulation paths
- Supports 8 uplink and 1 downlink channels
- 2 units of SX125x Tx/Rx front-ends for high and low frequency
- supports a power supply of 5 V and a transmit power of up to 27 dBm
- Receive a sensitivity of down to -139 dBm@ SF12 with a bandwidth of 125 kHz.
- Supports the most recent version of the LoRaWAN protocol (1.0.2)
- Compatible with the worldwide licence-free frequency band (EU433, CN470, EU868, US915, AS923, AU915, and KR920)
- SPI, UART, and I2C interfaces are all supported

Figure 4.8 presents the wireless communication flow of the data processing and LoRa

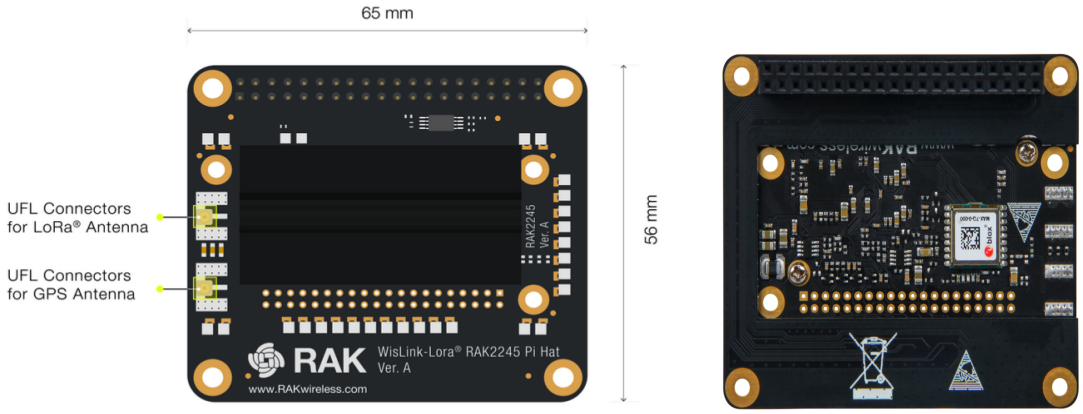

(a) (b)

Figure 4.6: RAK2245 Pi HAT WisLink LPWAN Concentrator (a) top view (b) bottom view (https://docs.rakwireless.com/Product-Categories/WisLink/RAK2245-Pi-HAT/Overview/)

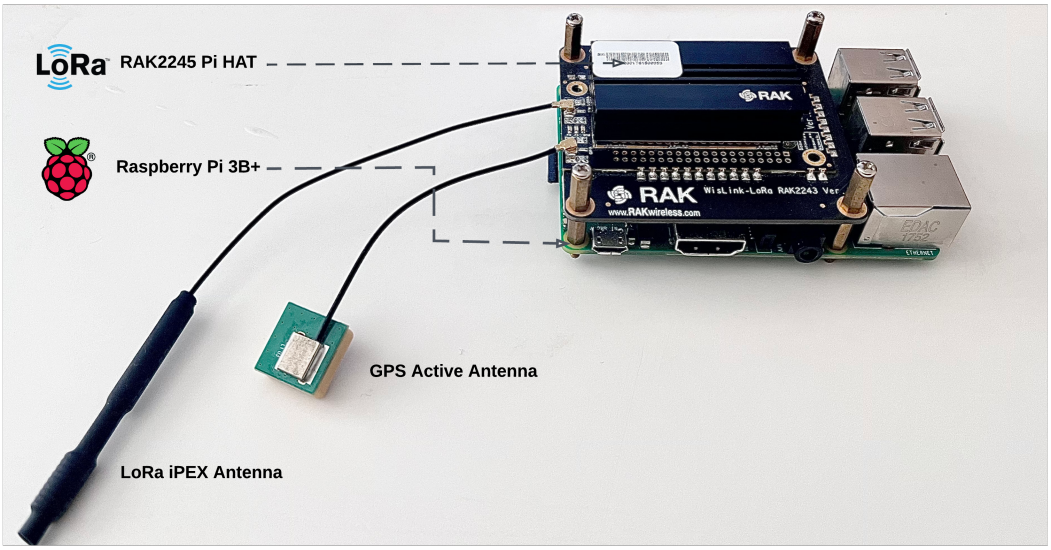

Figure 4.7: Devepoed LoRa gateway prototype

node transmission parts that are controlled by the RP2040 microcontroller (this part does not include the data storage flow of communication with the ESP32 S3, which is discussed in the following section). There are a total of 14 steps involved in the procedure. To be more specific, once the system has been powered on, it will initially wait for a ready signal in order to guarantee that the UART protocol will be able to begin

communication. The AT command is then sent out in order to trigger the LoRa node to communicate with the LoRa gateway, after which the LoRa gateway will join the TTN. While the RP2040 waits for the LoRa network to be successfully established, it issues data acquisition instructions to manage the bridge connection arrangement within the flexible strain sensor using the multiplexer. This allows it to alternately collect two strains: bending strain and axial strain. This data acquisition procedure has a sampling rate of 30 Hz, and after every 30 strain values are sampled, the multiplexer changes to a different strain collecting mode. Because of the low bandwidth limitation of the LoRa technology, as was discussed previously, and because the primary objective of utilising LoRa in this investigation is to monitor the irregularities in the strain field, LoRa will only broadcast the highest and lowest values within the range of 30 sample values for each strain mode. After passing through the LoRa node, the highest and lowest values will be sent to the LoRa gateway, which will subsequently send them to TTN. The end user is then able to view the maximum and minimum values of each strain configuration that are transmitted in real time to the TTN network server. This allows the end user to evaluate the state of health or damage to the local strain field of the structural members by observing whether or not there are abnormal values (either abnormally large or abnormally small). Figure 4.9 present the data/payload sent to the TTN application.

In addition to the development of a LoRa gateway, the focus of this study is on the development of a user access interface for the gateway. This is done with the intention of resolving the issue of network configuration that was brought about as a result of the gateway's requirement to access TTN. When developing a traditional gateway, developers are required to build the network configuration in advance and integrate it into the embedded operating system (such as the Raspberry 3B+ that was utilised for this study). Even though the gateway is often installed in a stationary location, the

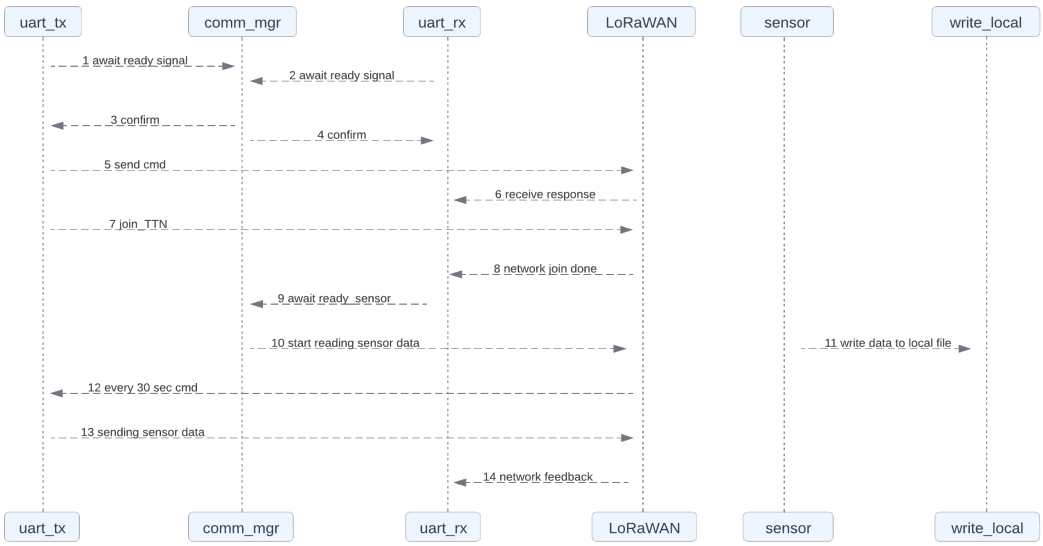

Figure 4.8: Proposed workflow for the intergrated wireless SHM system

network configuration on the gateway does not require frequent updating. Users, on the other hand, are required to carry out local network configuration every time they change the location where the gateway was installed; in other words, the developer must recompile them. This is the case regardless of how often they move the gateway's installation. This is a very laborious development effort for practical applications in any outdoor location or civil building context. In order to overcome this challenge, the author of this study built a user access interface for the LoRa gateway that they had developed (as can be seen in Figure 4.10). Assuming that the LoRa gateway is installed in a new location, users will only need to set their electronic devices, such as mobile phone hotspots, to the default SSID and password. Once the LoRa gateway is connected to the power supply, it will automatically connect to the hotspot network, which will serve as a temporary network for the LoRa gateway. After that, the user can log into the access interface (it does not need to be the same device as the temporary network of the LoRa gateway; any electronic device will work), enter the network name (SSID) available in the new area, the password, and the address of the TTN server where the

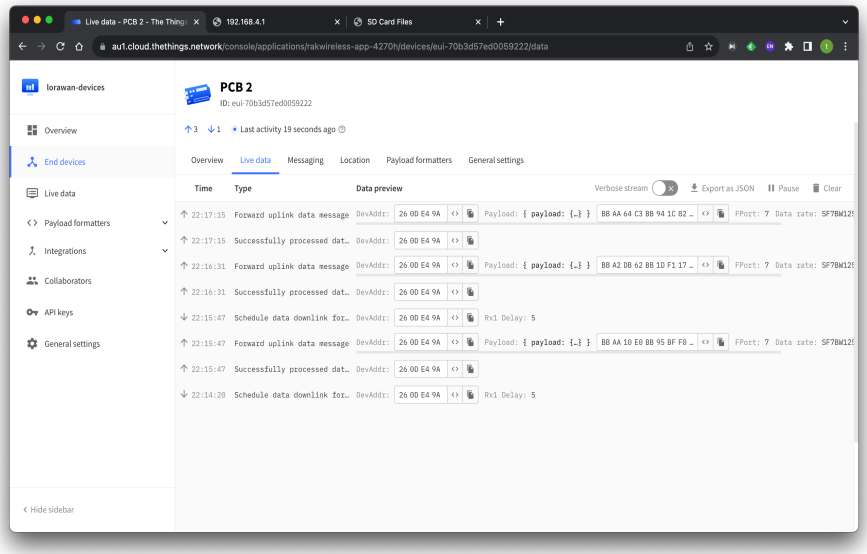

(a)

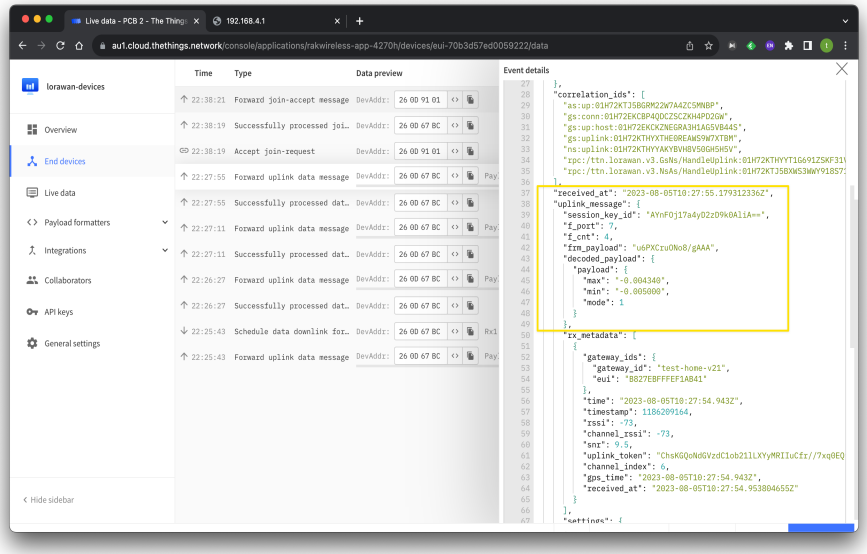

(b)

Figure 4.9: TTN platform overview (a) TTN application page (b) Data received on TTN - min and max value

LoRa system is located, and then click the connect button. The network configuration file that is stored inside the LoRa gateway is immediately overwritten, and the hotspot is disabled. It can be accomplished for the LoRa gateway to automatically connect to the new network after it has been restarted (also known as the system being rebooted). This will allow it to establish communication with the LoRa sensor nodes and the TTN.

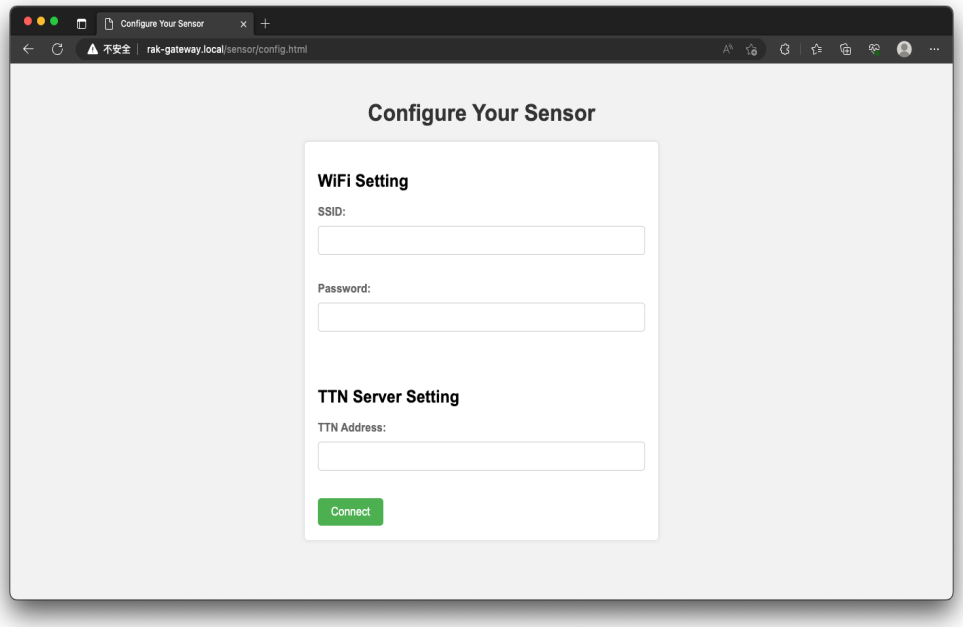

Figure 4.10: Nerwork configuration interface for the developed LoRa gateway

4.3.4 Data Storage and Extraction

The main MCU-RP2040 will alternate between collecting two different types of strain data, sending the highest and lowest values to the LoRa gateway, and also sending the whole raw data to the SD card module. The RP2040 and the second microcontroller, the ESP32 (ESP32 S3), are primarily responsible for managing this stage in terms of data storage and extraction, respectively. The ESP32 S3 is a dual-core microcontroller

unit (MCU) that incorporates long-range support for 2.4GHz, 802.11b/g/n Wi-Fi, and Bluetooth 5 (LE) connectivity. The ESP32-S3 has 45 programmable GPIO, SPI, I2S, and I2C pins, as well as PWM, RMT, ADC, and UART hosts, SD/MMC hosts, and TWAITM. For HMI-related applications, a total of 14 GPIOs are capable of being set as capacitive touch inputs. In addition to all of these peripherals, the ESP32-S3 features an ultra-low-power (ULP) core that allows for various different modes that consume less power. In this research, the RP2040 sends all of the data to the ESP32 S3, which then saves the information in a local memory near the sensor. In addition to that, this research builds a web server by utilising the built-in access point that comes standard on the ESP32. The maximum range that the access point can cover is 100 metres. This brings a new data extraction mode to the SHM framework. The present traditional SHM framework can be broken down into two categories: academic and commercial, as was discussed in the previous literature review in Chapter 2. However, one of the most challenging aspects of both is the extraction of data. The following are the two categories that can be used to classify common problems:

1. The data is stored locally on the sensor system

The majority of sensors place an emphasis on storing data locally as a primary means of protecting data integrity and mitigating the risk of packet loss during wireless transmission. However, in order to make SHM systems useful in real-world applications, sensors are frequently positioned either on the inside or the exterior of structures of varying heights and lengths. Users are required to make routine trips to the monitoring area in order to retrieve data when it is kept locally. When extracting the data, the user must first pause the sensor collection in order to preserve the integrity of the data that is recorded in the sensor system. If the sensor is placed in an area that is difficult to access or reach, it will be more difficult for the user to extract data from the sensor.

2. Data is stored on a remote or central system

SHM systems that are equipped with wireless communication capabilities will typically communicate data wirelessly to a central processing unit; nevertheless, in this circumstance, it is necessary to take into consideration the installation location of the terminal device. LoRa is not ideal for sensors like accelerometers that demand high bandwidth and throughput because of its low bandwidth, despite the fact that LoRa offers the possibility of long-distance transmission. This is because LoRa offers the possibility of long-distance transmission. In the application of SHM, if it is a large infrastructure, such as a bridge, there are no cellular network conditions due to the fact that the structure itself is located outside. As a result, when the SHM system is installed on the bridge, the central processor that is used for processing wireless transmission data needs to have the ability to access the network in order to receive data. Real-time monitoring over a protracted period of time incurs substantial costs. Furthermore, a power system is necessary to guarantee that the central processing unit can operate without interruption and on schedule.

To address these challenges, the web server designed in this study allows users to access the local storage of the proposed wireless SHM system free of charge and download the complete data file within a distance of 100 metres. Real-time monitoring is made possible by the simultaneous control of RP2040 and ESP32. Users are able to constantly open the wireless system at any moment, are free to enter the system locally, simply refresh the web page, and will be able to collect real-time data.

4.3.5 Development of Data Storage System

Figure 4.11 (a) shows the proposed prototype of the data storage system. It features a Micro SD card module, an ESP32 S3 module, and header pins for connection with

the LoRa-based wireless data processing and transmission system. Figure 4.11 (b) demonstrates a complete view of this subsystem connected to the main wireless system. The data storage system initiates the opening of its very own hotspot as soon as it becomes operational. As shown in Figure 4.12 (a), the RP2040 will store all of the information that it has gathered by moving it through the ESP32 S3 and onto the microSD card module. The files are in text file format(Figure 4.12 (b)), and their names are generated by a programme to correspond with the date and time when the wireless sensor system started to function and gather data. Users have access to the ESP32 S3's internal hotspot, which gives them access to the current internal server (192.168.4.1) of the storage system. Users can browse through all of the data that is saved on the SD card, and they have the option to either download it or delete it. It is also possible to pick the most recent files in order to watch the data that has been collected in real time, and these actions taken by the end user do not interfere with the instruction and data transmission that occur between the RP2040 and the ESP32 S3. To put it another way, when the sensor collects new data, all the end user needs to do is reload the most recent file in order to quickly view the most recent real-time data. This is of the utmost importance for the monitoring system of the SHM framework, which genuinely realises the real-time monitoring of the monitoring object by the wireless system.

4.4 Summary

This chapter primarily discusses the process of developing wireless intelligent sensor hardware based on LoRa and LoRa networks to meet the needs of monitoring the local strain field of structural components and civil building emergency monitoring. The wireless smart sensor board could be connected with the flexible strain sensor, and the two modes can be switched alternately without affecting the installation position of the



(a)

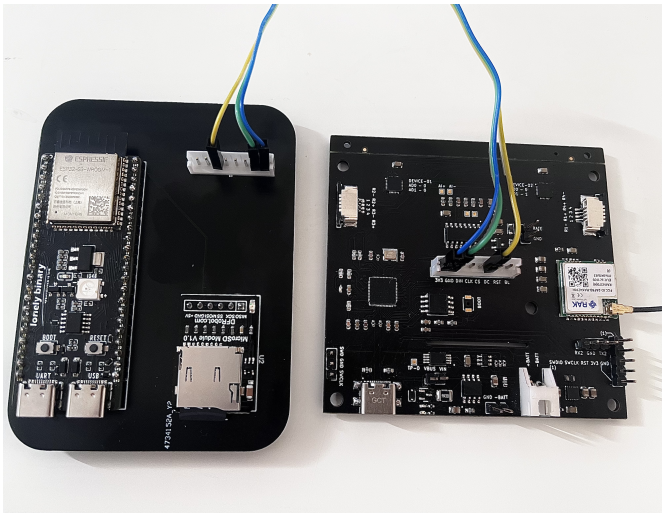

(b)

Figure 4.11: PCB prototypes (a) data storage system (b) connected to the LoRa-based wireless system

strain sensor. This allows for the measurement of both bending strain and axial strain simultaneously. In the first section of this chapter, the overall design architecture of wireless smart sensors is presented. This architecture can be broken down into three parts: the collection of data, the processing and transmission of data, and the storage of data. Since the flexible strain sensor that is used for data gathering was discussed in the chapter before this one, the primary focus of this chapter is on the design and

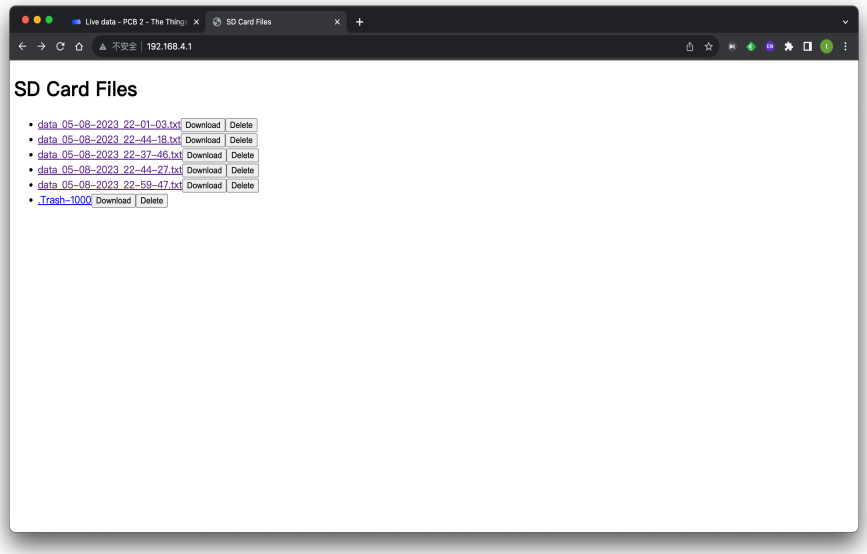

(a)

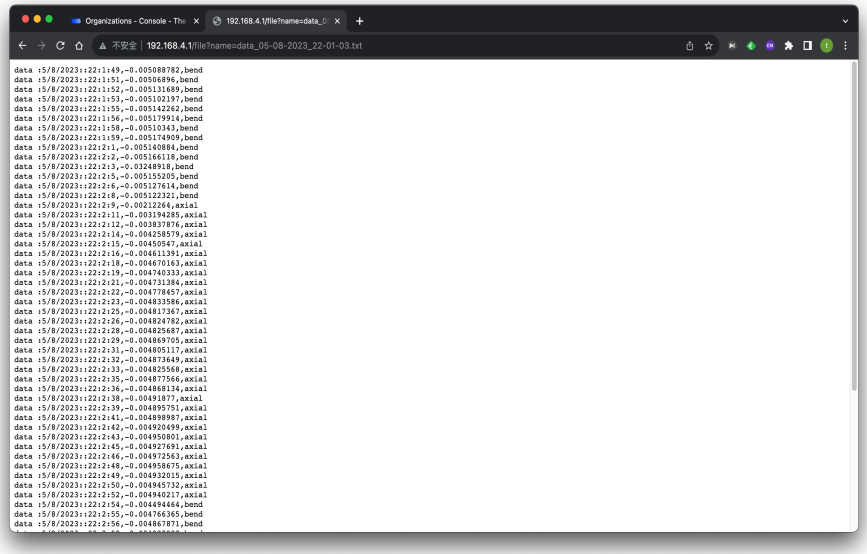

(b)

Figure 4.12: End user access file (a) webserver main page (b) webserver test file

development of the hardware that is used for data processing and transmission, as well as data storage systems. In general, the wireless sensor intelligent system that was

developed in this study could be freely installed and replaced with a half-bridge flexible strain sensor. This results in a significant reduction in the replacement cost required for sensor damage when compared to the conventional strain sensor. In addition, the wireless sensor is fitted with LoRa communication technology, which enables it to send the extreme strain field values of essential structural components. This provides the rapid monitoring and assessment capabilities that are required for civil building crises. The data storage system is responsible for providing comprehensive data storage for the entire wireless system. Users are able to log into the local server of the storage system in real time without having to pause the sensor device in order to receive the entirety of the data being measured. The process can be performed in parallel with data collection and LoRa transmission, which allows for the realisation of real-time monitoring and assessment of wireless smart systems inside the SHM framework.

Chapter 5

Development of MQTT-based Data Visualisation and Storage for SHM Applications

5.1 Introduction

The rapid development of information and communication technology (ICT) is making the implementation of applications for the internet of things (IoT) increasingly accessible and economically feasible. For an integrated SHM system, developing and maintaining the storage and visualisation of data collected by sensors is critical. The Internet of Things Industry (TTI) (*The things industries*, 2015) came up with the idea to build The Things Network (TTN) (Network, 2015) in order to make the planning and implementation of networked systems for IoT devices more approachable. As a global collaborative IoT ecosystem platform, TTN makes use of LoRaWAN to provide solutions for LoRa-based IoT devices. These solutions include the establishment of

networks, the development of gateways, and the deployment of device nodes. The Things Stack server is a free shared web hosting platform that is made available to developers by TTN. As introduced in the previous chapter, the LoRa gateway developed by this research is integrated with the TTN server. Although TTN could help developers greatly simplify the deployment of the architecture of the IoT system, the design and build of gateways and the development of Lorawan-based IoT devices need to be done by the end users. In addition, it does not provide application servers for things such as long-term data cloud storage, data visualisation, sending data early warning, and so on, as TTN works to provide the foundation for the setup of network servers. Despite this, there are a large number of third-party APIs available to developers, such as MQTT, AWS IoT, and Azure IoT, for the application server development environment.

In order to be able to visualise the data collected by the sensor for the initial occasion, so that the user is able to make a quick preliminary assessment within a short period of time. In this research, the MQTT protocol is utilised to construct a user-friendly graphical interface for SHM real-time monitoring for a LoRa-based wireless sensor that was developed. MQTT is a very lightweight network protocol that is used for message queuing services. It is a frequent practise to use it to link remote devices in order to make connections for devices that have restricted bandwidth. In this study, MQTT is used to add an application layer to the deployment of the TTN server. This is performed in order to realise more control of the user's data and to make it easier to analyse the data produced by the proposed LoRa-based flexible strain sensor. In this chapter, the design requirements and practical applications of the overall system architecture are presented.

5.2 Related Work

The proliferation of IoT devices in the field of SHM can be attributed to the rapid growth of information and communication technology over the past decade (Firdaus Hashim, Kassim, Suliman, Anas & Bakar, 2019; Wadhwani, Singh, Singh & Dwivedi, 2018; Plageras, Psannis, Stergiou, Wang & Gupta, 2018). There is currently no low-cost integrated SHM system that combines direct monitoring of strain field anomalies, flexible sensors, wireless connection, and on-site real-time data monitoring and extraction. The vast majority of applications for wireless SHM systems that aim to do real-time data monitoring rely on cloud computing platforms such as Amazon Simple Storage Service (S3). The cost of this kind of cloud monitoring platform is significant, in spite of the fact that it is capable of providing real-time monitoring of data storage in the cloud (Pramukantoro, Luckies & Bakhtiar, 2019). When it comes to SHM systems that require the transfer of data over extended periods of time, this is not the most effective approach. This chapter focuses mostly on the presentation of the development of the network platform monitoring layer and the application layer. Additionally, this section discusses the lightweight MQTT protocol that was utilised in this research for the application layer, which integrated with the TTN server for the LoRaWAN system.

5.2.1 MQTT Protocol

Message Queuing Telemetry Transport (MQTT) is a communication protocol that is extensively used in the M2M industry and was proposed by Andy Stanford-Clark of IBM and Arlen Nippe of Arcom Control Systems Ltd. (Eurotech). It employs the Transmission Control Protocol (TCP) as the transport protocol and TLS/SSL as the security protocol. Because it is commonly used for the transmission of lightweight

information over networks with limited bandwidth, this research employs it as the communication protocol for the TTN server application layer in order to convey data for developing the data visualisation dashboard for end users. MQTT was formerly employed for machine-to-machine communication (Yasmin et al., 2018); however, it is currently also frequently utilised for Internet of Things devices. There are two components that make up the MQTT protocol: the client and the message broker. Clients will provide data to the message broker in the form of "messages," which will eventually be available for other clients to subscribe to, or they can be saved for future subscriptions. Due to the fact that MQTT is a binary protocol, its message payloads typically consist of very short 2-byte fixed headers, and their storage capacity can reach up to 256MB. Kang et al. (Kang et al., 2017) developed an Internet of Things-based smart home system that saves its data on AWS. As a result, they proposed an Internet of Things system that uses MQTT agents on AWS to perform operational temperature sensors and provide the capability to send early warning notifications. These notifications are ultimately displayed on the mobile app of the end user using Gluon.

5.2.2 Development of the Application Layer - Data visualisation

The use of data dashboards as a method of visualising data has gained significant traction in recent years. It can basically be segmented into three categories (Saha & Majumdar, 2017), which are as follows:

1. Strategic dashboard: It's a tool that enables an organisation to define strategic goals for a predetermined period of time (often quarterly or annually), monitor performance indicators, and summarise the results of their efforts. It is designed to assist business decision-makers in producing high-level data analysis reports, with the end goal

of assisting firms in more effectively achieving their objectives. Quantitative and qualitative analyses are typically components of the data analysis process.

2. Operation dashboard: It's mostly used for the purpose of monitoring and managing procedures. The primary function of this kind of dashboard is to provide users with alert information, thereby prompting them to pay attention to data abnormalities and allowing them to complete further research when it is most convenient for them.
3. Tactical Dashboard: It's a subset of the operational dashboard that focuses on more specific information. Its primary purpose is to take advantage of the interactive capabilities of the dashboard, enabling users to investigate the data; however, it is also frequently regarded as an analytical dashboard.

5.3 System Architecture Overview

The entire flexible wireless strain direct monitoring system based on LoRa that has been suggested has a total of two data streams, as can be seen in Figure 5.1 which depicts the architecture of the system. In the first part, the maximum and minimum values of each strain mode are extracted from the flexible strain sensor through two multiplexers. The data flows to the TTN server through the LoRa node and then through the developed application layer data visualisation user interface for real-time monitoring and storage. This is done because of the low-bandwidth characteristics of LoRaWAN. The second step is to store the complete raw data on the SD card after transferring it to the ESP32 S3 microcontroller. A built-in hotspot is also made available to the user by the ESP32 S3, which enables the user to access all of the data on any device without restrictions, in real time,to access and extract all of the data files.

The dashboard of data visualisation is the primary focus of the development of the application layer that is proposed by this research. Multiple sensor nodes are connected

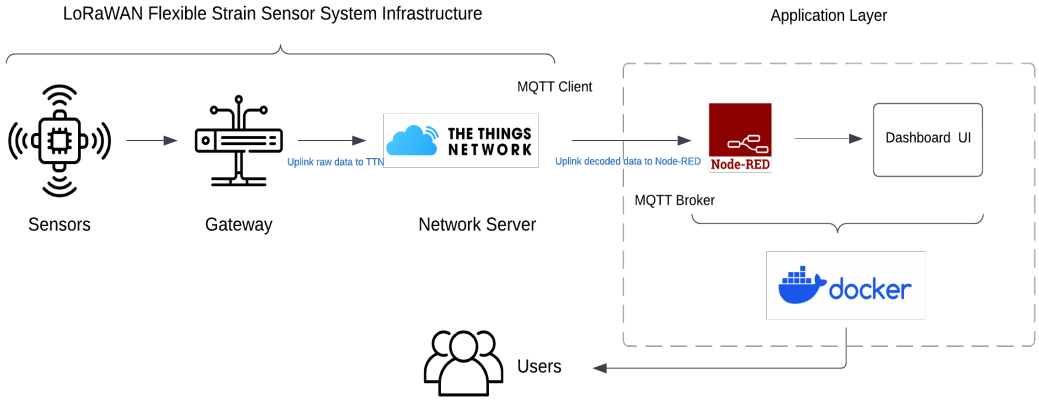

Figure 5.1: LoRa-based IoT system architecture diagram for the strain monitoring application

to the LoRa gateway via LoRaWAN. The sensor readings are then released to the TTN server correspondingly. Ultimately, the data is communicated to the data visualisation dashboard that was built using the MQTT client that is located on the TTN server. The dashboard that was produced for this research work is an example of an event-driven application. Event-driven data can be transmitted in near real time, so end users can respond immediately to events as they occur. In this study, a LoRa gateway can simultaneously establish communication connections with a number of LoRa nodes; thus, the data visualisation dashboard is required to be able to accommodate the flow of numerous threads of data. SHM systems are often comprised of many sensor nodes in practical applications as well; hence, the amount of time and frequency of time that need to be processed centrally necessitate the utilisation of numerous threads. What is most worth mentioning is that the whole process is different from the high cost of data transmission and storage on other cloud platforms. The entire data transmission is free of charge because of the integration of the proposed dashboard application with the TTN server carried out by the MQTT client. This allows for the achievement of practical zero-cost data monitoring as well as accelerated user access. Additionally,

MQTT clients are not started unless the user specifically requests quick access to data or monitoring dashboards. Users are required to install the integrated dashboard application on their own local computers in order for the data to be stored. This ensures that a high level of security is provided to the data to prevent its loss.

5.3.1 Design Requirements

In order to fulfil the objectives of the application while operating within the SHM framework, the TT server integrated data visualisation application needs a collaborative effort from a number of different elements. Firstly, the LoRa-based sensor node that is deployed must successfully establish a connection with the LoRa gateway while simultaneously ensuring that the LoRa gateway is connected to the TTN network server. This is necessary to ensure that the sensor is able to successfully send information to the TTN network server in order to provide real-time data. The data must be compiled using JavaScript into a form that is readable and understandable to the end user. In addition, the data needs to be able to be transferred via the MQTT client to the designed Node-RED-based data visualisation application so that end users are able to access it whenever they need to. Secondly, in order for the system to be constructed in a way that is both sustainable and capable of meeting the cost demands of a wide range of users, it needs to have the lowest possible operating costs in terms of the data transmission and storage it performs. Last but not least, the application in consideration needs to be user-friendly, easy to understand, and simple in terms of its deployment, operation, and maintenance for end users.

5.3.2 System Implementation

As can be seen in the system architecture 5.1, the flexible strain sensor infrastructure, which is based on LoRaWAN, is broken up into two parts: the LoRaWAN-based flexible strain sensor system infrastructure 5.2, and the application layer, which is integrated with the TTN server through MQTT. The TTN server is communicated with by the MQTT client.

Earlier on, the designing and building of the hardware component of the flexible strain sensor system that is based on LoRa was discussed. This component functions as an Internet of Things (IoT) sensing device for the purpose of data collection and can also be simplified for use in that capacity. The flexible strain sensor is primarily accountable for detecting and monitoring the strain field of the monitored object in addition to the data collection process. The following is a brief overview of the hardware development of flexible strain sensors and wireless sensing systems, as stated in Chapters 3 and 4. These two components implement the primary processing unit of the system with the assistance of the most recent microcontroller, the RP2040, produced by Raspberry PI. They bring the first phase of the integrated system to a successful conclusion, which allows the system to be considered fully functional. In order to gather data regarding strain, the microcontroller has the ability to operate the bridge connection arrangement of the flexible strain sensor. In the second stage, the gateway server must be functioning along with other servers to set up a communication network in order to be able to send the information that is acquired by the embedding layer. The system architecture that was built for this study has the goal of making it achievable for SHM applications to have secure and stable long-distance data transmission as well as IoT device connections. The Internet of Things (IoT) is an open-source architecture, and LoRaWAN enables communication over great distances (up to 15 km) with minimal power consumption

and bandwidth. The amount of power that is consumed by LoRaWAN is extremely low when compared to that of Bluetooth, WiFi, ZigBee, and other networks that generally have high coverage. The gateway that is based on LoRaWAN is included in this system along with the TTN server. The system will instantly establish a communication network with TTN when the gateway device is powered on. This is done to ensure that the data gathered by the embedded layer may be uploaded to the TTN server at the same time that it is transferred to the LoRa gateway using LoRaWAN. When the gateway device is powered off, the system will not establish a communication network with TTN. On the TTN server, uploaded hex-formatted and space-separated bytes are simultaneously decoded into meaningful and readable fields.

The development of the application layer's primary goal is to make it easier for the end user to monitor and read data. The application layer is constructed by using the MQTT client, which is then connected to the MQTT brokers that are hosted on the TTN server. This allows the user to receive data that is updated in real time. The MQTT broker uploads the data to the application layer dashboard system as soon as TTN receives it. Users are able to access the dashboard system on any of the different computers. The system is built using Node-RED, as can be seen in Figure 5.3; it is also capable of being integrated into the TTN server, which enables cost-free data uploading and downloading. Node-RED is a visual process-based programming development tool developed by IBM. In addition, the system makes use of Docker to host the containerized application that was designed to simplify the process of dashboard installation for end users. Docker is chosen for the majority of reasons related to the following benefits that it offers:

1. Consistent Environment: This is one of Docker's outstanding characteristics. It provides developers with a consistent environment from design, development, testing, production, and maintenance, enabling programmes to run unconstrained in diverse contexts and lowering the number of difficulties encountered when deployment in

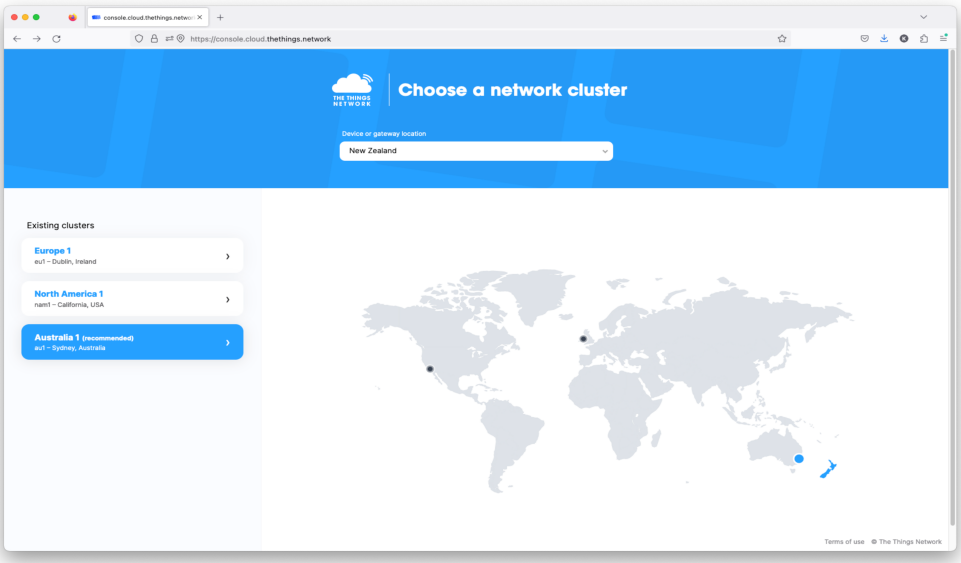

(a) AU Server home page

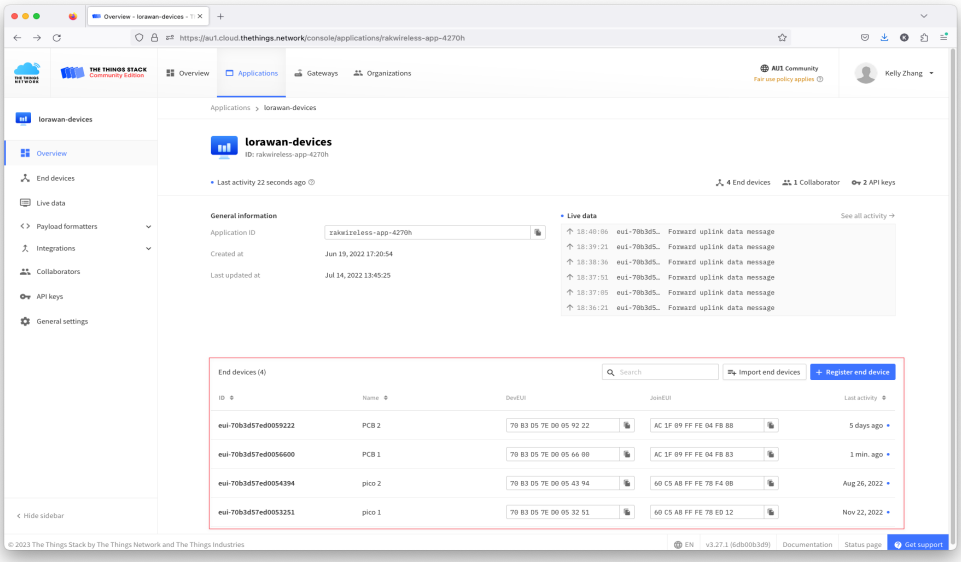

(b) TTN applications page for monitoring the registred IoT devices(sensors)

Figure 5.2: TTN server interface

new environments.

2. Speed and agility: These are two other important benefits that come with using

Docker. It enables the building of containers for each process, and because of the environmental consistency and hands-free operating system limits it provides, the deployment of these containers may be accomplished in only a few seconds. Users have the ability to rapidly start, pause, or delete containers at any time.

3. A high level of security Isolating containers from one another ensures that every container has access to its own set of resources and is shielded from influence from the outside world. Users can deploy it on their own devices, which provides an additional layer of protection.
4. Optimisation of costs Docker's benefits are also contained in the fact that it enables users to significantly lower the cost of their infrastructure while simultaneously allowing applications to be run at a very low cost. This is one of the ways in which Docker enables users to optimise costs.

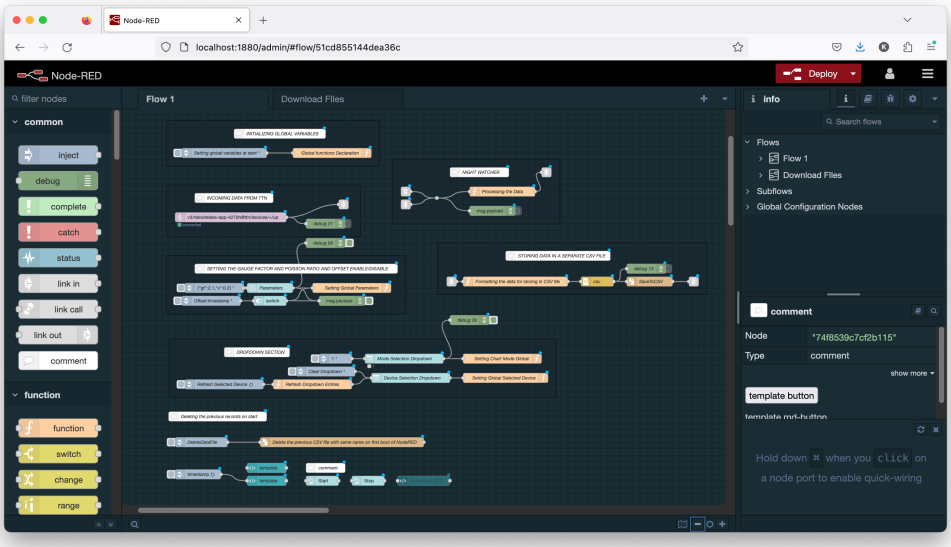

Figure 5.3: Backend view of the designed dashbaord work flow on Node-RED

The differences and similarities between Docker and virtual machines are illustrated in Figure 5.4. In the present day, the majority of SHM system applications have

stringent criteria for users in actual deployment, and some of these applications require the deployment of professional developers. This problem can be resolved with this application. Developing the designed system with Docker has the primary goal of empowering end users with the ability to swiftly deploy apps, easily create new instances, and freely migrate programmes on their own devices. And offer users improved safety, fewer privileges for accessing the system, and less software dependency overall.

Narration	Virtual Machine	Docker
Infrastructure Management	Hypervisor Layer	Docker Engine layer
Memory Usage	Very high	Very low
Memory Reallocation	Not possible	Unused memory can be reallocated to other containers
Performance	As virtual machines increase, the performance decreases	As Docker uses a single engine, the performance is high, regardless of the increase in containers
Portability	Virtual machines depend on the Host OS, libraries and dependencies. So, portability is a challenge	Docker is highly portable
Boot Time	VMs take time to boot	Docker containers take milliseconds to boot on.

Figure 5.4: Backend view of the designed dashbaord work flow on Node-RED (CloudTern, 2021)

The user is only required to execute one command line on the terminal: docker pull strain-sensors-realtime-monitoring:1.6.0, users will be able to download and save the application for data visualisation dashboard on their own machine. Figure 5.5 is the main interface of the Docker Desktop. Once the user has successfully pulled the docker image, which is the designed application locally, they can access the application via Docker Desktop and click the Run button to run the application. When the user executes the application, they will see the interface that is shown in Figure 5.6. Launch the browser and type localhost:1880/ui. Users are able to access the homepage of the dashboard, as shown in Figure 5.7. This should be done after verifying that the connection between the application programme and the TTN server has been successfully established.

The following are the primary functions that the dashboard home page provides: Firstly,

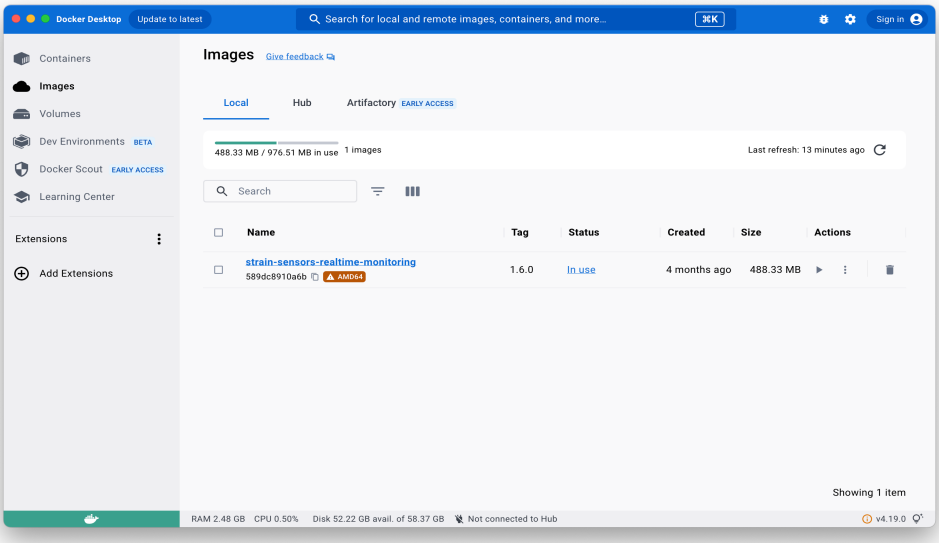

Figure 5.5: Docker desktop

the user selects the device that is going to be monitored. There is no inconsistency between the device ID and the EUI number of the LoRa node device that is connected to the TTN server. Any new devices on the TTN server are automatically updated on the dashboard, eliminating the need for users to manually add devices. Secondly, the user is able to select the data for the various strain configurations that they are interested in tracking since the flexible strain sensor gathers both axial strain and bending strain in a switching way. Because the flexible strain sensor made by different manufacturers will cause the GF value to float due to their differences in terms of production capacity, it can be seen that the dashboard provides the user the option of entering the desired GF value and the Poission Ratio. This is done so that the user can calculate the measured strain more accurately by inputting the calibrated GF value. The user also has the option of activating or deactivating the function of data offset. This is because, in a real-world monitoring situation, the measurement cannot be guaranteed to start completely from 0 due to ambient noise and the components of the hardware itself. The data on the primary

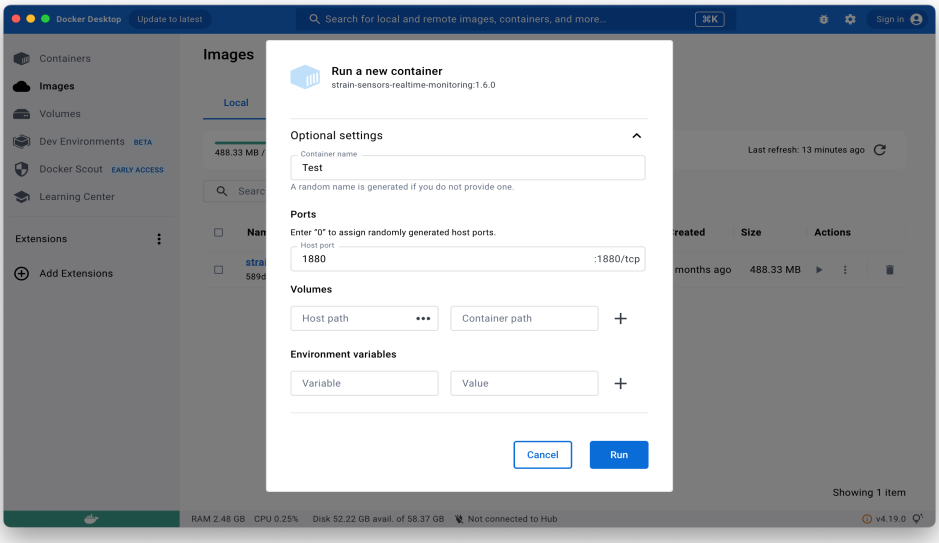

(a) application installed on local

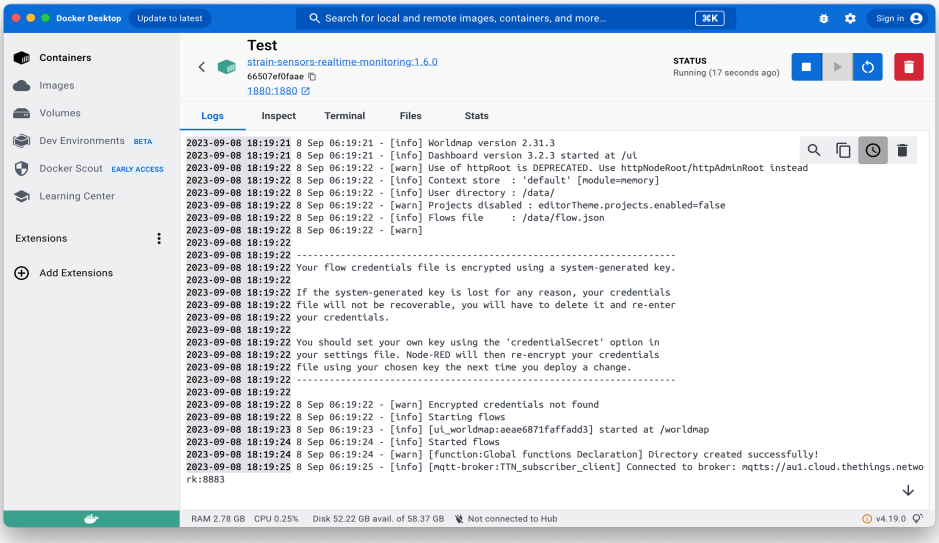

(b) application running status

Figure 5.6: Docker Desktop interface

page of the dashboard is displayed primarily through the use of line charts and gauges. This is due to the fact that line charts are able to demonstrate the pattern of data within

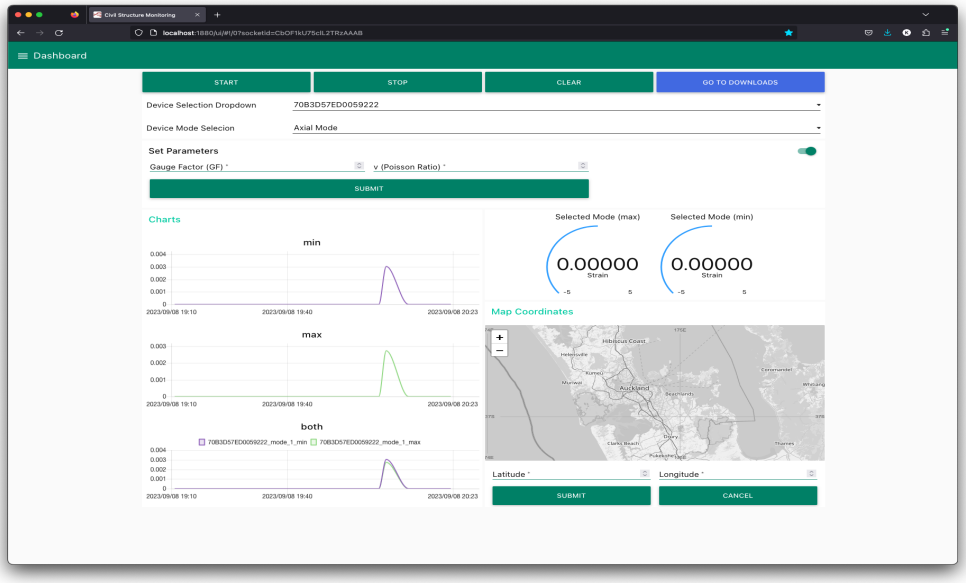

Figure 5.7: The designed dashboard main interface

a specific period of time and are excellent for demonstrating abnormal changes in data. Guage offers a depiction of value that is simpler and easier to understand. Finally, the dashboard also provides a map to show the actual installation location of the gateway device.

This system is different from the standard dashboard in that it additionally possesses the capability to download and store data. Although TTN servers also provide data storage, it needs to charge for cloud data storage like other cloud storage platforms. In order to reduce the cost of the whole system as much as possible, the data storage function was developed in the dashboard system when the system was designed. Figure 5.8 demonstrates the download function. Data stores start to gather locally as soon as the user begins to run the application; however, these data stores are not visible until the user chooses a device from the home page. The data stored by default is the same as the data that is published on the TTN server. The programme will first check to see if the offset function is applied when the user selects the file for download. If the offset

function is applied, the programme will apply the offset function to all of the data in the file and download the offset data for the user. If the offset function is not applied, the programme will not apply the offset function and will only download the original raw data. If the user has submitted the GF and Poisson ratio in the main interface, they could click the "Convert Raw Data" button in the download interface. And the system will create a new folder to keep the file containing the calculated data after it has finished calculating the original data based on the value that was submitted. Additionally, the download interface provides the user with a preview of the file.

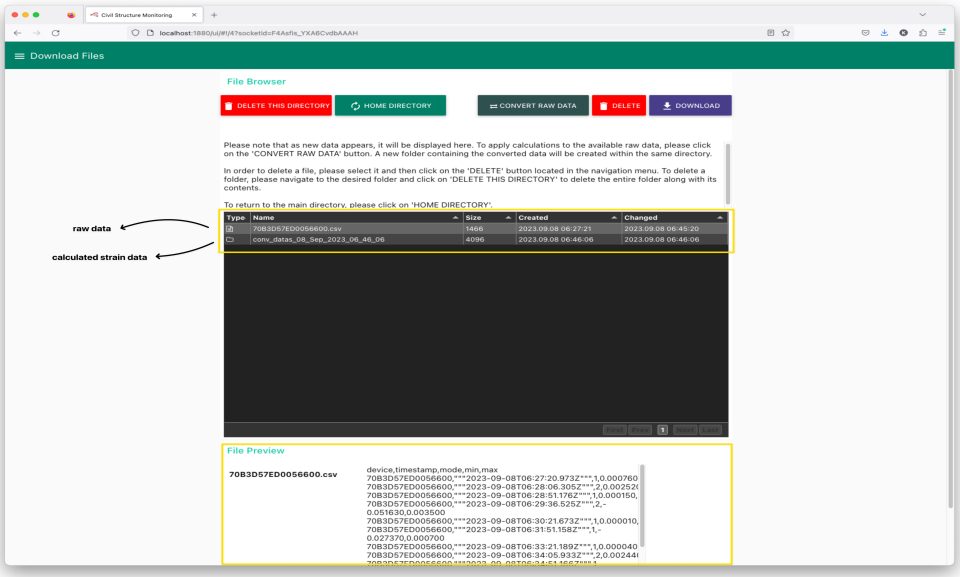

Figure 5.8: The designed dashboard download function interface

5.4 Summary

In this chapter, the focus is mostly on introducing the data visualisation application that was developed for the LoRaWAN-based wireless sensor system. Despite the fact that there has been a significant amount of progress made in the development

of IoT devices and applications, the deployment and actual implementation of many systems are highly complex and fraught with the issue of excessive cost. As a result, the process of developing and deploying application devices within the IoT remains a challenge. The visualisation application that was developed by this research institute has no additional costs in data transmission and storage; its local storage and operation make it efficient and highly secure; and the programme takes advantage of Docker to substantially simplify the process of deployment for end users. In addition, the application transmits data to the TTN server mostly through the implementation of the MQTT protocol. The IoT devices and the TTN network server are integrated so that data can be visualised in nearly real time. This system is also capable of automatically establishing communication across different LoRa nodes on the TTN server without the need for point-to-point integration and possesses the capability to process events simultaneously using multiple threads of processing. This also gives the end user the ability to respond instantly whenever anomalous data is generated (or whenever an event takes place).

Chapter 6

Experimental Validation of Flexible Strain Sensors and LoRa-based Wireless Sensor System

6.1 Introduction

This chapter focuses primarily on introducing the experimental verification of the performance of the designed flexible strain sensor and wireless sensor system, as well as the findings of the structural component health monitoring within the SHM framework. The testing platform includes cyclic loading tests on a full-scale precast reinforced concrete (RC) frame structure in the laboratory to evaluate the efficacy of flexible strain sensors to detect structural damage and assess the state of the building structure. Another goal was to assess the performance of the system that was built in order to rapidly evaluate the strain fields of crucial structural components when SHM applications are used. In addition to this, the functionality of a LoRa-based

wireless sensor system network that was designed for long-term monitoring in an outside environment was tested and evaluated.

In order to accomplish these goals, two distinct periods of testing were conducted. In the first step of the process, multiple cyclic loading experiments were performed in the lab on a full-scale precast concrete frame structure. At the same time, the flexible strain sensor that was built was put on the major structural components of the structure so that it could monitor two separate strains. Increasing the load that is being exerted on the structure at the same time allows for the simultaneous monitoring of any localised damage, such as cracks, that may occur in the structure's essential components. The second experiment is a bending test, mainly to evaluate the overall performance of the developed flexible wireless sensing system under bending conditions.

Furthermore, the third test is to evaluate the performance of the established LoRa network. The test site is an existing medium-rise building (the WZ building at Auckland University of Technology) to conduct remote testing of the developed LoRa wireless system. The LoRa network management system is deployed on fixed levels, and LoRa nodes are tested on the fourth to 12th floors of the building to evaluate the system's dependability and stability over long distances.

6.2 Full-Scale RC Frame Cyclic Loading Test

In order to evaluate the monitoring ability of the proposed flexible strain sensors on the shear behaviour of the RC frame with shear critical beam, two full-scale one-story RC frames with shear critical beam, shown in Figure 6.1, was subjected to testing under the condition of increasing lateral load applied to the top of the column. This was done so that the monitoring potential of the developed flexible strain sensors could be

analysed. It is the purpose of the frame to concentrate the shear failure on the principal components of the structure. Due to the limitations of the laboratory, a single-story frame structure has been implemented here rather than a multi-story frame structure. Despite the fact that single-story frames are more uncommon than multi-story frames, nevertheless, the test delivers an important contribution to the inadequate available information for monitoring the strain field anomalies that are induced by shear critical frame testing under lateral loads.

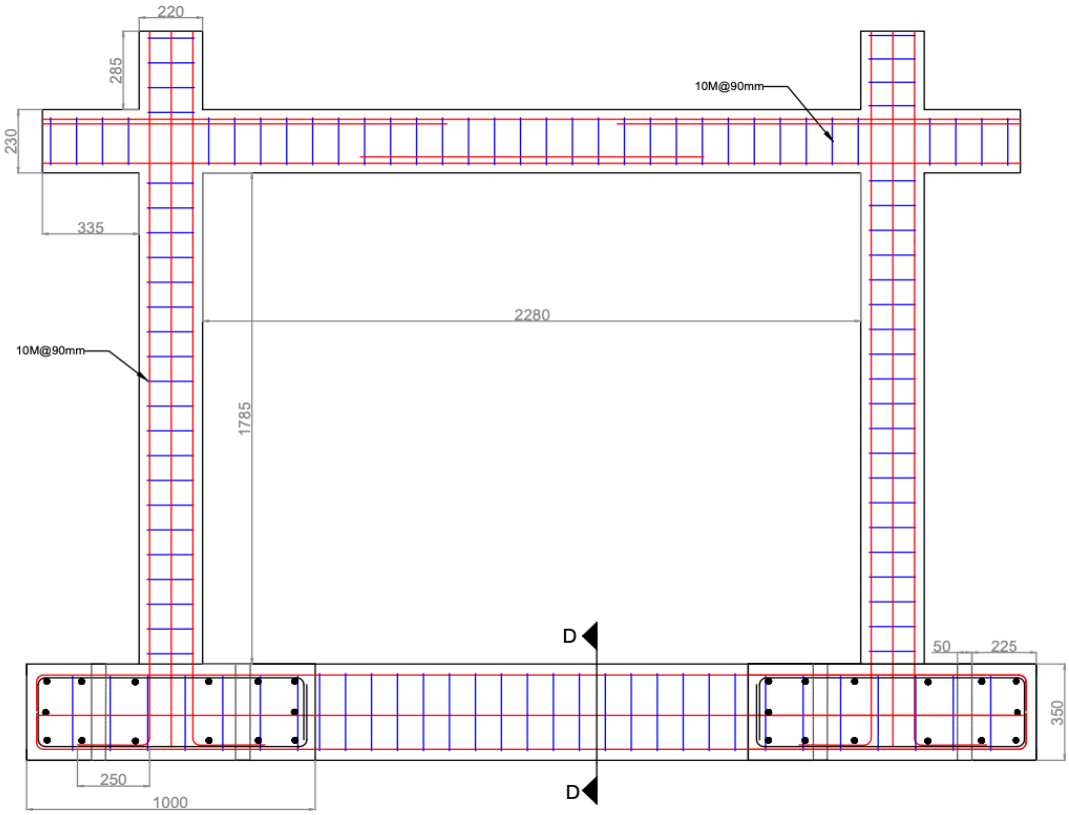

Figure 6.1: RC frame geometry

One of the primary goals of this investigation is to provide direct monitoring that is quick, reliable, and cost-effective for monitoring existing buildings. As a result, the experimental structure that was ultimately chosen had to demonstrate that it was capable of fulfilling the design requirements of a significant number of existing RC structures in

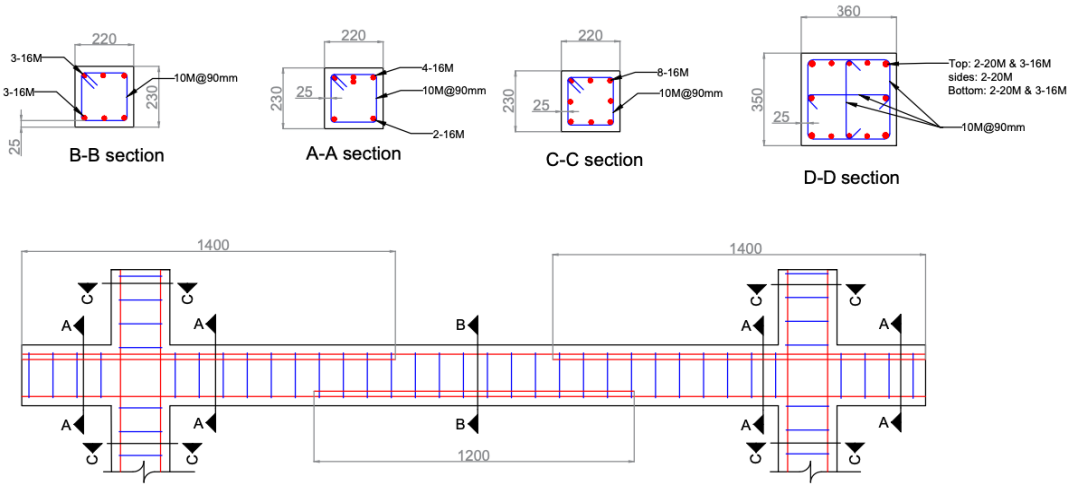

(a)

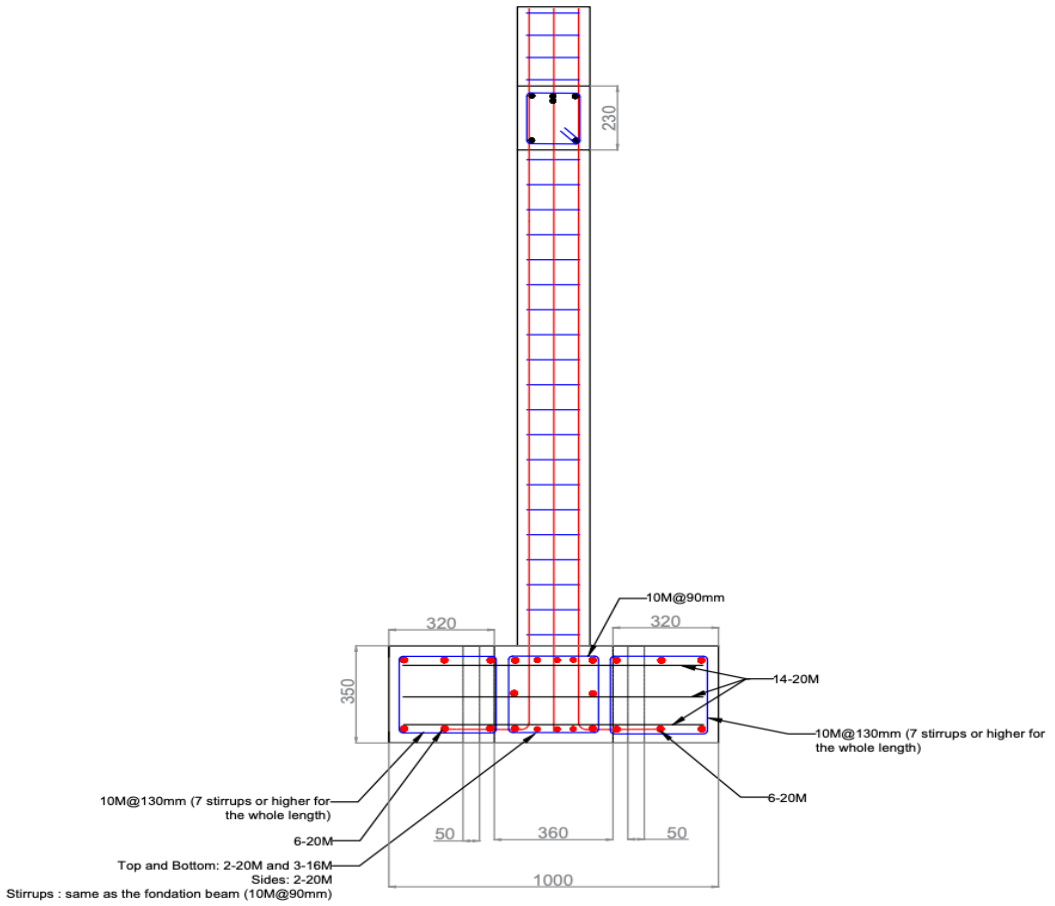

(b)

Figure 6.2: RC frame reinforcement (a) top view (b) side view

New Zealand.

The centre-to-centre span of the frame design is 2500 millimetres, the height is 1900 millimetres, and the overall height is 2365 millimetres. The base of the frame is a low strength concrete base that measures 400 millimetres. Beams with a width of 220 mm and a height of 230 mm; columns with a width of 350 mm and a height of 360 mm. The material that was utilised in the construction of the concrete frame was subjected to preliminary laboratory testing, during which it was determined that the material possessed a compressive strength of 20 MPa. Furthermore, in order to provide a more accurate representation of the low-strength concrete frame, the design of the frame takes into account the relatively low compressive strength value of the concrete. In addition to this, the quantity of transverse steel bars in the frame column and the design of the spacing between the adjacent steel bars are also crucial. The transverse steel bars produce a specific confinement on the concrete and prevent the longitudinal steel bars from buckling. The structural design of the RC frame that was tested is, in general, mostly based on the design concept of strong columns and weak beams that was first established in the New Zealand Concrete Code 1982 (NZS 3101, 1982). It is possible to adapt the structure to the significant number of reinforced concrete (RC) buildings that were constructed in New Zealand prior to the 1970s. The structure was developed to fulfil the requirements of the SHM system for practical applications. Due to the age of these structures, many of them do not comply with the most recent design code criteria.

The RC frame experiment is being conducted in the Structural Laboratory of Auckland University of Technology. Figure 6.4 presents the installation of the RC frame. The concrete material that was used for the experiment has a maximum aggregate size of 10 mm and consists of two different compressive strengths. The concrete compressive strength of the beams and columns is low (about 20 MPa), as indicated above; however, this criterion does not need to be met for the foundation. The general frame is built

to benchmark existing ancient New Zealand buildings, and while this requirement is necessary for the beams and columns, it is not required for the foundation. Because of this, the foundation components of the tested RC frame was built independently from one another. Additionally, the concrete used in both foundations has a high compressive strength of 30 MPa, and the primary portion of the structure is joined to the foundation using drossbachs (Figure 6.3).

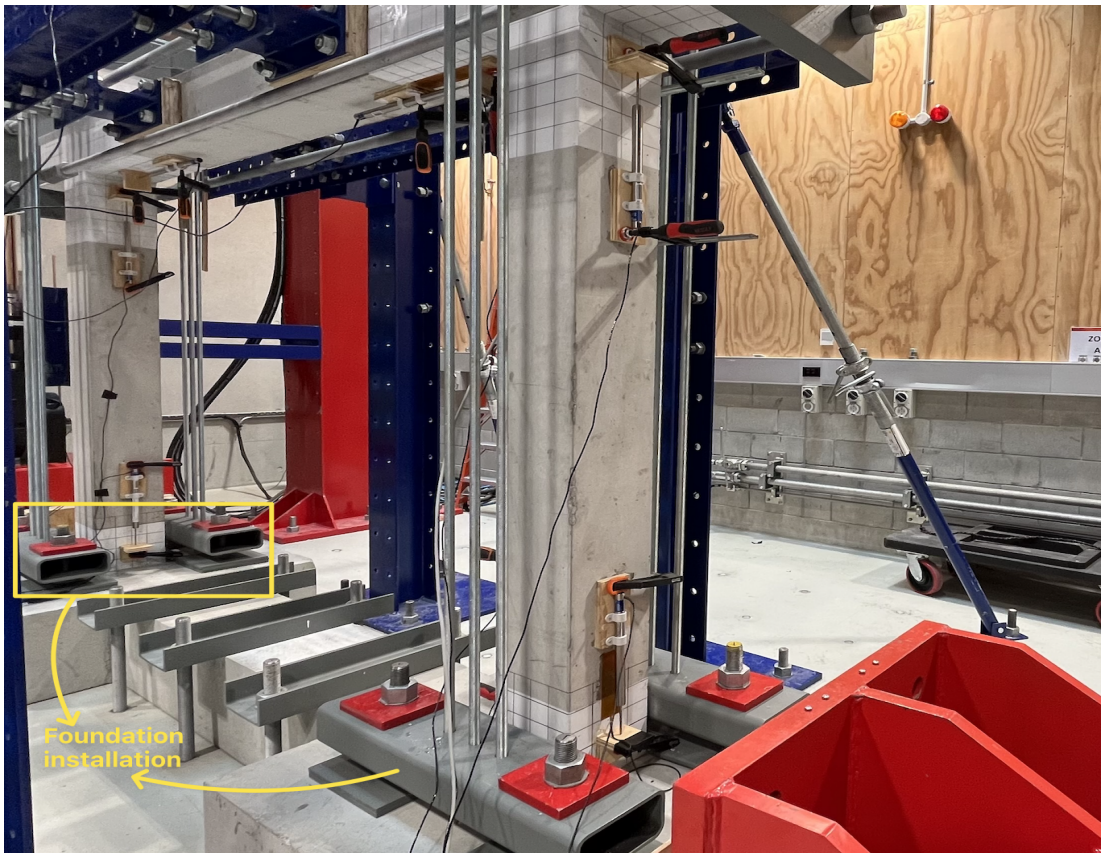

Figure 6.3: RC frame foundation installation

6.2.1 Experimental Sensors Setup

In the experiment, in order to validate the capability of the flexible strain sensor that was designed to measure the damage to the primary elements of the structure, the flexible strain sensor was placed on the surface where the potential damage (i.e., the

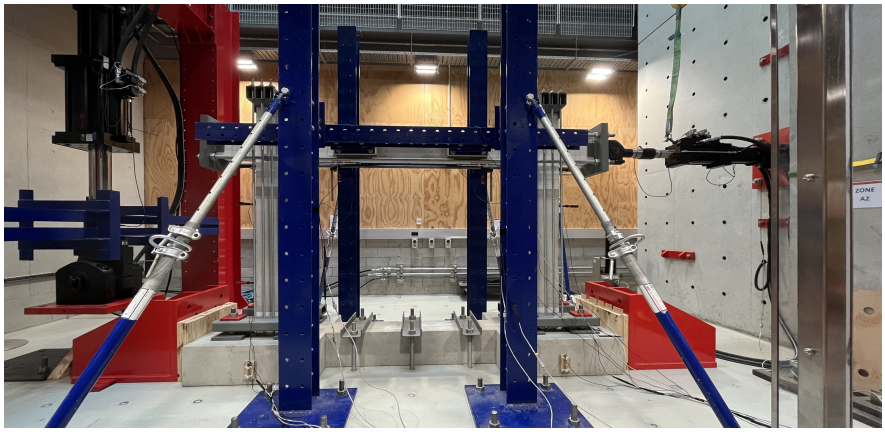

(a)

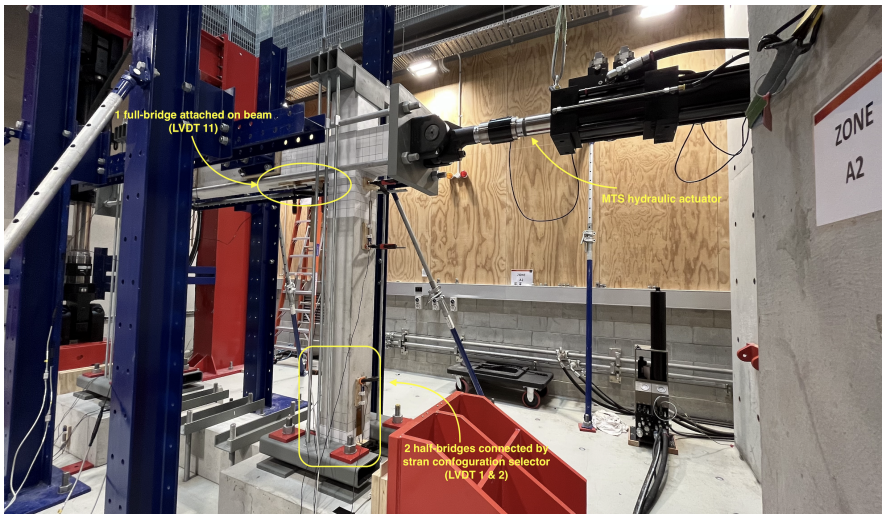

(b)

Figure 6.4: The RC frame installation (a) front view (b) side view (c) back view

more fragile section) occurs; specifically, the surface where the concrete cracks occur. A full bridge sensor was mounted close to the beam-column joint, as can be seen in Figure 6.6. There are two half-bridge sensors that were installed on both sides of the right column, and they are connected by the strain gauge configuration selector. These sensors can be found near the bottom of the right column. Additionally, in order to offer greater accuracy and precision and a multidimensional reference for the experiment, 14 linear variable differential transformers (LVDT) were installed. In addition to that, the rightmost end of the beam was outfitted with a draw-wire displacement sensor, which

performs the function of a baseline for the lateral displacement that was brought about by the load that was applied to the frame.

Figure 6.5 demonstrates the location of all sensor installations along with the frame setup. During the course of the experiment, an MTS hydraulic actuator was utilised in order to provide a load that was carried horizontally in the opposite direction from the construction of the frame. Hydraulic actuators are capable of applying loads of up to 1000 kN and have a static stroke of up to 500m at their disposal. The cyclic loads are gradually applied to the transverse frame beams by the hydraulic actuator as it moves. In each loading step, LVDTs were used to examine the vertical displacement of the beam in addition to the transverse displacement of the column.

Flexible strain sensors were utilised as the direct sensing measurement device to capture strain information and monitor the performance of the structural members in order to determine the strain value on the concrete surface of the beam and column, respectively. The LVDT that was placed in close proximity to the flexible strain sensor was used to measure the accuracy of the sensor by comparing it with the data that was acquired regarding the strain. The LVDT was attached to the base of the RC frame so that it could measure any bumps that could occur during the experiment. In addition, the column of the frame is installed with 6 prestressed rods, each of which has a capacity of 220 kN; this results in the frame being subjected to a total vertical force of 440 kN. The lateral load is applied by a 250kN MTS rod with a 125mm process in this experiment.

6.2.2 Cyclic Testing and Strain Field Monitoring

The primary purpose of this section is to present the findings of experiments using quasi-static cyclic loading as well as the data acquisition of flexible strain sensors. The loading procedure is presented in Figure 6.7. During the period of the experiment,

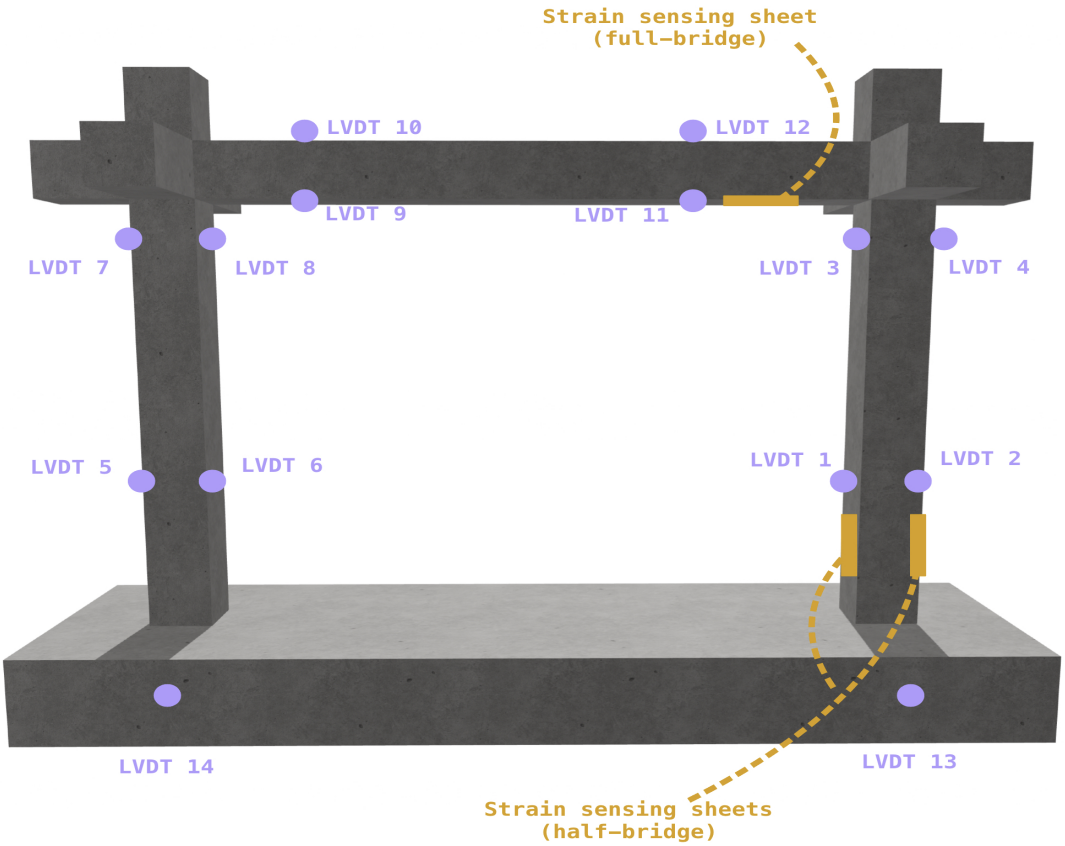

Figure 6.5: All sensors installation on the RC frame

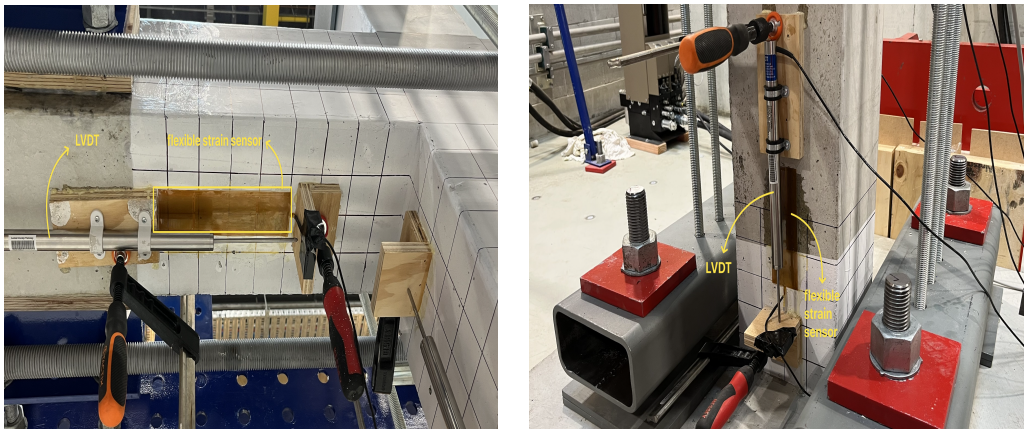

(a) (b)

Figure 6.6: Flexible strain sensors installation (a) 1 full-bridge installed on beam with LVDT 11 (b) 2 half-bridges connected as 1 full-bridge installed on column with LVDT 1 and 2.

the framework was subjected to progressive and cyclic loading that was conducted up to a drift of 2.5% (Δ52.5mm). The push-pull rod was being evaluated using the displacement mode, and the loading rate being used was 0.5mm/s. Each drift level is repeated for a total of three cycles, with the exception of the third cycle, during which the highest value in the direction of the pull is maintained to the right. As shown in Table 6.1, in the experiment, the reinforced concrete frame was gradually loaded from an initial drift of 0.25% (5.3mm) to a drift of 1.25% (26.3mm) in 0.25% increments with each test.

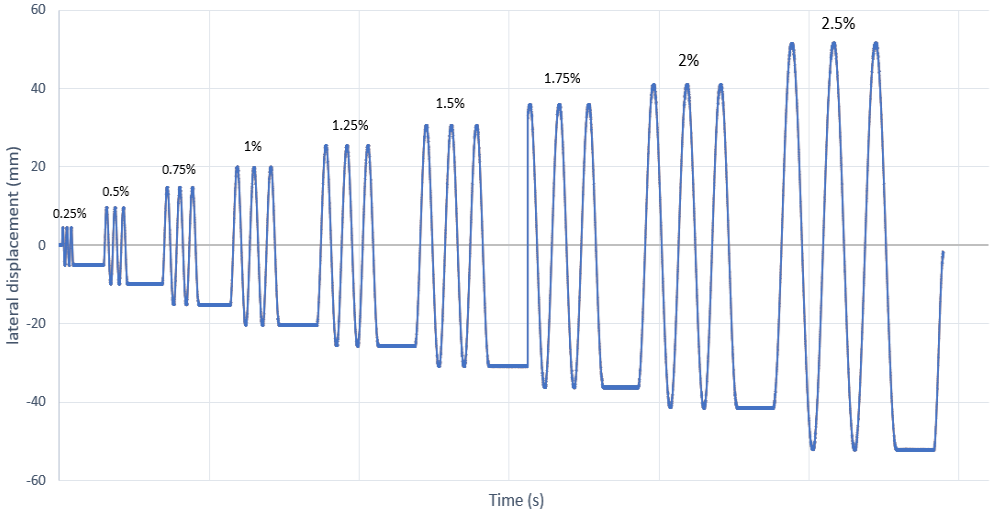

Figure 6.7: Lateral loading protocol of the RC frame

Table 6.1: Cyclic Test Procedure

Test Cycle	Drift (%)	Lateral Displacement (mm)
1	0.25	5.3
2	0.50	10.5
3	0.75	15.8
4	1.00	21.0
5	1.25	26.3
6	1.50	31.5
7	1.75	36.8
8	2.00	42.0
9	2.50	52.5

In order to observe and detect the change in crack morphology of the RC frame during the experiment, the following four distinct crack categories have been preset according to the crack width Cw, and the corresponding cracks occurring on the frame have been noted according to the classification:

1. Cw < 0.2mm: Green mark - subtle cracks on shallow surfaces
2. 0.2mm ≤ Cw < 1mm: Blue mark - cracks are apparent; however, they are quite narrow and small
3. 1mm ≤ Cw < 2mm: Red mark - the presence of local squeeze cracks caused by the overlying layer of concrete
4. Cw ≥ 2mm: Black mark - the surface layer flaking off the concrete, which results in apparent breakage

Cracks appear in RC frames when the lateral drift approaches 0.5%, 1%, 1.5%, and 2%, as shown in Figure 6.8. It can be seen that during the initial phase of the 0.5% drift process, the RC frame only exhibited small flexural cracks at both the top and bottom of the column. When the drift grew to 1%, the number of cracks as well as the width of the cracks increased. It is important to note that the cracks in the column were more evident than the fractures at the two ends of the beam, but in the process, the width of the cracks was less than 1mm (green and blue marks). When the transverse drift of the frame reaches 1.5%, more noticeable cracks that are larger than 1mm occur on the top and bottom of the frame columns (marked with red), and some narrow cracks are seen on the diagonal of the beam-column connection area (marked with green). As the drift increased to 2%, the bottom of both columns revealed quite visible concrete breakage greater than 2mm, and big flexural cracks (black marks) emerged on the beams.

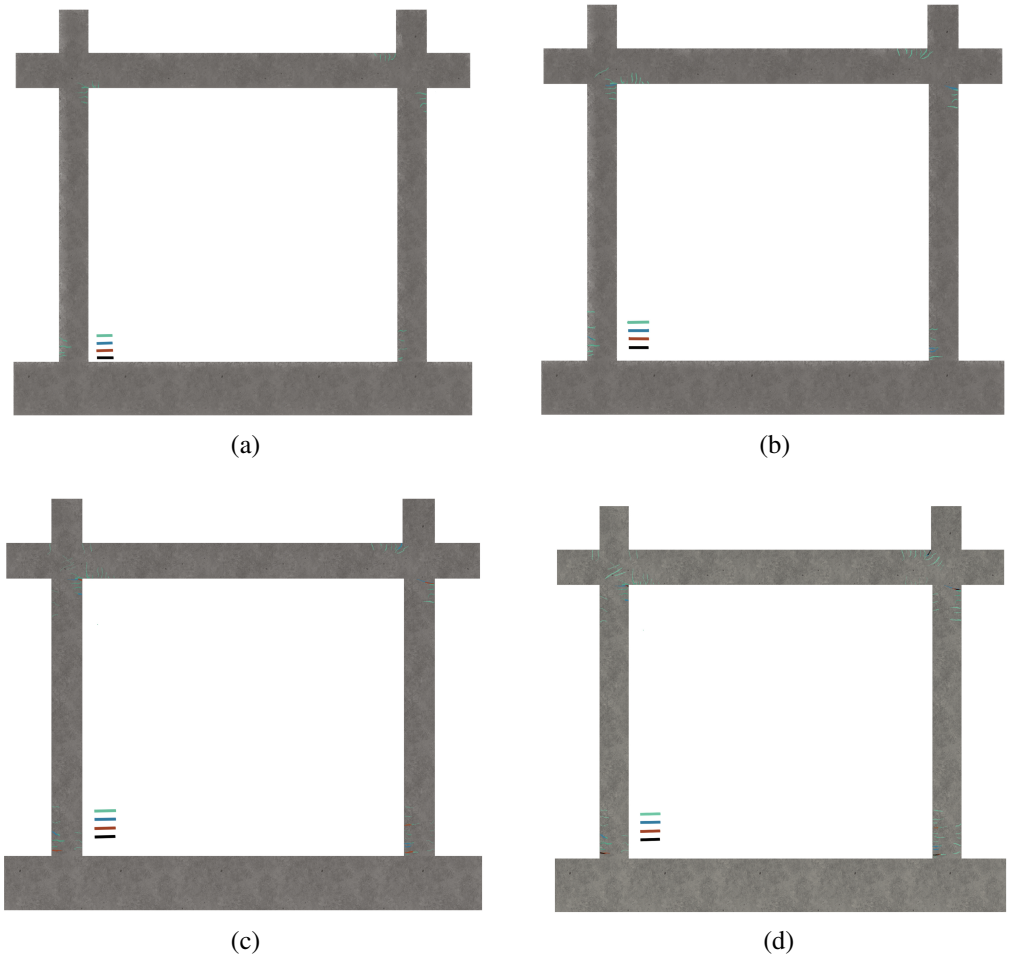

Figure 6.8: Crack patterns of the bare frame in different drift levels (a) 0.5% drift (b) 1.0% drift (c) 1.5% drift (d) 2.0% drift.

6.2.3 Hysteretic Response and Load Capacity

The lateral load-displacement relationship of the frame is demonstrated in Figure 6.9 (the drift up to 2.5%—52.5 mm). The lateral load-drift relationship of the frame is demonstrated in Figure 6.10 (the drift up to 2.5%—52.5 mm). Figure 6.11 and Figure 6.12illustrates the cracking of the RC frame surrounding the area where the flexible strain sensor was installed with different drift levels. These figures indicate very clearly that the mode of failure of an RC bare frame is primarily concentrated at the end of the column and beam, where it forms flexural cracks. This is in accordance with the

assumption that was brought up prior to this, which states that flexible strain sensors ought to be positioned in the most vulnerable locations of structural components. When the drift reaches 1.5%, it can be seen from the pattern of cracks that the framework starts to cause relatively considerable damage.

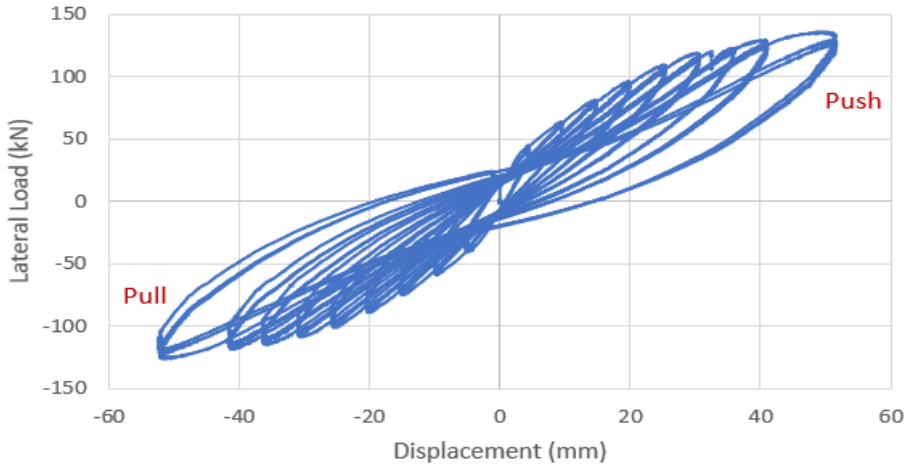

Figure 6.9: Lateral load-displacement hysteresis of RC frame

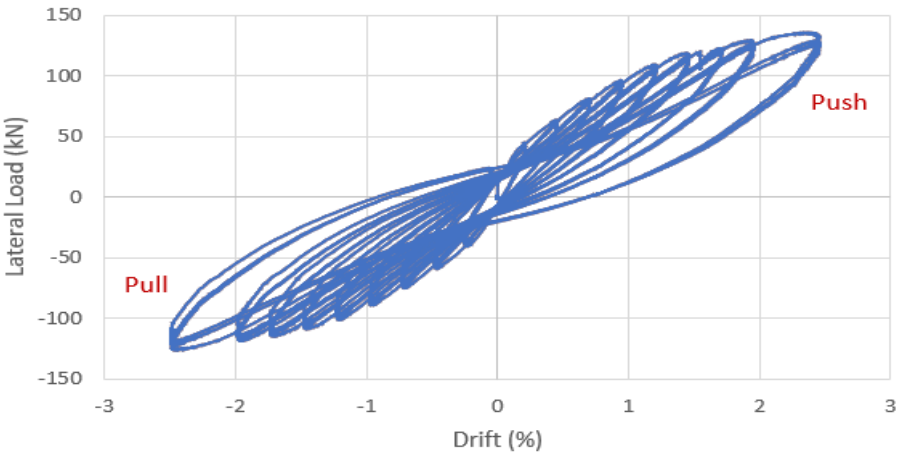

Figure 6.10: Lateral load-drift hysteresis of RC frame

As was indicated earlier, by monitoring the crack creation of the RC frame, it was discovered that in the process of drift approaching 1.5%, the frame examined had more noticeable cracks larger than 1mm (marked in red). As can be seen from the

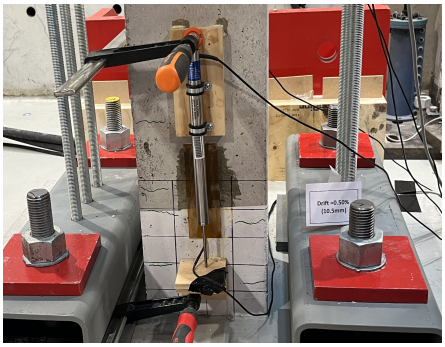

(a) 0.5% drift - flexible strain sensors on column

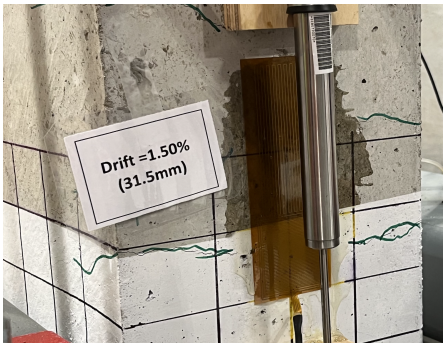

(b) 1.5% drift - flexible strain sensors on column

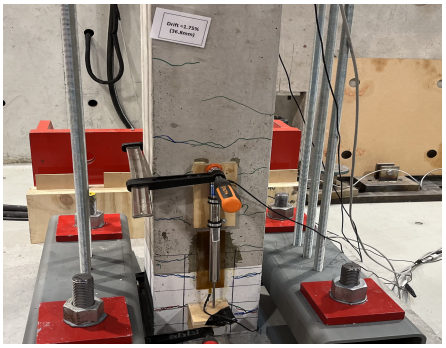

(c) 1.75% drift - flexible strain sensors on beam

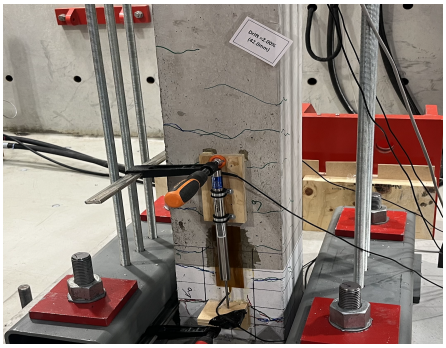

(d) 2.0% drift - flexible strain sensors on beam

Figure 6.11: Crack patterns in different drift levels (half-bridge flexible strain sensors)

strain measurements monitored by the flexible strain sensor attached at the bottom of the frame column, as shown in Figure 6.13(a), the sensor detects a considerable change in the strain field around it when the frame drift approaches 1.5%. When the drift reaches 1.5%, as shown in Figure 6.14, cracks begin to appear around the flexible strain sensor. Because the flexible strain sensor is placed at the bottom of the column, which is the location where the cracks first occur and are most dense (the weak region of the structural element), the measured strain is greater after the obvious cracks are found. This is because the bottom of the column is the area where the cracks are most concentrated. In addition, because the cracks in the frame have been continuously becoming larger, the strain field continues to remain in a very high strain value range in comparison to what it was like before the drift of less than 1mm

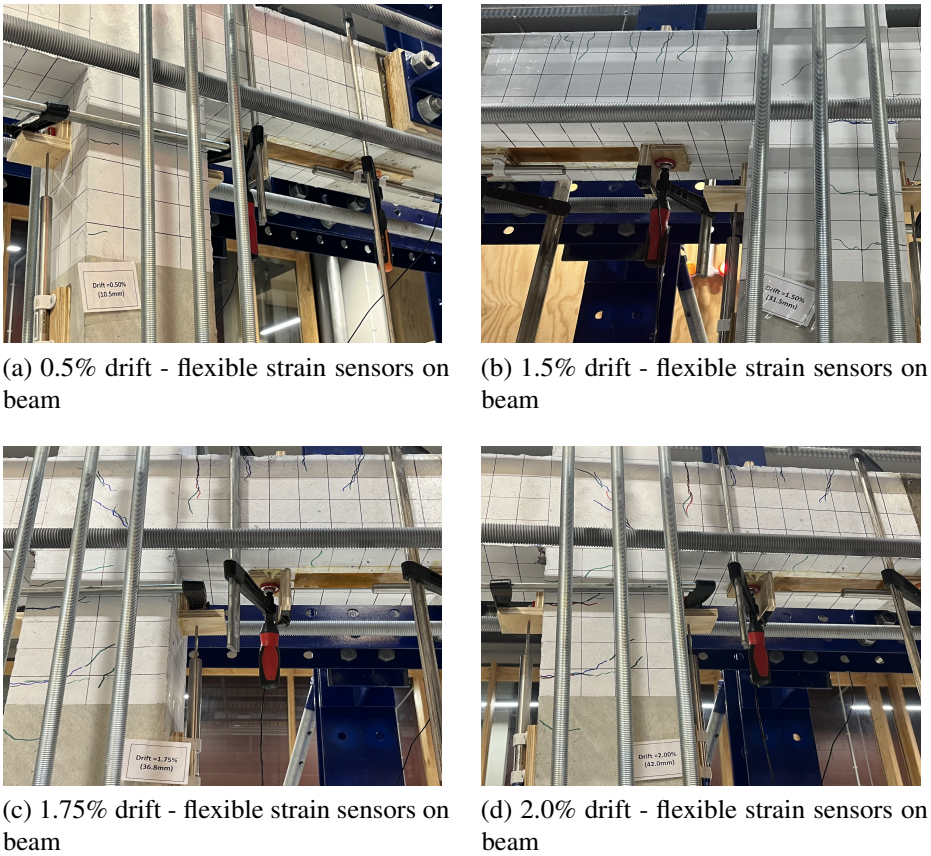

(a) 0.5% drift - flexible strain sensors on beam

(b) 1.5% drift - flexible strain sensors on beam

(c) 1.75% drift - flexible strain sensors on beam

(d) 2.0% drift - flexible strain sensors on beam

Figure 6.12: Crack patterns in different drift levels (full-bridge flexible strain sensors)

cracks was identified. The specific strain reading obtained by the flexible strain sensor is displayed in Figure 6.13(b). This reading was collected just prior to the detection of considerable damage. Within the scope of this study, it is of utmost importance to investigate the levels of strain that can be sustained by the critical components of the full-scale structures. The objective of the study is to gather valuable strain information on the growth of structural crack damage in order to facilitate the speedy identification of any potential damage to critical structural members.

Figure 6.17 demonstrates the findings obtained from a half-bridge flexible strain sensor that was attached to both sides of the bottom RC frame. The rate of relative resistance change of the flexible strain sensor is shown in Figure 6.17 (a), which illustrates the

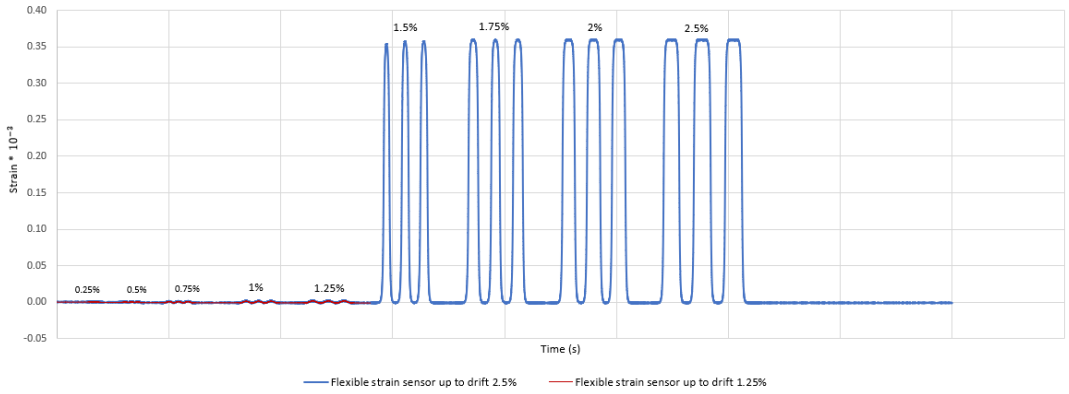

(a) drift up to 2.0%

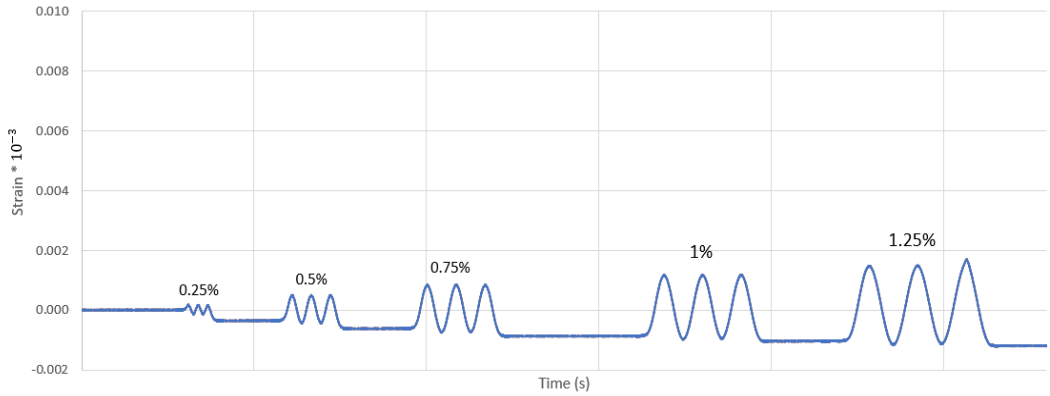

(b) drift up to 1.25%

Figure 6.13: Strain measurements collected by the flexible strain sensor - column

results of the first cycle test. During the entire cyclic loading procedure, it is clear that the response time (loading) and recovery time (unloading) of the flexible strain sensor are both fairly quick. The resistance increases and decreases almost in sync as the sensor deforms. Figure 6.17 (b) illustrates how sensitive a newly developed flexible strain sensor is when subjected to cyclic testing. It proves that the GF value obtained in the calibration test conducted in Section 5 of Chapter 3 is accurate. The value of GF that was achieved through the calibration test is 2.15, while the value of GF that was obtained through the cyclic test is 2.17. Additionally, it can be seen that the developed flexible strain sensor is still capable of maintaining acceptable linearity despite being subjected to high-strength cyclic loading. Previous research has demonstrated that

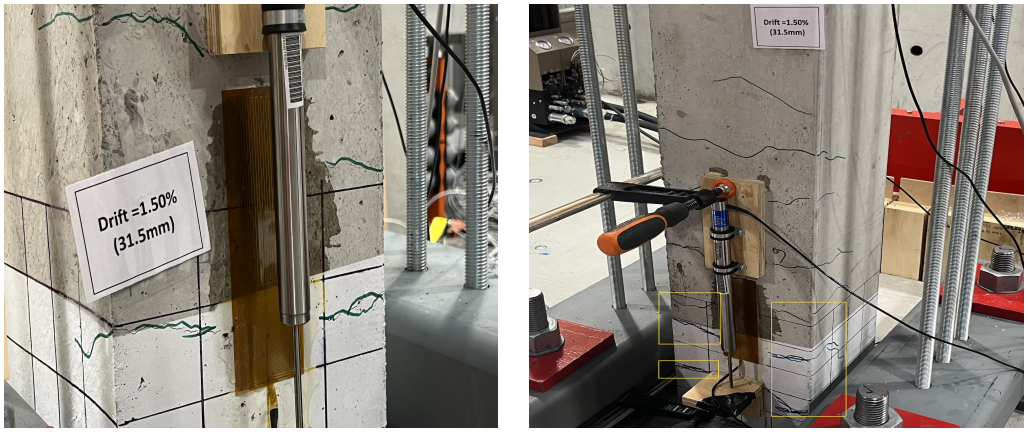

(a) (b)

Figure 6.14: Column damage condition surrounding the flexible strain sensor - drift 1.5%

linearity decreases when strain sensors are sensitive to changes in strain. The flexible strain sensor developed in this research differs from the research results in that it not only has high sensitivity and can detect strain field anomalies, but it also has very low hysteresis (as shown in Figure 6.17 (a), during cyclic test load, the resistivity during loading and unloading is almost the same).



Figure 6.15: Cracks pattern on the beam (full-bridge flexible strain sensor) at 2%drift

The findings of the tests performed on a full-bridge strain sensor that was positioned on the inner surface of the beam are shown in Figure 6.16. The outcomes are different from

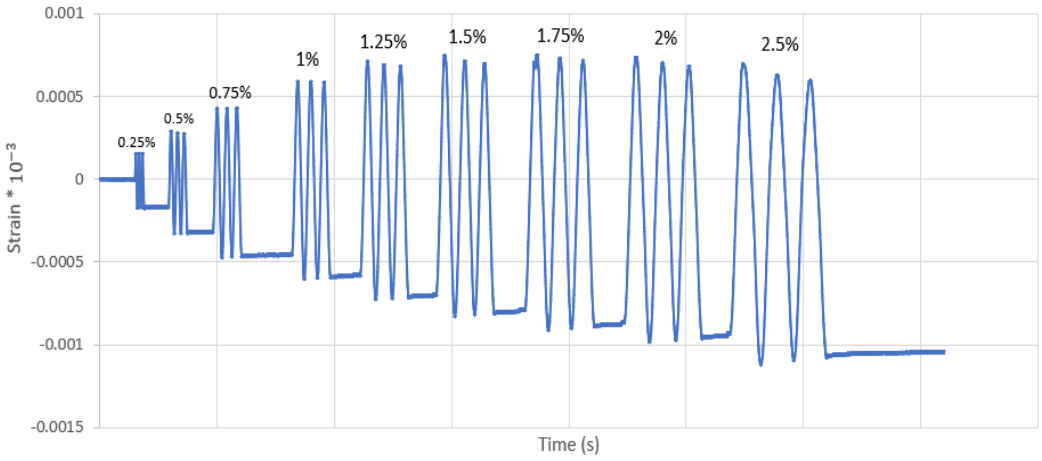

Figure 6.16: Strain measurements collected by the flexible strain sensor - beam

what was observed with the sensors installed on the frame columns. Throughout the entirety of the cyclic loading test, it was observed that no visible strain field anomalies brought on by cracks located around the column were seen. This conclusion is supported by the photo presented in Figure 6.15. It is clear from inspection of the RC Frame beam that there were no obvious cracks (cracks that are greater than 1 mm) around the full-bridge flexible strain sensor at any of the drift levels. The majority of the fractures can be found in the beam's upper surface section and the column's topmost section, respectively. As a result, there aren't any noticeable strain field abnormalities that may be detected. This indicates that direct damage monitoring as part of the SHM framework needs to be carried out as close as feasible to the region that could potentially sustain damage. This is one of the most difficult aspects of assessing the structural health of a building. The performance of a full-bridge flexible strain sensor is depicted in Figure 6.17, which demonstrates the variation in the relative resistance rate of the sensor as a function of time (during the first cyclic loading cycle). Figure 6.17 (a) demonstrates that, similar to the developed half-bridge flexible strain sensor, the response time and recovery time of the sensor are quick, the change in resistance is proportional to the change of the sensor, and the resistivity remains the same during loading and unloading.

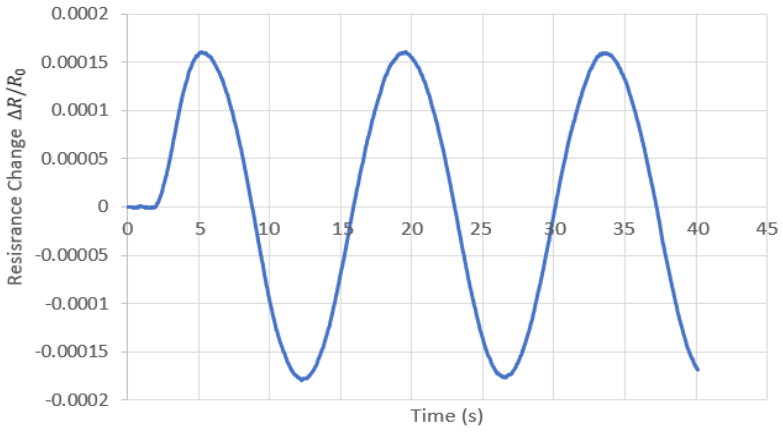

(a) Relative resistance change during the first cycling

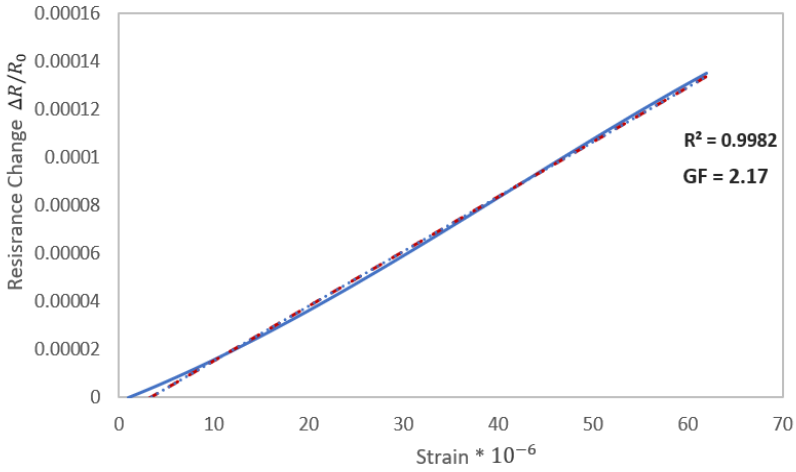

(b) Flexible strain sensor linearity and sensitivity

Figure 6.17: Flexible strain sensor performance during cyclic testing - on column

In the prior calibration test, the results that were obtained were quite similar to those shown in Figure 6.17 (b), indicating that there is no substantial difference between the two sets of findings about the sensitivity of the sensor.

In conclusion, it was determined from the cyclic loading studies carried out on the full-scale RC frame that the proposed flexible strain sensors have great performance, high sensitivity, excellent linearity, and low hysteresis. These qualities make it possible for the sensor to monitor the strain field in a manner that is accurate and linear. It is

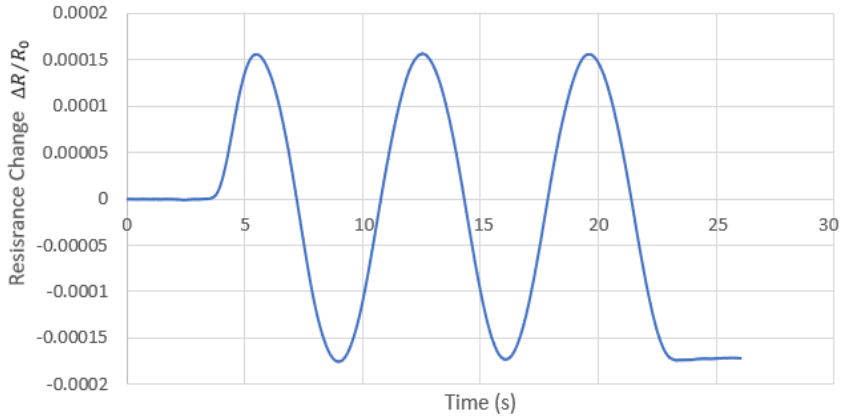

(a) Relative resistance change during the first cycling

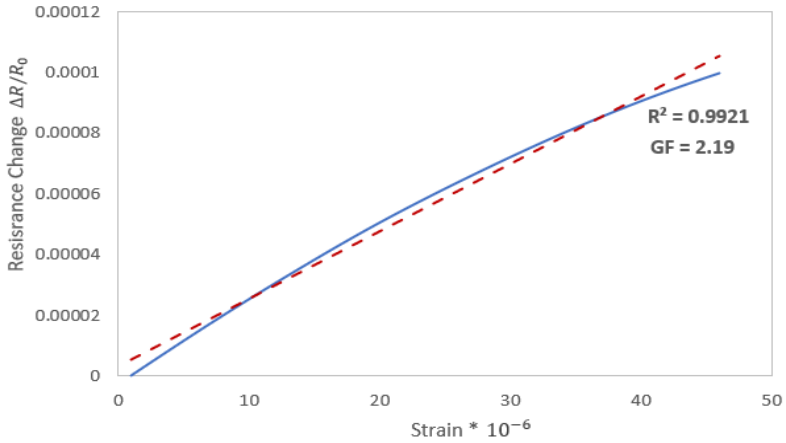

(b) Flexible strain sensor linearity and sensitivity

Figure 6.18: Flexible strain sensor performance during cyclic testing - on beam

possible to monitor the strain field condition of the full-scale structure using only one set of sensors for each structural element, which provides a low-cost sensor system for SHM local direct monitoring applications.

6.3 Full system Lab Bending Test

Sensing strain is an essential part of advanced engineering technology, and it plays an essential part in the monitoring of structural health, the detection of deformation, and the maintenance of various levels of structural integrity. There has been a recent increase in interest in the exploration of flexible strain sensors, which can be incorporated into wearables, soft robots, and other applications that demand consistency and adaptability. However, the performance of these sensors, particularly under conditions of bending, is still a subject of substantial research in the field of SHM.

This section discusses a three-point bending test using a Universal Testing Machine (UTM) to assess the sensitivity, performance, and dependability of the proposed flexible strain sensor system under bending conditions. The objective is to perform a comprehensive and cohesive examination of all the software and hardware systems discussed in Chapters 3, 4, and 5.

The test results provide important insights and an evaluation of the many uses for flexible strain sensors in the context of SHM, in addition to pointing out any potential limitations that they might have.

6.3.1 UTM Bending Test Setup

The bending test that was carried out at the AUT Structural Lab. The configurations and processes that are presented in this section are an essential component of the analysis of the results of the three-point bending test, with a particular emphasis on the performance evaluation of strain gauge sensors. The test is designed to fully evaluate the function and reliability of the strain gauge sensor under controlled bending conditions. Test

sample is mild steel with the 0.3 Poisson's ratio. The total length of the test specimen is 750mm. There is a distance of 340 mm between the left bottom support and the loading point.

As a result of the fact that the AUT laboratory is situated one level below ground, there are major constraints that prevent the potential LoRa-based system from being tested in its entirety. It is anticipated that the underground laboratory, which is constructed out of steel and concrete, will provide a significant obstacle to the transmission of information and communication systems. To ensure the continued effectiveness of the bending test in the event of a signal disruption, two experimental setups were created. One was established using NI DAQ to record the dataset. Another one was established by employing the LoRa-based wireless system to evaluate the full functionality of all suggested software and hardware systems.

As can be seen in Figure 6.19, the strain gauge sensor is attached to the specimen loading point on the right-hand side of the equipment. Each strain gauge's original dimensions are 16 mm across and 56 mm in length. Two half-brigde flexible strain sensors were used in this experiment. The specimen is sandwiched between two half-bridge flexible strain sensors, one of which is situated above it and the other underneath it. Then it is connected by the designed strain configuration selector to form a full bridge configuration to measure the bending strain. The strain configuration selector includes an interface to connect the sensor to the NI DAQ system via RJ50.

Figure 6.20 demonstrates an experimental setup designed to evaluate the functionality of the full system in its entirety. The LoRa gateway is connected to the power source located at the rear of the UTM. Because the flexible cable has a limited length, the LoRa infinite node is placed in close proximity to the flexible strain sensor, which is situated on the right side of the specimen. The ESP microcontrol processor's data storage system

is located adjacent to the LoRa wireless node. To validate the functionality of the developed software system designed for real-time data storage and retrieval, a computer was used to monitor the collected data in real-time using the integrated Bluetooth feature offered by the data storage system during the experiment.

The bend test was carried out with the flexible sensor installed in such a way that it is perpendicular to the longitudinal axis of the specimen. This configuration enables the sensor to measure the amount by which the length of the specimen changes. The width of this long gauge was originally 20 mm, and the length was originally 100 mm. It consists of 20 traces with a total trace length of 2000 mm. In contrast, the shorter gauge is primarily employed for the purpose of temperature compensation. Its original length is 50 mm, its width is 40 mm, and it consists of 50 traces with the same total trace length of 2000 mm. In the first experiment, UTM was set to run at a displacement rate of 5 mm/min until a deflection of -15 mm was achieved.

The second bending test was set up as shown in Figure 6.20, in order to evaluate the performance of the developed LoRa-based sensor system under the bending condition.

6.3.2 Bending Test Results

The performance of the strain sensor shows a consistent linear response to the applied strain in the initial set of bending tests. The linearity of the relationship between strain and relative resistance change, as shown in Figure 6.21, is evidence that the strain sensor possesses both a high degree of sensitivity and an extremely low degree of hysteresis in its measurement. When a sensor is linear, it signifies that it provides accurate readings across the whole strain range that was evaluated in this experiment. The reliability of the strain sensor in precisely detecting sample deformation is further emphasised by the consistency of the signals, which capture the deformation of the sample.

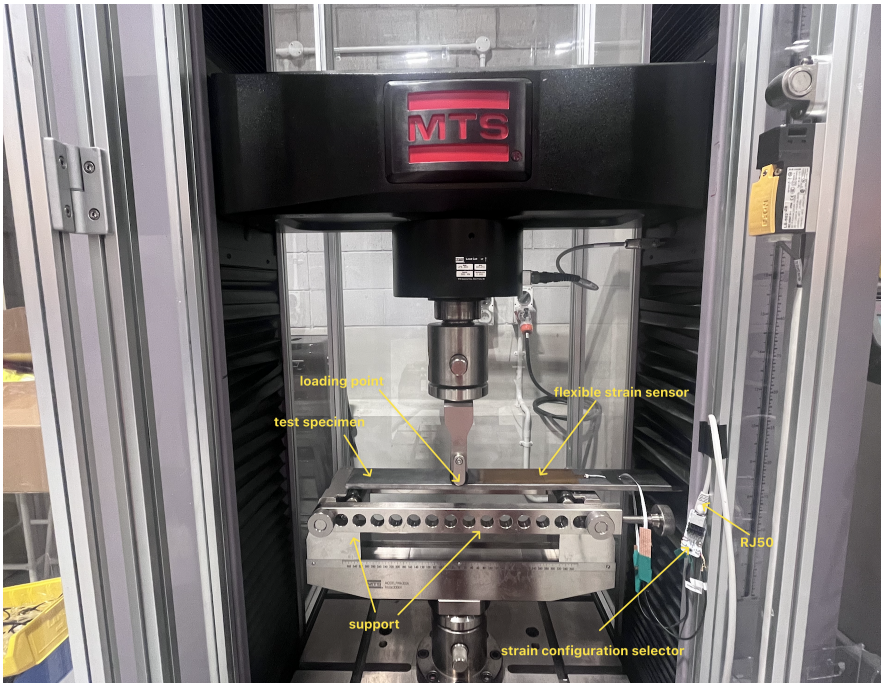

(a)

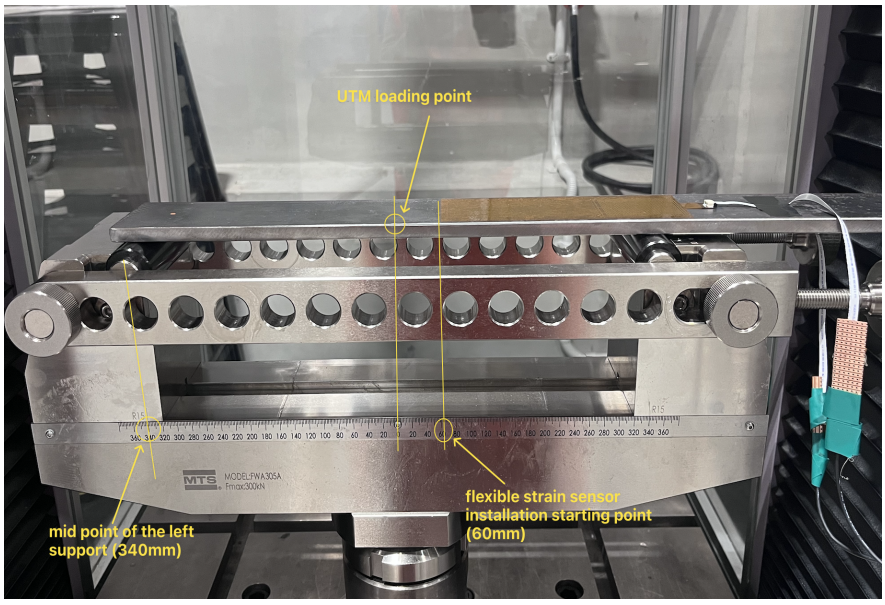

(b)

Figure 6.19: UTM bending test setup - NI DAQ

During the bending test, the strain as well as the relative resistance are both shown in Figure 6.22 to demonstrate how their values fluctuate over time. Within the linear range, the sensor demonstrates both high sensitivity and excellent linearity. The resistance

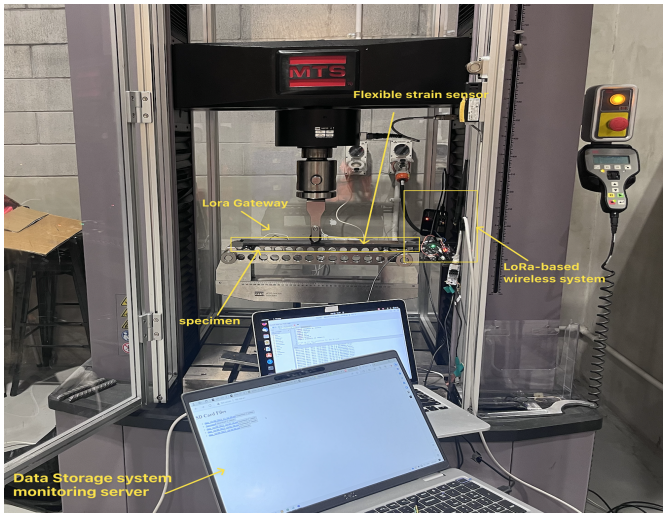

(a)

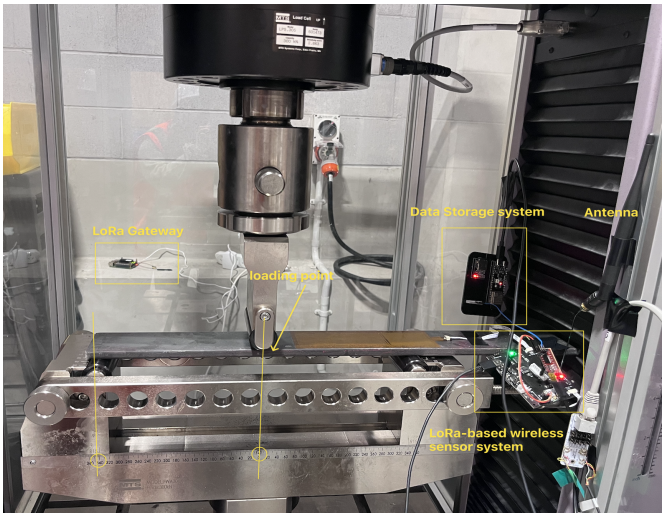

(b)

Figure 6.20: UTM bending test setup - LoRa-based wireless flexible strain sensor system

changes as the sensor deforms. The sensor's response time is relatively quick, with a small lag. However, once the specimen material passes the yield threshold, some of the deformation that occurred will be permanent and irreversible. The results of the tests show that the sensor response has a latency of approximately six seconds (sample rates of 31 Hz). The results of the tests demonstrate that there is no noise or unstable readings in the data, which indicates that the strain sensor is both reliable and

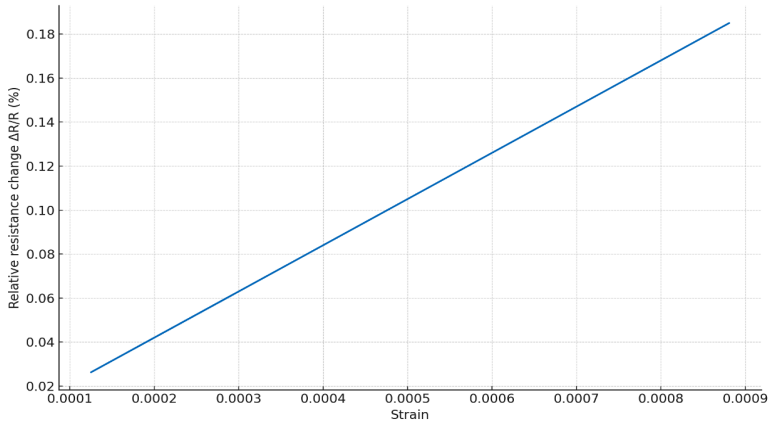

Figure 6.21: Relative resistance change during the bending test

sensitive. Additionally, the results reveal that there is no instability in the readings. It is able to continually capture strain and then interpret that captured strain into changes in resistance. It should be pointed out that the primary purpose of the flexible strain sensor developed in this research is not to accurately measure strain but rather to monitor abnormal changes in the structural strain field. Because of this, it is more important to assess the linearity and sensitivity of the sensor.

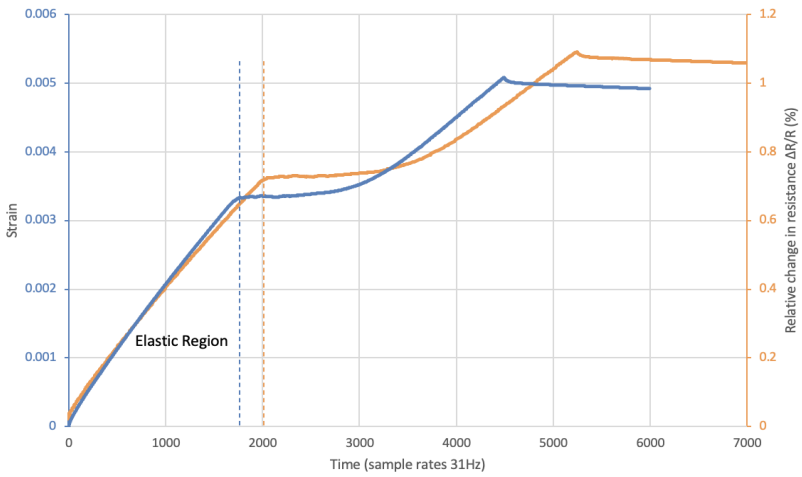

Figure 6.22: Strain and relative resistance change over time

6.4 LoRa-based Wireless Sensor System Performance Test

The previous literature review, which can be found in Chapter 2, introduces a number of applications related to the Internet of Things (IoT), including smart cities (Cook, Duncan, Sprint & Fritz, 2018), smart healthcare (Mettler, 2016), smart grids (Fang, Misra, Xue & Yang, 2011), smart buildings (Ghosh, 2018; Shrouf, Ordieres & Miragliotta, 2014), and so on. However, the majority of the wireless sensor nodes that are utilised in these applications within the framework of the Internet of Things are designed to collect parameters such as temperature, humidity, noise,etc. Research on the application of wireless sensor nodes to the direct sensing of structural key components and remote structural health monitoring (RSHM) is very limited, and the majority of the research focuses on one area of interest. Additionally, there is no research that is aimed at monitoring the strain field anomalies of structural components and integrating them into a complete SHM system. At the same time, it is equipped with the capabilities of real-time monitoring as well as fast detection.

6.4.1 Test Purpose and Scope

Due to the constraints of the AUT underground laboratory, as described earlier, conducting tests on the full system alone is inadequate to showcase the capabilities of a wireless system using LoRa technology, despite its ability to verify the system's wireless transmission functionality. The purpose of this supplementary test is to assess the efficiency of long-distance data transmission in wireless networks that use LoRa technology. To evaluate the capability of the designed system to handle complex scenarios in real-world applications.

The scope of the test is to determine the performance of the proposed LoRa network, including the range and distance in terms of data transmission range, the quality of the signal, and the volume of data packet loss. Long-range transmission is one of the essential features of LoRa. There are various studies being conducted on the implementation of LoRa in rural regions. These studies have shown that LoRaWAN signals can be carried up to 15km away in situations where the terrain is level and there are no noticeable barriers to the outside. Cattani et al. (Cattani, Boano & Römer, 2017) conducted research to determine how changes in the outdoor environment, such as variations in temperature and humidity, affect the functioning of the LoRaWAN communication system. As a result, the primary objective of this research is to obtain an in-depth comprehension of the transmission performance of the proposed LoRa system in a variety of circumstances in order to fulfil the objective of developing integrated SHM applications for real-world scenarios.In order to simulate the real environmental conditions, two environmental modes were tested: indoors - indoor of a medium-rise buildings and outdoors. The indoor experiment was carried out in the WZ building at AUT University in Auckland, New Zealand. Because the experiment was carried out inside, the factors that could have been affected by the weather outside were not considered in the analysis of the findings. This experiment is important in understanding how the performance of a LoRa network is affected by the presence of barriers inside a building. The LoRa node sends information to the LoRa gateway during transportation. This investigation contributes to a better understanding of the influence that dynamic outside environments have on the performance of LoRa transmissions.

6.4.2 Indoor Test with Obstacles

The experiment was carried out at Auckland University of Technology in the WZ building, which is the ECMS Faculty building. It is a 12-storey tower (Figure 6.23)

spanning 18,000 square metres. The external of the tower is covered in aluminium screens (Figure 6.24), which are connected to cables to form a high-performance light screen. The interior of the building (figure), as seen in Figure 6.25, comprises a full 12-storey glass atrium. The building's structural framework is composed of 10,000 tonnes of seismic-resistant steel, concrete floors, and exposed ceiling designs. The majority of the space on floors 1 to 4 is taken up by wood and laboratories. In order to properly evaluate the performance of the proposed LoRa network in the more complicated indoor environment (design), the design of the building can be considered because it provides various indoor obstacles for this experiment.

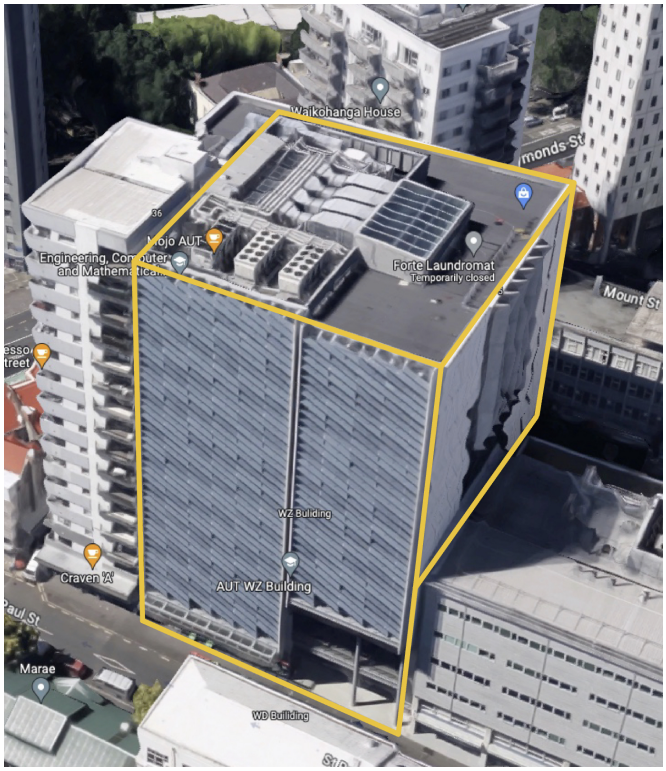

Figure 6.23: Testing site - AUT WZ Building 3D view

The experiment is carried out primarily on a LoRa network that consists of a gateway and a wireless sensor that is based on LoRa. The first experiment was conducted indoors; the LoRa gateway was always located on the third floor of the test building. This was because it was unable to locate an appropriate location for supplying power

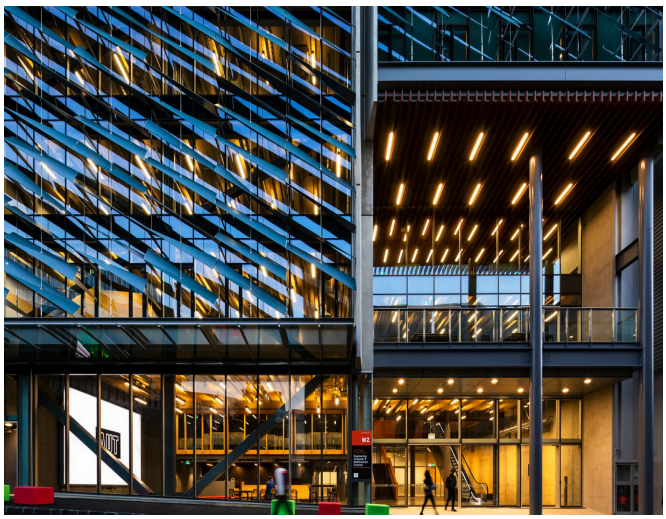

(a) Front view of the building entrance



(b) External aluminium screens

Figure 6.24: Testing site - AUT WZ Building external view (Mann, 2019)

on the ground and second floors of the building due to the constraints imposed by the internal architectural design of the building. During each phase of the testing, the LoRa node device was alternately configured to capture bending strain and axial strain. It then extracted the highest and lowest values of each configuration mode and transmitted them to the LoRa gateway at a sample rate of 31 Hz. It is important to simulate rapid transmission by IoT smart sensors for local strain field monitoring of crucial components of building structures. If the Lora node moves to a new location (a

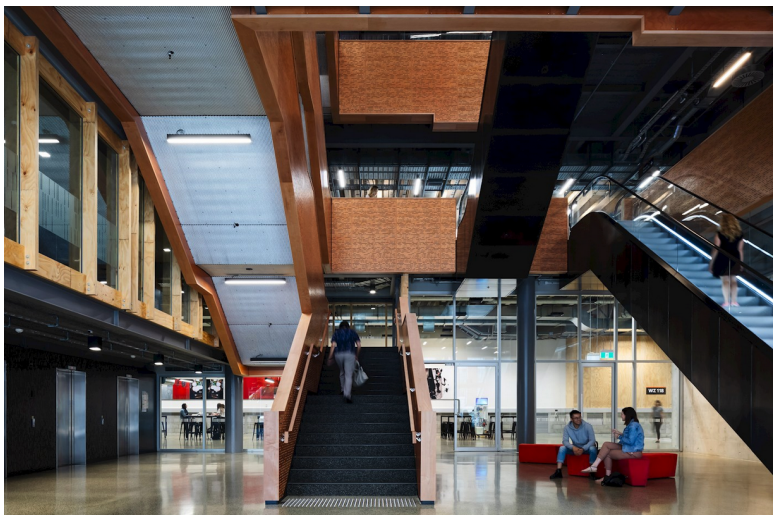

(a) Front view of the ground floor hall

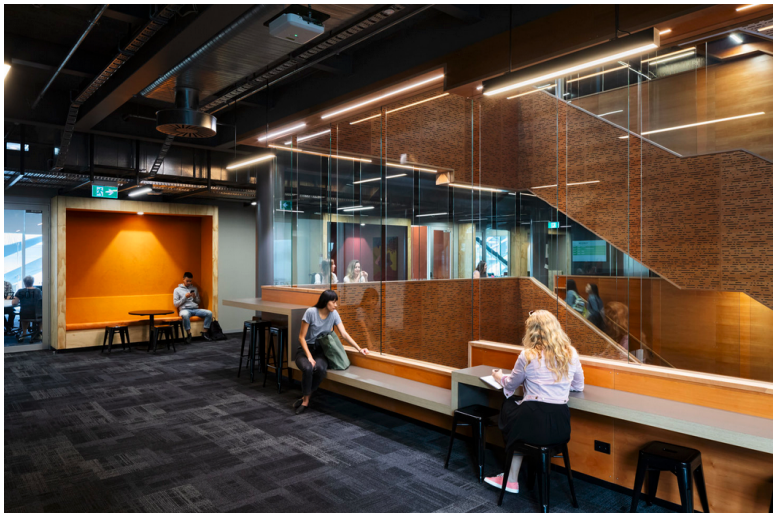

(b) one of the floors

Figure 6.25: AUT WZ Building - internal view (Mann, 2019)

higher floor), it will force a reboot so that it can establish an entirely new connection with the LoRa gateway. Throughout the entire test, the LoRa gateway did not require a restart and instead stayed in the state of being connected to a communication network.

The installation of the proposed LoRa network is depicted in Figure 6.26. The beginning of the experiment was carried out on the fourth floor as shown in the Figure 6.27, and the measuring position of the LoRa node was set up at the end of the diagonal that was furthest away from the LoRa gateway. The LoRa node was moved vertically up

one story for each trial, and its signal strength was monitored all the way up to the 12th floor, which is the highest floor in the tested building. There were a total of 9 sets of experiments conducted, and each set lasted between 30 and 35 minutes. This was done to guarantee that at least 30 sets of data packets were transmitted, as there was an instance of data packet loss when the measurement reached a high level.

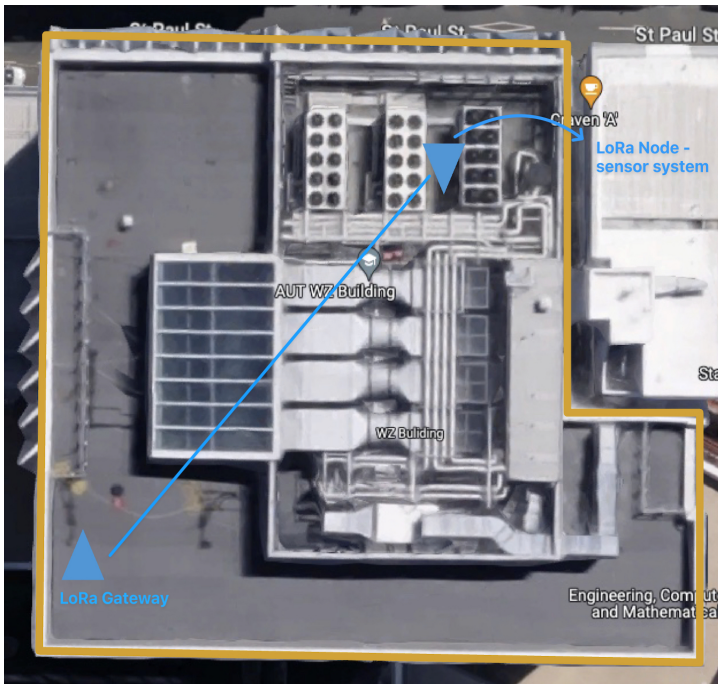

Figure 6.26: LoRa network installation top view

6.4.3 Indoor Test Results and Findings

LoRa itself is a radio technology that operates on the basis of spread-spectrum modulation and has the ability to demodulate information despite very low signal levels. The signal-to-noise ratio (SNR), which is defined as the ratio between the received signal power and the environmental noise power level, can be used to show the ambient noise level. The term "noise floor" refers to all of those zones that are unnecessary and can result in interference with the signal source. The interference signal will prevent the

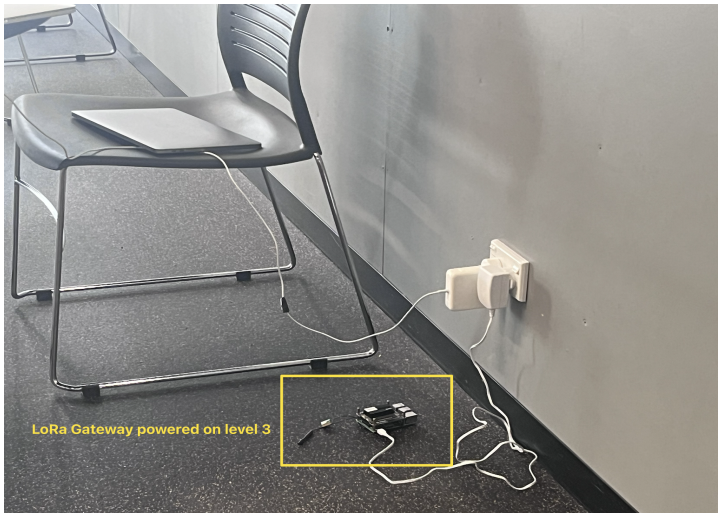

(a) LoRa gateway installed on Floor 3

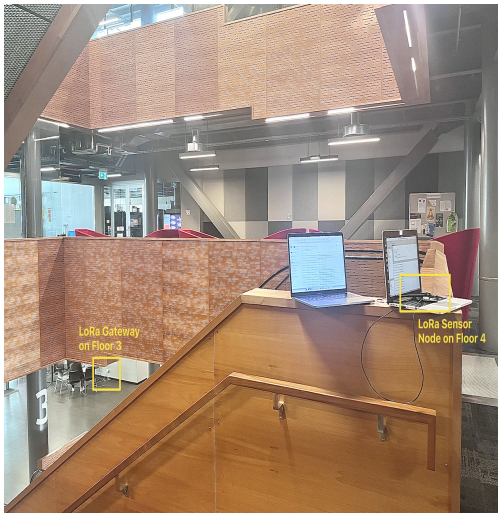

(b) Field test - sensor on floor 4

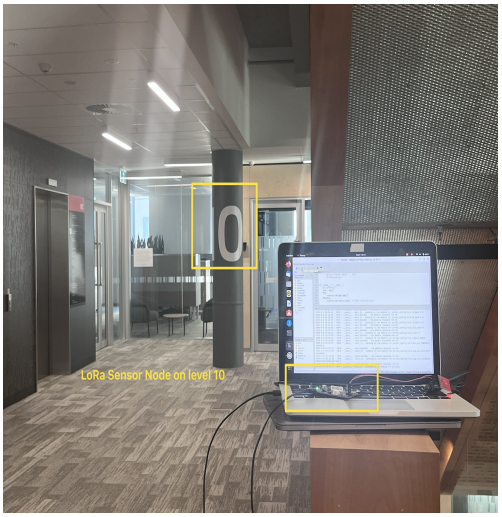

(c) Field test - sensor on floor 10

Figure 6.27: Field testing of Lora network performance in AUT WZ Building

LoRa signal transmission from being successful, which will result in the occurrence of retransmission. The SNR (6.1) value of LoRa is typically between -20 dB and +10 dB, and the received signal is considered to be extremely low damage when it is closer to +10 dB.If the SNR is greater than 0, the signal that was received operates above the noise floor; otherwise, the signal operates below the noise floor. The Received Signal Strength Indication (RSSI) provides an indication of the received signal's power level in milliwatts. The value of the RSSI, which is measured in dBm and is a negative value,

can be used to determine the maximum strength at which the receiver is able to receive the signal it originally sent. The more closely it approaches zero, the better the reception will be. Therefore, the objective of the indoor test is to collect RSSI and SNR data in order to assess how effectively the LoRa network that was built in the mid-rise building is functioning.

$$SNR_{dB} = P_{signal,dBm} - P_{noise,dBm} \tag{6.1}$$

Each floor was measured for a total of 30 minutes, and a minimum of 30 groups of data were collected in order to ensure the reliability of the results of the experiment. Table 6.2 presents the settings for each group of trials, as well as the RSSI (maximum, minimum, and average value), SNR (maximum, minimum, and average value), and packet received rate (PPR%). The experimental data that was obtained from the TTN server is depicted in Figure 6.28. Transmission power (TP), carrier frequency (CF), bandwidth (BW), spreading factor (SF) (6.2), and coding rate (CR) are the LoRa communication parameters configured at the physical layer. The parameters of TP and CF for this experiment were determined by the LoRa component manufracture. The SF and CR values are chosen in an automated process by taking into account the amount of time it takes for the gateway to acknowledge the packet. The SF remained consistent at 7 during all of the tests, and the CR was 4/5 during the test. When SF = 7, the receiver has a sensitivity of -123dBm for a bandwidth that is set at 125kHz.

The bandwidth expansion factor, additionally referred to as the spreading factor (SF), can be calculated using the relationship that exists between the ratio of the chip rate Rc to the data symbol rate Rs. Data in binary form dt (information to be transmitted), with a symbol rate of Rs equal to 1/Ts. Pseudo-noise code, also known as chip sequence pnt, in which the chip rate Rc is equal to 1/Tc, where Rs is a divisor of Tc.

$$SF = \frac{BW_{ss}}{BW_{data}} = \frac{Rc}{Rs} = \frac{Tc}{Ts} = Nc \tag{6.2}$$

Table 6.2: LoraWAN communication range performance test

	RSSI (dBm)			SNR(dB)			Packets Received Rates	
Sensor node location	Min	Max	Average	Min	Max	Average	no. of the PRR	% PRR
Floor 4	-61	-55	-58.875	7	9.5	8.75	30 of 30	100%
Floor 5	-70	-65	-67.375	7.8	9.5	8.663	30 of 30	100%
Floor 6	-73	-71	-82.375	7.6	9.2	8.15	30 of 30	100%
Floor 7	-92	-89	-90.125	6	9.2	7.463	30 of 30	100%
Floor 8	-103	-99	-98.35	6	7.8	6.863	28 of 30	93.33%
Floor 9	-110	-101	-102.625	5.2	7.2	6.538	28 of 30	93.33%
Floor 10	-111	-101	-106.25	4.2	9	6.913	27 of 30	90%
Floor 11	-111	-101	-107.75	4.2	9	6.663	27 of 30	90%
Floor 12	-123	-120	-122.285	-8.5	-6	-6.871	23 of 30	76.77%

The results indicate that the developed hardware continues to provide a signal that is reasonably reliable and maintain a high level of data transmission capability despite the complex features of the indoor environment in the mid-rise building. The packet doesn't produce a negligible amount of loss due to the poor signal quality until the measurement height reaches floor 10 (Figure 6.29). As can be seen from Figure 6.31, at floor 8, the average signal-to-noise ratio (SNR) of the data packets that were successfully passed is 6.863dB, which is maintained at a good level. This indicates that the noise didn't reach the degree of signal blur. However, at this point, the average RSSI had dropped to -98.35dBm (Figure 6.30), and a small number of data packets to be dropped. The RSSI value, the SNR, and the packet reception rate all start to decrease as the floor height increases. This results in a reduction in the strength of the LoRa transmission signal. In an indoor experimental setting, signal attenuation occurs because the signal needs to travel through a variety of barriers and materials before reaching the location of the receiver. These obstacles and materials include things like concrete floors and glass atriums. Assuming that the attenuation rate of air at around 900 MHz is 0, the attenuation rate of wood is 5dB/m, and the attenuation rate of concrete can reach up to

22dB/m. This demonstrates that the type of building material used in the construction of a building can have a significant effect on the quality of the signal received indoors. Overall, in Test A, there was only one LoRa gateway employed, which is a challenge for surroundings that are very complicated indoors. Despite this, both the LoRa device and the LoRa network demonstrate excellent performance. This also indicates that there is potential for significant cost savings when deploying LoRa devices and gateways on a large scale.

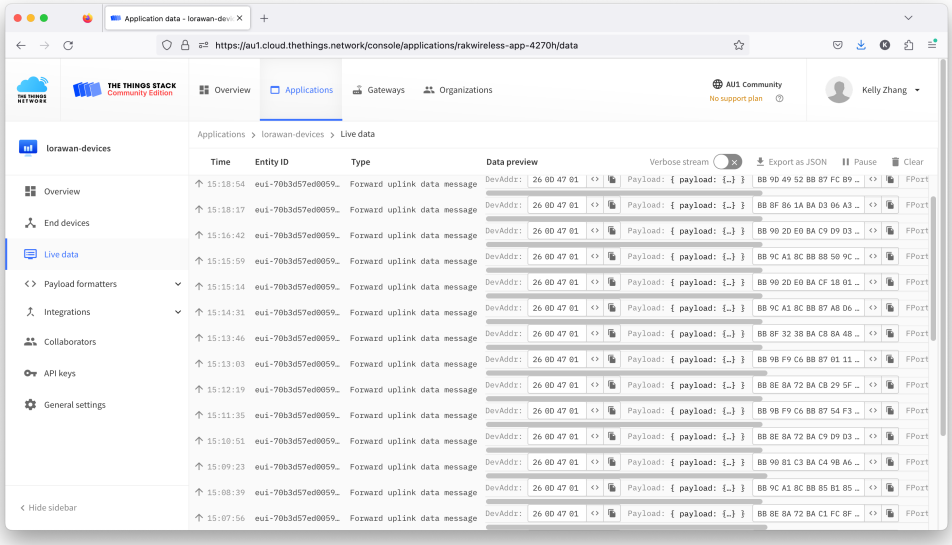

Figure 6.28: TTN server monitoring panel for indoor test - floor 4

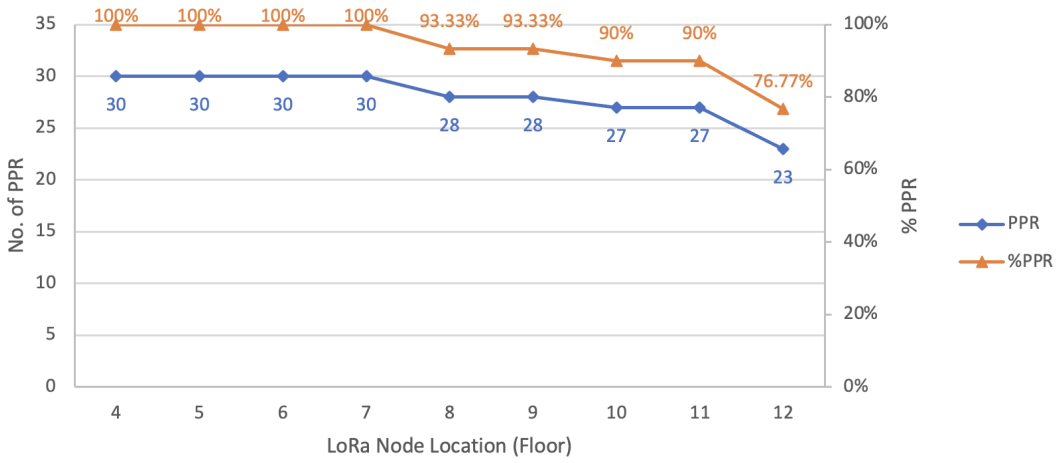

Figure 6.29: PPR values for indoor test

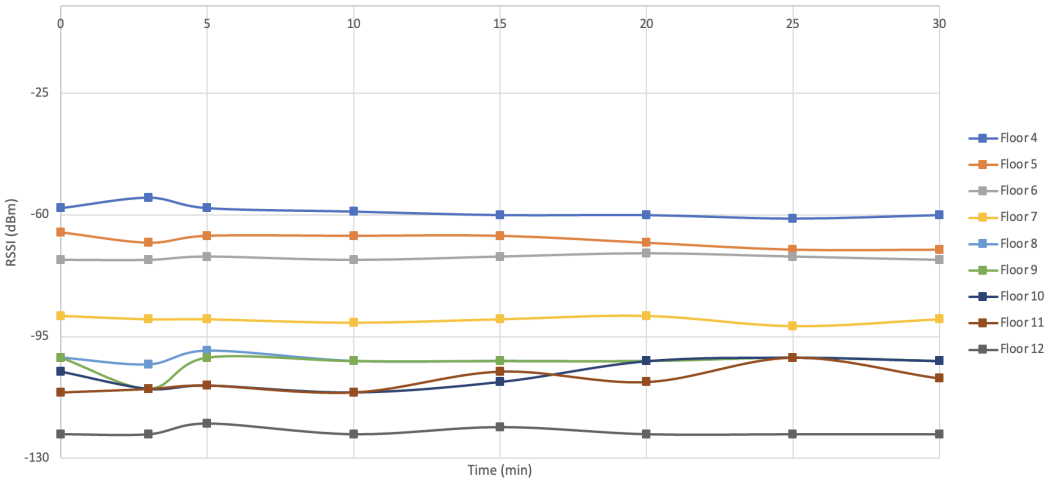

(a) RSSI values over time

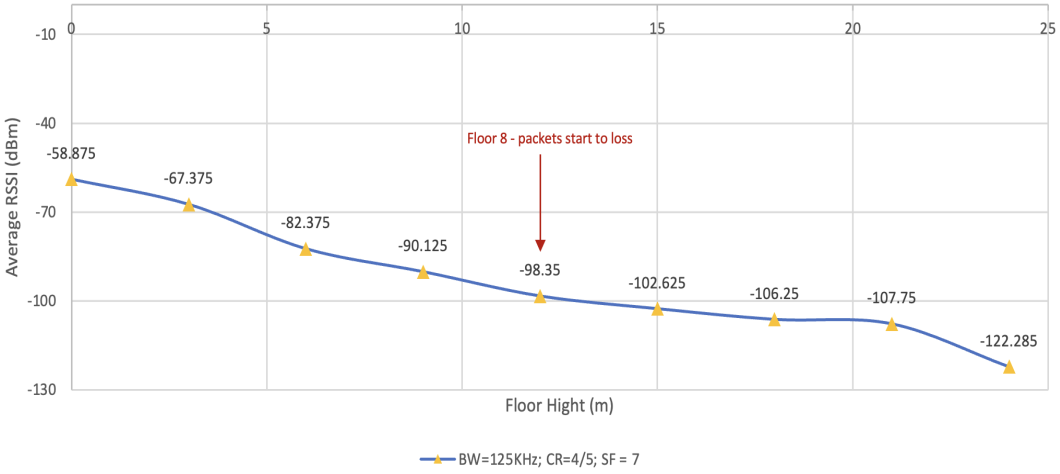

(b) Average RSSI values over height

Figure 6.30: RSSI values for indoor test - SF = 7

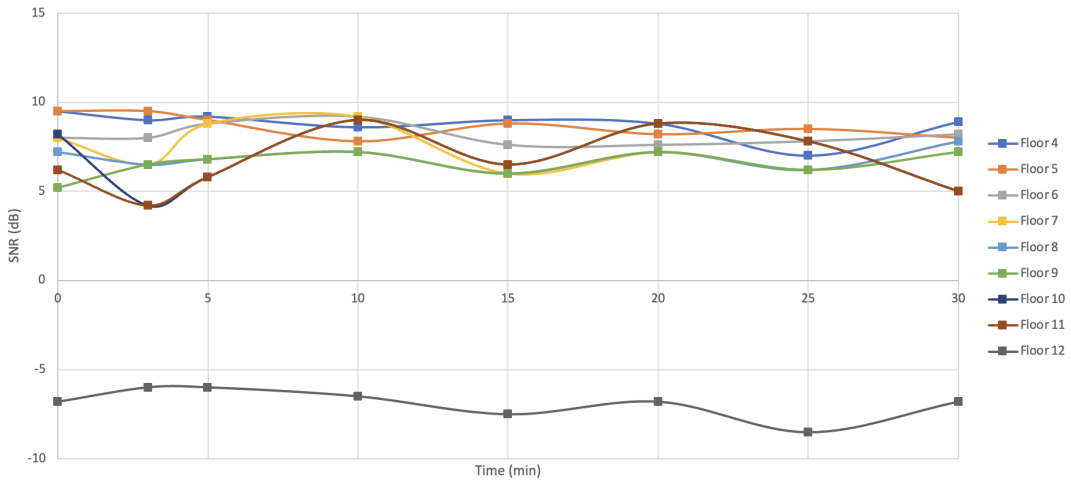

(a) SNR values over time

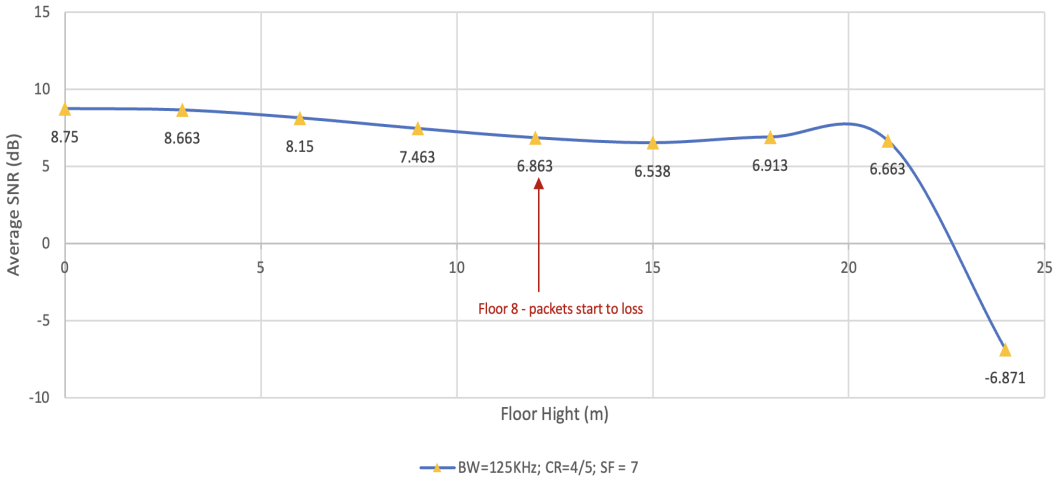

(b) Average SNR values over height

Figure 6.31: SNR values for indoor test - SF = 7

Chapter 7

Future Work Exploration

7.1 Introduction

This chapter primarily aims to examine the impact and feasibility of machine learning on structural health monitoring (SHM) applications. Furthermore, it acts as an illustration to other scholars of the prospective interdisciplinary orientation for forthcoming research. This study utilises deep learning techniques to analyse the possible applications of a wireless sensor based on LoRa technology. The results indicate that combining machine learning techniques with wireless sensor systems using embedded software can unleash the potential for research and practical applications in predicting the real-time condition of structures.

In recent years, algorithms proposed in the field of Machine Learning (ML) and Deep Learning (DL) are widely applied to SHM. For instance, the structural damage identification framework based on an auto-encoder obtains the optimal solution of modal identification of highly nonlinear structures through a deep neural network (Pathirage et al., 2018). Genetic algorithms (GA) and artificial neural networks (ANN) are used to

simplify the modal shapes of structures and apply them to the layered recognition of composite plates (Gomes, De Almeida, Junqueira, da Cunha Jr & Ancelotti Jr, 2019). Author (Chang, Lin & Chang, 2018) propose a new artificial intelligence-based structural health monitoring strategy based on neural network modelling. Author (R.-T. Wu & Jahanshahi, 2020) present a comprehensive review of the recent data fusion applications in structural health monitoring. (Avci et al., 2021) reviews the application of DL from traditional ML in the field of vibration-based structural damage detection.

However, in recent years, the development of structural health monitoring has entered a relatively slow stage, which is mainly due to the lack of a bridge between scientific research and industry deployment (Cawley, 2018). At present, the research direction combined with big data is more based on computer vision (CV) techniques (Tong, Gao, Han & Wang, 2018; Chen & Jahanshahi, 2017; B. Kim & Cho, 2018; Li, Ma, He, Ren & Liu, 2020), while this type of crack detection based on CV technology has limitations, such as small data set and ideal laboratory receipt data (H. Kim, Ahn, Cho, Shin & Sim, 2017), resulting in limited application of its training and verification results in real-life civil engineering scenarios. Computer vision technology cannot be widely used as a performance indicator of structural health monitoring.

In addition, most of the research focuses on the failure of a single structural element or material using deep neural networks. Therefore, a prediction model based on DL is developed in this study to predict the change of strain value of full-scale reinforced concrete frame structure, which is also the preparation study for the deployment of the prediction model into the flexible wireless smart sensor in the future work.

7.2 Deep Neural Network-Based Strain Values Prediction Models

As a kind of exploration and analysis technology with high prediction accuracy, the deep neural network can provide very good insights into complex nonlinear data in the scientific research field. DNN is a multi-layer sequence architecture composed of a collection of neurons (Fig.7.1). The neuron accepts neuron activation from the previous layer as input to the current layer and then performs a calculation that results in a complex nonlinear mapping from input to output. In this study, the back-propagation (BP) (Rumelhart, Hinton & Williams, 1986) learning method was also used to adjust the weights of each neuron learning from the tested data set. It minimizes the difference between the predicted output vector and the expected output vector by repeatedly adjusting the weighted value in the neural network.

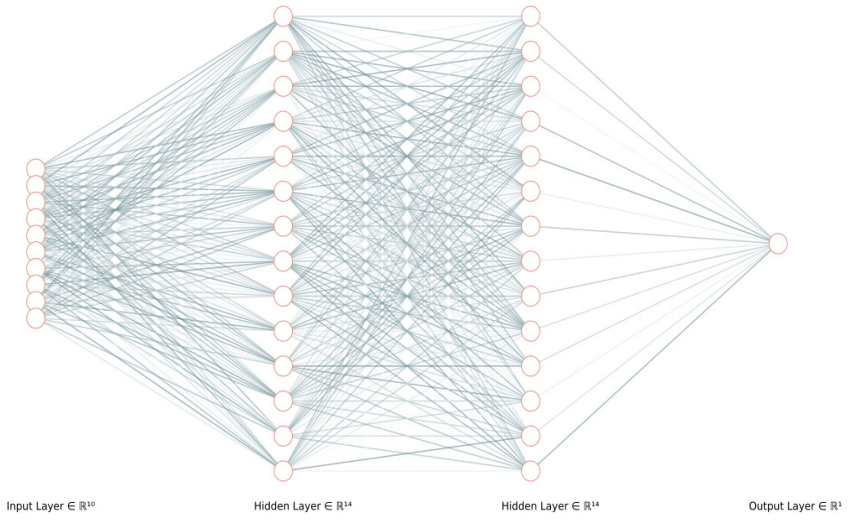

Figure 7.1: A typical DNN model architecture

7.2.1 Model Evaluation

Evaluation and detection model is an important part of model building, indispensable. In order to verify the accuracy of the established model, this study adopted two model evaluation methods, mean square error (MSE) and R-Squared (R^2).

7.2.2 Mean Square Error (MSE)

As a signal fidelity unbiased estimation, MSE aims to identify the accuracy of the model by comparing the fidelity (similarity) or distortion (error) between two signals. MSE has several significant advantages (Wang & Bovik, 2009):

1. The calculation results are based on a single sample, so they are independent of other samples.
2. MSE has a definite physical meaning and remains unchanged after any orthogonal linear transformation. For example, the Fourier transform.
3. When considering model optimization problems, MSE can be used as an excellent indicator due to its symmetry and differentiability.
4. MSE can also be used as an excellent metric in statistical and estimation models.

As one of the evaluation criteria of the regression model, the MSE of the model relative to the test set is the mean square prediction error of all samples in the test set. Here, the prediction error is mainly the difference between the real value of the test sample and the predicted value of the model (Ostertagová, 2012):

$$MSE = \frac{SSE}{dfE} = \frac{\sum_{i=1}^{D}(x_i - y_i)^2}{n - (k+1)} \tag{7.1}$$

Where y_i is the true target value of the data test set, $\hat{y}_i$ is the predicted target value in the ith case, and n is the number of the test. The root mean square is estimated from the standard deviation σ of the random error term, and the mean value in the mean square error is obtained by the primary degree of freedom.

7.2.3 R-Squared (R^2)

R^2 (Coefficient of Determination) is used to represent the proportion of variance of the dependent variable to the variance of the independent variable in the regression model:

$$R^2 = 1 - \frac{SSE}{SST} = 1 - \frac{\sum_{i=1}^{D}(y_i - \hat{y}_i)^2}{\sum_{i=1}^{D}(y_i - \bar{y}_i)^2} \tag{7.2}$$

Where SST is the sum of squares, R^2 as an important indicator to measure the fitting data of the regression model, can be used to explain the difference between variable x and dependent variable y.

R^2 does not directly quantify the dataset itself; it represents the correlation between dependent variables and independent variables. Therefore, in ML or DL, it is often used to identify the correlation between the predicted value of the model and the target value of the actual training sample. Usually, the value is between [0, 1]. In some cases, R^2 will also be negative, which may be due to improper algorithm or over-fitting of the model.

7.3 Deep Neural Network Design Considerations

If the neural network is not complex enough, it will lead to under-fitting. On the other hand, if it is too complicated and provides too many unnecessary inputs to the network, it will lead to over-fitting. In order to avoid the occurrence of the above two situations, before establishing the network, this study classifies and filters the input data to find the correlation between variables. The collected data of 19 channels are preliminary analysed to determine which sensor data of nodes can be used as input to train the model The steps are as follows:

1. Use a correlation heatmap to determine the correlation between variables.
2. According to the relational values in (1), select appropriate inputs for the outputs (strain values at the two locations-beam and column).
3. Build a deep neural network based on input and output.
4. Conduct group training, verify the model, and adjust and improve the accuracy of the model.

First of all, correlation is used here to determine the input characteristics of the training set. Correlation is widely used in statistics and usually refers to the degree of linear correlation between two or more variables. The most common measure to judge the degree of correlation between variables is the Pearson correlation coefficient, but it is only sensitive to the linear relationship between two variables. Spearman's Rank correlation is more sensitive to nonlinear relations.

Figure 7.2 shows the correlation among 19 data channels. This heatmap can visualize the relative strength between numerical variables, each variable is represented by a column, and each row represents the relationship between the corresponding two variables. The value in the small cell unit directly reflects the relationship between a pair of variables

corresponding to the row and column, and the value range is [-1, 1]. The larger the value is, the higher the correlation degree is, which can be selected as input values to train models and predict target values. The X_Value in the Figure 7.2 is the calibrated draw-wire sensor that reading the frame displacements during the RC frame Cyclic tests. And the Draw_Wire_2 is the calibrated draw-wire sensor that reading damper displacements.

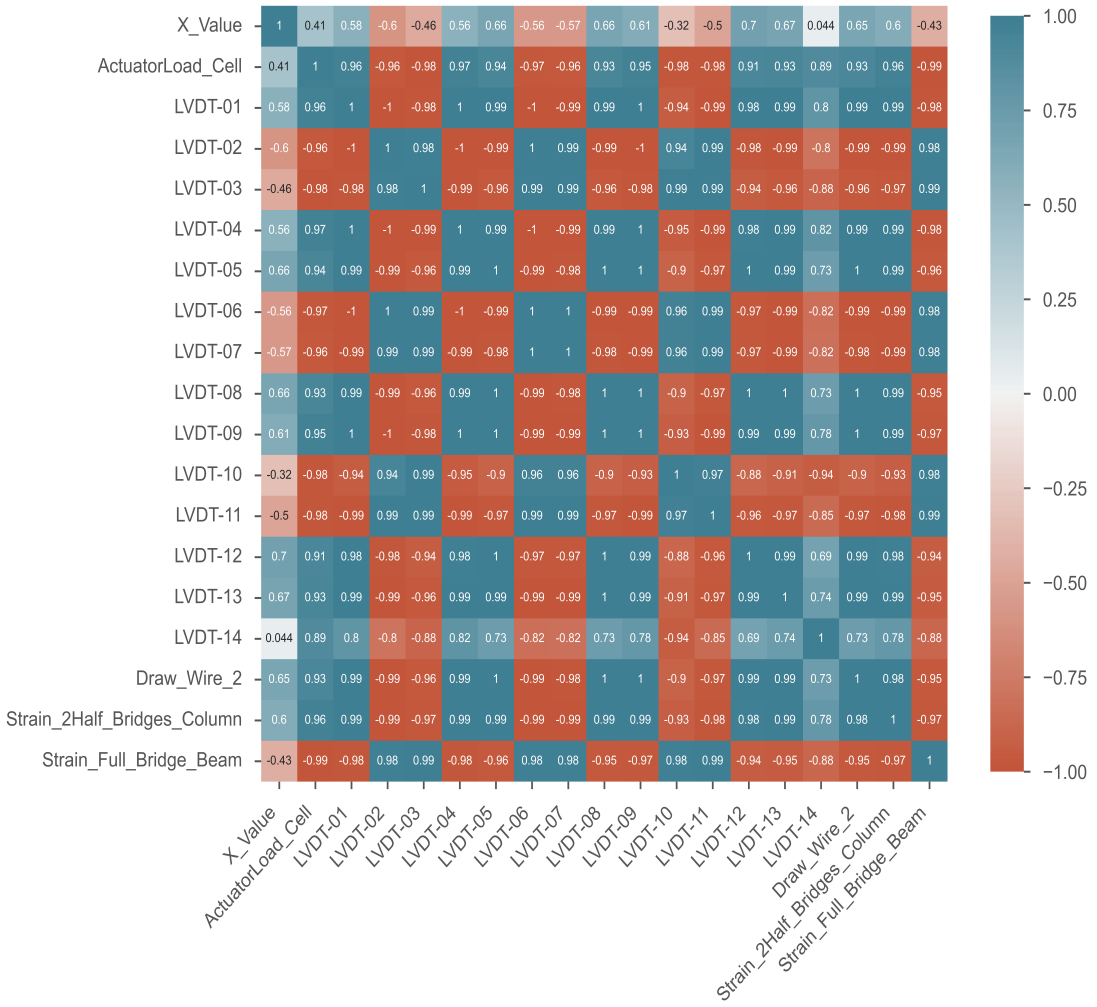

Figure 7.2: Correlation heatmap of 19 data channels

7.4 Training Neural Network Preparation

The strain data measured by experiments have high nonlinear characteristics, and the deep neural network has an excellent ability to deal with nonlinear relations. In this study, a fully connected strain value prediction model based on a deep neural network is designed and trained. As part of the Structural Health Monitoring System (SHM), the prediction model can be used as a threshold monitoring system for strain sensors to pre-process the collected raw data. This reduces the pressure on sensor data internal storage and SHM system data processing.

The determination of hidden layers and the number of neurons is complex and usually requires an iterative process. Studies on damage recognition show that the number of hidden layers and neurons in neural networks is usually determined by model trial and error. Early studies (Yam, Yan & Jiang, 2003; Vafaei, Alih, Shad, Falah & Halim, 2018; Zang & Imregun, 2001) indicated that one hidden layer was enough, but such studies did not prejudge the correlation of input values, so the reliability of input variables would be reduced, thus affecting the selection of the number of hidden layers. This study found that the model with two hidden layers can better carry out feature recognition and extraction, thus improving the accuracy of the model.

Figure 7.3 shows the model architecture adopted in this study, which is a fully connected multi-layer deep neural network. Built-in the PyTorch framework, the network is trained using feed-forward and BP which is also a technique of supervised learning. Gradient descent (GD) is used to optimise the accuracy of the model. As a strain prediction model, it needs to be applied to nonlinear data, so the activation function selection of neurons must also be nonlinear. Therefore, the Sigmoid function is chosen as the activation function. It can help the neural network to discover the nonlinear relationship

between data features.

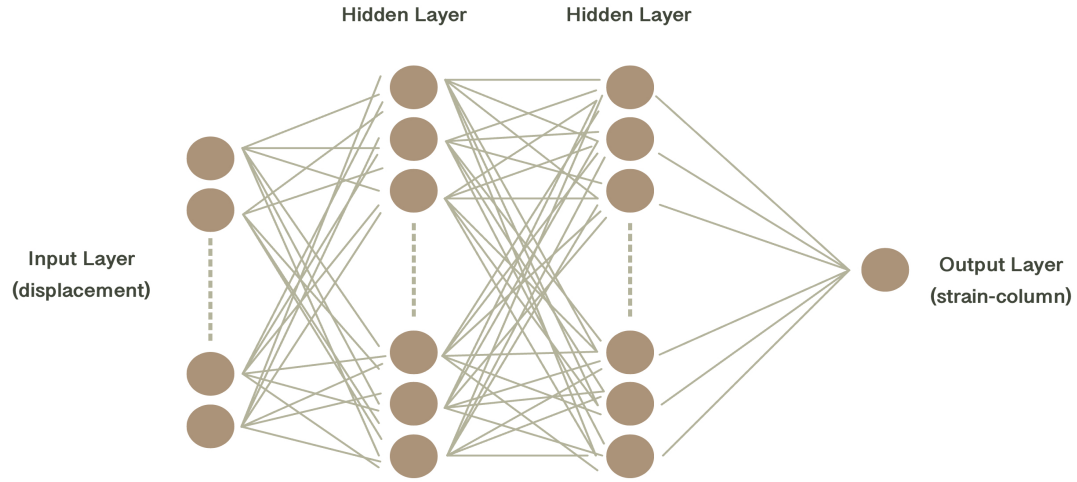

(a) 2 hidden layers deep neural network for the sensor on column

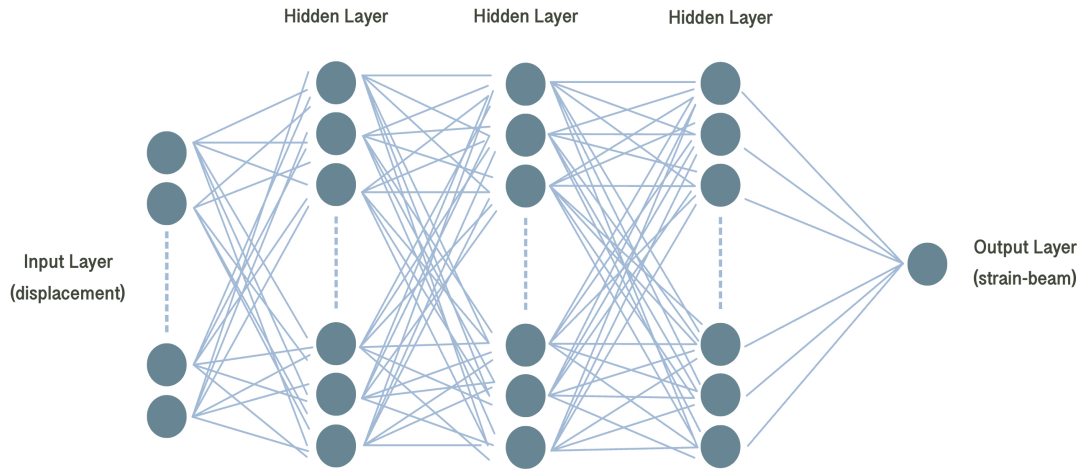

(b) 3 hidden layers deep neural network for the sensor on beam

Figure 7.3: Architecture of the proposed neural network

The data set is divided into three groups: training, and testing/validation, where 80% of the total data set is used to train the network and 20% to test/validate the network. The train and validation datasets are divided into x_train, x_est, and y_est, y_train. Each training process is randomly assigned in accordance with the above ratio. To avoid over-fitting, the generalization ability of a deep neural network is tested by using test samples. The training and verification process of the model built in this study is shown

in Figure 7.4.

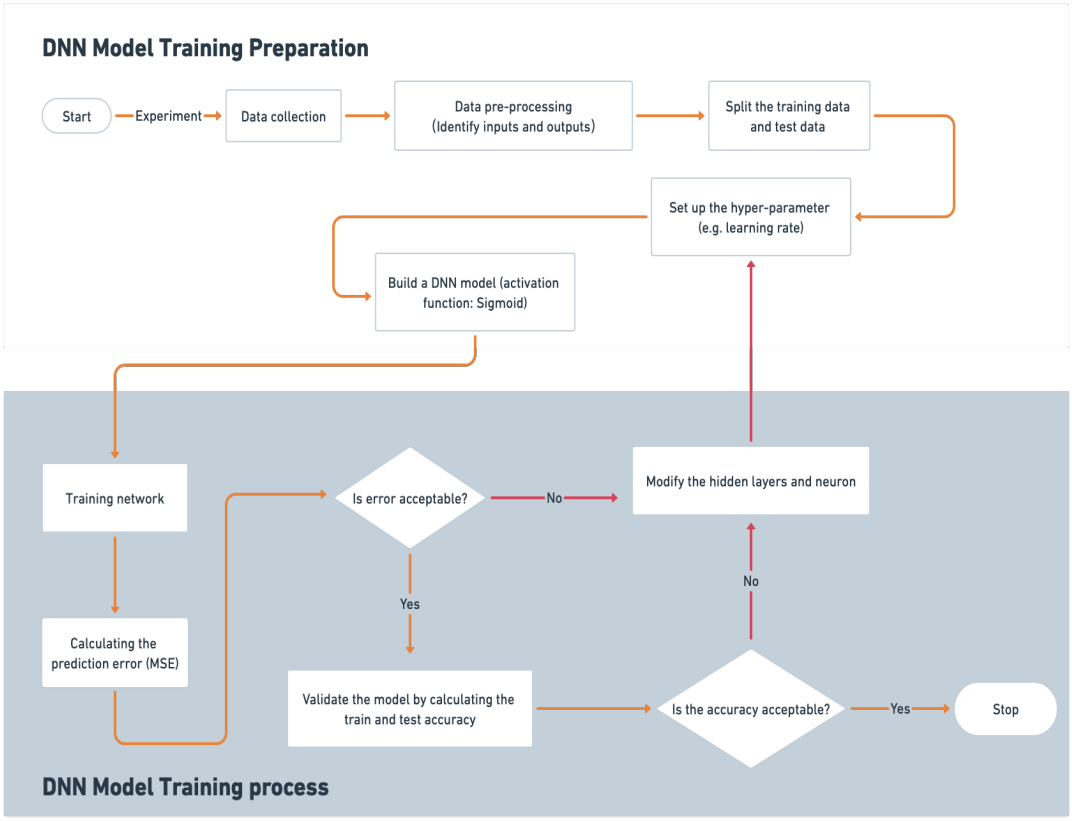

Figure 7.4: Flowchart of DNN model preparation and training

7.5 Model Training Results

As mentioned above, strain prediction results of the trained deep neural network are evaluated by two methods, MSE and R-squared, as part of verifying the accuracy of the model. The results are shown in Figure 7.5 the neural network established in this study accurately estimated the concrete surface strain value located near the bottom of the column. It is also obvious that the trained network model can successfully predict the strain value in the linear range and the strain trend in the non-linear range.

The results obtained from Figure 7.5 (a) show that for strain gauges installed on both

sides near the bottom of the column during the RC frame test, the accuracy of training and strain prediction of this deep neural network can reach 86%, test accuracy is 85%, and the root mean square deviation (RMSE) of the whole training is only 0.016%, and the mean absolute error (MAE) is 0.0089%. Figure 7.5 (b) shows the strain prediction results where the sensor was installed on the beam during the RC frame test. The training accuracy and test accuracy both reach 87%. RMSE of the whole training result is 0.0042% and MAE is only 0.0036%.

Figure 7.6 shows the comparison results of experimental data and predicted data. Eighty samples are randomly selected from the experimental data set and the predicted data set respectively. It can be seen that there is a high linear correlation between the real strain value and the predicted strain value, indicating that both two DNN models for beam and column elements proposed in this study have great generalization ability.

7.6 Summary

In this chapter, deep neural networks are applied to predict the strain values of full-size concrete frame structural members. The data set used to build the deep neural network was derived from the cyclic loading of the RC Frame to its limit, and a highly stretchable strain gauge was used to collect the strain values of the concrete surface. The two network architectures are suitable for beam and column respectively, and the prediction accuracy is 86% and 87%. Furthermore, random sampling is carried out in the predicted data set, and then compared with the real strain value, to prove the high generalization of the proposed deep neural network.

It is worth mentioning that in this study, gradient descent was used to train the network. According to (Wilson, Shenhav, Straccia & Cohen, 2019) , Eighty-Five Percent Rule

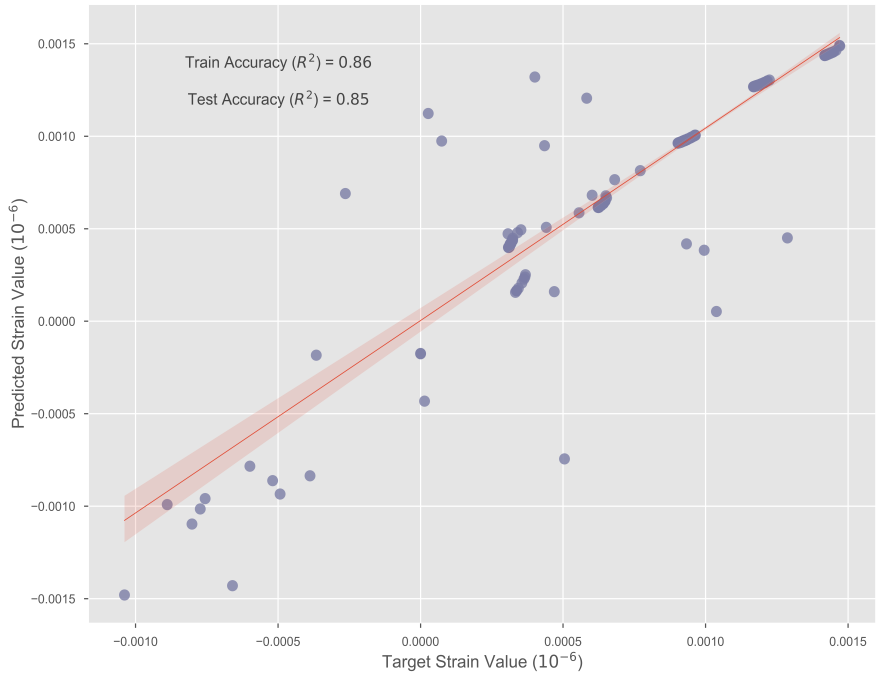

(a)

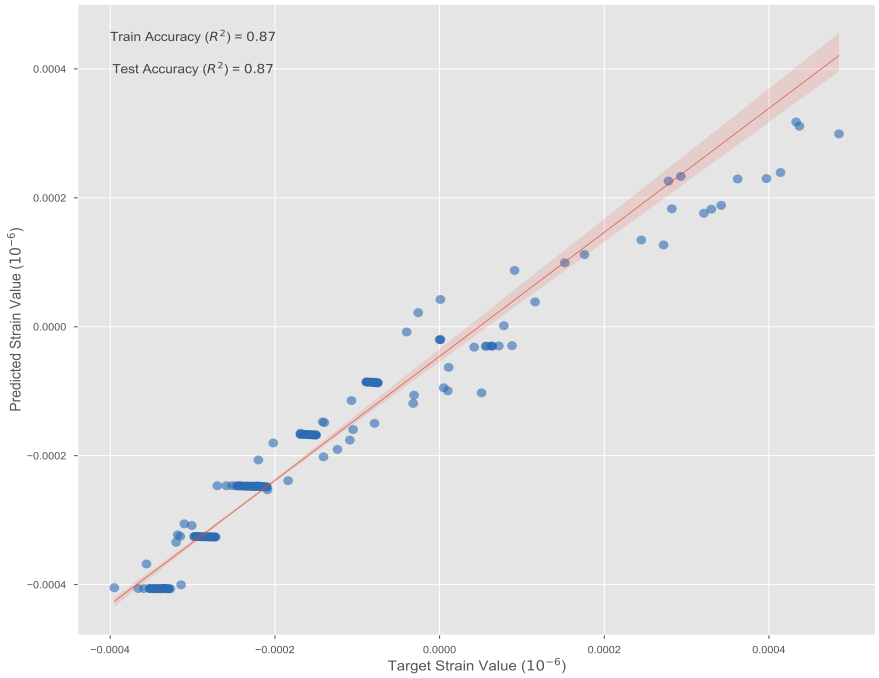

(b)

Figure 7.5: Training and Testing accuracy of proposed deep neural networks

for optimal learning, the best training point for the neural network was when the training accuracy was about 85% and the training rate and difficulty were moderate.

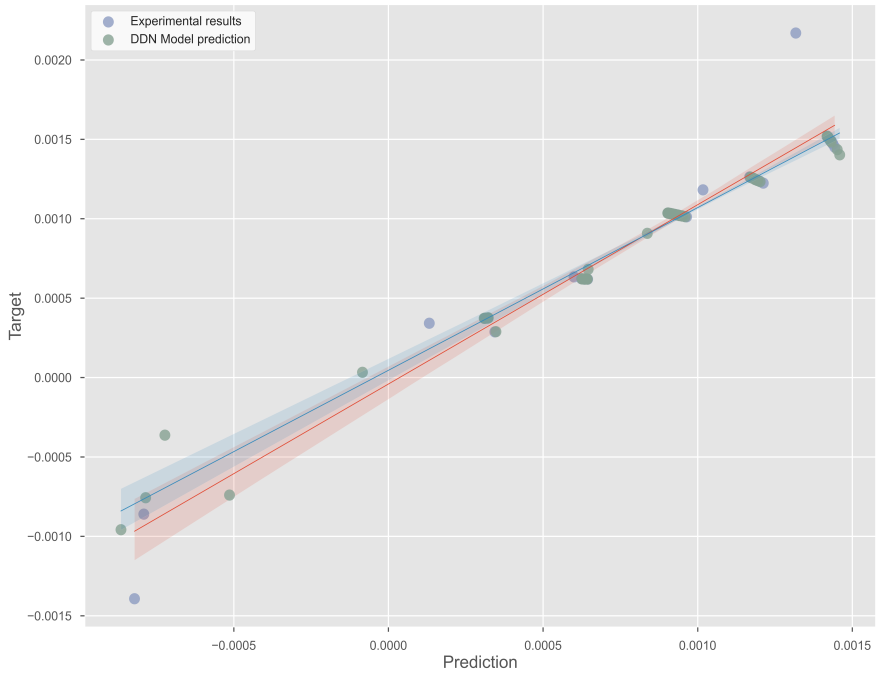

(a)

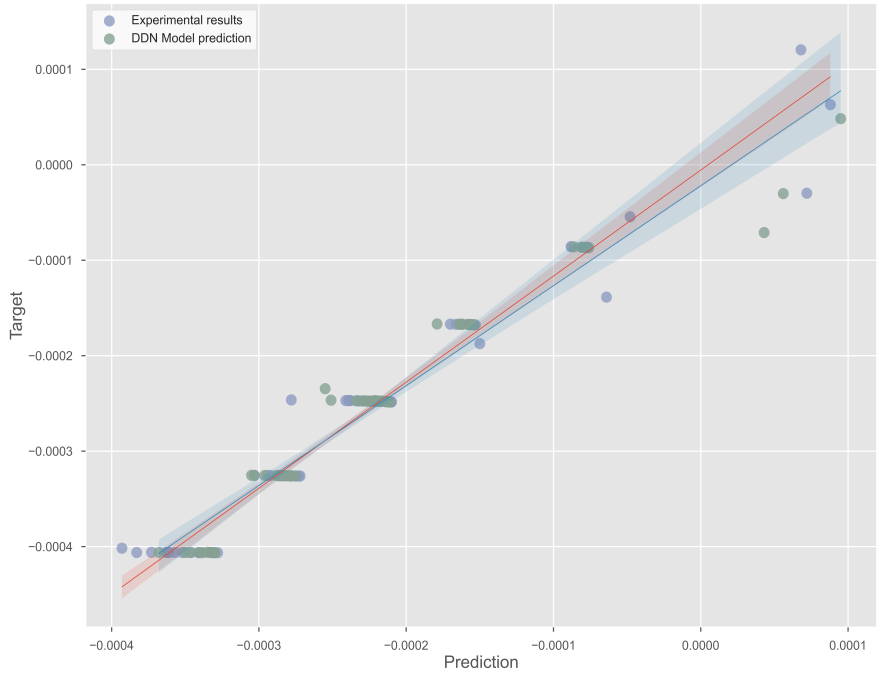

(b)

Figure 7.6: Comparison between experimental measurements and predictions

Optimization improves the most. It also avoids over-fitting due to the pursuit of high accuracy.

In addition, the proposed two neural networks can be served as the basis for future research. For future work, the proposed neural network prediction model can be deployed in the wireless sensor system to application layer to establish the threshold value for strain measurement and realize the data pre-processing and outlier alarm of the sensor board in the SHM application.

Chapter 8

Conclusion

8.1 Conclusion

The primary goal of this research is to expand the implementation of flexible electronic devices in structural health monitoring (SHM) by designing and developing an integrated flexible strain structure health monitoring system that is based on LoRaWAN. The developed system provides for monitoring local strain field anomalies in building structures in order to ensure the integrity of civil structures. It may be quickly and easily installed, making it accessible to asset owners and engineers. The system is made up of three essential components: a highly stretchable and flexible strain sensor that is used for detecting anomalies in the local strain fields of essential structural elements; a hardware system for data collection and wireless transmission; and data management systems for storing and extracting collected data. The following is a summary of the development process of this system and gives the corresponding conclusions.

In Chapter 3, the development and specifications of two forms of flexible strain sensors were introduced. In the first part of this chapter, the theoretical foundations of strain

sensing techniques as well as the process that led to their creation were discussed. The challenges associated with SHM applications' strain monitoring nowadays were also brought up for discussion. Therefore, the proposed flexible strain sensor system is designed to address the limitation of a single strain sensor's ability to measure numerous strains at the same time without changing the position of the sensor or adding new sensors. After that, the chapter provided the design and development of the flexible strain sensor in detail, explained the characteristics of the materials that were determined, and designed two different circuit topologies for measuring bending strain and axial strain. In addition to this, a strain configuration selector was developed so that the alternating measurement of the two strains could be carried out. In order to realise the idea of detecting two strains, the flexible strain sensor that was designed features a connection that uses alternating switching as a bridge. In addition to that, in order to evaluate the performance of the flexible strain sensor, both the calibration test and the tensile test of the flexible strain sensor were carried out. The findings indicate that the design that was proposed possesses the qualities of high resolution and sensitivity, and it was found that the installation of strain sensor sheets may be lowered to the fullest extent possible when two strains can be detected concurrently. In order to facilitate the deployment of sensors on a massive scale at a reduced cost.

In Chapter 4, the hardware development of a wireless sensor node that is based on LoRaWAN was introduced. The development of the hardware is primarily split into two components, the first of which is the design and development of smart sensor nodes based on LoRaWAN. Data transfer and remote monitoring are two of its primary functions. The design and development of this wireless node is significant because it integrates with the strain configurator that was developed in the preliminary stage and makes the process of installing flexible strain sensors and replacing them very easy. The master system development of wireless sensors mainly relies on the microcontroller

RP2040 (developed by Raspberry PI Company); its price is very low, but it has not been widely used in the development of wireless sensors. The use of a multiplexer enables the automatic switching of bridge connections between the two different strain configurations. The implementation of a LoRa node in the proposed system design enables minimal power consumption over long distances while also facilitating wireless transmission.

The second phase of the hardware system was aimed at providing storage and management for the data collection. In order to accomplish this objective, a system for data management that operates on a microcontroller (ESP32 S3) was built. This subsystem communicates with RP2040 in the main system to store the full raw data. Users are able to gain free access to the server through the built-in hotspot that is provided by the ESP32 S3. This allows users to achieve real-time monitoring data collection and provides them with the capability of downloading the original data file. This is the most notable feature that it possesses. Because the sensor will be installed in various locations throughout the structure, the design is primarily focused on finding a solution to the challenge that it is difficult for users of practical applications of SHM systems to get in close range of the sensor in order to extract data. For instance, it is not practical to expect users to be able to easily visit the bridge in order to access data when it is in operation. The capability of the subsystem to cover a distance of up to 1 km provides users with the greatest amount of flexibility and practicability possible while extracting data. The last step in the process of developing a comprehensive LoRaWAN network is the building of a gateway that incorporates wireless sensor nodes. The development of the LoRa gateway was successfully carried out in association with TTN. In addition to LoRa's long-distance transmission characteristics, this study also developed a local server that is easily accessible by users to access the established network. The purpose of this design is because most of the current gateway development requires a certain

level of user development ability. Common users' aspiration to construct their very own gateway presents a number of additional challenges. Furthermore, because LoRa and TTN have been integrated, it is required to make an initial intervention in the user's local network. Because the user is responsible for configuring the access network during setup, a minimum competency level is required for asset owners to be able to make use of such IoT devices. To address this challenge, this study also develops a system for the LoRa gateway to facilitate user configuration of the new network. And integrate it with the configuration settings on TTN. The user can access the local server via any device and is just required to enter the SSID and password of the local network and the server address of the TTN, and then enable the LoRa gateway to connect to the new network. In general, the developed wireless sensor system that is based on LoRaWAN possesses the qualities of low cost, low power consumption, long distance transmission, and a high level of end-user friendliness.

In Chapter 5, the focus is on introducing the application development process for visualising the collected data to enable users to make quick preliminary assessments. Within the LoRa application layer, a data visualisation dashboard for end users was developed with the implementation of the MQTT protocol. Users are able to download and install the application on their local devices in order to receive data from the TTN server in real time. This is made possible by integrating the developed software into a container using Docker, which makes it easier for end users to deploy the application. The dashboard is different from the general visualisation application, which additionally has the functions of data transformation and download. In addition, the application does not require point-to-point integration; rather, it only needs to connect with the LoRa gateway by way of an API interface (using the MQTT protocol). Once the application is running, it can automatically add all of the node devices that are under the control of the LoRa gateway and possess the capability of multiple processing threads.

In Chapter 6, the results of employing a new wireless flexible strain sensor system that is based on LoRa were discussed. The experiment first used a full-scale RC frame as the target structure and carried out the cyclic loading test. A major objective of the test was to evaluate the performance of the developed flexible strain sensor in a full-scale structure to assess the strain field status of key structural members. In addition to that, the GF values of the flexible strain sensor that were calibrated in the tensile test were also verified by the cyclic loading test. Furthermore, in order to test the performance of the LoRa network that was developed, remote tests were carried out in an engineering building at Auckland University of Technology in New Zealand. The purpose of these tests was to evaluate the data transmission capability of LoRa in complex indoor environments. In general, the findings obtained from the experiment indicate that the new wireless sensor system is reliable in its monitoring of the strain field anomalies of the essential elements of the structure and that it is able to maintain good and stable long-distance transmission. To draw the conclusion that the wireless sensor nodes that are based on LoRa can be employed in a dependable manner for the purpose of monitoring and analysing the local strain field anomalies of full-scale structural elements.

In chapter 7, the strain prediction model that is based on a deep neural network is presented. This model builds a model that can be used for full-scale strain prediction, and it does so by using data from RC frame cyclic loading tests as a training set. As part of the ongoing effort to give data predictions to end users, the model can be included in the application layer of the TTN server that is currently being developed.

8.2 Future Work

The work that was presented in this paper highlights the significance of flexible strain instruments that are based on LoRa for the purpose of monitoring and evaluating the strain fields of full-scale building structural elements. The process of completing projects typically consists of the following steps: designing a flexible electronic, calibrating sensors, designing hardware, doing integrated troubleshooting, and testing the system. The final goal of the project that is given in this thesis is to develop and implement an integrated SHM functional system, combined with flexible electronics, so that it can have more flexible technical advances and practises. The whole system is designed to improve the feasibility of practical SHM applications as the core. The following is a list of valuable technical aspects:

1. A flexible strain sensor with an adhesive layer eliminates the need for the common strain gauge's complex installation process, requiring liquid glue.
2. A flexible strain sensor equipped with a ZIF connector makes it easier and more flexible to connect with the hardware element. Additionally, the sensor can be freely disassembled and replaced after heavy use.
3. The development of low-cost and low-power wireless sensor nodes as well as an integrated LoRa network with the TTN server.
4. Dashboards for data visualisation that allow end users to browse and quickly assess TTN data in real time.

This study presents a summary of some of the challenges faced during the process of development as well as some ideas for future research, with the intention of assisting other researchers in the identification of relevant research gap:

1. The developed flexible strain sensor is mostly appropriate for use in circumstances

involving abnormalities in the local strain field and damage to full-scale or large structures. It is theoretically hard to accurately record very small strains since they are so close to or below the level of ambient noise. Because of this, numerous kinds of sensor components can be added to the system in order to monitor a wide variety of physical properties, including accelerations, natural frequencies, and so on.

2. Combine the ESP32 S3-controlled subsystem with the RP2040-controlled main system to achieve a higher degree of integration.
3. Expand the capabilities of the data visualisation dashboard so that it can perform a wider range of monitoring tasks.
4. Implement the proposed deep neural network based model into the application layer, to provide the strain data trend prediction to end users.
5. Continue to develop the power supply equipment of the system so that it can be equipped with a portable power system that has a large capacity. Facilitate the extension of the system's life cycle.

During the course of the development process, the most significant setback was the significant delay that occurred in the production and shipment of the equipment because of the COVID-19 epidemic. As a result, the development of the hardware is available only for the half-bridge flexible strain sensor. It is conceivable, for future development, to add an interface to the proposed full-bridge flexible strain sensor on a highly integrated device. This would make it possible for the mutiplixer to also regulate the connection of the sensor's internal bridge. Finally, flexible electrical devices are not frequently used in integrated SHM systems. The development of flexible electrodes and connectors is currently meeting the greatest demand in this field. This study has provided a good practise demonstration for this research field, which demonstrates that this is a very worthy field to pay attention to.

References

Abdulkarem, M., Samsudin, K., Rokhani, F. Z. & A Rasid, M. F. (2020). Wireless sensor network for structural health monitoring: a contemporary review of technologies, challenges, and future direction. *Structural Health Monitoring*, *19*(3), 693–735.

Alvandi, A. & Cremona, C. (2006). Assessment of vibration-based damage identification techniques. *Journal of sound and vibration*, *292*(1-2), 179–202.

Alvear-Puertas, V., Rosero-Montalvo, P. D., Michilena-Calderón, J. R., Arciniega-Rocha, R. P. & Erazo-Chamorro, V. C. (2021). Urban air pollution monitoring by neural networks and wireless sensor networks based on lora. In *Proceedings of the future technologies conference (ftc) 2020, volume 2* (pp. 907–919).

An, H., Youn, B. D. & Kim, H. S. (2022). A methodology for sensor number and placement optimization for vibration-based damage detection of composite structures under model uncertainty. *Composite Structures*, *279*, 114863.

Avci, O., Abdeljaber, O., Kiranyaz, S., Hussein, M., Gabbouj, M. & Inman, D. J. (2021). A review of vibration-based damage detection in civil structures: From traditional methods to machine learning and deep learning applications. *Mechanical systems and signal processing*, *147*, 107077.

Aygün, B. & Gungor, V. C. (2011). Wireless sensor networks for structure health monitoring: recent advances and future research directions. *Sensor Review*, *31*(3), 261–276.

Aygun, L. E., Kumar, V., Weaver, C., Gerber, M., Wagner, S., Verma, N., ... Sturm, J. C. (2020). Large-area resistive strain sensing sheet for structural health monitoring. *Sensors*, *20*(5), 1386.

Baghrous, M., Ezzouhairi, A. & Benamar, N. (2020). Smart farming system based on fog computing and lora technology. In *Embedded systems and artificial intelligence: Proceedings of esai 2019, fez, morocco* (pp. 217–225).

Bhuiyan, M. Z. A., Wang, G., Cao, J. & Wu, J. (2013). Deploying wireless sensor networks with fault-tolerance for structural health monitoring. *IEEE Transactions on Computers*, *64*(2), 382–395.

Caballero-Russi, D., Ortiz, A. R., Guzmán, A. & Canchila, C. (2022). Design and validation of a low-cost structural health monitoring system for dynamic characterization of structures. *Applied Sciences*, *12*(6), 2807.

Carden, E. P. & Fanning, P. (2004). Vibration based condition monitoring: a review. *Structural health monitoring*, *3*(4), 355–377.

Cattani, M., Boano, C. A. & Römer, K. (2017). An experimental evaluation of the reliability of lora long-range low-power wireless communication. *Journal of Sensor and Actuator Networks*, *6*(2), 7.

Cawley, P. (2018). Structural health monitoring: Closing the gap between research and industrial deployment. *Structural health monitoring*, *17*(5), 1225–1244.

Chan, T. H., Yu, L., Tam, H.-Y., Ni, Y.-Q., Liu, S., Chung, W. & Cheng, L. (2006). Fiber bragg grating sensors for structural health monitoring of tsing ma bridge: Background and experimental observation. *Engineering structures*, *28*(5), 648–659.

Chang, C.-M., Lin, T.-K. & Chang, C.-W. (2018). Applications of neural network models for structural health monitoring based on derived modal properties. *Measurement*, *129*, 457–470.

Chen, F.-C. & Jahanshahi, M. R. (2017). Nb-cnn: Deep learning-based crack detection using convolutional neural network and naïve bayes data fusion. *IEEE Transactions on Industrial Electronics*, *65*(5), 4392–4400.

Chintalapudi, K., Fu, T., Paek, J., Kothari, N., Rangwala, S., Caffrey, J., ... Masri, S. (2006). Monitoring civil structures with a wireless sensor network. *IEEE Internet Computing*, *10*(2), 26–34.

CloudTern. (2021, 8). *Top 5 Advantages of using Docker.* Retrieved from `https://www.cloudtern.com/cloud/top-5-advantages-of-using-docker/`

Cook, D. J., Duncan, G., Sprint, G. & Fritz, R. L. (2018). Using smart city technology to make healthcare smarter. *Proceedings of the IEEE*, *106*(4), 708–722.

Corbally, R. & Malekjafarian, A. (2022). A data-driven approach for drive-by damage detection in bridges considering the influence of temperature change. *Engineering Structures*, *253*, 113783.

Cruz, N., Cota, N. & Tremoceiro, J. (2021). Lorawan and urban waste management—a trial. *Sensors*, *21*(6), 2142.

Das, S., Saha, P. & Patro, S. (2016). Vibration-based damage detection techniques used for health monitoring of structures: a review. *Journal of Civil Structural Health Monitoring*, *6*(3), 477–507.

Day-Lewis, F. D., Slater, L. D., Robinson, J., Johnson, C. D., Terry, N. & Werkema, D. (2017). An overview of geophysical technologies appropriate for characterization and monitoring at fractured-rock sites. *Journal of environmental management*, *204*, 709–720.

De Reus, R., Gulløv, J. O. & Scheeper, P. R. (1999). Fabrication and characterization of a piezoelectric accelerometer. *Journal of Micromechanics and Microengineering*, *9*(2), 123.

Doebling, S. (1996). Damage identification and health monitoring of structural and mechanical system from changes in their vibration characteristics: a literature survey. *Los Alamos National Laboratory, Report*.

Dondi, D., Di Pompeo, A., Tenti, C. & Rosing, T. Š. Š. (2010). Shimmer: A wireless harvesting embedded system for active ultrasonic structural health monitoring. In *Sensors, 2010 ieee* (pp. 2325–2328).

Doshvarpassand, S., Wu, C. & Wang, X. (2019). An overview of corrosion defect characterization using active infrared thermography. *Infrared physics & technology*, *96*, 366–389.

Fan, W. & Qiao, P. (2011). Vibration-based damage identification methods: a review and comparative study. *Structural health monitoring*, *10*(1), 83–111.

Fang, X., Misra, S., Xue, G. & Yang, D. (2011). Smart grid—the new and improved power grid: A survey. *IEEE communications surveys & tutorials*, *14*(4), 944–980.

Farrar, C. R., Park, G., Allen, D. W. & Todd, M. D. (2006). Sensor network paradigms for structural health monitoring. *Structural Control and Health Monitoring: The Official Journal of the International Association for Structural Control and Monitoring and of the European Association for the Control of Structures*, *13*(1), 210–225.

Farrar, C. R. & Worden, K. (2007). An introduction to structural health monitoring. *Philosophical Transactions of the Royal Society A: Mathematical, Physical and Engineering Sciences*, *365*(1851), 303–315.

Firdaus Hashim, R. M., Kassim, M., Suliman, S. I., Anas, N. M. & Bakar, A. Z. A. (2019). Implementation of embedded real-time monitoring temperature and humidity system. *Indonesian Journal of Electrical Engineering and Computer Science*, *16*(1), 184–190.

Fu, H., Khodaei, Z. S. & Aliabadi, M. F. (2018). An event-triggered energy-efficient wireless structural health monitoring system for impact detection in composite airframes. *IEEE Internet of Things Journal*, *6*(1), 1183–1192.

Gambi, E., Montanini, L., Pigini, D., Ciattaglia, G. & Spinsante, S. (2018). A home automation architecture based on lora technology and message queue telemetry transfer protocol. *International Journal of Distributed Sensor Networks*, *14*(10), 1550147718806837.

Ghosh, S. (2018). Smart homes: Architectural and engineering design imperatives for smart city building codes. In *2018 technologies for smart-city energy security and power (icsesp)* (pp. 1–4).

Gkotsiopoulos, P., Zorbas, D. & Douligeris, C. (2021). Performance determinants in lora networks: A literature review. *IEEE Communications Surveys & Tutorials*, *23*(3), 1721–1758.

Glisic, B. (2022). Concise historic overview of strain sensors used in the monitoring of civil structures: The first one hundred years. *Sensors*, *22*(6), 2397.

Gomes, G. F., De Almeida, F. A., Junqueira, D. M., da Cunha Jr, S. S. & Ancelotti Jr, A. C. (2019). Optimized damage identification in cfrp plates by reduced mode shapes and ga-ann methods. *Engineering Structures*, *181*, 111–123.

Gordan, M., Sabbagh-Yazdi, S.-R., Ismail, Z., Ghaedi, K., Carroll, P., McCrum, D. & Samali, B. (2022). State-of-the-art review on advancements of data mining in structural health monitoring. *Measurement*, 110939.

Gubbi, J., Buyya, R., Marusic, S. & Palaniswami, M. (2013). Internet of things (iot): A vision, architectural elements, and future directions. *Future generation computer systems*, *29*(7), 1645–1660.

Han, J., Song, W., Gozho, A., Sung, Y., Ji, S., Song, L., ... Zhang, Q. (2020). Lora-based smart iot application for smart city: an example of human posture detection. *Wireless Communications and Mobile Computing*, *2020*.

He, Y., Zhang, L., Chen, Z. & Li, C. Y. (2022). A framework of structural damage detection for civil structures using a combined multi-scale convolutional neural network and echo state network. *Engineering with Computers*, 1–19.

Herrera-Iriarte, A., Alvarez-Montoya, J. & Sierra-Pérez, J. (2020). Study of sensitivity for strain-based structural health monitoring. In *Iop conference series: Materials science and engineering* (Vol. 836, p. 012001).

Hou, R. & Xia, Y. (2021). Review on the new development of vibration-based damage identification for civil engineering structures: 2010–2019. *Journal of Sound and Vibration*, *491*, 115741.

Hu, C., Gao, Y. & Sheng, Z. (2000). The piezoresistance coefficients of copper and copper-nickel alloys. *Journal of materials science*, *35*, 381–386.

IoT, L. (2022, 7). *Waspmote.* Retrieved from `https://www.libelium.com/iot-products/waspmote/`

Islam, R., Rahman, M. W., Rubaiat, R., Hasan, M. M., Reza, M. M. & Rahman, M. M. (2022). Lora and server-based home automation using the internet of things (iot). *Journal of King Saud University-Computer and Information Sciences*, *34*(6), 3703–3712.

Iyer, S., Patro, P., Kapadia, R., Das, A., Cheriyan, S. & Ansari, N. (2020). Iot based cost-effective centralised smart irrigation system using lora. In *Proceedings of the 3rd international conference on advances in science & technology (icast).*

Jain, Y., Soni, B., Goyal, A. & Sharma, C. (2020). Novel wearable device for health monitoring and tracking of soldiers based on lora module. In *2020 ieee 4th conference on information & communication technology (cict)* (pp. 1–5).

Jang, S. & Spencer Jr, B. F. (2015). Structural health monitoring for bridge structures using smart sensors.

Jang, W.-S., Healy, W. M. & Skibniewski, M. J. (2008). Wireless sensor networks as part of a web-based building environmental monitoring system. *Automation in Construction*, *17*(6), 729–736.

Jo, H., Park, J.-W., Spencer, B., Jung, H.-J. et al. (2013). Develoment of high-sensitivity wireless strain sensor for structural health monitoring. *Smart Struct. Syst*, *11*(5), 477–496.

Kang, D.-H., Park, M.-S., Kim, H.-S., Kim, D.-y., Kim, S.-H., Son, H.-J. & Lee, S.-G. (2017). Room temperature control and fire alarm/suppression iot service using mqtt on aws. In *2017 international conference on platform technology and service (platcon)* (pp. 1–5).

Kim, B. & Cho, S. (2018). Automated vision-based detection of cracks on concrete surfaces using a deep learning technique. *Sensors*, *18*(10), 3452.

Kim, H., Ahn, E., Cho, S., Shin, M. & Sim, S.-H. (2017). Comparative analysis of image binarization methods for crack identification in concrete structures. *Cement and Concrete Research*, *99*, 53–61.

Kim, J., Nadukuru, S., Pour-Ghaz, M., Lynch, J., Michalowski, R., Bradshaw, A.,

... Weiss, W. (2012). Assessment of the behavior of buried concrete pipelines subjected to ground rupture: experimental study. *Journal of Pipeline Systems Engineering and Practice*, *3*(1), 8–16.

Kim, J.-T., Ryu, Y.-S., Cho, H.-M. & Stubbs, N. (2003). Damage identification in beam-type structures: frequency-based method vs mode-shape-based method. *Engineering structures*, *25*(1), 57–67.

Kohler, M. D., Hao, S., Mishra, N., Govinda, R. & Nigbor, R. (2015). Shakenet: a portable wireless sensor network for instrumenting large civil structures.

Lee, J., Stanley, M., Spanias, A. & Tepedelenlioglu, C. (2016). Integrating machine learning in embedded sensor systems for internet-of-things applications. In *2016 ieee international symposium on signal processing and information technology (isspit)* (pp. 290–294).

Lee, J.-L., Tyan, Y.-Y., Wen, M.-H. & Wu, Y.-W. (2017). Development of an iot-based bridge safety monitoring system. In *2017 international conference on applied system innovation (icasi)* (pp. 84–86).

Li, G., Ma, B., He, S., Ren, X. & Liu, Q. (2020). Automatic tunnel crack detection based on u-net and a convolutional neural network with alternately updated clique. *Sensors*, *20*(3), 717.

Lin, M., Guo, S., He, S., Li, W. & Yang, D. (2022). Structure health monitoring of a composite wing based on flight load and strain data using deep learning method. *Composite Structures*, *286*, 115305.

Liu, P., Yuan, S. & Qiu, L. (2012). Development of a pzt-based wireless digital monitor for composite impact monitoring. *Smart Materials and Structures*, *21*(3), 035018.

Loh, K. J., Kim, J., Lynch, J. P., Kam, N. W. S. & Kotov, N. A. (2007). Multifunctional layer-by-layer carbon nanotube–polyelectrolyte thin films for strain and corrosion sensing. *Smart Materials and Structures*, *16*(2), 429.

Lousado, J. P. & Antunes, S. (2020). Monitoring and support for elderly people using lora communication technologies: Iot concepts and applications. *Future Internet*, *12*(11), 206.

Ltd., S. R. (2022, 12). *Wearable Sensor Technology | Wireless IMU | ECG | EMG | GSR.* Retrieved from `https://shimmersensing.com/`

Lu, P., Lalam, N., Badar, M., Liu, B., Chorpening, B. T., Buric, M. P. & Ohodnicki, P. R. (2019). Distributed optical fiber sensing: Review and perspective. *Applied Physics Reviews*, *6*(4), 041302.

Lueth, K. L. (2015). The 10 most popular internet of things applications right now. *IoT Analytics*.

Lueth, K. L. (2018, 2). *The Top 10 IoT Segments in 2018 – based on 1,600 real IoT projects.* Retrieved from `https://iot-analytics.com/top-10-iot-segments-2018-real-iot-projects`

Lynch, J. P. & Loh, K. J. (2006). A summary review of wireless sensors and sensor networks for structural health monitoring. *Shock and Vibration Digest*, *38*(2), 91–130.

Madakam, S., Lake, V., Lake, V., Lake, V. et al. (2015). Internet of things (iot): A literature review. *Journal of Computer and Communications*, *3*(05), 164.

Mahmud, M. A., Abdelgawad, A., Yelamarthi, K. & Ismail, Y. A. (2017). Signal processing techniques for iot-based structural health monitoring. In *2017 29th international conference on microelectronics (icm)* (pp. 1–5).

Mann, J. (2019, 7). *AUT Nga Wai Hono Building, Auckland — Jason Mann Photography.* Retrieved from `https://jasonmann.co.nz/architectural-photography/aut-ecms`

Marais, J. M., Malekian, R. & Abu-Mahfouz, A. M. (2017). Lora and lorawan testbeds: A review. *2017 Ieee Africon*, 1496–1501.

Maurya, A. K., Kumar, S., Singh, M. & Manik, G. (2022). Polyamide fiber reinforced polymeric composites: a short review. *Materials Today: Proceedings*.

Measuring Strain with Strain Gages. (n.d.). Retrieved from `https://www.ni.com/en-nz/shop/data-acquisition/sensor-fundamentals/measuring-strain-with-strain-gages.html`

Mettler, M. (2016). Blockchain technology in healthcare: The revolution starts here. In *2016 ieee 18th international conference on e-health networking, applications and services (healthcom)* (pp. 1–3).

Mikhaylov, K., Petaejaejaervi, J. & Haenninen, T. (2016). Analysis of capacity and scalability of the lora low power wide area network technology. In *European wireless 2016; 22th european wireless conference* (pp. 1–6).

Mikhaylov, K., Petäjäjärvi, J. & Janhunen, J. (2017). On lorawan scalability: Empirical evaluation of susceptibility to inter-network interference. In *2017 european conference on networks and communications (eucnc)* (pp. 1–6).

Misra, D., Das, G. & Das, D. (2020). An iot based building health monitoring system supported by cloud. *Journal of Reliable Intelligent Environments*, *6*(3), 141–152.

Misra, R., Jalali, H., Rizzo, P. & Dickerson, S. J. (2021). Wireless node for highly nonlinear solitary wave transducers. *IEEE Sensors Journal*, *22*(4), 3540–3552.

Montalvao, D., Maia, N. M. M. & Ribeiro, A. M. R. (2006). A review of vibration-based structural health monitoring with special emphasis on composite materials. *Shock and vibration digest*, *38*(4), 295–324.

Morassi, A. & Vestroni, F. (2008). *Dynamic methods for damage detection in structures*. Springer Science & Business Media.

Moreu, F., Kim, R. E. & Spencer Jr, B. (2017). Railroad bridge monitoring using wireless smart sensors. *Structural Control and Health Monitoring*, *24*(2), e1863.

Mutlib, N. K., Baharom, S. B., El-Shafie, A. & Nuawi, M. Z. (2016). Ultrasonic health monitoring in structural engineering: buildings and bridges. *Structural Control and Health Monitoring*, *23*(3), 409–422.

Myers, A., Mahmud, M. A., Abdelgawad, A. & Yelamarthi, K. (2016). Toward integrating structural health monitoring with internet of things (iot). In *2016 ieee international conference on electro information technology (eit)* (pp. 0438–0441).

Nagayama, T., Spencer, B. & Rice, J. (2008). Structural health monitoring using smart sensors. In *World forum on smart materials and smart structures technology* (pp. 278–278).

National Instruments. (n.d.). *Measuring strain with strain gages.* Retrieved 2023-03-21, from https://www.ni.com/en-nz/shop/data-acquisition/sensor-fundamentals/measuring-strain-with-strain-gages.html

National Instruments. (n.d.). Retrieved from https://www.ni.com/docs/en-US/bundle/pxie-4339-rm-4339-seri/resource/375963a.pdf

Network, T. T. (2015). *The Things network.* Retrieved from https://www.thethingsnetwork.org/

The New Zealand Infrastructure Strategy 2022-2052: A foundation for progress (Tech. Rep.). (2022, 10). Retrieved from https://www.minterellison.co.nz/insights/the-new-zealand-infrastructure-strategy-2022-2052

Ni, Y.-Q., Wang, B. S. & Ko, J. M. (2000). Simulation studies of damage location in tsing ma bridge deck. In *Nondestructive evaluation of highways, utilities, and pipelines iv* (Vol. 3995, pp. 312–323).

Nicolescu, R., Huth, M., Radanliev, P. & De Roure, D. (2018). Mapping the values of iot. *Journal of Information Technology*, *33*(4), 345–360.

Ostertagová, E. (2012). Modelling using polynomial regression. *Procedia Engineering*, *48*, 500–506.

Ou, J. & Li, H. (2010). Structural health monitoring in mainland china: review and future trends. *Structural health monitoring*, *9*(3), 219–231.

Pathirage, C. S. N., Li, J., Li, L., Hao, H., Liu, W. & Ni, P. (2018). Structural damage identification based on autoencoder neural networks and deep learning. *Engineering structures*, *172*, 13–28.

Petersen, H., Baccelli, E., Wählisch, M., Schmidt, T. C. & Schiller, J. (2014). The role of the internet of things in network resilience. In *International internet of things summit* (pp. 283–296).

Plageras, A. P., Psannis, K. E., Stergiou, C., Wang, H. & Gupta, B. B. (2018). Efficient iot-based sensor big data collection–processing and analysis in smart buildings. *Future Generation Computer Systems*, *82*, 349–357.

Pramukantoro, E. S., Luckies, M. & Bakhtiar, F. A. (2019). Bridging iot infrastructure and cloud application using cellular-based internet gateway device. *TELKOMNIKA (Telecommunication Computing Electronics and Control)*, *17*(3), 1439–1446.

Qiu, L., Deng, X., Yuan, S., Huang, Y. & Ren, Y. (2018). Impact monitoring for aircraft smart composite skins based on a lightweight sensor network and characteristic digital sequences. *Sensors*, *18*(7), 2218.

RAKWireless. (2023, 8). *RAK2245 PI HAT WiSLink LPWAN Concentrator.* Retrieved from https://docs.rakwireless.com/Product-Categories/WisLink/RAK2245-Pi-HAT/Overview/

Rappaport, T. S. (2002). Wireless communications–principles and practice, (the book end). *Microwave Journal*, *45*(12), 128–129.

Rumelhart, D. E., Hinton, G. E. & Williams, R. J. (1986). Learning representations by

back-propagating errors. *nature*, *323*(6088), 533–536.

Rytter, A., Brincker, R. & Hansen, L. P. (1991). Vibration based inspection of civil engineering structures. *Bygningstekniske Meddelelser*, *62*(4).

Saha, S. & Majumdar, A. (2017). Data centre temperature monitoring with esp8266 based wireless sensor network and cloud based dashboard with real time alert system. In *2017 devices for integrated circuit (devic)* (pp. 307–310).

Sahota, J. K., Gupta, N. & Dhawan, D. (2020). Fiber bragg grating sensors for monitoring of physical parameters: A comprehensive review. *Optical Engineering*, *59*(6), 060901.

Sánchez Sutil, F. & Cano-Ortega, A. (2020). Smart public lighting control and measurement system using lora network. *Electronics*, *9*(1), 124.

Schulz, M. & Sundaresan, M. (2006). *Smart sensor system for structural condition monitoring of wind turbines: 30 may 2002–30 april 2006* (Tech. Rep.). National Renewable Energy Lab.(NREL), Golden, CO (United States).

Shrouf, F., Ordieres, J. & Miragliotta, G. (2014). Smart factories in industry 4.0: A review of the concept and of energy management approached in production based on the internet of things paradigm. In *2014 ieee international conference on industrial engineering and engineering management* (pp. 697–701).

Sidorov, M., Nhut, P. V., Matsumoto, Y. & Ohmura, R. (2019). Lora-based precision wireless structural health monitoring system for bolted joints in a smart city environment. *IEEE Access*, *7*, 179235–179251.

Sohn, H., Farrar, C. R., Hemez, F. M., Shunk, D. D., Stinemates, D. W., Nadler, B. R. & Czarnecki, J. J. (2003). A review of structural health monitoring literature: 1996–2001. *Los Alamos National Laboratory, USA*, *1*.

Spark NZ network coverage. (2023). Retrieved from `https://www.spark.co.nz/shop/mobile/network.html`

Spencer Jr, B., Park, J.-W., Mechitov, K., Jo, H. & Agha, G. (2017). Next generation wireless smart sensors toward sustainable civil infrastructure. *Procedia engineering*, *171*, 5–13.

STMicroelectronics. (n.d.). *Stm32l0 discovery kit lora, sigfox, low-power wireless.* Retrieved 2023-01-16, from `https://www.st.com/en/evaluation-tools/b-l072z-lrwan1.html`

The things industries. (2015). Retrieved from `https://www.thethingsindustries.com/`

Tong, Z., Gao, J., Han, Z. & Wang, Z. (2018). Recognition of asphalt pavement crack length using deep convolutional neural networks. *Road Materials and Pavement Design*, *19*(6), 1334–1349.

Vafaei, M., Alih, S. C., Shad, H., Falah, A. & Halim, N. H. F. A. (2018). Prediction of strain values in reinforcements and concrete of a rc frame using neural networks. *International Journal of Advanced Structural Engineering*, *10*, 29–35.

Vega-Rodríguez, R., Sendra, S., Lloret, J., Romero-Díaz, P. & Garcia-Navas, J. L. (2019). Low cost lora based network for forest fire detection. In *2019 sixth international conference on internet of things: Systems, management and security (iotsms)* (pp. 177–184).

Vermesan, O., Friess, P., Guillemin, P., Gusmeroli, S., Sundmaeker, H., Bassi, A., ... others (2022). Internet of things strategic research roadmap. In *Internet of things-global technological and societal trends from smart environments and spaces to green ict* (pp. 9–52). River Publishers.

Wadhwani, S., Singh, U., Singh, P. & Dwivedi, S. (2018). Smart home automation and security system using arduino and iot. *International Research Journal of Engineering and Technology (IRJET)*, *5*(2), 1357–1359.

Wang, Z. & Bovik, A. C. (2009). Mean squared error: Love it or leave it? a new look at signal fidelity measures. *IEEE signal processing magazine*, *26*(1), 98–117.

Wilson, R. C., Shenhav, A., Straccia, M. & Cohen, J. D. (2019). The eighty five percent rule for optimal learning. *Nature communications*, *10*(1), 4646.

Wixted, A. J., Kinnaird, P., Larijani, H., Tait, A., Ahmadinia, A. & Strachan, N. (2016). Evaluation of lora and lorawan for wireless sensor networks. In *2016 ieee sensors* (pp. 1–3).

World Internet Users Statistics and 2022 World Population Stats. (2022). Retrieved from `https://www.internetworldstats.com/stats.htm`

Wu, R.-T. & Jahanshahi, M. R. (2020). Data fusion approaches for structural health monitoring and system identification: past, present, and future. *Structural Health Monitoring*, *19*(2), 552–586.

Wu, Y., Liu, W. & Li, K. (2017). A novel wireless acoustic emission sensor system for distributed wooden structural health monitoring. *Int J Innov Comput Inf Control*, *13*(4), 1289–1306.

Xu, S., Fan, Z., Yang, S., Zhao, Y. & Pan, L. (2021). Flexible, self-powered and multi-functional strain sensors comprising a hybrid of carbon nanocoils and conducting polymers. *Chemical Engineering Journal*, *404*, 126064.

Yam, L., Yan, Y. & Jiang, J. (2003). Vibration-based damage detection for composite structures using wavelet transform and neural network identification. *Composite Structures*, *60*(4), 403–412.

Yao, H., Cao, H. & Li, J. (2016). Design and implementation of a portable wireless system for structural health monitoring. *Measurement and Control*, *49*(1), 23–32.

Yao, Y. & Glisic, B. (2012). Reliable damage detection and localization using direct strain sensing. In *6th international conference on bridge maintenance, safety and management, iabmas 2012* (pp. 714–721).

Yasmin, R., Salminen, M., Gilman, E., Petäjäjärvi, J., Mikhaylov, K., Pakanen, M., ... Pouttu, A. (2018). Combining iot deployment and data visualization: experiences within campus maintenance use-case. In *2018 9th international conference on the network of the future (nof)* (pp. 101–105).

Zang, C. & Imregun, M. (2001). Structural damage detection using artificial neural networks and measured frf data reduced via principal component projection. *Journal of sound and vibration*, *242*(5), 813–827.

Zhang, L., Zhou, G., Han, Y., Lin, H. & Wu, Y. (2018). Application of internet of things technology and convolutional neural network model in bridge crack detection. *Ieee Access*, *6*, 39442–39451.

Zhao, Y., Zhu, Y., Yuan, M., Wang, J. & Zhu, S. (2016). A laser-based fiber bragg grating

ultrasonic sensing system for structural health monitoring. *IEEE Photonics Technology Letters*, *28*(22), 2573–2576.

Zhu, L., Fu, Y., Chow, R., Spencer Jr, B. F., Park, J. W. & Mechitov, K. (2018). Development of a high-sensitivity wireless accelerometer for structural health monitoring. *Sensors*, *18*(1), 262.

Zymelka, D., Togashi, K., Ohigashi, R., Yamashita, T., Takamatsu, S., Itoh, T. & Kobayashi, T. (2017). Printed strain sensor array for application to structural health monitoring. *Smart Materials and Structures*, *26*(10), 105040.

Zymelka, D., Yamashita, T., Takamatsu, S., Itoh, T. & Kobayashi, T. (2018). Printed strain sensors for early damage detection in engineering structures. *Japanese Journal of Applied Physics*, *57*(5S), 05GD05.

Appendix A

LoRa-Based Wireless Sensor Node Hardware Design

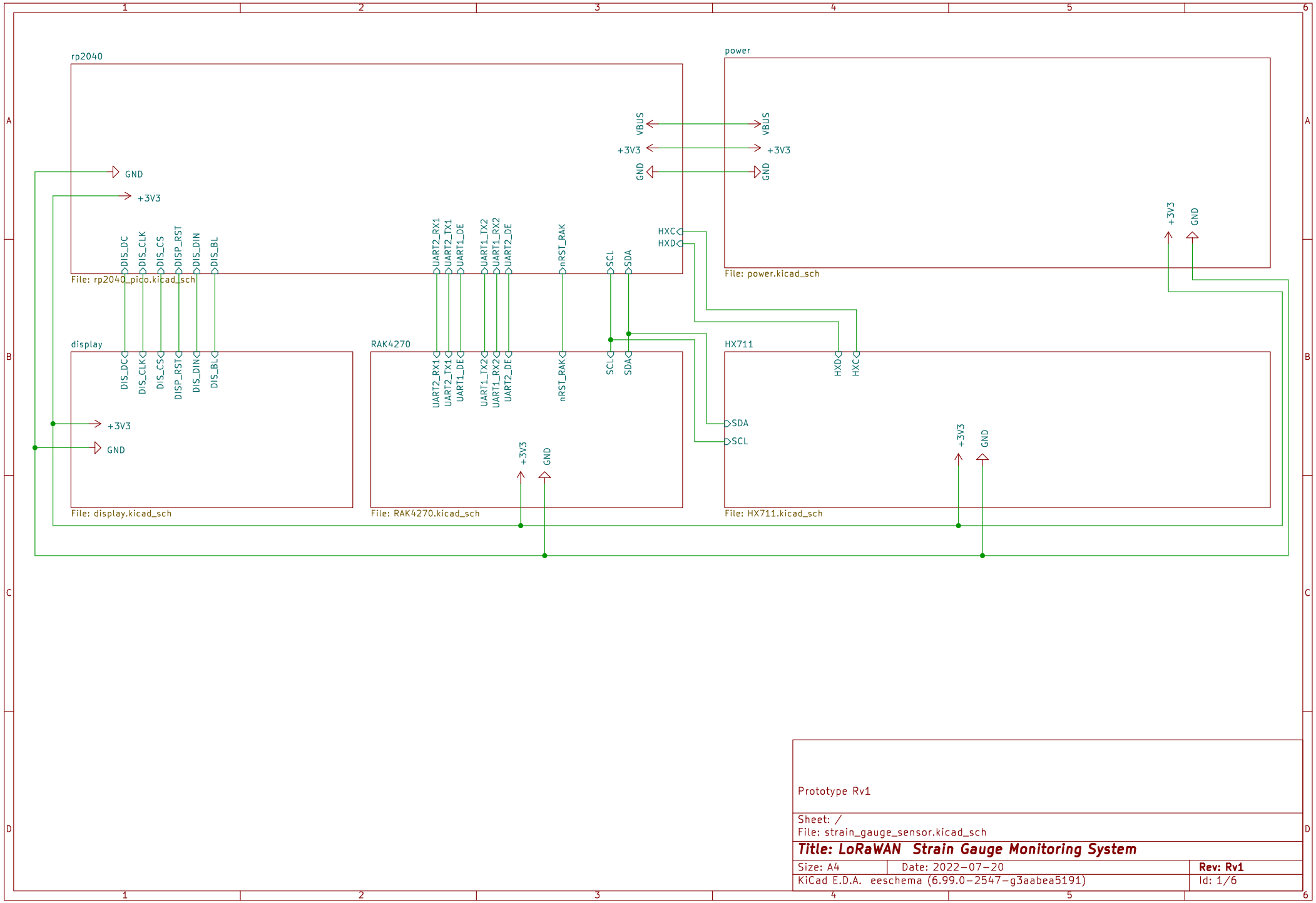

Prototype Rv1

Sheet: /
File: strain_gauge_sensor.kicad_sch

Title: LoRaWAN Strain Gauge Monitoring System

Size: A4	Date: 2022-07-20	**Rev: Rv1**
KiCad E.D.A. eeschema (6.99.0-2547-g3aabea5191)		Id: 1/6

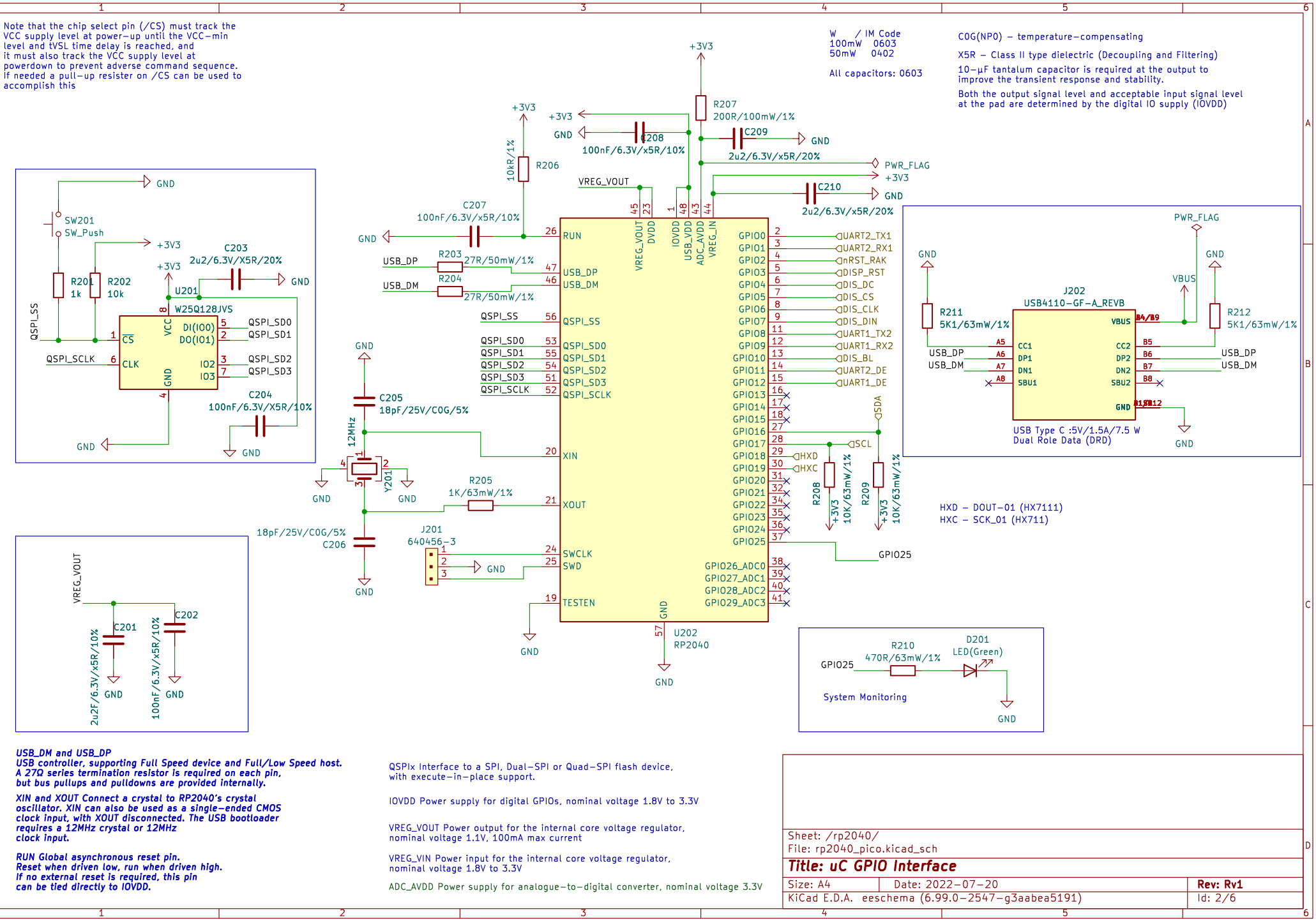
Note that the chip select pin (/CS) must track the VCC supply level at power-up until the VCC-min level and tVSL time delay is reached, and it must also track the VCC supply level at powerdown to prevent adverse command sequence. If needed a pull-up resister on /CS can be used to accomplish this
W / IM Code
100mW 0603
50mW 0402
All capacitors: 0603
C0G(NP0) - temperature-compensating
X5R - Class II type dielectric (Decoupling and Filtering)
10-µF tantalum capacitor is required at the output to improve the transient response and stability.
Both the output signal level and acceptable input signal level at the pad are determined by the digital IO supply (IOVDD)
SW201
SW_Push
R201 1k
R202 10k
C203 2u2/6.3V/X5R/20%
U201
W25Q128JVS
QSPI_SS
QSPI_SCLK
QSPI_SD0
QSPI_SD1
QSPI_SD2
QSPI_SD3
C204 100nF/6.3V/X5R/10%
R207 200R/100mW/1%
C208 100nF/6.3V/x5R/10%
C209 2u2/6.3V/x5R/20%
C210 2u2/6.3V/x5R/20%
PWR_FLAG
R206 10KR/1%
C207 100nF/6.3V/x5R/10%
VREG_VOUT
R203 27R/50mW/1%
R204 27R/50mW/1%
USB_DP
USB_DM
C205 18pF/25V/C0G/5%
12MHz
Y201
R205 1K/63mW/1%
C206 18pF/25V/C0G/5%
J201 640456-3
SWCLK
SWD
TESTEN
RUN
XIN
XOUT
U202 RP2040
GPIO0 UART2_TX1
GPIO1 UART2_RX1
GPIO2 nRST_RAK
GPIO3 DISP_RST
GPIO4 DIS_DC
GPIO5 DIS_CS
GPIO6 DIS_CLK
GPIO7 DIS_DIN
GPIO8 UART1_TX2
GPIO9 UART1_RX2
GPIO10 DIS_BL
GPIO11 UART2_DE
GPIO12 UART1_DE
GPIO16 SDA
GPIO17 SCL
GPIO18 HXD
GPIO19 HXC
GPIO25
R208 10K/63mW/1%
R209 10K/63mW/1%
HXD - DOUT-01 (HX7111)
HXC - SCK_01 (HX711)
J202 USB4110-GF-A_REVB
R211 5K1/63mW/1%
R212 5K1/63mW/1%
USB Type C :5V/1.5A/7.5 W Dual Role Data (DRD)
C201 2u2F/6.3V/x5R/10%
C202 100nF/6.3V/X5R/10%
R210 470R/63mW/1%
D201 LED(Green)
System Monitoring
USB_DM and USB_DP
USB controller, supporting Full Speed device and Full/Low Speed host. A 27Ω series termination resistor is required on each pin, but bus pullups and pulldowns are provided internally.
XIN and XOUT Connect a crystal to RP2040's crystal oscillator. XIN can also be used as a single-ended CMOS clock input, with XOUT disconnected. The USB bootloader requires a 12MHz crystal or 12MHz clock input.
RUN Global asynchronous reset pin. Reset when driven low, run when driven high. If no external reset is required, this pin can be tied directly to IOVDD.
QSPIx Interface to a SPI, Dual-SPI or Quad-SPI flash device, with execute-in-place support.
IOVDD Power supply for digital GPIOs, nominal voltage 1.8V to 3.3V
VREG_VOUT Power output for the internal core voltage regulator, nominal voltage 1.1V, 100mA max current
VREG_VIN Power input for the internal core voltage regulator, nominal voltage 1.8V to 3.3V
ADC_AVDD Power supply for analogue-to-digital converter, nominal voltage 3.3V
Sheet: /rp2040/
File: rp2040_pico.kicad_sch
Title: uC GPIO Interface
Size: A4
Date: 2022-07-20
Rev: Rv1
KiCad E.D.A. eeschema (6.99.0-2547-g3aabea5191)
Id: 2/6

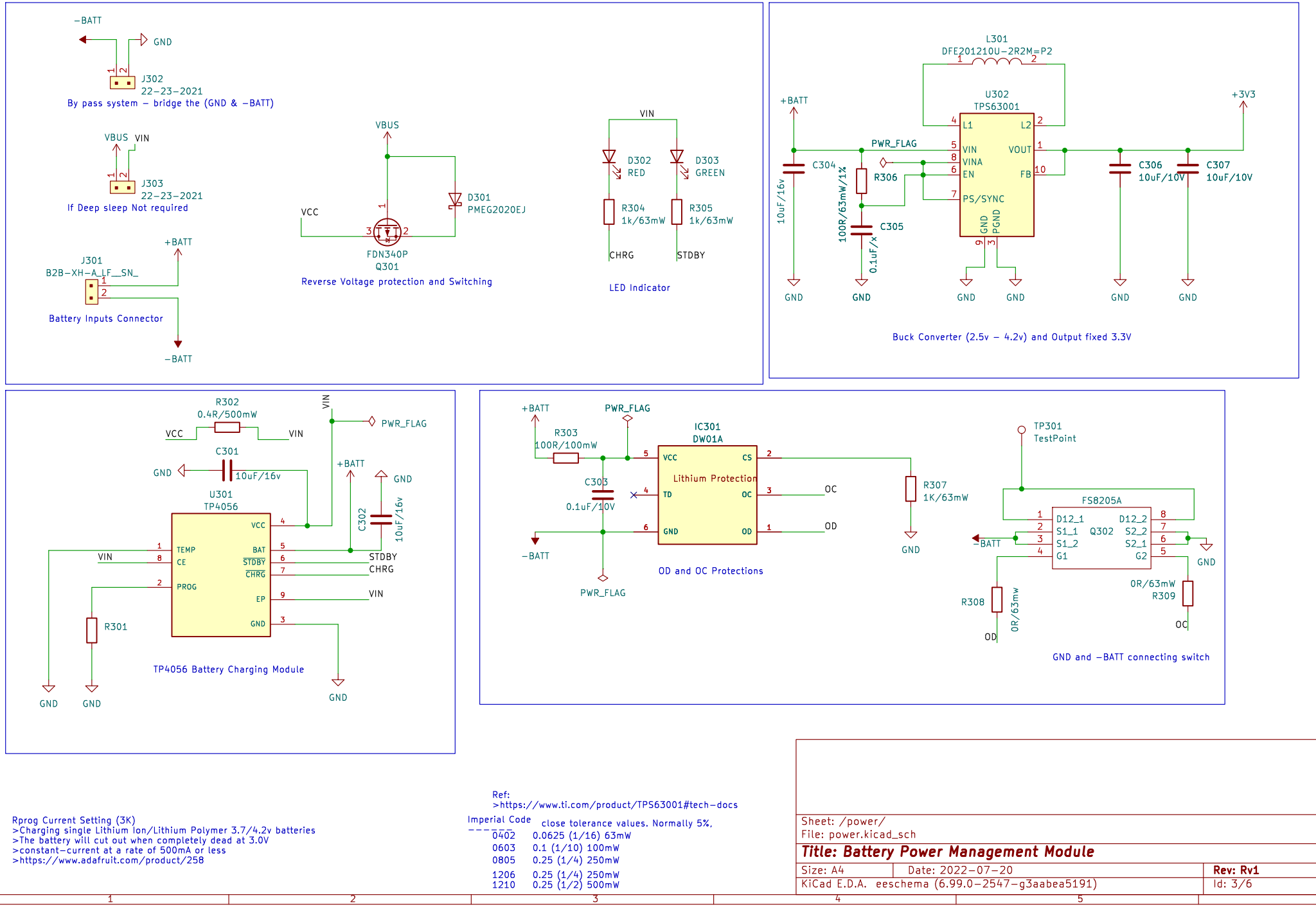

Rprog Current Setting (3K)
>Charging single Lithium Ion/Lithium Polymer 3.7/4.2v batteries
>The battery will cut out when completely dead at 3.0V
>constant−current at a rate of 500mA or less
>https://www.adafruit.com/product/258

Ref:
>https://www.ti.com/product/TPS63001#tech−docs

Imperial Code	close tolerance values. Normally 5%,
0402	0.0625 (1/16) 63mW
0603	0.1 (1/10) 100mW
0805	0.25 (1/4) 250mW
1206	0.25 (1/4) 250mW
1210	0.25 (1/2) 500mW

Sheet: /power/
File: power.kicad_sch

Title: Battery Power Management Module

Size: A4	Date: 2022−07−20	**Rev: Rv1**
KiCad E.D.A. eeschema (6.99.0−2547−g3aabea5191)		Id: 3/6

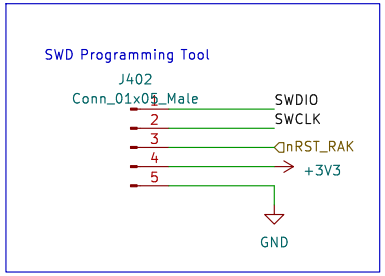

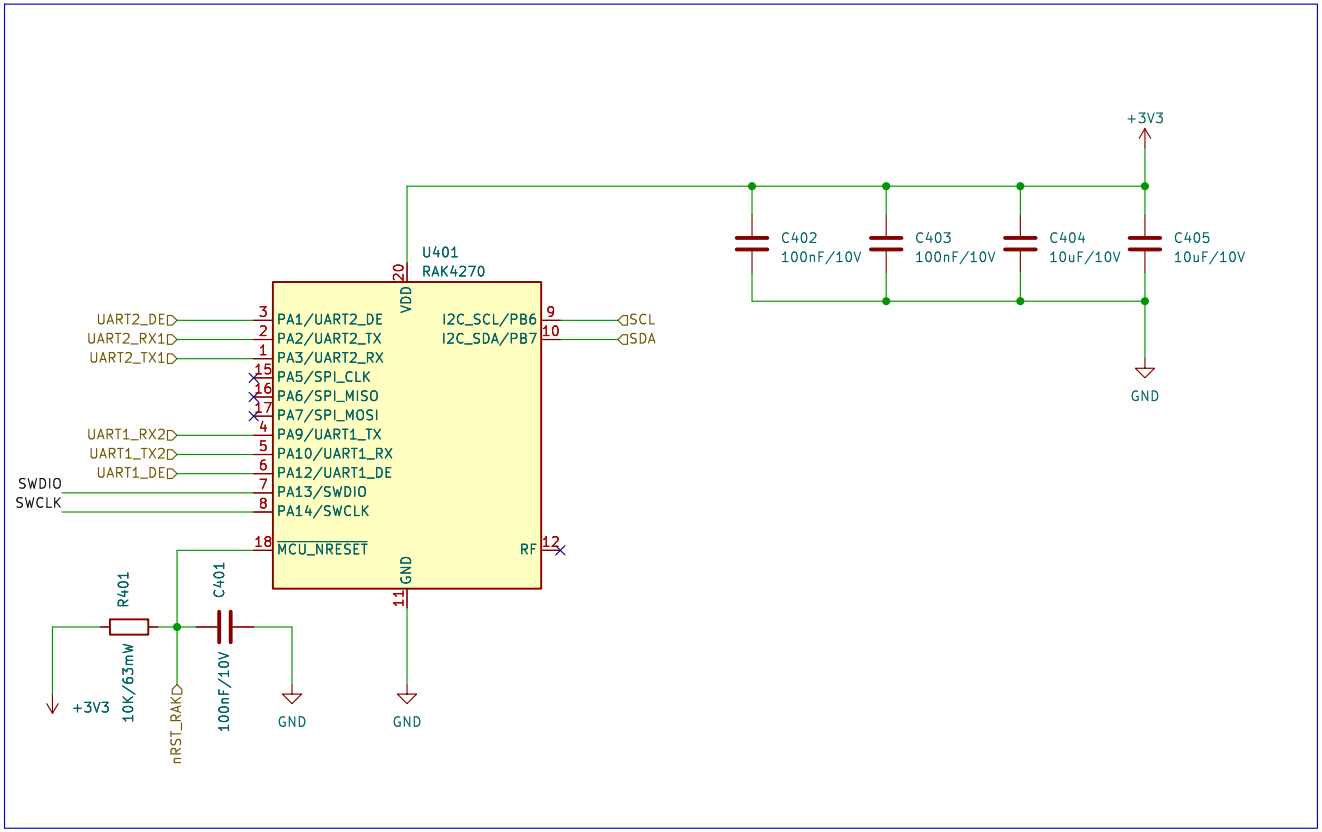

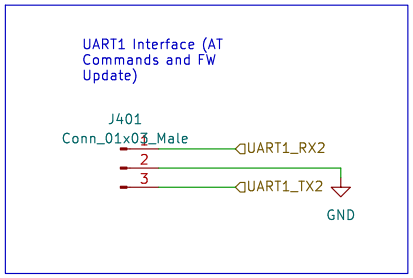

UART1-TX1 ->> EX: TXn -> n =1,2 (rp2040 TX1 0r TX2)
Uart1 – At Commands
Uart2 – Firmware Update

Sheet: /RAK4270/
File: RAK4270.kicad_sch

Title: RAK4270 Module

Size: A4	Date: 2022-07-20	**Rev: Rv1**
KiCad E.D.A. eeschema (6.99.0-2547-g3aabea5191)		Id: 4/6

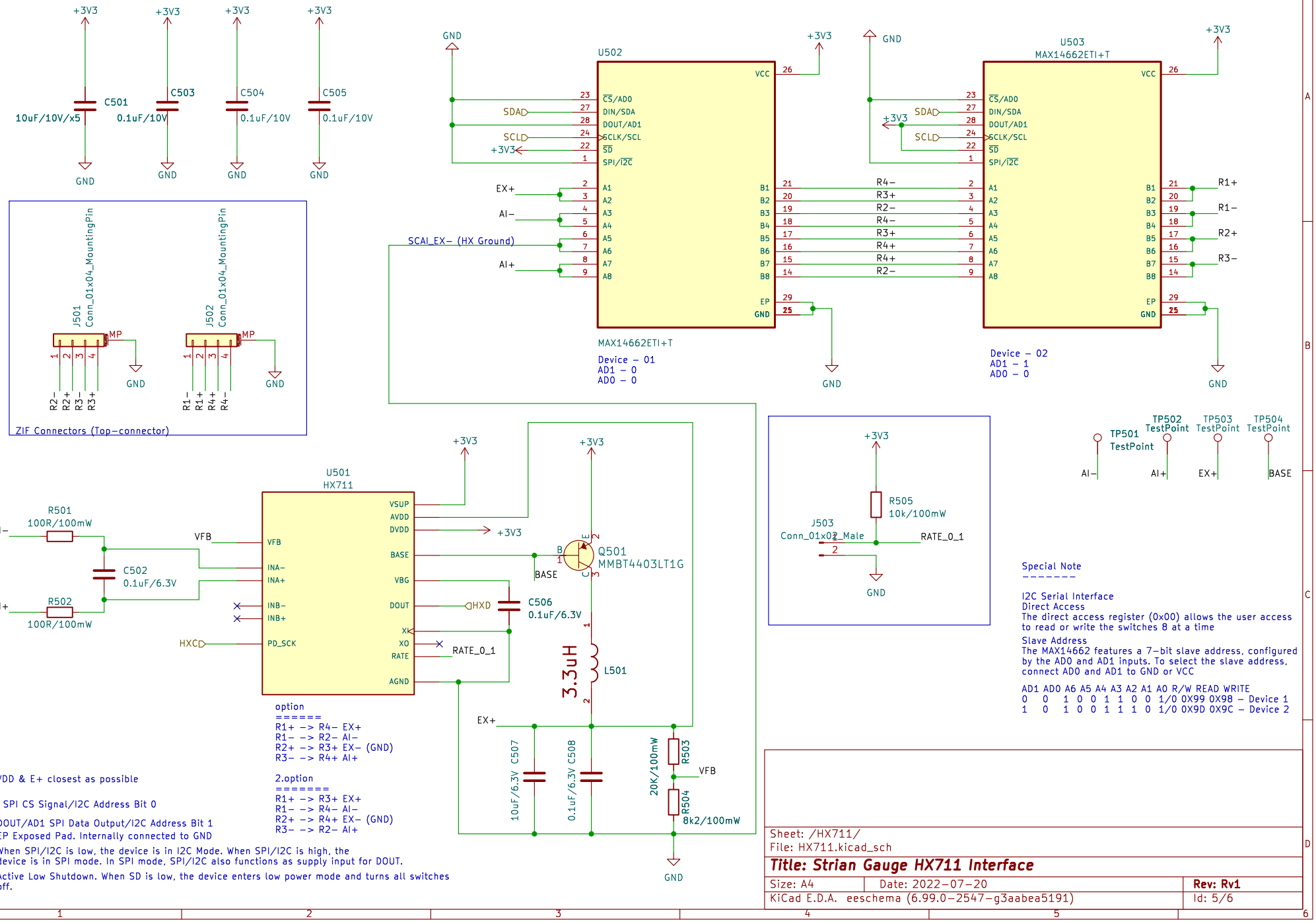
+3V3
C501
10uF/10V/x5
GND
C503
0.1uF/10V
C504
0.1uF/10V
C505
0.1uF/10V
U502
MAX14662ETI+T
Device – 01
AD1 – 0
AD0 – 0
U503
MAX14662ETI+T
Device – 02
AD1 – 1
AD0 – 0
SDA
SCL
SCAI_EX– (HX Ground)
EX+
AI–
AI+
R4–
R3+
R2–
R4–
R3+
R4+
R4+
R2–
R1+
R1–
R2+
R3–
J501
Conn_01x04_MountingPin
J502
Conn_01x04_MountingPin
MP
R2–
R2+
R3–
R3+
R1–
R1+
R4+
R4–
ZIF Connectors (Top–connector)
U501
HX711
VSUP
AVDD
DVDD
BASE
VBG
DOUT
XI
XO
RATE
AGND
VFB
INA–
INA+
INB–
INB+
PD_SCK
HXD
HXC
RATE_0_1
R501
100R/100mW
R502
100R/100mW
C502
0.1uF/6.3V
C506
0.1uF/6.3V
Q501
MMBT4403LT1G
L501
3.3uH
C507
10uF/6.3V
C508
0.1uF/6.3V
R503
20K/100mW
R504
8k2/100mW
VFB
J503
Conn_01x02_Male
R505
10k/100mW
RATE_0_1
TP501
TestPoint
TP502
TestPoint
TP503
TestPoint
TP504
TestPoint
AI–
AI+
EX+
BASE
Special Note
I2C Serial Interface
Direct Access
The direct access register (0x00) allows the user access to read or write the switches 8 at a time
Slave Address
The MAX14662 features a 7–bit slave address, configured by the AD0 and AD1 inputs. To select the slave address, connect AD0 and AD1 to GND or VCC
AD1 AD0 A6 A5 A4 A3 A2 A1 A0 R/W READ WRITE
0 0 1 0 0 1 1 0 0 1/0 0X99 0X98 – Device 1
1 0 1 0 0 1 1 1 0 1/0 0X9D 0X9C – Device 2
option
======
R1+ –> R4– EX+
R1– –> R2– AI–
R2+ –> R3+ EX– (GND)
R3– –> R4+ AI+
2.option
=======
R1+ –> R3+ EX+
R1– –> R4– AI–
R2+ –> R4+ EX– (GND)
R3– –> R2– AI+
* Analog VDD & E+ closest as possible
SPI CS Signal/I2C Address Bit 0
DOUT/AD1 SPI Data Output/I2C Address Bit 1
EP Exposed Pad. Internally connected to GND
When SPI/I2C is low, the device is in I2C Mode. When SPI/I2C is high, the device is in SPI mode. In SPI mode, SPI/I2C also functions as supply input for DOUT.
Active Low Shutdown. When SD is low, the device enters low power mode and turns all switches off.
Sheet: /HX711/
File: HX711.kicad_sch
Title: Strian Gauge HX711 Interface
Size: A4
Date: 2022–07–20
Rev: Rv1
KiCad E.D.A. eeschema (6.99.0–2547–g3aabea5191)
Id: 5/6

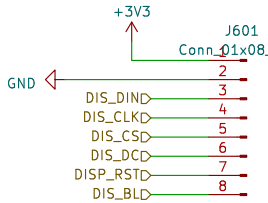

VCC Power (3.3V/5V input)
GND Ground
DIN SPI data input
CLK SPI clock input
CS Chip selection, low active
DC Data/Command selection (high for data, low for command)
RST Reset, low active
BL Backlight

OPERATING VOLTAGE	3.3V/5V
RESOLUTION	240 × 135 pixels
COMMUNICATION INTERFACE	4-wire SPI
DISPLAY SIZE	24.91 × 14.86mm
DISPLAY PANEL SIZE	IPS PIXEL 0.1101 × 0.1035mm
DRIVER	ST7789

https://www.waveshare.com/1.14inch-LCD-Module.htm

Sheet: /display/
File: display.kicad_sch

Title: SPI 1.4" Display Interface

Size: A4	Date: 2022-07-20	**Rev: Rv1**
KiCad E.D.A. eeschema (6.99.0-2547-g3aabea5191)		Id: 6/6